


2-4-2013

Analysis of Coal Combustion By-Products Disposal Practices at the San Juan Mine: Hydrologic and Water Quality Issues

Bruce Thomson

Follow this and additional works at: https://digitalrepository.unm.edu/ce_fsp

 Part of the [Civil Engineering Commons](#), and the [Environmental Engineering Commons](#)

Recommended Citation

Thomson, Bruce. "Analysis of Coal Combustion By-Products Disposal Practices at the San Juan Mine: Hydrologic and Water Quality Issues." (2013). https://digitalrepository.unm.edu/ce_fsp/1

This Technical Report is brought to you for free and open access by the Engineering Publications at UNM Digital Repository. It has been accepted for inclusion in Civil Engineering Faculty Publications by an authorized administrator of UNM Digital Repository. For more information, please contact disc@unm.edu.

Analysis of
Coal Combustion By-Products Disposal Practices
at the San Juan Mine:
Hydrologic & Water Quality Issues

Final Report

Submitted to
Mining and Minerals Division
Energy Minerals and Natural Resources Department
State of New Mexico
Santa Fe, NM

Bruce Thomson, John Stormont, Mark Stone, Ryan Webb, Cheryl Parker, Kirsty Bramlett
Department of Civil Engineering
University of New Mexico
Albuquerque, NM

July 2012

Abstract

Coal Combustion By-Products (CCBs) are generated by the burning of coal for electric power generation and as waste streams from emissions control systems. They consist of bottom ash from the furnaces, fly ash from electrostatic precipitators, and flue gas desulfurization sludge from air pollution scrubbers. Depending on the characteristics of the coal, CCBs may contain high concentrations of metals or other constituents that present a threat to ground or surface water resources if not properly managed. This report describes results of an investigation of CCBs generated by a power plant in northwestern New Mexico. Coal Combustion By-Products from this plant are disposed in mined out areas of a nearby surface coal mine. The objective of this project was to determine the potential for leachate from CCB disposal to contaminate underlying ground water. This was done by: 1) measuring the physical characteristics of fresh and buried CCBs that affect their unsaturated hydraulic properties; 2) determining the chemical, mineralogical, and leaching characteristics of these materials, and 3) through development of a numerical simulation of water migration through an unsaturated column of cover material and buried CCBs.

The CCBs were found to have a dry bulk density of about 1100 kg/m^3 and 800 kg/m^3 for fly and bottom ash respectively, however, both are highly compressible and their density varies with effective stress. The saturated hydraulic conductivity of these materials was about $1 \times 10^{-4} \text{ cm/s}$ for fly ash, $5 \times 10^{-3} \text{ cm/s}$ for bottom ash, and less than $8.5 \times 10^{-6} \text{ cm/s}$ for spoil material used for cover. Soil moisture characteristic curves were measured to permit calculation of unsaturated hydraulic conductivities.

Acid digestion and subsequent elemental analysis of the fly and bottom ash found them to consist primarily of aluminum, barium, calcium, potassium, sodium, and silicon. The mineralogy of these samples is dominated by amorphous glass along with mullite ($\text{Al}_6\text{Si}_2\text{O}_{13}$), quartz (SiO_2), calcite (CaCO_3) and clay minerals. Flue gas desulfurization sludge primarily consists of gypsum ($\text{CaSO}_4 \cdot 2\text{H}_2\text{O}$). Batch and column leach tests of fresh and aged CCBs suggest some dissolution of amorphous materials occurs, but elemental concentrations in the leachates were moderate. Arsenic was present in both the ash material and subsequent leachates but at very low concentrations.

Numerical simulation of water flow through 2 m of cover material into buried CCBs predict very low infiltration rates, less than 0.4 mm/yr , due to low hydraulic conductivity of the cover and water uptake by vegetation. At the bottom of the pit, infiltration from the CCBs into underlying sandstone was predicted to be near zero, and some modeled scenarios actually predicted an upward flux of water.

The very low (or possibly zero) downward flow of ground water through the unsaturated waste predicted by the modeling study, together with the low concentrations of contaminants in leachates from buried CCBs provides evidence that the potential for contamination of the underlying regional aquifer at this site is small.

Table of Contents

Abstract.....	ii
Table of Contents	iii
List of Figures.....	vi
List of Tables.....	x
Acknowledgments.....	xi
1 Introduction.....	1
1.1.1 Concerns Regarding CCB Disposal.....	1
1.1.2 Site Description.....	3
1.1.2.1 Mine Site.....	3
1.1.2.2 Local Geology.....	5
1.1.2.3 Site Hydrology.....	6
1.1.3 Issues of Concern.....	16
1.1.4 Project Objectives.....	16
1.1.5 Report Organization.....	16
Part I – Geotechnical Properties of CCBs and Cover Materials at the San Juan Mine	18
2.1 - Introduction	18
2.2 - Previous Research.....	19
2.2.1 Compressibility of CCBs.....	19
2.2.2 Saturated Hydraulic Conductivity of CCBs.....	19
2.2.3 Unsaturated Hydraulic Properties of CCBs.....	20
2.3 - Research Methods.....	22
2.3.1 Source of Samples.....	22
2.3.2 Physical Properties.....	22
2.3.3 Compressibility.....	23
2.3.4 Saturated Hydraulic Conductivity.....	23
2.3.5 Moisture Characteristic Curve (MCC) Measurements	23
2.4 - Results & Discussion.....	26
2.4.1 Physical Properties.....	26
2.4.2 Compressibility.....	28
2.4.3 Saturated Hydraulic Conductivity.....	29
2.4.4 Moisture Characteristic Curves.....	31
2.4.5 Moisture Characteristic Curve Comparisons.....	32
2.5 Discussion of Laboratory Results	42
2.5.1 Specific Gravity & Calculated Porosity of Fly Ash & Bottom Ash	42
2.5.2 Fly Ash.....	43
2.5.3 Bottom Ash	44
2.6 Conclusions.....	46
Part II – Geochemical Properties of Coal Combustion By-Products and Cover Materials.....	47
3.1 Introduction.....	47
3.2 Background Information.....	48
3.2.1 Fly Ash.....	48
3.2.2 Bottom Ash	50
3.2.3 Flue Gas Desulfurization Sludge	51
3.2.4 Reuse of Coal Combustion Byproducts.....	51

3.2.5 Potential Impacts of Coal Combustion Byproduct Disposal	51
3.3 Research Methods	54
3.3.1 Sample Collection and Preservation	54
3.3.1.1 Core Sampling	54
3.3.1.2 Sample Preparation	59
3.3.2 Chemical Analysis	59
3.3.2.1 Sample Digestion & Leaching	60
3.3.2.2 Mineralogical Characterization	62
3.3.2.3 Column Studies	63
3.4 Results and Discussion	67
3.4.1 Chemical Characteristics of CCBs	67
3.4.1.1 Composition of CCBs and Leachate Characteristics	67
3.4.1.2 Variation of CCB Composition with Depth	71
3.4.1.3 Column Tests	79
3.4.2 Mineralogical Results	93
3.4.2.1 SEM Investigations	94
3.4.2.2 X-Ray Diffraction Investigation	100
3.4.3 Potential Ground Water Impacts of Leachate from Buried CCBs	108
3.5 Conclusions	110
3.5.1 Analytes of Concern	110
3.5.2 Leaching Sequence	110
3.5.3 Evidence of Aging of Buried CCBs	111
3.5.4 Comparison of Results with Historical Data	111
Part III One Dimensional Modeling of Unsaturated Flow	112
4.1 Introduction	112
4.2 Previous research	112
4.2.1 Methods	113
4.2.1.1 Profile Development	113
4.2.1.2 Material Properties	114
4.2.1.3 Upper Boundary Condition for Baseline Model	117
4.2.1.4 Baseline Root Water Uptake	117
4.2.1.5 Lower Boundary Condition for Baseline Model	118
4.2.1.6 Initial Moisture Content	119
4.2.1.7 Root Water Uptake	120
4.2.1.8 Upper Boundary Condition	120
4.2.1.9 Extended Simulation Duration	120
4.2.1.10 Focused Recharge on Surface	120
4.2.1.11 Presence of Water Table	121
4.2.1.12 Lowering of Water Table	122
4.3 Results and Discussion	123
4.3.1 Results of Baseline Model Simulation	123
4.3.1.1 Initial Moisture Content	129
4.3.1.2 Effect of Root Water Uptake	129
4.3.1.3 Impact of the Upper Boundary Condition	132
4.3.1.4 Extended Simulation Duration	132
4.3.1.5 Impact of Focused Surface Recharge	132

4.3.1.6 Impact of the Presence of a Water Table.....	136
4.3.1.7 Impact of Lowering of the Water Table	136
4.4 Discussion.....	141
4.4.1 Sensitivity Analyses.....	146
4.4.2 Importance of the Lower Boundary Condition.....	146
4.4.3 Properties as a Function of Density	147
4.5 Conclusions.....	148
5.0 Overall Project Conclusions	149
5.1.1 Physical Properties.....	149
5.1.2 Geochemical Properties	150
5.1.3 Modeling Studies	151
References.....	153
Appendix I – Results of Column Leach Tests.....	157
Appendix II - Abbreviations	173

List of Figures

Figure 1 General location of San Juan Coal Mine within the state of New Mexico (Mining and Minerals Division, New Mexico 2011).....	4
Figure 2. Pinon, Juniper and Underground areas within the San Juan Coal Mine. The brown area is where several sections overlap and near the active CCB dumping site.	5
Figure 3. CCB disposal locations in the Juniper Pit at San Juan Coal Mine (Mining and Minerals Division, New Mexico 2011).....	7
Figure 4. Geologic map the San Juan Coal Mine and surroundings (Figure 803.A-1 in San Juan Mine Permit 09-01).....	8
Figure 5. Cross Section of Geology at the San Jan Coal Mine from Fruitland Formation to Lewis Shale (Figure 803.A-2 in San Juan Mine Permit 09-01)	9
Figure 6. MMD vegetation classification map for San Juan Coal Mine (Mining and Minerals Division, New Mexico 2011).....	10
Figure 7. Panorama of the San Juan Coal Mine showing vegetative cover following mine reclamation.....	10
Figure 8. Total dissolved solids (TDS) concentration in the No 8 Coal Seam wells G-26 and G3 from 2006 to 2009.....	11
Figure 9. Map of monitoring wells at the San Juan Coal Mine.....	12
Figure 10. Historical ground water elevations in the alluvial well GL in the Shumway Arroyo from 1979 to 2007 (Norwest 2009)	13
Figure 11. Measured potentiometric gradients between the GL and GE alluvial wells in the Shumway Arroyo (Norwest 2009).....	14
Figure 12. Potentiometric surface at No 8 Coal Seam monitoring well G3 from 1990 to 2009 (Norwest 2009)	15
Figure 13. Grain size distribution for fly ash and bottom ash.	27
Figure 14. Compressibility data with fitted curves for fly ash and bottom ash.	30
Figure 15. Plot of saturated hydraulic conductivity (K_{sat}) vs. dry density.	31
Figure 16. Fitted data (top) and saturation moisture characteristic curves (bottom) for fly ash at lowest dry density.	34
Figure 17. Fitted data (top) and saturation moisture characteristic curves (bottom) for fly ash at intermediate dry density.....	35
Figure 18. Fitted data (top) and saturation moisture characteristic curves (bottom) for fly ash at greatest dry density.	36
Figure 19. Fitted data (top) and saturation moisture characteristic curves (bottom) for bottom ash at lowest dry density.....	37
Figure 20. Fitted data (top) and saturation moisture characteristic curves (bottom) for bottom ash at intermediate dry density.....	38
Figure 21. Fitted data (top) and saturation moisture characteristic curves (bottom) for bottom ash at greatest dry density.....	39
Figure 22. Best fit moisture characteristic curves for fly ash as function of dry density.....	40
Figure 23. Van Genuchten parameters vs. dry density.....	41
Figure 24 - Comparison of linear trend line and parabolic trend line.....	45
Figure 25. Geoprobe ® coring samples diagram	55
Figure 26. Example photo of core samples from sonic drilling.....	56

Figure 27. Logs of holes drilled by sonic drilled showing location at which samples were collected.....	58
Figure 28. Photo of samples before leach tests by ASTM D3987-06.....	61
Figure 29. Samples placed in mixer for leach tests	62
Figure 30. Photo of 2 in ID by 10 in tall columns used in column leach studies.	64
Figure 31. Average total arsenic concentrations in fresh and aged CCBs and spoil material.....	70
Figure 32. Concentration of Nickel in buried CCBs versus sample depth	71
Figure 33. Concentration of Barium and Boron in buried CCBs versus sample depth.....	72
Figure 34. Concentration of Iron in buried CCBs versus sample depth	73
Figure 35. Concentration of Strontium in buried CCBs versus sample depth.....	74
Figure 36. Concentration of Magnesium in buried CCBs versus sample depth.....	74
Figure 37. Normalized concentrations of Barium and Arsenic in Fly Ash leachates versus sample depth.....	75
Figure 38. Normalized concentrations of elements with depth (B, Co, Cr, Ni, Si).....	76
Figure 39. Normalized concentrations of elements with depth (Al, Cd, Fe, Mg, Mo, Se, As)....	77
Figure 40. Normalized concentrations of elements which varied little with depth (Ca, K, Li, Sr, V).....	78
Figure 41. Normalized anion concentrations versus depth (F^- , Cl^- , NO_2^- , NO_3^- , SO_4^{2-} , Alkalinity).....	79
Figure 42. Column test concentration changes over time for Na with largest initial concentration	82
Figure 43. Normalized concentrations of constituents in DI water column leachate of fresh fly ash	83
Figure 44. Normalized concentrations of constituents in DI water column leachate of fresh fly ash with Ba, and Sr removed	84
Figure 45: Normalized concentrations of constituents in DI water column leachate of fresh bottom ash.....	85
Figure 46: Normalized concentrations of constituents in DI water column leachate of old buried fly ash.....	86
Figure 47: Normalized concentrations of constituents in DI water column leachate of old buried bottom ash.....	87
Figure 48: Normalized concentrations of constituents in DI water column leachate of young buried fly ash.....	88
Figure 49: Normalized concentrations of constituents in DI water column leachate of spoil.....	89
Figure 50: Normalized concentrations of constituents in No 8 Coal Seam Water column leachate of fresh fly ash	90
Figure 51: Normalized concentrations of constituents in No 8 Coal Seam Water column leachate of fresh fly ash with Al, Li and V not plotted	91
Figure 52: Normalized concentrations of constituents in No 8 Coal Seam Water column leachate of old buried fly ash	92
Figure 53: Normalized concentrations of constituents in No 8 Coal Seam Water column leachate of old buried fly ash with Ba, Al and Si removed.....	93
Figure 54. SEM micrograph of fly ash using secondary electron imaging showing spherical morphology of particles. Original magnification = 400x. Scale bar = 100 μ m.	95
Figure 55. SEM micrograph of fly ash using back scattered electron imaging. Original magnification = 1500x. Scale bar = 20 μ m.....	95

Figure 56. SEM image of bottom ash samples using back scattered electron imaging. Original magnification = 180x. Scale bar =200 μ m.....	96
Figure 57. SEM micrograph of bottom ash using back scattered electron imaging. Original magnification = 1000x. Scale bar = 50 μ m.....	97
Figure 58. SEM micrograph of flue gas desulfurization (FGD) sludge using back scattered electron imaging. Original magnification = 430x. Scale bar = 100 μ m.....	98
Figure 59. SEM micrograph of old buried bottom ash using back scattered electron imaging. Original magnification = 500x. Scale bar = 100 μ m.....	99
Figure 60. SEM micrograph of old buried fly ash using secondary electron imaging. Original magnification = 3000x. Scale bar = 10 μ m.....	100
Figure 61. XRD pattern for fresh fly ash. The library patterns are for mullite (top), quartz (middle) and hematite (bottom).....	101
Figure 62. XRD pattern for fresh bottom ash. The library patterns are for mullite (top), quartz (second from top), calcite (third from top) and albite (bottom).....	102
Figure 63. XRD pattern for fresh flue gas desulfurization ash. The library patterns are for gypsum (top), calcite (middle) and quartz (bottom).....	103
Figure 64. XRD pattern for old fly ash. The library patterns are for mullite (top), quartz (second from top), aluminum phosphate (third from top), ferrierite (fourth from top), clintonite (fifth from top), and paragonite (bottom).....	104
Figure 65. XRD pattern for fresh bottom ash. The library patterns are for mullite (top), quartz (second from top), calcite (third from top), ferrierite (fourth from top), and anorthite (bottom).....	105
Figure 66. XRD pattern for spoil material. The library patterns are for quartz (top), nontronite (second from top), kaolinite (third from top), calcite (fourth from top), albite (fifth from top), annite (sixth from top) and illite (bottom).....	106
Figure 67. XRD diffraction patterns for fresh fly ash (top), fly ash buried at 10 ft (middle) and fly ash buried at 125 ft (bottom).....	107
Figure 68. XRD diffraction patterns for fresh bottom ash (top), fly ash buried at 120 ft (middle) and bottom ash buried at 109 ft (bottom).....	108
Figure 69. Fly Ash (top) and Bottom Ash (bottom) Dry Density vs. Pressure Curves.....	116
Figure 70. Example of Profile Spreadsheet.....	117
Figure 71. Diagram of baseline model materials and boundary conditions.....	119
Figure 72. Precipitation (left) and Surface Runoff (right).....	121
Figure 73. Soil water flux predictions for fly ash only profile (top) and bottom ash only profile (bottom).....	125
Figure 74. Soil moisture content vs. depth for fly ash only profile (top) and bottom ash only profile (bottom).....	126
Figure 75. Soil water flux predictions for random profiles 3 (top) and 8 (bottom).....	127
Figure 76. Soil moisture content vs. depth for random profiles 3 (top) and 8 (bottom).....	128
Figure 77. Flux at bottom of CCB pit as a function of initial water content.....	129
Figure 78. Baseline results: cumulative infiltration.....	130
Figure 79. Cumulative root water uptake (top) and cumulative evaporation (bottom) for baseline model.....	131
Figure 80. Cumulative evaporation without root water uptake.....	132
Figure 81. Cumulative infiltration for focused recharge scenario.....	133
Figure 88. Predicted water flux at the interface between the soil cover and buried CCBs.....	141

Figure 89. Predicted water flux at the interface between the buried CCBs and the Pictured Cliffs Sandstone.....	142
Figure 90. Moisture characteristic curves for materials used in the modeling study.....	143
Figure 91. log K vs. log h for materials in profile 3	143
Figure 92. log K vs Water Content for materials in profile 3	144
Figure 93. Moisture characteristic curve for top soil, fly ash, and bottom ash at the interface between top soil and CCBs for focused recharge simulations.....	145
Figure 94. K vs. Suction Head for top soil, fly ash, and bottom ash at interface between top soil and CCBs for focused recharge simulations.....	146
Figure 95 : Results of column leach tests for silver (Ag).....	166
Figure 96: Results of column leach tests for aluminum (Al).....	166
Figure 97: Results of column leach tests for boron (B).....	167
Figure 98: Results of column leach tests for barium (Ba)	167
Figure 99: Results of column leach tests for calcium (Ca).....	168
Figure 100: Results of column leach tests for potassium (K).....	168
Figure 101: Results of column leach tests for chromium (Cr).....	169
Figure 102: Results of column leach tests for lithium (Li).....	169
Figure 103: Results of column leach tests for magnesium (Mg).....	170
Figure 104: Results of column leach tests for copper (Cu)	170
Figure 105: Results of column leach tests for molybdenum (Mo)	171
Figure 106: Results of column leach tests for silicon (Si).....	171
Figure 107: Results of column leach tests for strontium (Sr).....	172
Figure 108: Results of column leach tests for vanadium (V)	172

List of Tables

Table 1 Summary of physical properties of selected materials.....	26
Table 2. Water contents measured in Geo-Probe samples.	27
Table 3. Clod density results of sample from Juniper Pit 04 at 42 m depth.	27
Table 4. Summary of compressibility measurements and parameters for Eq. 1.....	28
Table 5. Saturated hydraulic conductivity measurements.....	29
Table 6. Van Genuchten model parameters for fly ash (FA) and bottom ash (BA) samples.	33
Table 7. Van Genuchten model parameters for best fit curves at each dry density.....	33
Table 8. Calculated Porosity and Saturated Water Content Comparison.....	43
Table 9. Dissolved trace element concentrations in groundwater and deionized water leachate (Luther, Musslewhite, and Brown 2009).	49
Table 10. Mean trace element concentrations in Bottom Ash, Fly Ash and Overburden at the SJCM (Luther, Musslewhite, and Brown 2009)	50
Table 11. Comparison of New Mexico ground water standards for domestic consumption and irrigation use to the range of water quality in SJCM monitoring wells.....	53
Table 12. Locations of the sample groups used for each test procedure.....	60
Table 13. Mineral phases present in the fly ash, bottom ash, and flue gas desulfurization sludge.	63
Table 14. Comparison of the composition of No 8 Coal Seam Water used in column leach studies to the range of water quality measurements from monitoring data.	65
Table 15. Previous leach tests of CCBs from the San Juan Coal Mine and results for key parameters.	67
Table 16. Elemental composition of CCBs following nitric acid digestion.	68
Table 17. Anionic constituents in DI water extracts for surface cover materials (spoil), fresh and buried ash samples	69
Table 18. Water Quality Results for No 8 Coal Seam Water used for column leach and historical data compared to typical water quality data	81
Table 19. Comparison of maximum concentration of elements in CCB column leachate to concentrations in SJCM ground water. All concentrations in mg/L.	109
Table 20. Hydraulic Properties of Top Soil and Pictured Cliffs Sandstone.	114
Table 21 - Root Distribution Input Values	118
Table 22. Day and Magnitude of Runoff Events	121
Table 23. Material distribution for random vertical profiles 3 and 8.....	124
Table 24. Range of fluxes and water contents for the baseline model simulation.	124
Table 25. Chemical analyses of column leach tests.....	158

Acknowledgments

This study benefitted from the assistance of several key participants. Brent Musslewhite and Kara Hart of BHP Billiton provided considerable insight into the history and operation of the San Juan Coal Mine as well as access to data and assistance in sample collection. Ms. Hart also provided guidance and technical support to Ms. Parker and Mr. Webb. Jim O'Hara, Dave Clark and Charles Thomas with the Mining and Minerals Division of the State of New Mexico Energy Minerals and Natural Resources Department provided funding, information on hydrology and policies, and technical review and comment. Drs. Abdul Mehdi Ali, Jim Connolly and Mike Spilde, all of the Department of Earth and Planetary Sciences at the University of New Mexico provided extraordinary support in chemical analyses and collection and interpretation of the mineralogical data. Technical staff at the consulting firm of Daniel B. Stephens and Associates provided assistance with measurement of the geotechnical properties of the samples.

Analysis of Coal Combustion By-Products Disposal Practices at the San Juan Mine: Hydrologic & Water Quality Issues

Bruce Thomson, John Stormont, Mark Stone, Ryan Webb, Cheryl Parker, Kirsty Bramlett

1 Introduction

Coal Combustion By-Products (CCBs), often referred to as simply “ash,” from the San Juan Generating Station is disposed of in the San Juan Coal Mine (SJCM) owned and operated by BHP Billiton adjacent to the power plant. The Mining and Minerals Division (MMD) of the NM Energy, Minerals and Natural Resources Department regulates the impact of this disposal on surface and ground water.

The SJCM is a large open pit mine located west of Farmington, NM and north of the San Juan River. The mine was permitted in 1973 and ash has been disposed of in the mine apparently since it opened. The Surface Mining Control and Reclamation Act (SMCRA) was passed in 1977 and established federal guidelines for surface coal mine operation that included a permit process. Permit provisions at the SJCM addressing ash disposal began in 1985.

The MMD has developed considerable knowledge of the location of the ash disposal areas and also has a fairly substantial data set of ground water samples at the mine. Ground water use near the mine is limited due to poor quality and limited quantity (Luther et al., 2007). Few contaminants are present above NM ground water standards. To date, there has been no direct linkage between groundwater quality in the vicinity of the SJCM and contamination from CCB disposal.

1.1.1 Concerns Regarding CCB Disposal

National attention was drawn to disposal of CCBs following failure of the TVA Kingston Fossil Plant’s fly ash disposal pond on December 22, 2008 resulting in release of 4.2 million m³ of fly ash slurry and extensive contamination of surface and ground water resources. However, industry and regulatory interest extend back at least 40 years, eventually resulting in passage of SMCRA of 1977. This law resulted in development of extensive regulations that deal with surface mining, mine land reclamation, and mine waste disposal. It is enforced by the Office of Surface Mining Reclamation and Enforcement within the U.S. Department of Interior at the federal level. As with many other environmental laws, SMCRA allows for delegation of authority to the states. In New Mexico, SMCRA is enforced by the MMD of the Energy Minerals and Natural Resources Department under authority granted by the New Mexico Surface Mining Act. The MMD administers four programs: Abandoned Mine Land Program, Coal Mine Reclamation Program, Mining Act Reclamation Program, and the Mine Registration Program. The Coal Mine Reclamation Program deals specifically with regulation of coal mines.

CCBs may consist of a variety of materials including fly ash, bottom ash, flue gas desulfurization sludge (FGDS), and boiler slag. CCB disposed at the San Juan Mine typically consists of 70% fly ash, and 15% each of bottom ash and FGD products (Luther et al., 2007). Fly ash consists of small particles of light inorganic materials transported from the boiler by the hot flue gasses and subsequently captured by emissions control equipment such as electrostatic precipitators, scrubbers, and bag filters. Bottom ash is the agglomerated inorganic material too heavy to be carried in the flue gases. It is removed through open grates to an ash hopper at the bottom of the boiler. Bottom ash is typically gray to black in color, is quite angular, and has a porous surface structure. Both the fly and bottom ash materials frequently have high concentrations of metals and inorganics that, under some circumstances, can leach into water producing water contamination problems. This leachate is the source of contaminants that were released by the Kingston Fossil Plant's ash pond failure. FGD products consist of a thick slurry of gypsum ($\text{CaSO}_4 \cdot 2\text{H}_2\text{O}$) from the lime scrubbers used to remove SO_2 .

Ash from the San Juan Generating Station is disposed of in the San Juan Mine, an open pit mine located adjacent to the power plant. The adjacent underground mine does not receive CCBs. It is the only state-regulated mine in NM currently receiving CCBs (OSMRE, 2009). It is important to recognize that there is very little similarity between this ash disposal practice and that at the Kingston plant. The Tennessee ash was disposed as a slurry to an above-grade pond. Thus, it was an elevated pond; containment was provided by an earth berm. At the SJGS fly and bottom ash are disposed as solids in empty mine pits. The low water content minimizes the amount of water that moves downward through the waste to underlying formations and increases the stability of unconsolidated waste materials. Because the disposal site is in a pit, there is negligible probability that the containment will suffer a catastrophic failure.

The principal concerns regarding ash disposal at the San Juan Mine relate to protection of underlying ground water formations by CCB leachate as well as possible water quality impacts to nearby streams such as the Shumway Arroyo. A general description of ash disposal practices at the San Juan Mine and the nearby Navajo Mine was provided by Young (2003). A combination of engineered controls and natural barriers is used to protect the environment. Engineered controls focus on final covers of the ash as well as grading, vegetation, and drainage strategies to minimize surface water infiltration into the ash. The natural barriers include placement of ash only in inactive pits that are underlain by low permeability materials.

CCB has been disposed of at the San Juan Mine since 1973, although prior to SMCRA information about the amounts and disposal location was limited. O'Hara et al. (2009) have used GIS technology to compile information on the location and amounts of CCBs disposed of to facilitate development of improved monitoring programs aimed at protecting ground water resources. Although there is a potential for high concentrations of contaminants, leaching tests with CCB materials disposed of at the San Juan Mine has shown relatively modest concentrations of contaminants in these leachates (Luther et al., 2007). This study found limited evidence of ground water contamination below the San Juan Mine. Further, the evidence collected to date could not be attributed to disposal of CCBs with any confidence as other potential sources of contamination are present including "natural" contamination from geologic formations in the vicinity of the SJM. Formations of interest include the No. 8 Seam aquifer, Pictured Cliffs Sandstone (PCS) Formation, Fruitland Formation, Kirtland Formation, and

unconsolidated alluvial deposits associated with the San Juan River and Shumway-Westwater Arroyos. The general groundwater quality is saline with total dissolved solids typically greater than the Safe Drinking Water Act (SDWA) secondary standard of 500 mg/L.

1.1.2 Site Description

The San Juan Coal Mine (SJCM) is located near Farmington, New Mexico in the northwest part of the state (Figure 1). The SJCM began operation in 1972 and contains estimated coal reserves that are sufficient to last another 25 years.

1.1.2.1 Mine Site

The permitted mining area of the SJCM is broken up into three general sections as shown in Figure 2. The dotted red line denotes the approximate boundary of the BLM lease. The approximate extent of the Pinon pit is shown in light blue and is located in the northwest section of the mine. The Pinon pit has several ponds and topsoil stockpiles within the area. The Juniper pit area is seen in pink and is located in the southwestern part of the SJCM. The Shumway Diversion runs along the western boundary of the Juniper Pit. The Juniper Pit was the reclaimed area that was the focus of the research described in this report. The Underground mining area is highlighted in green and is where active underground mining and support structures are in place.

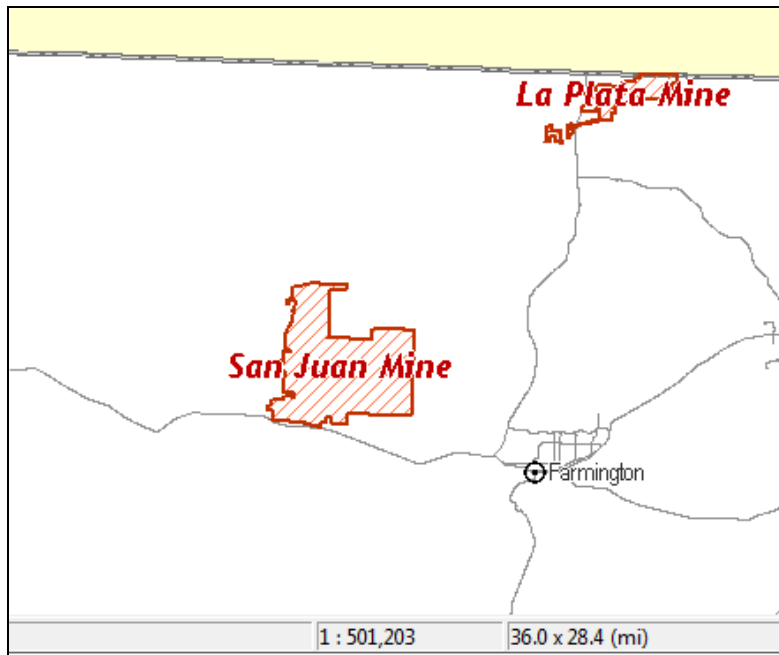
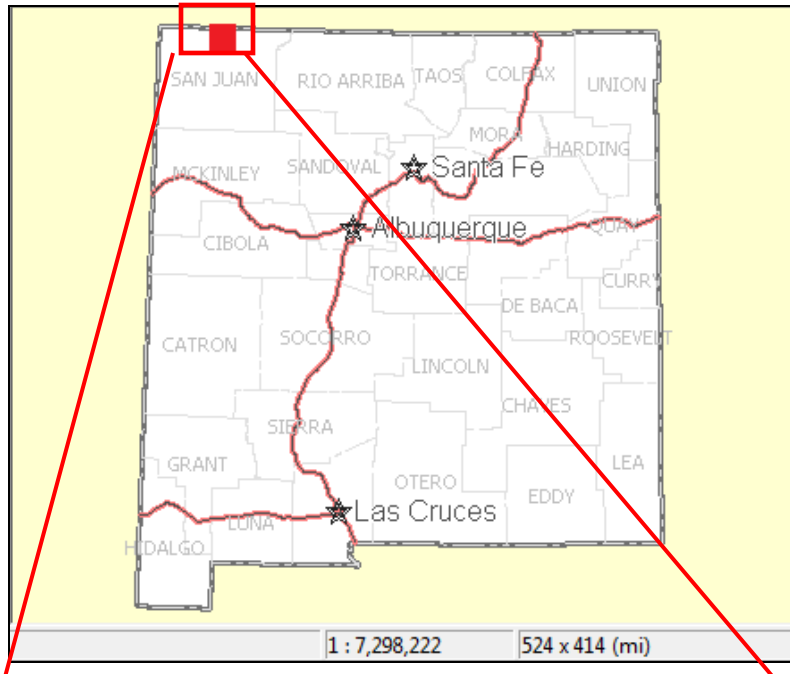


Figure 1 General location of San Juan Coal Mine within the state of New Mexico (Mining and Minerals Division, New Mexico 2011)

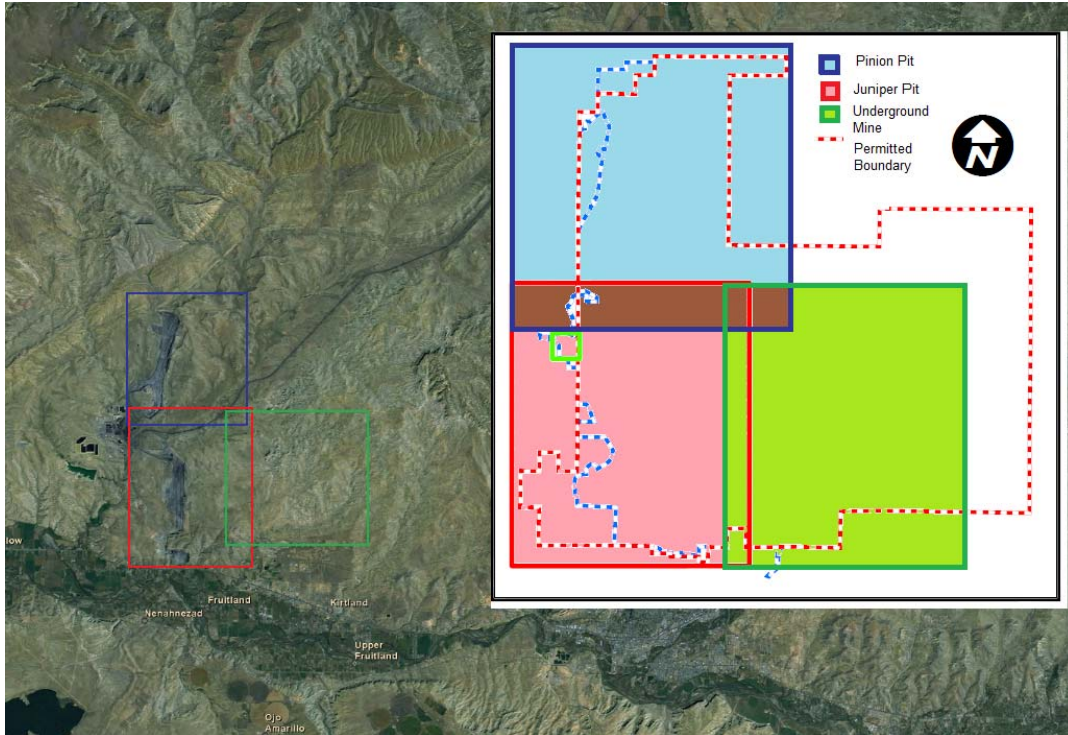


Figure 2. Pinion, Juniper and Underground areas within the San Juan Coal Mine. The brown area is where several sections overlap and near the active CCB dumping site.

Figure 3 provides a closer view of the locations within the Juniper Pit at which CCBs have been disposed. The year in which each site was covered is listed. This year therefore establishes a minimum age of the buried CCBs. Detailed records of CCB disposal have not been kept so the age of deeper material is not known.

1.1.2.2 Local Geology

The SJCM is located on the western edge of the San Juan Structural Basin with the geologic strata dipping towards the east. The classification of the MMD for the SJCM can be seen in Figure 4 (Mining and Minerals Division, New Mexico 2011). The geologic formations are from the Cretaceous Period and consist of Pictured Cliffs Sandstone, Fruitland formations, Kirtland formation and unconsolidated alluvial deposits (Mining and Minerals Division, New Mexico 2011). Nearly all of the mine property is located atop Kirtland shale.

A cross section of the typical geology throughout the permitted area can be seen in Figure 5 with Fruitland formation nearest the surface, which contains the coal layer that is overlying Pictured Cliffs Sandstone on top of Lewis Shale.

Natural vegetation in the vicinity of the SJCM is shown in Figure 6 and is classified as Great Basin desert scrub. A photo showing vegetation on a reclaimed part of the mine is presented in Figure 7. The picture was taken facing north at a the sonic drilling sample site. In the distance steam from the San Juan Generating Station can be seen.

1.1.2.3 Site Hydrology

The site poses unique hydrologic properties as its southern boundary approaches the San Juan River which likely affects ground water flow; the exact direction and magnitude of ground water flows under the SJCM are unknown. As part of the permitting process the SJCM submitted a reclamation plan to protect the hydrologic balance of the area. The purpose of the reclamation plan is to assure protection of the surface and ground water quality by monitoring mine water inflows, minimizing surface runoff and sedimentation into streams. Ground water is present due to perched aquifers, location of the ground water table within the area, leakage from water pipe used by SJCM and PNM, a native river, arroyos and storm water runoff (Ginn, Perkins, and O'Hayre 2009).

Annual precipitation at the SJCM averages about 9 in/yr. Farmington, NM is the nearest site at which evaporation is measured with a period of record from 1978 to 2008. Over this time the average pan evaporation rate was 66.81 in/yr. The precipitation-to-evaporation ratio is thus 0.13 in/in which results in the climate being classified as arid.

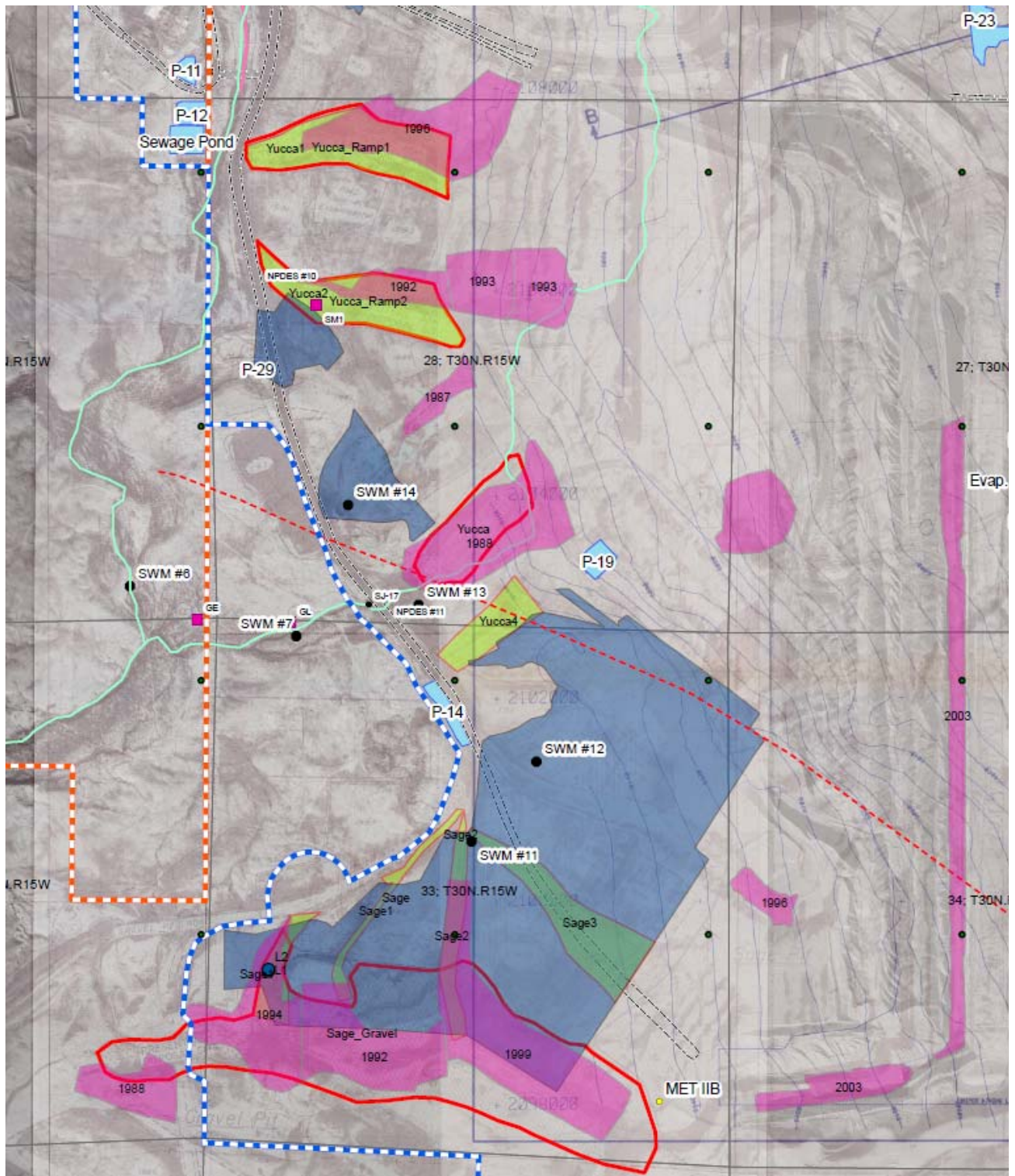
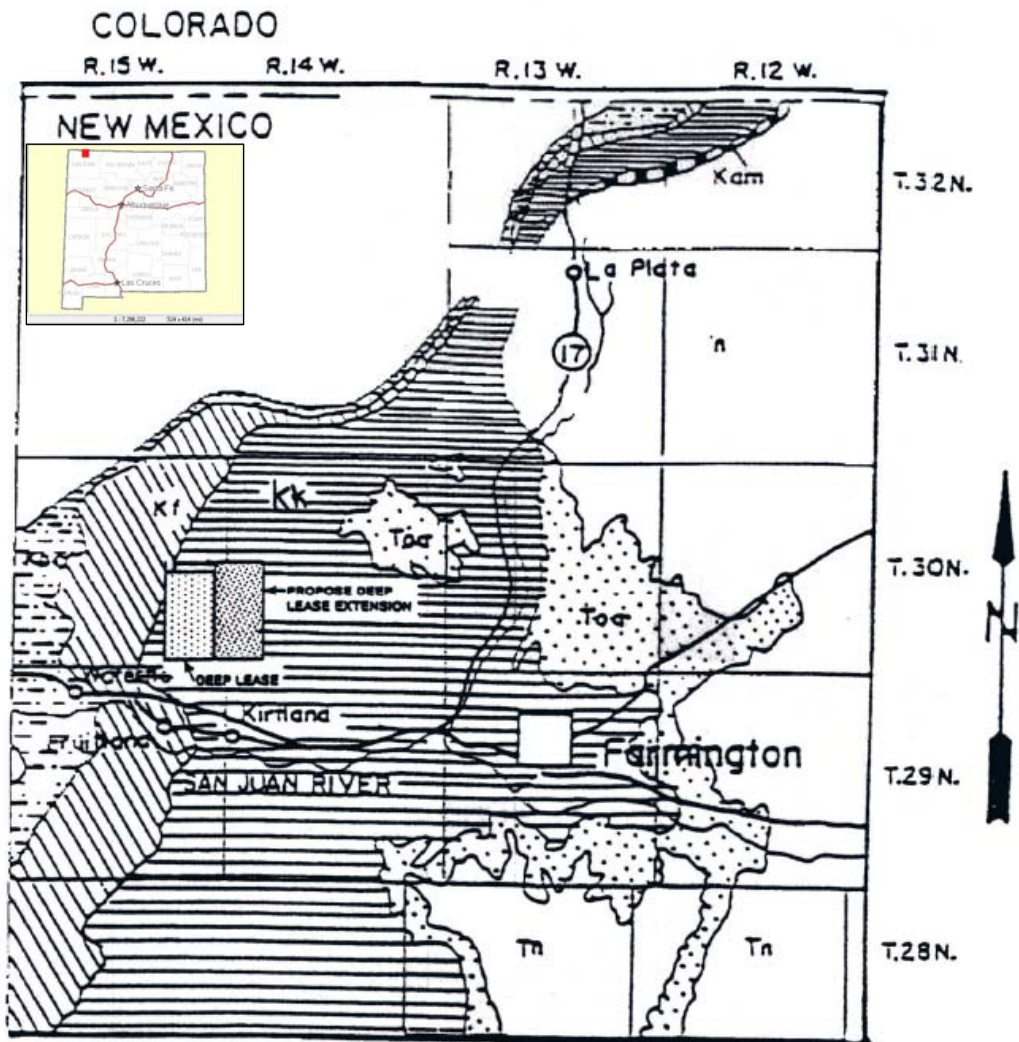


Figure 3. CCB disposal locations in the Juniper Pit at San Juan Coal Mine (Mining and Minerals Division, New Mexico 2011).



Source:
Fassett and Hinds,
U.S.G.S.
Prof. Paper 676, 1971

Legend:
1 Mile
1 Kilometer

Fruitland Formation

Ojo Alama Sandstone

McDermott Member,
Animas Formation

Kirtland Shale

Pictured Cliffs Sandstone

Figure 4. Geologic map the San Juan Coal Mine and surroundings (Figure 803.A-1 in San Juan Mine Permit 09-01)

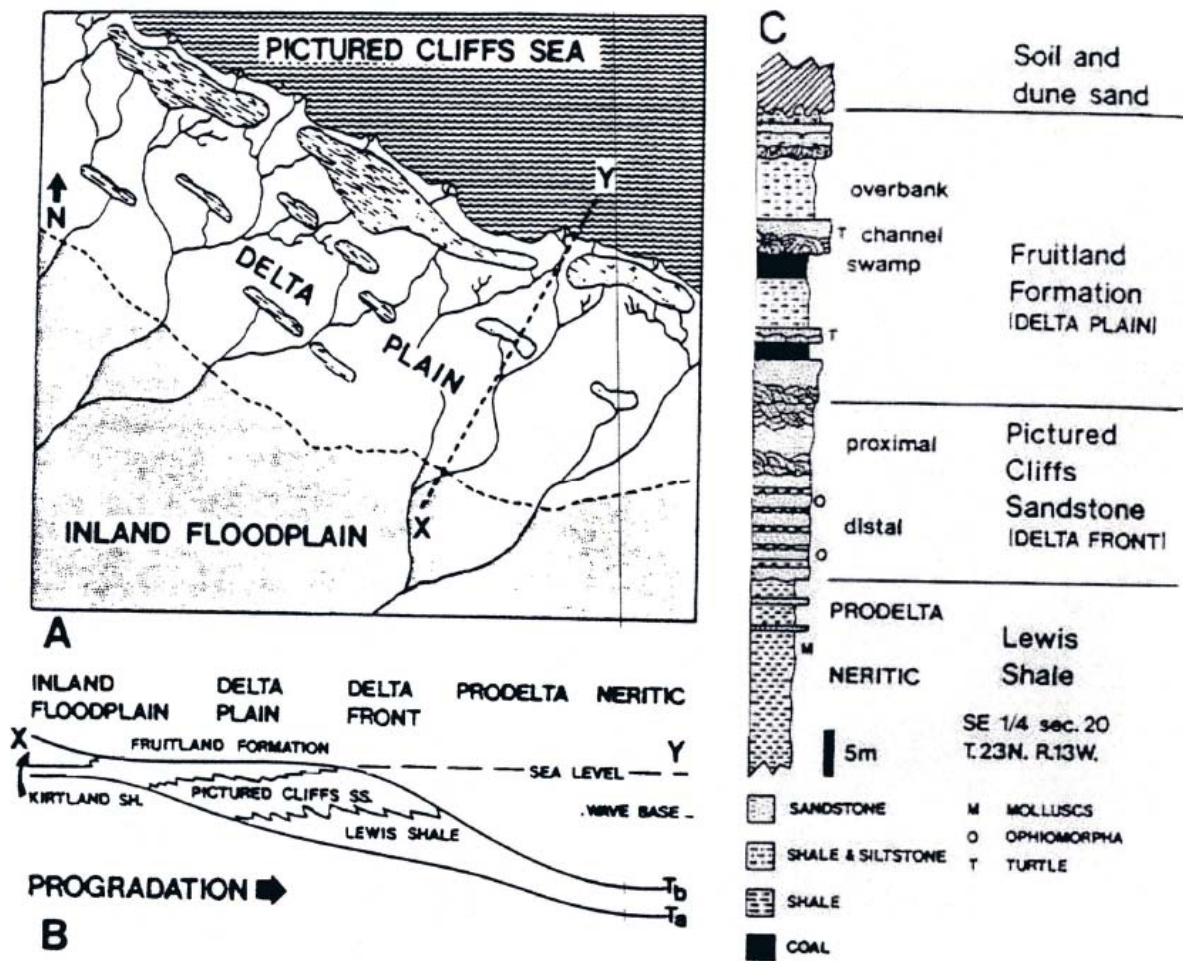


Figure 5. Cross Section of Geology at the San Jan Coal Mine from Fruitland Formation to Lewis Shale (Figure 803.A-2 in San Juan Mine Permit 09-01)

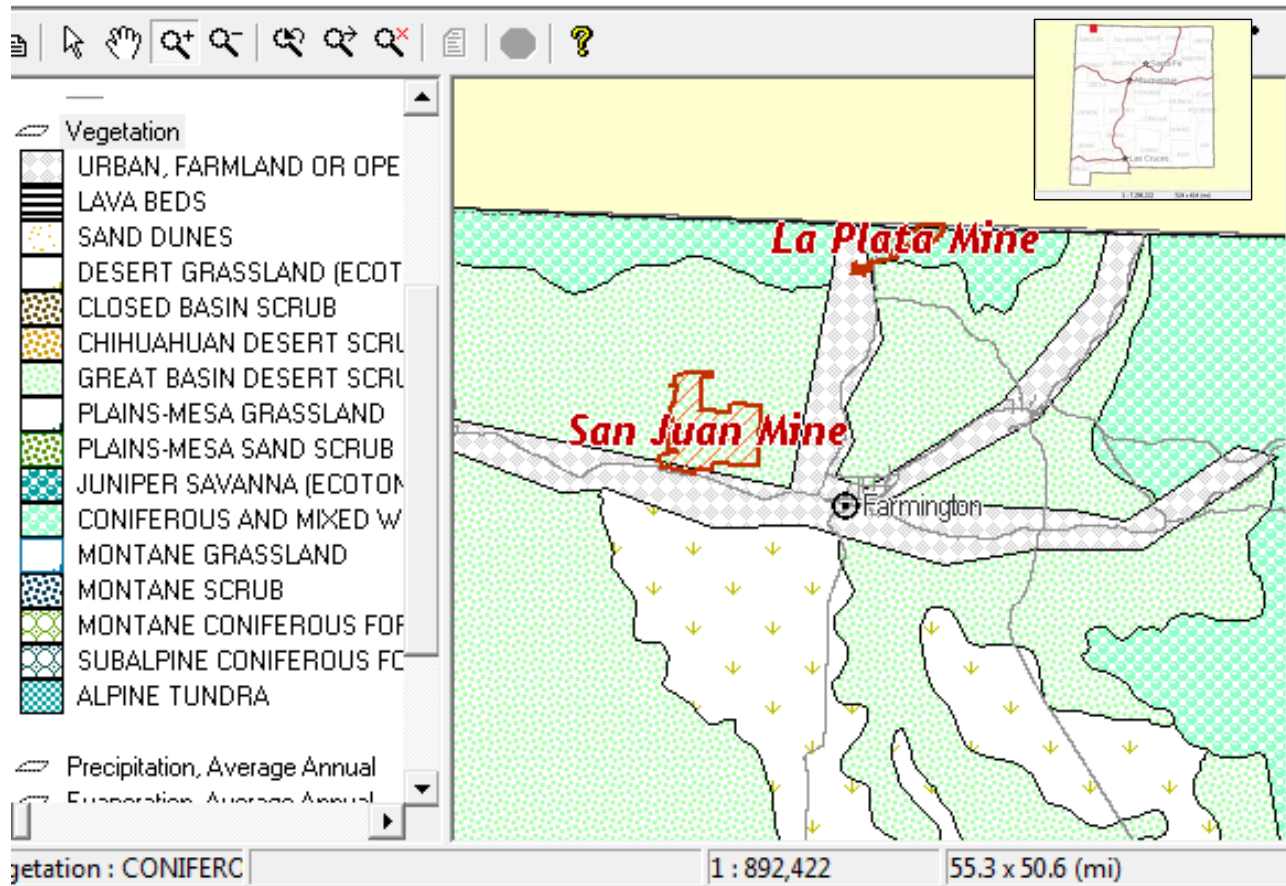


Figure 6. MMD vegetation classification map for San Juan Coal Mine (Mining and Minerals Division, New Mexico 2011)



Figure 7. Panorama of the San Juan Coal Mine showing vegetative cover following mine reclamation.

Within the permitted area of the SJCM there are no existing springs or domestic or livestock wells (Ginn, Perkins, and O'Hayre 2009). Surface water channels have been constructed to divert water around current and past mining areas. Ground water pumping has been conducted to dewater the underground mine. The total volume of pumping ranges from 12 to 20 acre feet/month with an average of 15 acre feet/month from January 2006 to February 2009 (Ginn, Perkins, and O'Hayre 2009).

There are four identified aquifers within the permitted area: the Pictured Cliffs Sandstone (PCS), Fruitland formation coal Unit No 8 Coal Seam, Fruitland formation coal Unit No 9 Coal Seam, and the Westwater-Shumway Arroyo alluvial (Luther, Musslewhite, and Brown 2009). Figure 9 shows the location of monitoring wells at the SJCM (Mining and Minerals Division, New Mexico 2011). The purple dots show the locations of the most recent monitoring wells drilled in June 2011.

Monitoring wells have been installed near areas where CCBs have been disposed (Figure 9). Monitoring wells in the Picture Cliff Sandstone (PCS) are labeled GB and monitoring wells placed within the Shumway and Westwater Arroyo are labeled GE and GL respectively. G26 and G3 are the current monitoring wells with water in them from the No 8 Coal Seam water (Ginn, Perkins, and O’Hayre 2009). Total dissolved solids (TDS) in water samples from the No 8 Coal Seam are shown in Figure 8 for wells G26 and G3.

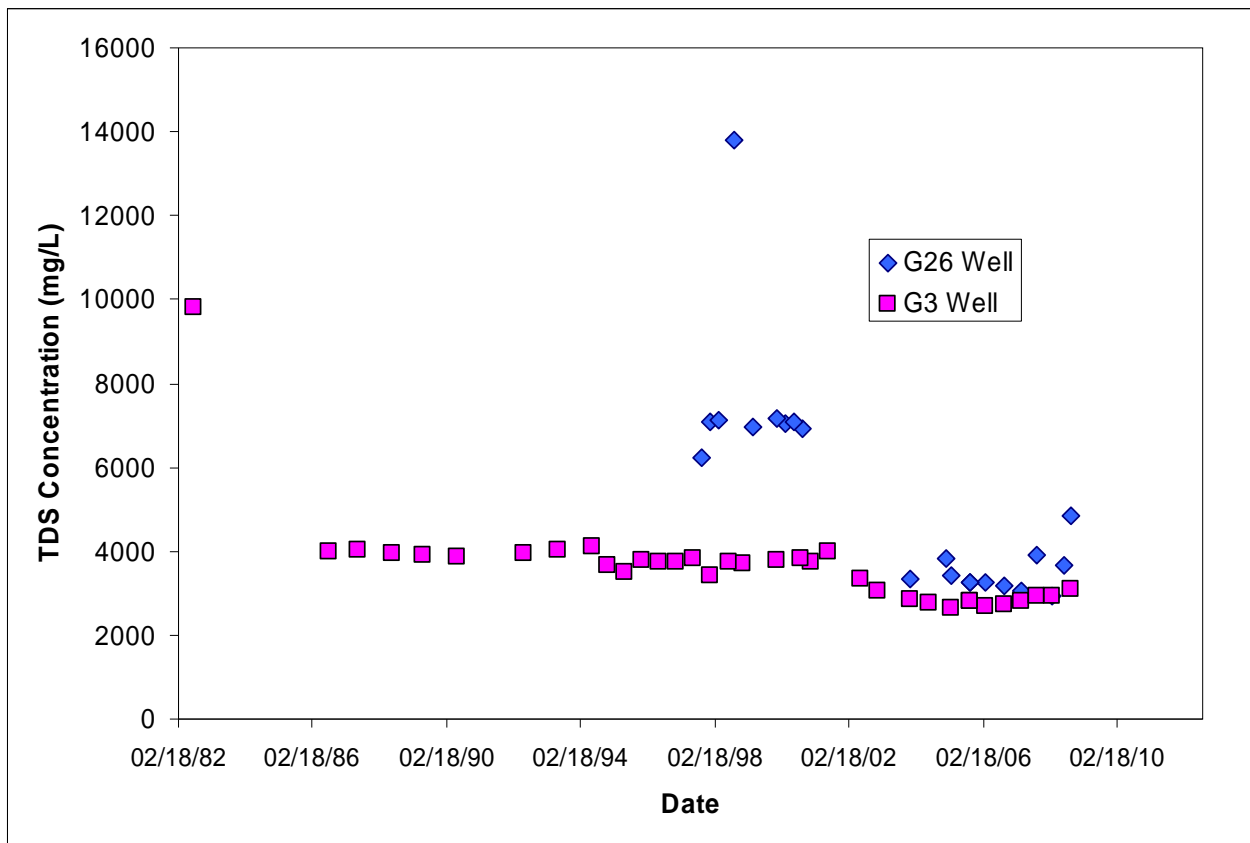


Figure 8. Total dissolved solids (TDS) concentration in the No 8 Coal Seam wells G-26 and G3 from 2006 to 2009

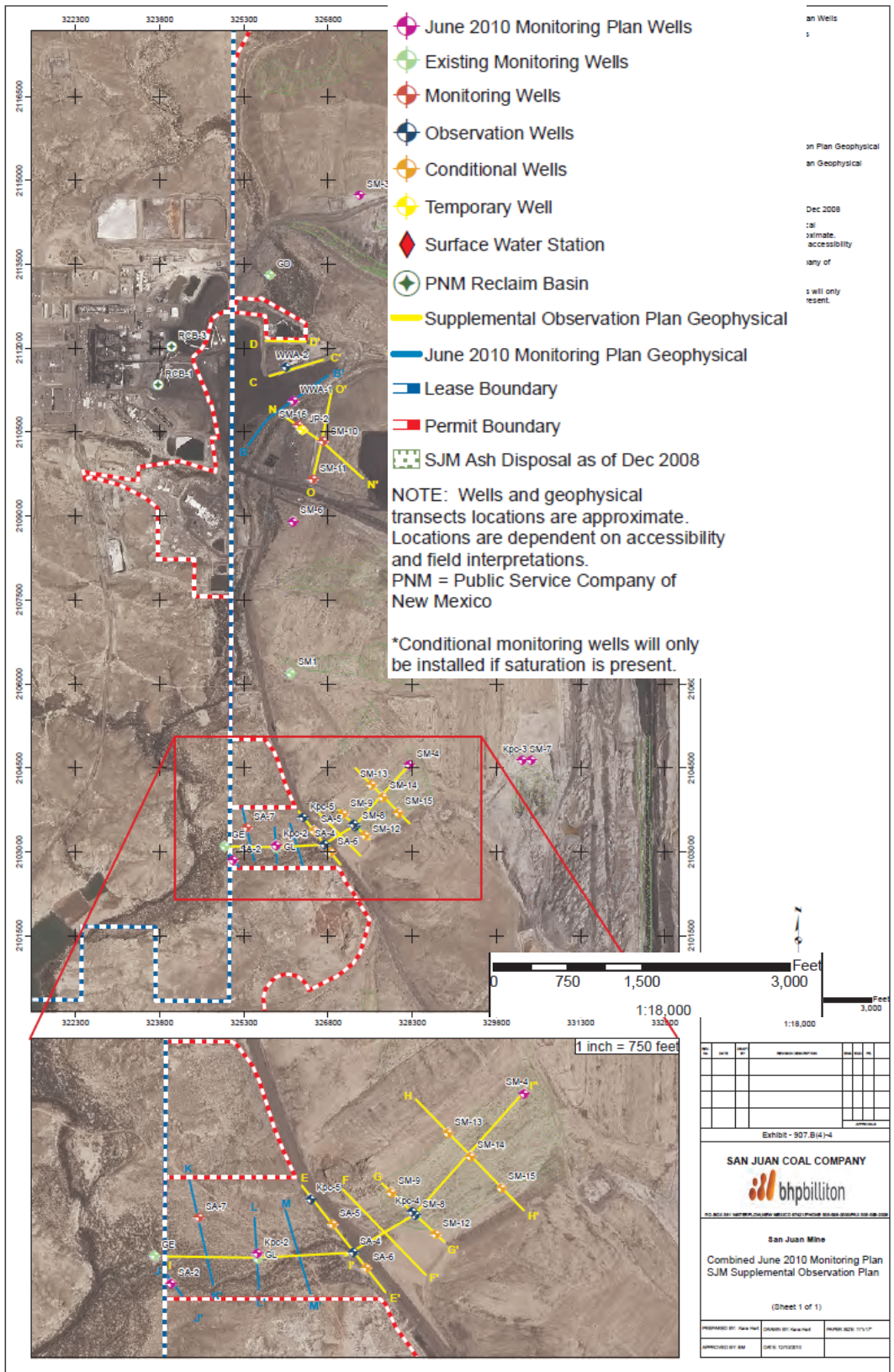


Figure 9. Map of monitoring wells at the San Juan Coal Mine

Near the mine the Pictured Cliffs Sandstone averages about 120 feet thick and dips one to two degrees to the east southeast. The PCS does not yield usable quantities of ground water due to low permeability. The groundwater is classified as sodium-bicarbonate-chloride and contains elevated concentrations of sulfide (S), fluoride (F), and sulfate (SO₄). In 1979 a test measured the transmissivity of the PCS at 1.12 ft²/d and hydraulic conductivity of 0.03 ft/d.(Luther, Musslewhite, and Brown 2009).

A small perched water table roughly 100 ft above the No 8 Coal Seam is associated with the No 9 Coal Seam but the amount of water it contains is negligible (Luther, Musslewhite, and Brown 2009).

The No 8 Coal Seam is a potential recharge source due to outcrops of the Coal Seam that intersect with intermittent stream channels within the SJCM. Ground water in the No 8 Coal Seam flows east with hydraulic gradients ranging from 0.001 to 0.011. The estimated transmissivity of this formation is extremely low at 0.183 ft²/d corresponding to a hydraulic conductivity of 0.005 ft/d. The water quality of No 8 Coal Seam is classified as sodium-sulfate-bicarbonate type and considered poor quality with high concentrations of chloride and calcium. No 8 Coal Seam water quality varies throughout the SJCM. For example the TDS concentrations are very high and range from 3,645 mg/ L to 18,560 mg/L. The pH of this water ranges from 8.5 to 12.6 (Luther, Musslewhite, and Brown 2009).

The water elevations collected from GL wells in the Shumway Arroyo since 1979 appear to be declining as seen in Figure 10. Some of the scatter in earlier years may be due to inaccurate or inconsistent measuring tools (Norwest 2009).

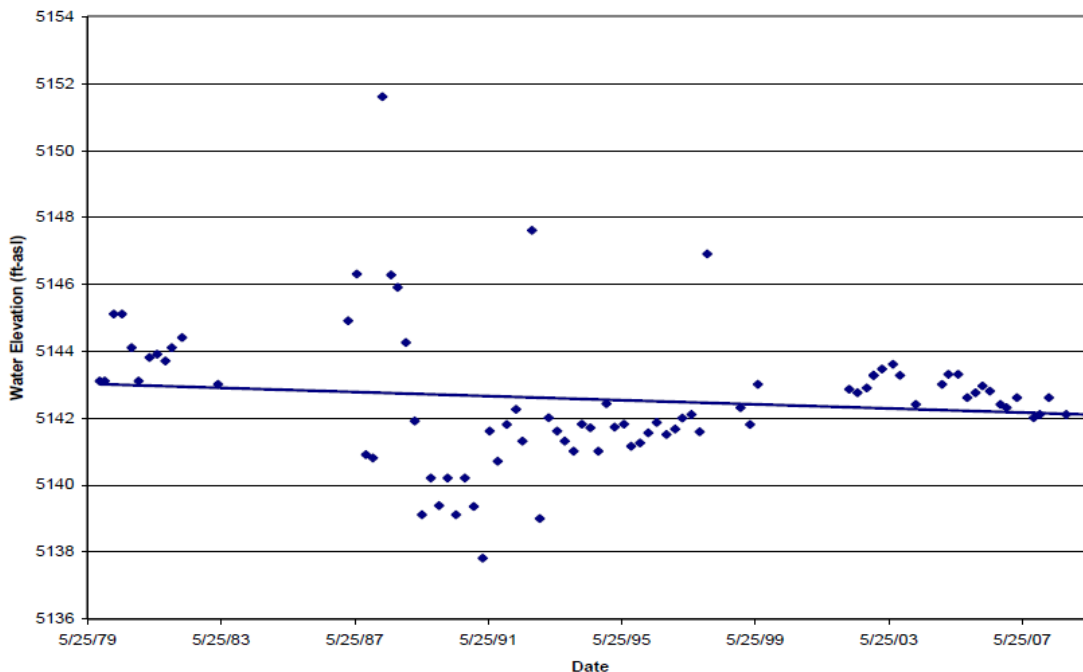


Figure 10. Historical ground water elevations in the alluvial well GL in the Shumway Arroyo from 1979 to 2007 (Norwest 2009)

Similar measurements were collected at GE wells and followed a similar trend. This led to the conclusion that the alluvial water table between the wells is flat with little to no groundwater flow along the Shumway Arroyo just east of the Westwater Arroyo (Norwest 2009).

Well data from the GE and GL wells was compiled to estimate the potentiometric gradient between them (Figure 11) (Norwest 2009). A positive value indicates a gradient between the GL and GE wells. The data show that the gradient between wells GE and GL is relatively small (Norwest 2009).

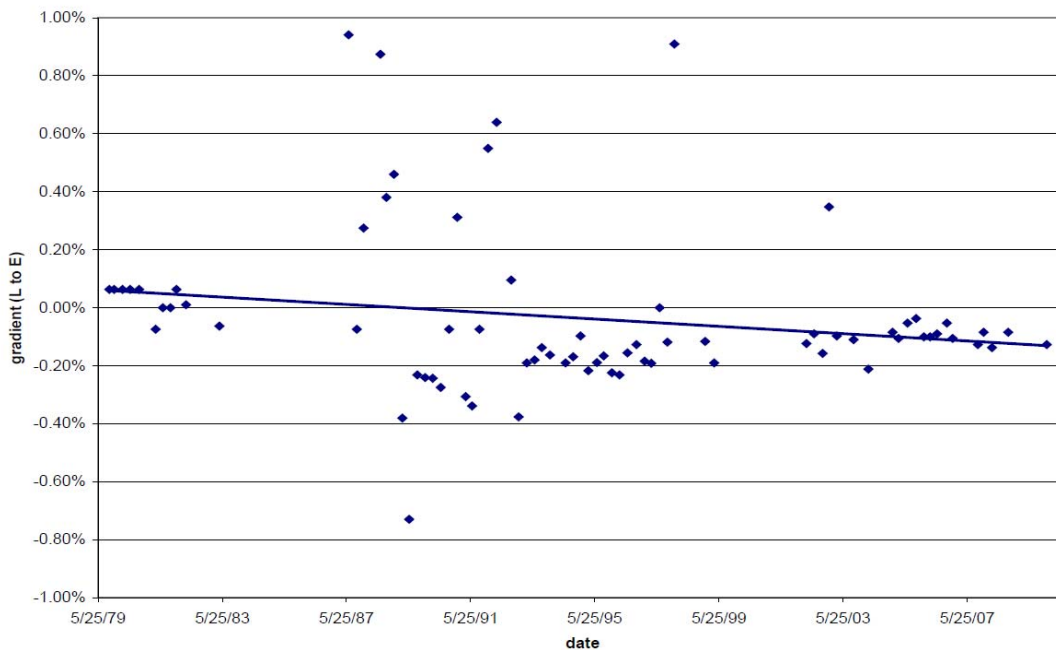


Figure 11. Measured potentiometric gradients between the GL and GE alluvial wells in the Shumway Arroyo (Norwest 2009)

As mentioned, G3 is one of the monitoring wells for the No 8 Coal Seam aquifer. The G3 well data was plotted to determine the draw down and recovery of mining in the Pinon Pit. Figure 12 shows initial drawdown followed by a slight recovery once mining was completed, most likely due to flow from near the highwall (Norwest 2009). It also shows an estimated original water elevation of 5325 ft and roughly where the water table is expected to return when site dewatering stops.

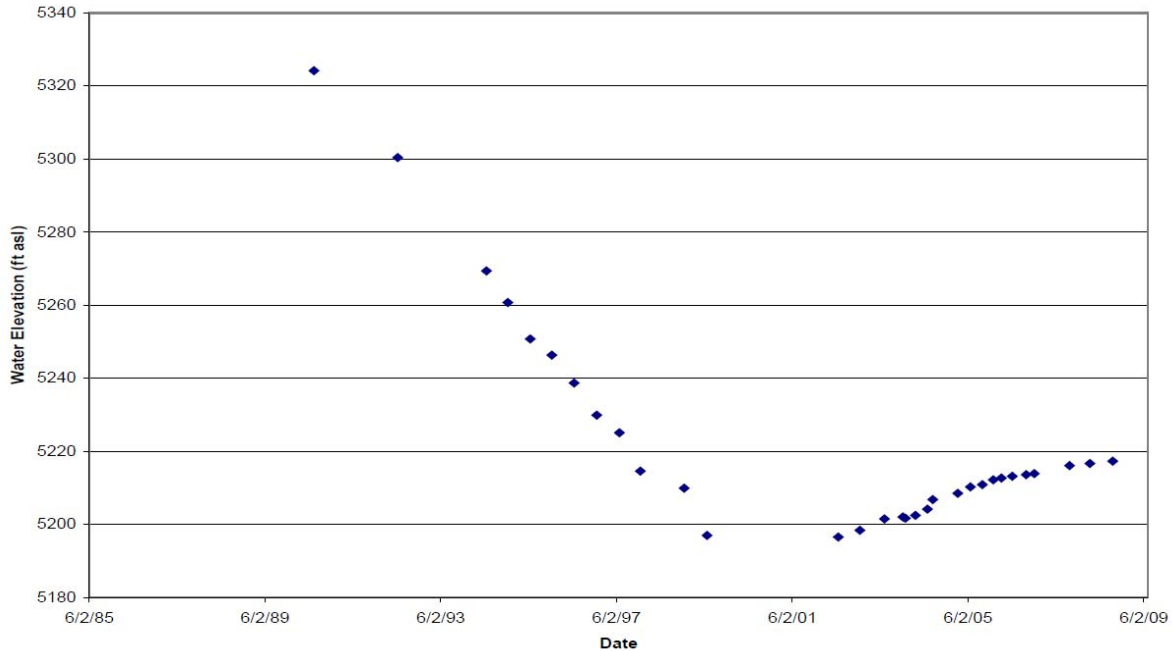


Figure 12. Potentiometric surface at No 8 Coal Seam monitoring well G3 from 1990 to 2009 (Norwest 2009)

Water from mine dewatering averaged 6.3 acre feet/month from 2006 to 2009. It is discharged to detention ponds and then combined with surface water and used for mine and power plant operations including reclamation, dust suppression, scrubbing of mine ventilation systems and cooling purposes. (Ginn, Perkins, and O’Hayre 2009).

The surface of the reclaimed mine is graded to achieve even sheet flow to detention ponds used to retain the water until it evaporates. Storm water that collects in the Juniper pit is stored in a retaining pond to evaporate. This was done to minimize infiltration and erosion potential (Ginn, Perkins, and O’Hayre 2009).

Two arroyos are located on the mine property, the Shumway and the Westwater arroyos. The arroyos have been relocated to divert flow around the pits to prevent water from entering the mine site (Norwest 2009). The Shumway and Westwater are referred to as the Shumway Diversion. Stormwater within the Shumway Diversion is characterized as a sodium-bicarbonate water. It exceeds NM drinking water standards for TDS and is therefore considered to be of poor water quality (Luther, Musslewhite, and Brown 2009).

The SJCM has estimated coal reserves for at least 25 more years at the current production rate so ground water pumping within the permitted area is likely to continue until 2036 to provide mine dewatering (Ginn, Perkins, and O’Hayre 2009),(Luther, Musslewhite, and Brown 2009). A study of ground water recharge found that recharge principally occurs through return of ground water from the No 8 Coal Seam and the Pictured Cliffs Sandstone, and by infiltration of ephemeral stream flow from the arroyos (Ginn, Perkins, and O’Hayre 2009).

1.1.3 Issues of Concern

The issues of concern associated with disposal of CCBs at the San Juan Coal Mine are principally associated with contamination of underlying ground water resources, not geotechnical stability of the buried waste. These include:

- What hazardous constituents are associated with CCBs and what is their potential for leaching from buried wastes?
- What are the geotechnical and hydraulic properties of the CCBs and how do they affect possible infiltration of ground water through the buried waste?
- What is the rate of infiltration through the disposed CCBs?
- Are geochemical processes occurring that affect leaching of contaminants from the wastes as well as their hydraulic properties that influence unsaturated and saturated flow of water through the wastes?

This project was designed and conducted to address these issues.

1.1.4 Project Objectives

The overall objective of this project was to determine what the potential for leachate from CCB disposal at the San Juan Mine is for contaminating underlying ground water. This was done by accomplishing the following tasks:

- Analyze and interpret existing data to facilitate understanding the geochemical environment at the SJCM
- Conduct leaching tests to characterize contaminant release from fresh and buried CCBs under saturated and unsaturated conditions.
- Measure the physical properties of soils and CCBs that govern the unsaturated flow of water through them
- Develop a one-dimensional unsaturated water flow model that can be used for estimating infiltration of water through disposed CCB materials.

1.1.5 Report Organization

This report has three separate sections that describe work done on this project. The first section describes laboratory work to measure the geotechnical properties of CCBs that are relevant to saturated and unsaturated flow of water through them. Measurements were made of the density, soil-moisture characteristics, and saturated hydraulic conductivity of the different components of the fresh and buried CCBs as well as of the soil used as overburden. This information was needed to estimate flow of water through the waste and used in development of a one-dimensional infiltration model.

The second section describes measurement of the geochemical characteristics of CCBs to determine their potential as a source term for contamination of underlying aquifers. Measurements of the chemical composition of the individual components of CCBs were done, as well as characterization of leachates from fresh and buried materials. Column experiments were conducted to measure leachate characteristics with time in an unsaturated environment. Instrumental analyses were conducted to determine the mineralogy of the CCBs and whether evidence of aging could be identified. The results are described in the context of potential impacts on underlying ground water quality.

The third section of the report describes development of a one-dimensional model of ground water flow through unsaturated spoil materials and CCB materials that are present at the SJM. A number of different scenarios representing stratification of disposed wastes, surface ponding of rain water, and alternative boundary conditions at the bottom of the pit were analyzed.

Part I – Geotechnical Properties of CCBs and Cover Materials at the San Juan Mine

2.1 - Introduction

The hydraulic properties of the CCBs will control the rate at which water moves through the buried material and potentially leaches contaminants. Because the disposal pit is above the regional water table, the unsaturated hydraulic properties (unsaturated hydraulic conductivity function and moisture characteristic curve) are of interest for each of the different buried materials.

A complication in understanding water movement through the buried waste is that the unsaturated hydraulic properties are likely a function of the depth of burial. As CCBs are disposed of in a landfill, effective stress increases with depth. As stress increases, particles will rearrange themselves into a higher density configuration with a corresponding decrease in porosity and void ratio. The manner in which a material's density changes in response to changes in stress is known as the material's compressibility. Changes in porosity can have a significant impact on both saturated and unsaturated hydraulic properties of a material (Lu and Likos, 2004) as flow through a porous material depends largely upon the size and distribution of pores within the material at any given time. Studies have found that for clay soils and silty soils, both saturated hydraulic conductivity and unsaturated hydraulic properties are impacted by compaction and variations in void ratio (e.g., Zeng et al., 2011; Richard et al., 2001).

The compressibility of fly ash and bottom ash materials was measured to develop a relationship between burial depth (i.e. over burden weight) and bulk density. Standard methods for measurement of unsaturated hydraulic properties were applied to fly ash and bottom ash materials compacted to different densities. Measurement of physical properties, including grain size distribution and specific gravity, are used to more completely characterize the tested materials.

2.2 - Previous Research

2.2.1 Compressibility of CCBs

Previous research concerning the compressibility of CCBs is focused largely upon using ash materials to produce hydraulic barriers for use as landfill covers and liners. This application was pursued because the majority of CCBs are fine grained particles that can be used to produce low permeability materials. Such studies have used standard and modified proctor tests to determine theoretical maximum dry densities at optimum water contents and have often used various admixtures along with the CCBs (e.g., Campbell et al., 1983; Martin et al., 1990; Prashanth et al., 1998; Prashanth et al., 2001; Kumar and Stewart, 2003).

Results from these studies indicate maximum dry densities for fly ash typically range from 980 to 1280 kg/m³ with a few of the results reaching as high as 1880 kg/m³ (Campbell et al., 1983; Martin et al., 1990; Prashanth et al., 1998; Prashanth et al., 2001). Bottom ash results show a range of maximum densities from 1050 to 1670 kg/m³ (Martin et al., 1990; Kumar and Stewart, 2003). Optimum gravimetric water contents for these proctor densities were reported from a range of 25 to 33% with one bottom ash having an optimum moisture content of 15% (Kumar and Stewart, 2003).

Admixtures such as bentonite and lime are sometimes added to the fly ash and bottom ash. Bentonite has characteristically low hydraulic conductivity, which is beneficial for hydraulic barriers, but it tends to crack as it dries. Fly ash and bentonite mixtures are an attempt to reduce the cracking behavior of bentonite liners. Lime is often mixed with fly ash in order to create a liner in which particles chemically react and form a weak concrete over time. Combinations of fly ash and bottom ash with bentonite or lime have been shown to create low permeable materials on the order of 10⁻⁷ cm/s or less. (Campbell et al., 1983; Martin et al., 1990; Prashanth et al., 1998; Prashanth et al., 2001; Kumar and Stewart, 2003).

Edil and Berthouex (cited by Palmer et al., 2000) found that for fly ash without any admixtures, increasing the water content and compactive effort increased the dry unit weight. Sivapullaiah and Lakshmikantha (2004) investigated the relative deformation vs. pressure of fly ash and produced similar results. Seals (1972) found bottom ash to have compressibility characteristics similar to that of sand. Because CCBs are subjected to a range of stresses corresponding to their depth of burial, it is important to determine the compressibility of CCBs.

2.2.2 Saturated Hydraulic Conductivity of CCBs

There have been some measurements of the saturated hydraulic conductivity of CCBs principally to support investigations of the use of fly ash and bottom ash in the construction of landfill covers and liners. These studies often use a single dry unit weight for testing, usually the theoretical maximum, and often incorporate various admixtures such as lime or bentonite (Campbell et al., 1983; Joshi et al., 1994; Prashanth et al., 2001; Kumar and Stewart, 2003; Mudd et al., 2000). Hydraulic conductivities ranging from 10⁻⁷ to 10⁻³ cm/s have been measured in pure fly ash samples (Campbell et al., 1983; Joshi et al., 1994; Prashanth et al., 2001).

Sivapullaiah and Lakshmikantha (2004) showed a change in hydraulic conductivity with a change in void ratio for fly ash. In this study, the range in void ratio was 1.12 to 1.15, which is near the maximum density, and hydraulic conductivities were on the order of 10^{-7} cm/s. Edil and Berthouex (cited by Palmer et al., 2000) found that increasing the water content and compactive effort not only increases the dry unit weight, it also decreases the saturated hydraulic conductivity. These studies cover only a narrow range of dry unit weights near the theoretical maximum for fly ash. Seals (1972) found the hydraulic conductivity of bottom ash samples to be similar to sand (10^{-2} cm/s) when the void ratio was approximately 50% of maximum relative density. No conductivity measurements were performed at other densities or void ratios. FGD gypsum has been shown, in one study, to have a low hydraulic conductivity (values were not reported) when compacted (Rudisell et al., 2001).

Saturated hydraulic conductivity of clay materials steadily decreases as the void ratio decreases (e.g., Zeng et al., 2011). Because CCBs in landfills experience various degree of compaction depending of burial depth and weight of overburden materials it is important to determine how the hydraulic conductivity changes increasing in dry bulk density.

2.2.3 Unsaturated Hydraulic Properties of CCBs

There has been limited research regarding the unsaturated hydraulic properties of CCBs. Truman et al. (2010) found that amending soils with amounts of FGD gypsum can increase water retention. Pathan et al. (2003) conducted research investigating the use of fly ashes to amend soils to increase plant available water, assuming the fine particle sizes of fly ash will assist in the retention of water. The water retention characteristics, however, were of samples at a single density not necessarily representative of any particular field conditions, aiming only to be indicative of relative differences between ash samples. Results showed that all fly ashes used retain more water than the sandy soils investigated. Mudd et al. (2007) studied numerous ash and soil samples for various geotechnical properties, including water retention characteristics. The 23 ash samples collected ranged from fly ash to bottom ash. Air entry pressures ranged from approximately -1 kPa (-10 cm of water) for bottom ash to -100 kPa (-1000 cm of water) for fly ash. Each sample was tested only at its proctor maximum dry density. In another study conducted by Chakrabarti et al. (2005), unsaturated properties of ash were incorporated into a water balance model to predict leaching behaviors. This study concluded that a thorough understanding of the unsaturated moisture characteristics of coal ash is essential to accurately predict moisture behavior in disposal sites.

Although there is no direct data regarding the change of unsaturated hydraulic properties of CCBs as a result of compaction, testing on other soils has shown that changes in porosity due to compaction have an impact on their unsaturated hydraulic properties (e.g., Richard et al., 2001; Assouline et al., 1997; Hill & Sumner, 1967). Therefore, it is expected that as the dry density of CCBs increase, the unsaturated hydraulic properties will vary. These variations may be vital in understanding the flow of water through CCB disposal cells.

CCBs can vary significantly depending upon the source coal and collection method. Disposal methods in landfill sites create a profile of varying overburden pressures and a potential range of hydraulic properties. Proper knowledge of the manner in which these properties vary with depth

in a landfill pit knowledge of the relationship between their hydraulic characteristics and compacted density is essential in analyzing leachate flow through buried CCBs.

2.3 - Research Methods

2.3.1 Source of Samples

The majority of fly and bottom ash samples for this study were received from the San Juan Generating Station in northwestern New Mexico. These samples were taken directly from the collection units (i.e. electrostatic precipitators, bottom of the furnace, or scrubber system) prior to transport to the landfill site, and are subsequently referred to as fresh samples. The samples were received by mail in June of 2011 and were contained in plastic bags specific to each of the 4 burning units. Approximately 10 kg were received for each unit. All samples used for this study were taken from Unit 4.

In addition to the fresh samples, geo-probe samples were also collected in the summer of 2010 in order to obtain the physical and hydraulic properties of in situ soils at the SJM (Chan, 2010). Also, in the Spring of 2011, observation wells were being installed at the SJM using a sonic drilling rig and samples were collected at a range of depths for analysis (Parker, 2011).

2.3.2 Physical Properties

Grain size distributions were determined for a sample mass of approximately 100 g of oven-dry fly ash and approximately a 230 g sample of oven-dry bottom ash following the methods of ASTM D422 (2007). The sample materials were washed through a #200 sieve, and a hydrometer test was conducted for the material passing through and a sieve analysis conducted for the retained material.

Specific gravity testing was conducted following the methods described by ASTM D854 (2009). Three tests were conducted on fly ash and three tests on bottom ash.

Relative density tests, as described by the Department of the Army Office of the Chief of Engineers (1970), were also conducted on one oven-dry sample of fly ash and one oven-dry sample of bottom ash using a 15 cm diameter proctor mold.

In-situ samples were collected by means of a geo-probe to determine field conditions present at the SJM. Moisture contents were determined gravimetrically according to procedures described in ASTM D-2216 (2010) and densities by ASTM D-7263 (2009), method B. The known volume from the density tests and mass of water from moisture content were then used to produce volumetric water contents.

Clod density tests were performed with methods similar to ASTM D-7263 (2009) method B. Copper rings measuring approximately 16 mm in diameter and 29 mm in length were sharpened on one end and inserted into the clods to collect samples of a known volume. Excess material was removed with a razorblade from either end of the rings to ensure the soil was level with the edges of the ring. Only two clods were large enough to be tested. Two samples were collected from one clod and one sample from the other.

2.3.3 Compressibility

Compressibility curves were developed for 4 samples of fly ash and 4 samples of bottom ash. Tests imposed one-dimensional loading on samples at gravimetric moisture contents consistent with field conditions at the SJM. The average moisture content of CCBs recovered from SJM disposal pits was determined to be 20% (Chan, 2010). Samples were contained in brass rings on top of a porous stone. The ring diameter was 60 mm with a height of 25 mm; samples filled the ring to a height of 22 mm. Each sample's initial dry density was the minimum dry density determined by relative density tests. Samples were compacted in a series of 4 lifts on top of the porous stone. Marks were made on the inside of the sample rings as well as on the tamper to ensure the sample was compacted to the proper height.

A series of 10 loadings, using a consolidometer, ranging from 50 to 1000 kPa were applied to prepared samples. The applied loads were approximately (in kPa): 50, 100, 165, 230, 330, 410, 555, 655, 885, and 985. Loads were selected on a basis of weights available in a manner to gradually increase pressure differences between loading increments. Dial gages with 0.025 mm precision were zeroed before the first applied load and used to measure changes in sample height for each loading cycle. Loads were applied for a period of one hour, after which a measurement was taken recording the change in height for each sample. It was observed that, for these particular materials, most of the volume change occurred in the first 15-30 minutes; there were no measurable sample height changes that occurred following 1 hour of load being applied.

2.3.4 Saturated Hydraulic Conductivity

Fly and bottom ash samples were tested for the coefficient of saturated hydraulic conductivity (K_{sat}) in accordance to ASTM D5856 (2007), method B (constant tail water). Porous stones were used on the bottom and top of each sample within a rigid-walled permeameter. Each compacted sample measured 76 mm in diameter and 25 mm in height. University of New Mexico tap water was used as the permeant liquid. Saturation of samples was accomplished by allowing constant flow of water through the compacted sample for at least 16 hours. Hydraulic gradients across each sample ranged from 4 to 25.

Fly ash and bottom ash samples were tested at three different dry densities. Two compacted samples at each dry density were tested.

2.3.5 Moisture Characteristic Curve (MCC) Measurements

Moisture characteristic curves during desorption were developed for three dry densities for both fly and bottom ash samples. The procedures used to measure soil MCCs consisted of hanging column tests similar to those described in ASTM D6836 (2008), pressure plate tests (Klute, 1986) for relative humidity box measurements, and Decagon Devices (2010) for chilled mirror hygrometer measurements.

For the hanging column and pressure plate tests, three samples at each of the three specified dry densities were prepared and tested for both fly and bottom ash, producing a total of 18 samples tested (9 fly ash and 9 bottom ash). Each sample was compacted to a target dry density so as to completely fill a brass ring of 60 mm diameter and 25 mm height. Synthetic nylon screening with openings measuring 25 microns were attached to the top and bottom of each sample ring by

a hose clamp to contain the sample while allowing free movement of water. Each sample was saturated in de-aired de-ionized water with a vacuum of 80 kPa for at least 24 hours.

Saturated samples were placed directly into saturated Buchner funnels connected to reservoirs/burettes by flexible tubing. The Buchner funnels were saturated in de-aired de-ionized water with a vacuum of 80 kPa for at least 24 hours. A thin layer of a diatomaceous earth was spread on each porous plate to improve the hydraulic contact with the sample. Negative pressures were then introduced to each of the samples by raising the Buchner funnel and/or lowering the reservoir/burette. Samples were allowed to equilibrate at 6 different pressure heads ranging from -5 cm to -160 cm of water, at which point the mass of each sample was taken to the nearest 0.01 g and subsequently used to determine volumetric water content. Equilibration at each pressure, determined by water ceasing to move from the sample to the burette for at least 24 hours, took 6 to 7 days for most samples.

After the final measurement in the hanging column, the samples were moved to the pressure plate apparatus. The porous plate was saturated in de-aired de-ionized water for a period of at least 24 hours with a vacuum of 80 kPa. A thin layer of a diatomaceous earth was spread on the plate to improve the hydraulic contact with the sample. The pressure plate test was used to produce pressure heads of -510 and -1275 cm of water. Pressures were introduced by sealing the samples on a porous plate in a pressure chamber and applying gas pressure to the chamber using compressed nitrogen gas. The porous plate has an outflow tube to a reservoir at atmospheric pressure at the bottom of each sample. Readings were taken from the pressure plate test by allowing the samples to equilibrate for 14 days at each pressure at which point the samples would be removed and masses measured to the nearest 0.01 g in order to determine the volumetric water content.

A chilled mirror hygrometer was used to collect data for the MCC at pressure heads ranging from -7,600 cm to -15,000 cm of water. A WP4 dew point potentiometer from Decagon Devices, Inc. was used as the testing apparatus. It was determined that, for values of pressure head less than -7,600 cm of water for bottom ash and -9,900 cm of water for fly ash, the WP4 readings were outside the range of accuracy (Decagon Devices, Inc., 2010). Five readings were taken for fly ash and 3 for bottom ash. Large amounts of ash (~200 g) were brought to target moisture contents and at least 25 g of moist sample was placed in a stainless steel WP4 sample cup. Plastic lids were used to seal the cups and allow samples to equilibrate for at least 16 hours. Following equilibration, water potential was read immediately upon removing the lid from the sample cup. The samples were then weighed immediately following the potential reading and removal from the WP4 apparatus. A drying oven was used for at least 16 hours to dry the samples. Once dry, samples were allowed to cool in a desiccator for 10 to 15 minutes and masses were measured to calculate the moisture content of each sample. Gravimetric water contents and water potentials were converted to volumetric water contents and pressure heads, respectively, for each specified density.

A relative humidity box was used to measure 2 final readings for the MCC. Saturated solutions of NaCl and LiCl were used to achieve negative pressure head equivalents of -4×10^5 cm and -3×10^6 cm of water, respectively (Lu and Likos, 2004). The saturated solutions were placed in the bottom of a desiccator. Fly and bottom ash samples (~10 g) were then placed directly above the

salt solution atop a plastic grate and allowed 7 days for equilibration, after which masses were measured and converted to volumetric water contents.

2.4 - Results & Discussion

2.4.1 Physical Properties

Grain size distribution curves for fly ash and bottom ash are shown in Figure 13. Grain size distribution for fly ash and bottom ash. Figure 13. Grain size distributions tests determined that 85.4% of fly ash material is finer than a #200 sieve (0.075 mm diameter) and bottom ash was 22.3% finer (Table 1). The average specific gravity measurements are also reported in Table 1. Fly ash was found to have an average specific gravity of 2.00 and bottom ash had 2.06 by these methods.

Relative density testing found that oven-dry fly ash had a loose dry density of 1007.4 kg/m³ and a maximum dry density of 1184.4 kg/m³. Oven-dry bottom ash had a loose dry density of 692.2 kg/m³ and a maximum dry density of 813.8 kg/m³ (Table 1).

Table 1 Summary of physical properties of selected materials.

Property	Fly Ash	Bottom Ash
% finer #200 sieve (0.075 mm)	85.4	22.3
% larger #200 sieve (0.075 mm)	14.6	77.7
Minimum Relative Density (kg/m ³)	1007.4	692.2
Maximum Relative Density (kg/m ³)	1184.4	813.8
Average Specific Gravity	2.00	2.06

Results of the geo-probe investigation by Chan (2010) are given in Table 2. These results, including samples from three different locations, show the average gravimetric moisture content of the soil to be 19%.

Clod density tests performed on clods collected from sonic drill samples at a depth of 42 m below the ground surface show an average dry density at this depth and location to be 1028.8 kg/m³ (Table 3). This material was determined to be bottom ash through a separate study (Parker, 2011).

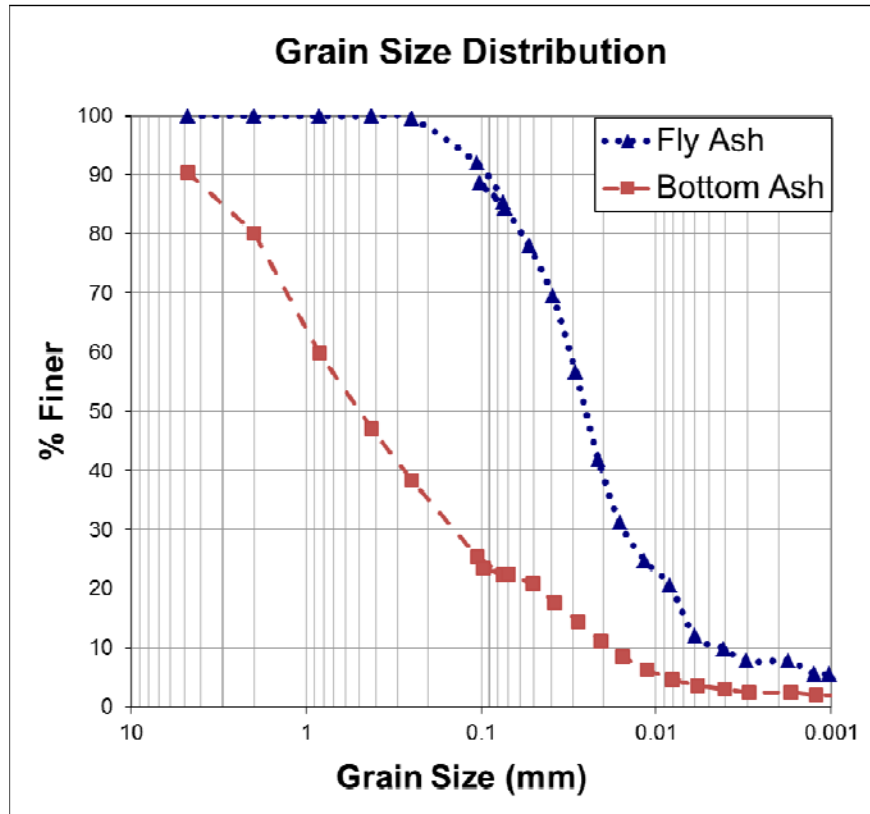


Figure 13. Grain size distribution for fly ash and bottom ash.

Table 2. Water contents measured in Geo-Probe samples.

Sample	Gravimetric Water Content	Volumetric Water Content	Depth of Sample (m)	Comments
1	24%	25%	4.2	Traces of ash (Yucca Ramp 1)
2	20%	18%	7.0	Traces of ash (Yucca Ramp 1)
3	22%	21%	6.7	Traces of ash (West Yucca Pit)
4	12%	18%	2.7	Layered core w/ clay (Juniper Pit)
5	19%	31%	4.9	Layered mostly clay (Juniper Pit)
6	19%	31%	9.4	Layered mostly clay (Juniper Pit)
Average	19%	24%		Top-soils not included

Table 3. Clod density results of sample from Juniper Pit 04 at 42 m depth.

	Volume (cm ³)	Dry Sample Mass (g)	Dry Density (kg/m ³)
Ring 1	561.9	5.69	1012.66
Ring 2	564.1	6.06	1074.21
Ring 3	566.3	5.66	999.43
		Average:	1028.76

2.4.2 Compressibility

Results of the compressibility tests and curve fitting parameters are summarized in Table 4 and presented graphically in Figure 14. It is important to note the differences in the scale of the vertical axes for fly ash (top graph) and bottom ash (lower graph). Fly ash and bottom ash samples experienced maximum changes in height ranging from 2.2 to 3.4 mm and 5.1 to 6.1 mm, respectively. These values represent a 10.0 to 15.3% and 23.0 to 27.5% change in sample height for fly ash and bottom ash, respectively. All samples experienced the largest deformation occurring at a pressure of 985 kPa. The maximum dry densities occurring under this pressure ranged from 1119.5 to 1189.0 kg/m³ for fly ash and 898.2 to 954.8 kg/m³ for bottom ash.

The compressibility data was fit to the following empirical equation:

$$\rho = r(1 - n^{-s} \sigma_v) + \rho_1 \quad (1)$$

Where:

- ρ = bulk density (kg/m³)
- r = total range of densities for curve (kg/m³)
- n = steepness of the curve (dimensionless)
- s = sharpness of curvature (kPa⁻¹)
- σ_v = overburden pressure (kPa)
- ρ_1 = Initial dry density of the material (kg/m³)

Table 4. Summary of compressibility measurements and parameters for Eq. 1.

Sample	Initial ρ_d (kg/m ³)	Total ΔH (mm)	Final ρ (kg/m ³)	r (kg/m ³)	n	s (kPa ⁻¹ x10 ⁻⁴)	R^2
Fly Ash A	1006.9	3.4	1189.0	193	3200	3.1	0.980
Fly Ash B	1006.9	2.2	1119.5	123	1580	2.9	0.974
Fly Ash C	1006.9	3.1	1168.5	173	700	3.5	0.974
Fly Ash D	1006.9	2.5	1136.9	141	500	3.4	0.979
Bottom Ash E	691.8	5.5	920.0	258	400	4.0	0.989
Bottom Ash F	691.8	5.1	898.2	236	1000	3.0	0.993
Bottom Ash G	691.8	6.1	954.8	283	800	4.0	0.981
Bottom Ash H	691.8	6.0	945.9	284	5000	2.8	0.981

The correlation coefficient (R^2) values for curves fit to the data using equation (1) range from 0.97 to 0.99. Selection of the equation was based upon the asymptotic approach towards a theoretical maximum dry density ($r-\rho_1$) and a predetermined vertical axis intercept for the loose dry density (ρ_1). The n and s parameters fit the curve to the data. A summary of the parameters used to fit equation (1) is given in Table 4.

Three selected dry densities to further test hydraulic properties are represented by the horizontal dashed lines in Figure 14. For fly ash, the selected values of dry density (in kg/m³) are 1028.4, 1113.3, and 1169.3. For bottom ash, the selected dry densities (in kg/m³) are 727.2, 800.9, and 913.1. The lowest density was chosen specifically to be near the initial uncompacted density but slightly greater than the minimum value since it is the minimum is not likely to be found in a disposal cell due to compaction occurring during waste emplacement. The highest density was selected to be near the higher end of the density curves. The third density to be tested was arbitrarily chosen in between the selected maximum and minimum dry densities to be tested.

2.4.3 Saturated Hydraulic Conductivity

Results measurements of saturated hydraulic conductivity (K_{sat}) by the falling head permeability method are presented in Table 5. Fly ash samples yielded K_{sat} values on the order of 10^{-4} to 10^{-5} cm/s while bottom ash samples K_{sat} values were on the order of 10^{-3} cm/s. The highest K_{sat} values measured were 1.3×10^{-4} cm/s and 6.5×10^{-3} cm/s for fly ash and bottom ash, respectively. These values were achieved at dry density values of 1024.0 kg/m³ for fly ash and 724.4 kg/m³ for bottom ash, which were the lowest dry density values that were tested for each material. The lowest K_{sat} values measured were 5.5×10^{-5} cm/s for fly ash and 1.5×10^{-3} cm/s for bottom ash. These values were measured at the highest densities tested for both fly ash (1163.0 kg/m³) and bottom ash (910.4 kg/m³). Graphical representation of K_{sat} vs. dry density is shown in Figure 15. Trend lines were fit to the data displaying an R^2 value of 0.61 for fly ash and 0.27 for bottom ash.

Table 5. Saturated hydraulic conductivity measurements.

Material	Target Dry Density (kg/m ³)	Actual Dry Density (kg/m ³)	Sample 1 K_{SAT} (cm/s)	Sample 2 K_{SAT} (cm/s)
Fly Ash	1028.4	1024.0	7.81E-05	1.30E-04
Fly Ash	1113.3	1108.2	6.62E-05	8.10E-05
Fly Ash	1169.3	1163.0	5.45E-05	5.96E-05
Bottom Ash	727.2	724.4	3.53E-03	6.45E-03
Bottom Ash	800.9	796.9	2.27E-03	6.26E-03
Bottom Ash	913.1	910.4	1.48E-03	3.90E-03

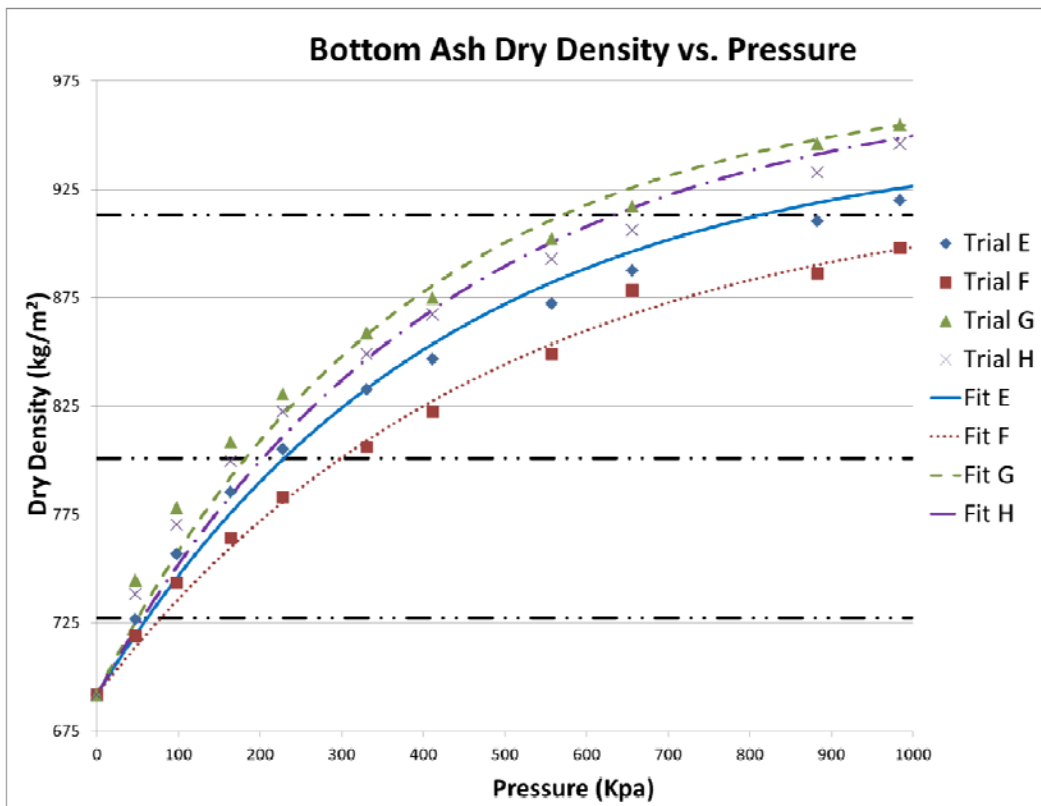
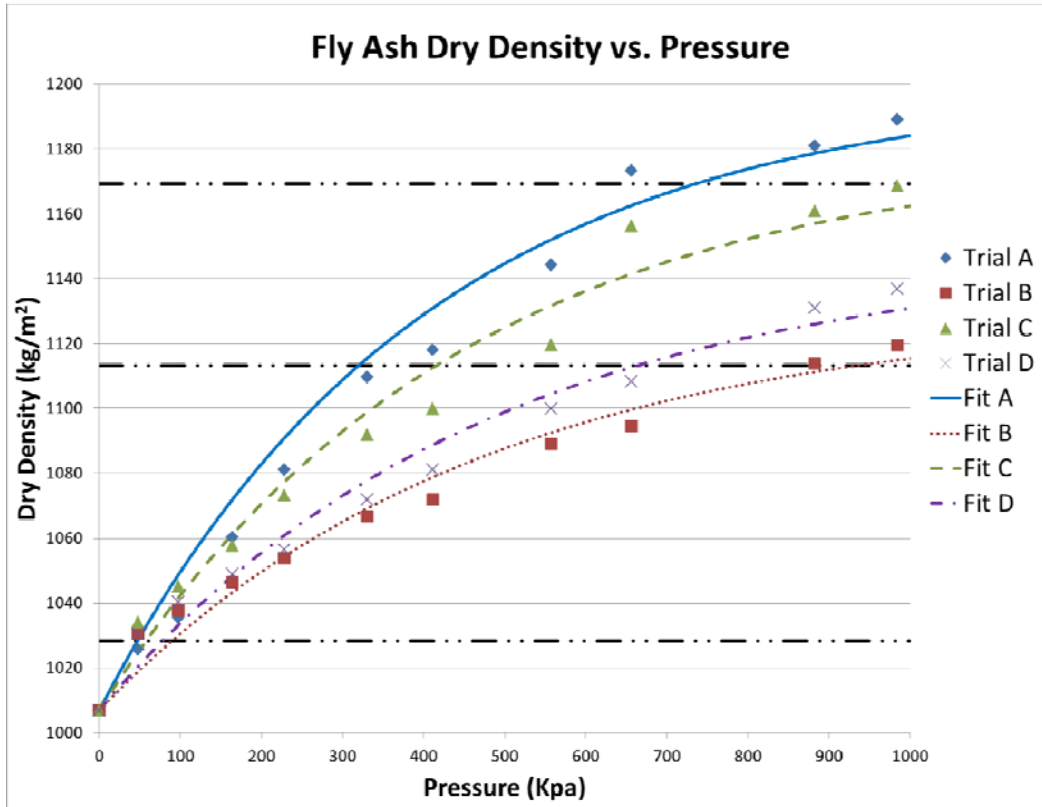


Figure 14. Compressibility data with fitted curves for fly ash and bottom ash.

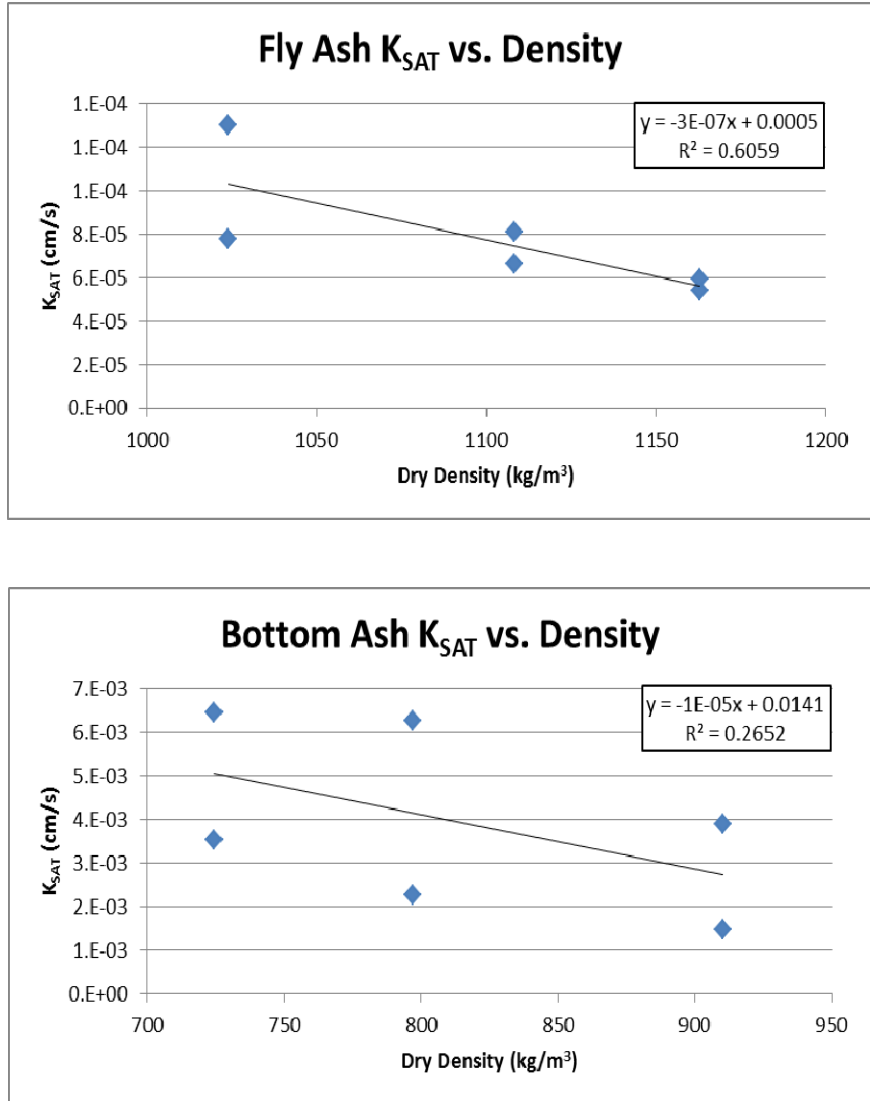


Figure 15. Plot of saturated hydraulic conductivity (K_{sat}) vs. dry density.

2.4.4 Moisture Characteristic Curves

Measured data points were fit to the van Genuchten model for the MCC, which is given as (van Genuchten et al., 1991):

$$\theta = \theta_r + (\theta_s - \theta_r) (1 + (\alpha h)^n)^{-m} \quad (2)$$

Where:

- θ = volumetric moisture content (dimensionless [L^3/L^3])
- θ_r = retained volumetric moisture content (dimensionless [L^3/L^3])
- θ_s = saturated volumetric moisture content (dimensionless [L^3/L^3])
- α = curve fitting parameter representing the inverse of air-entry suction (1/L)
- h = negative pressure head (L)
- n = curve fitting parameter (dimensionless)
- $m = 1 - 1/n$ (dimensionless)

The Retention Curve (RET) Program for Unsaturated Soils (van Genuchten et al., 1991) was used to fit the data to the van Genuchten model for MCCs. The model can be adjusted to observed data points by altering the weight of each measured value. Weighted values for this study were chosen in a manner such that all weighted values for a particular testing method are the same. Weighted values were altered, based upon accuracy of testing method for each data point, within the RETC program until an acceptable curve was observed through the data points. Weighted values ranged between one and three in increments of 0.5.

Once MCCs had been produced for each individual sample of CCBs, MCCs were created using RETC to be representative of each target dry density of material. This was done by including all of the data from the 3 samples at each respective dry density to create a single MCC for that dry density. The input data for RETC used the same calibrated weights for each data point as determined by MCC curve creation for individual samples.

2.4.5 Moisture Characteristic Curve Comparisons

Van Genuchten model parameters obtained using RETC are presented in Table 6. Graphical representation of the MCCs for the materials at their respective target densities are shown in Figure 16 through Figure 21. MCCs were then plotted as saturation instead of volumetric water content for comparison purposes. Saturation values (S) were calculated as follows:

$$S = \frac{\theta}{\theta_s} \quad (3)$$

Best fit MCCs for each target dry density are displayed graphically in Figure 22, and the parameters summarized in Table 7. Each best fit curve uses the data from all three samples of the same target dry density. The three fly ash best fit curves are displayed on the same graph to compare differences between dry densities; the same is done with bottom ash.

Van Genuchten model parameters are plotted vs. dry densities in Figure 23. Linear trend lines have been fitted with the data for θ_s , α , and n values. Fly ash shows a strong linear trend, with R^2 values of .59 and .94 for θ_s and α , respectively, where bottom ash does not, with R^2 values of .17 and .38 for θ_s and α , respectively. Values of n show low R^2 values for both fly ash and bottom ash, the values are 0.1 and 0.27, respectively.

Table 6. Van Genuchten model parameters for fly ash (FA) and bottom ash (BA) samples.

Sample	Target Dry Density (kg/m ³)	Actual Dry Density (kg/m ³)	θ_r (cm ³ /cm ³)	θ_s (cm ³ /cm ³)	α (1/cm)	n
FA A	1028.4	1030.83	0.00	0.52	4.0E-03	1.59
FA B	1028.4	1033.12	0.00	0.57	3.9E-03	1.64
FA C	1028.4	1034.74	0.02	0.56	3.7E-03	1.97
FA D	1113.3	1,113.3	0.00	0.51	2.4E-03	1.66
FA E	1113.3	1,113.3	0.00	0.49	2.4E-03	1.67
FA F	1113.3	1,118.8	0.00	0.57	2.8E-03	1.60
FA G	1169.3	1172.19	0.00	0.47	1.3E-03	1.80
FA H	1169.3	1173.41	0.00	0.46	7.3E-04	1.99
FA I	1169.3	1,175.2	0.00	0.49	1.4E-03	1.77
BA A	727.2	729.21	0.00	0.51	2.6E-02	1.51
BA B	727.2	726.52	0.00	0.58	4.6E-02	1.45
BA C	727.2	724.22	0.00	0.60	5.6E-02	1.44
BA D	800.9	795.18	0.00	0.66	5.4E-02	1.47
BA E	800.9	797.06	0.00	0.68	3.4E-02	1.61
BA F	800.9	798.68	0.00	0.64	4.6E-02	1.50
BA G	913.1	912.26	0.00	0.69	3.4E-02	1.51
BA H	913.1	913.47	0.00	0.60	2.4E-02	1.54
BA I	913.1	916.85	0.00	0.60	1.8E-02	1.57

Table 7. Van Genuchten model parameters for best fit curves at each dry density.

Material	Target Dry Density (kg/m ³)	θ_r (cm ³ /cm ³)	θ_s (cm ³ /cm ³)	α (1/cm)	n
Fly Ash	1028.4	0.003	0.55	3.9E-03	1.68
Fly Ash	1113.3	0.00	0.52	2.4E-03	1.66
Fly Ash	1169.3	0.00	0.47	1.1E-03	1.85
Bottom Ash	727.2	0.00	0.56	4.1E-02	1.46
Bottom Ash	800.9	0.00	0.66	4.3E-02	1.52
Bottom Ash	913.1	0.00	0.63	2.5E-02	1.54

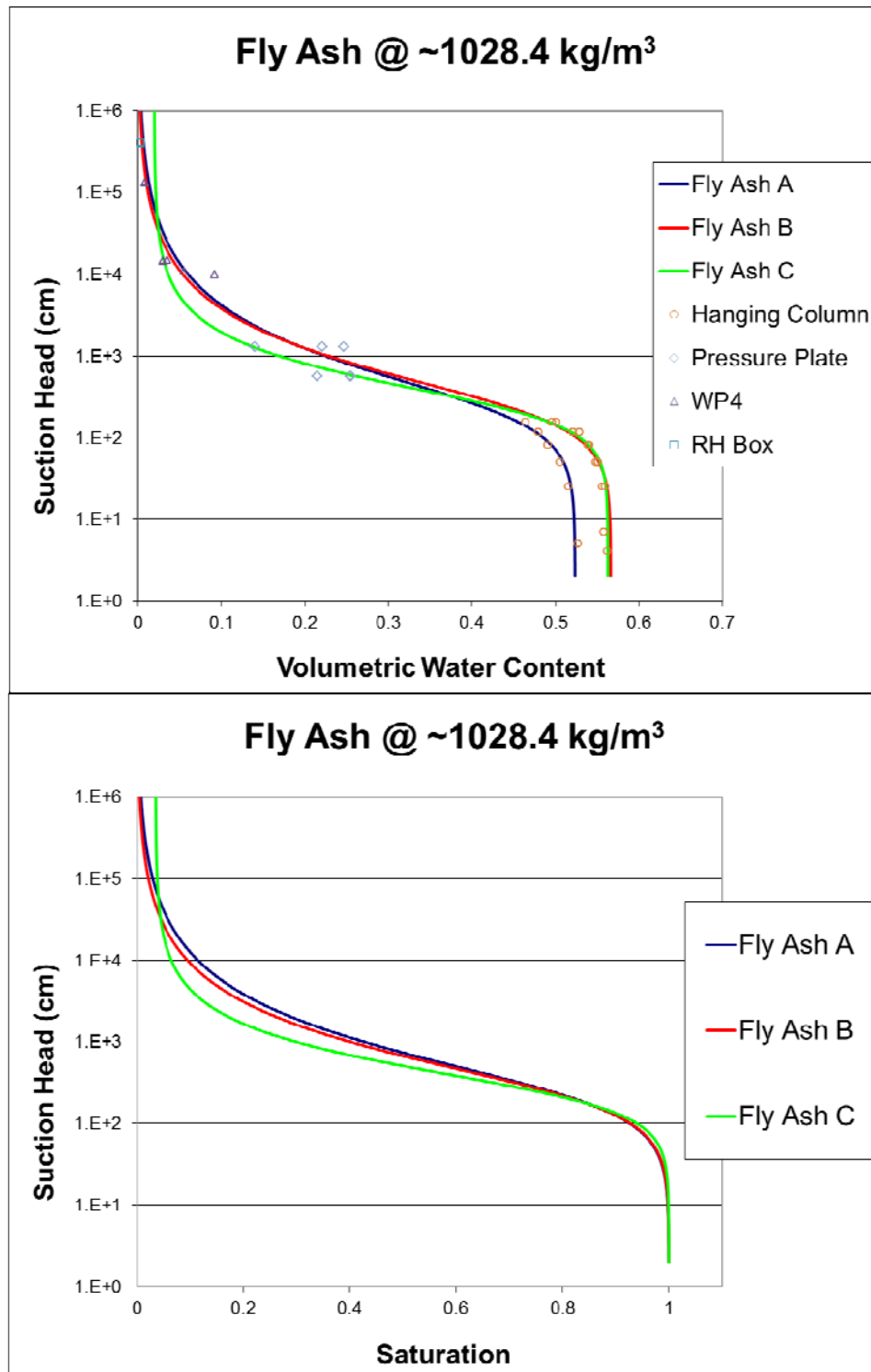


Figure 16. Fitted data (top) and saturation moisture characteristic curves (bottom) for fly ash at lowest dry density.

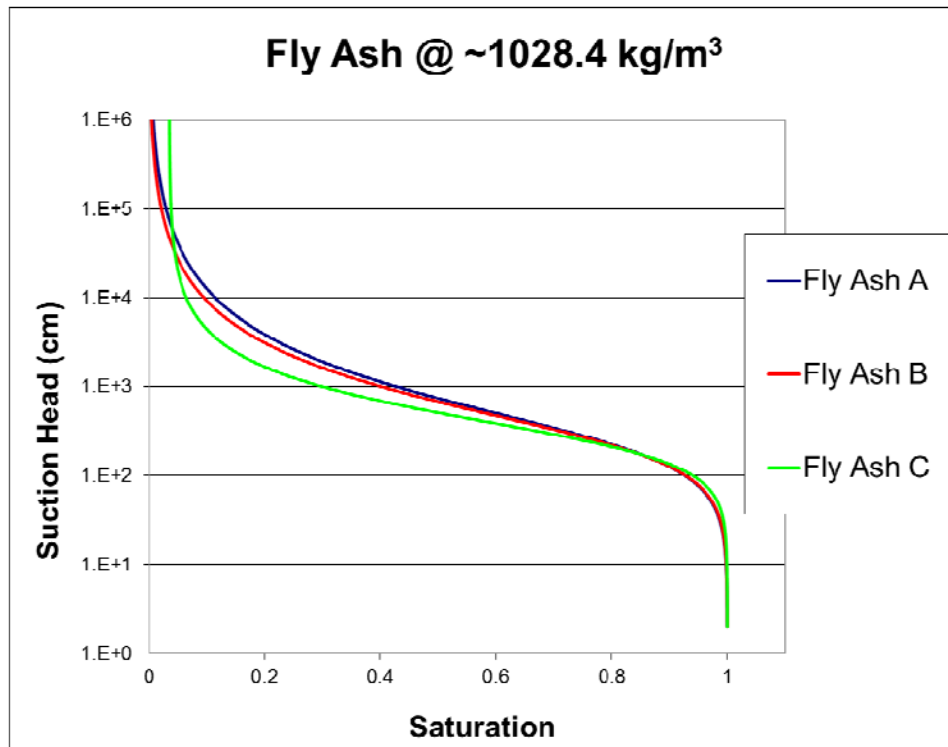
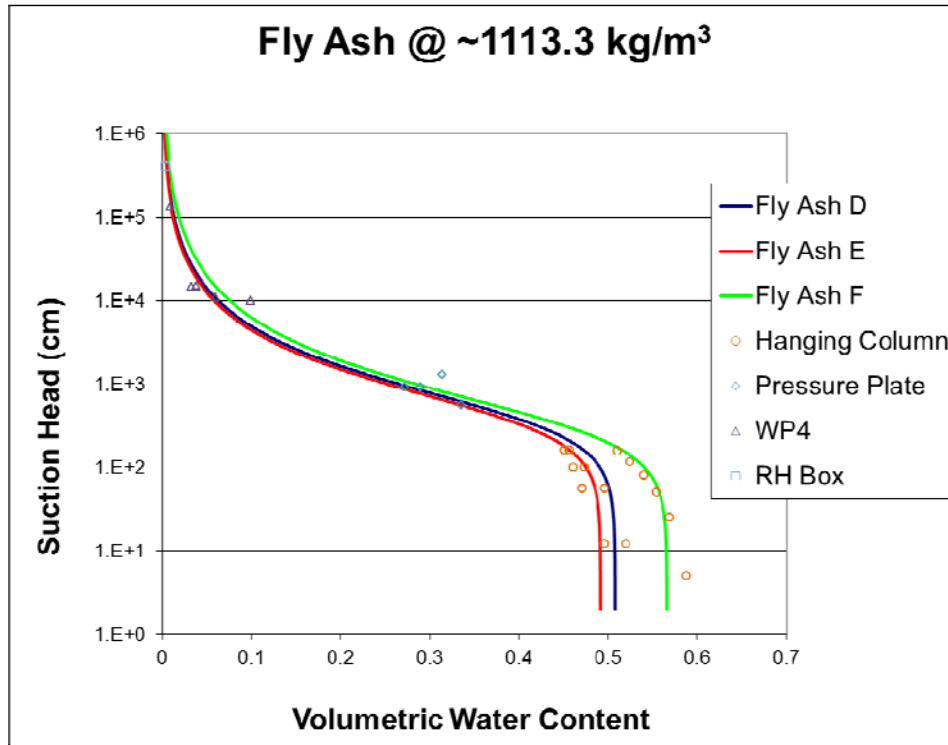


Figure 17. Fitted data (top) and saturation moisture characteristic curves (bottom) for fly ash at intermediate dry density.

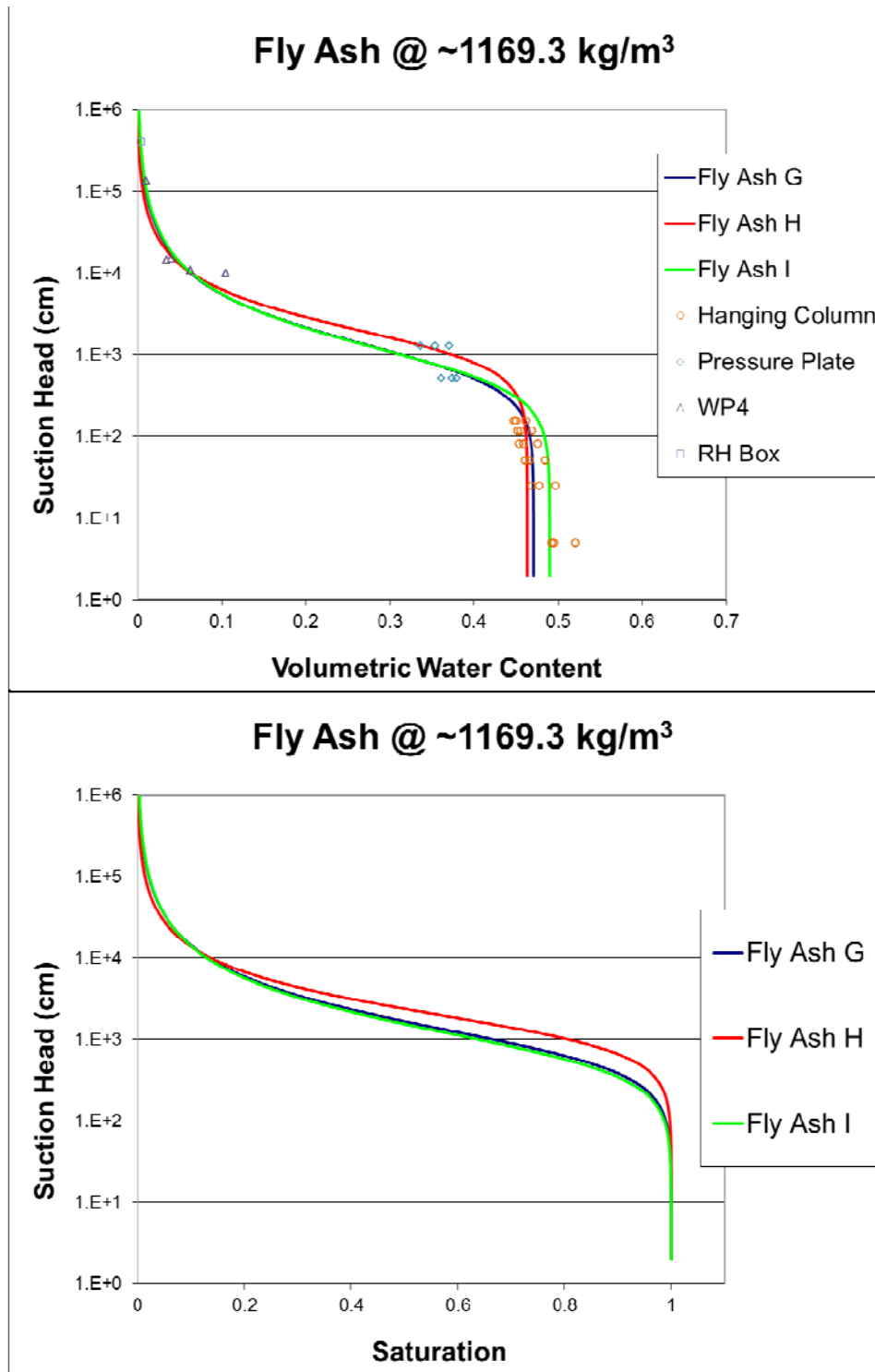


Figure 18. Fitted data (top) and saturation moisture characteristic curves (bottom) for fly ash at greatest dry density.

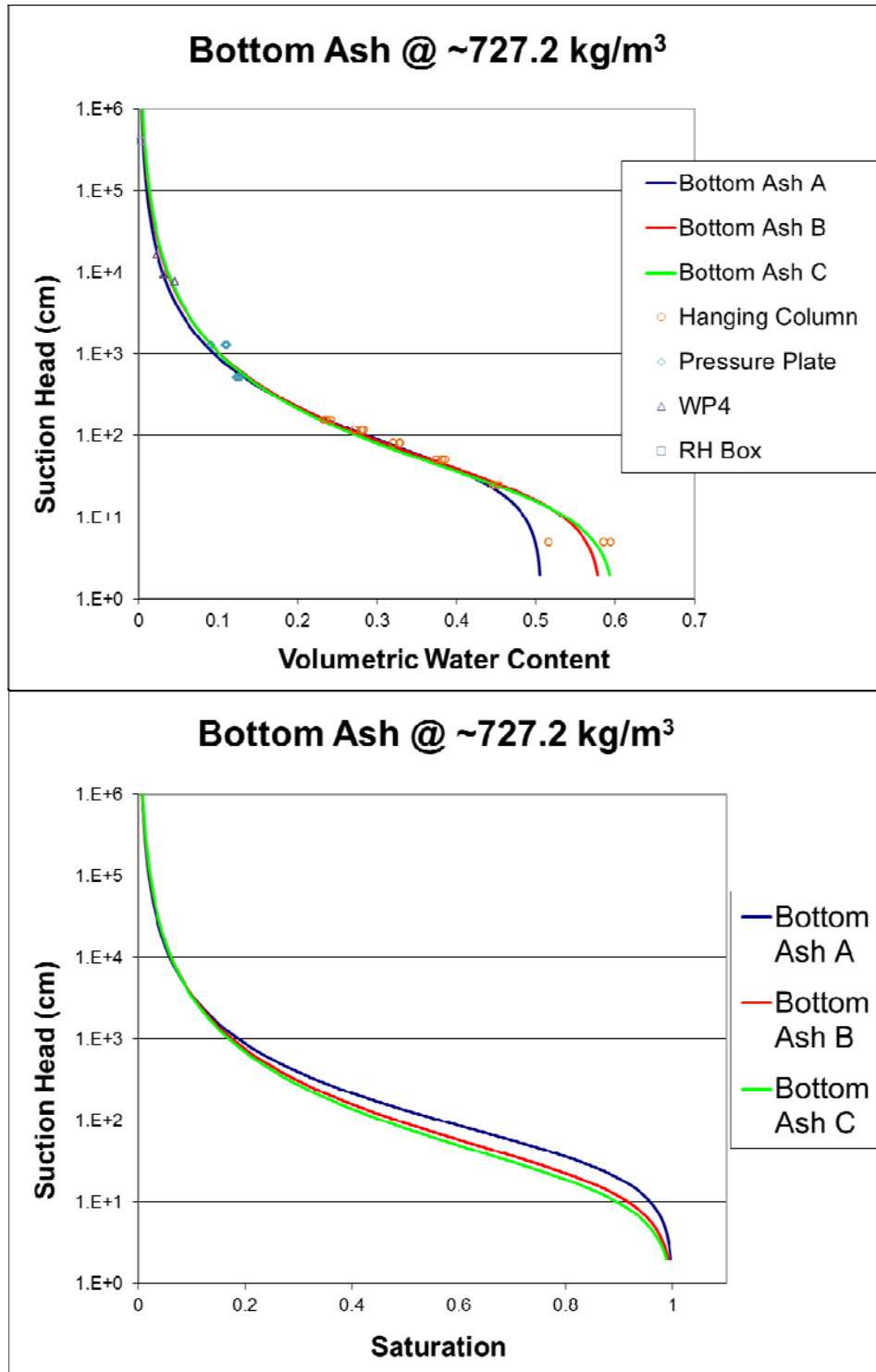


Figure 19. Fitted data (top) and saturation moisture characteristic curves (bottom) for bottom ash at lowest dry density.

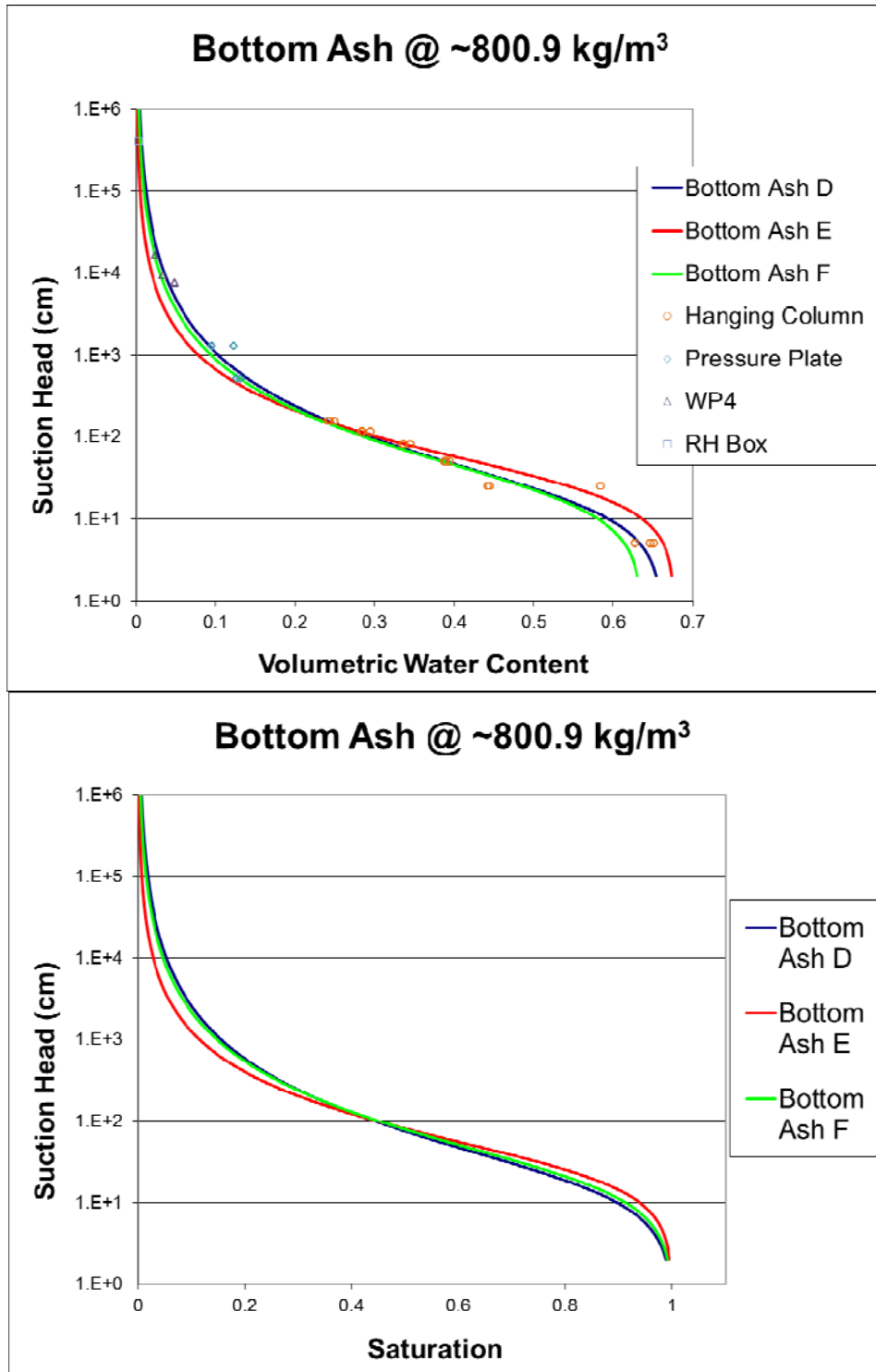


Figure 20. Fitted data (top) and saturation moisture characteristic curves (bottom) for bottom ash at intermediate dry density.

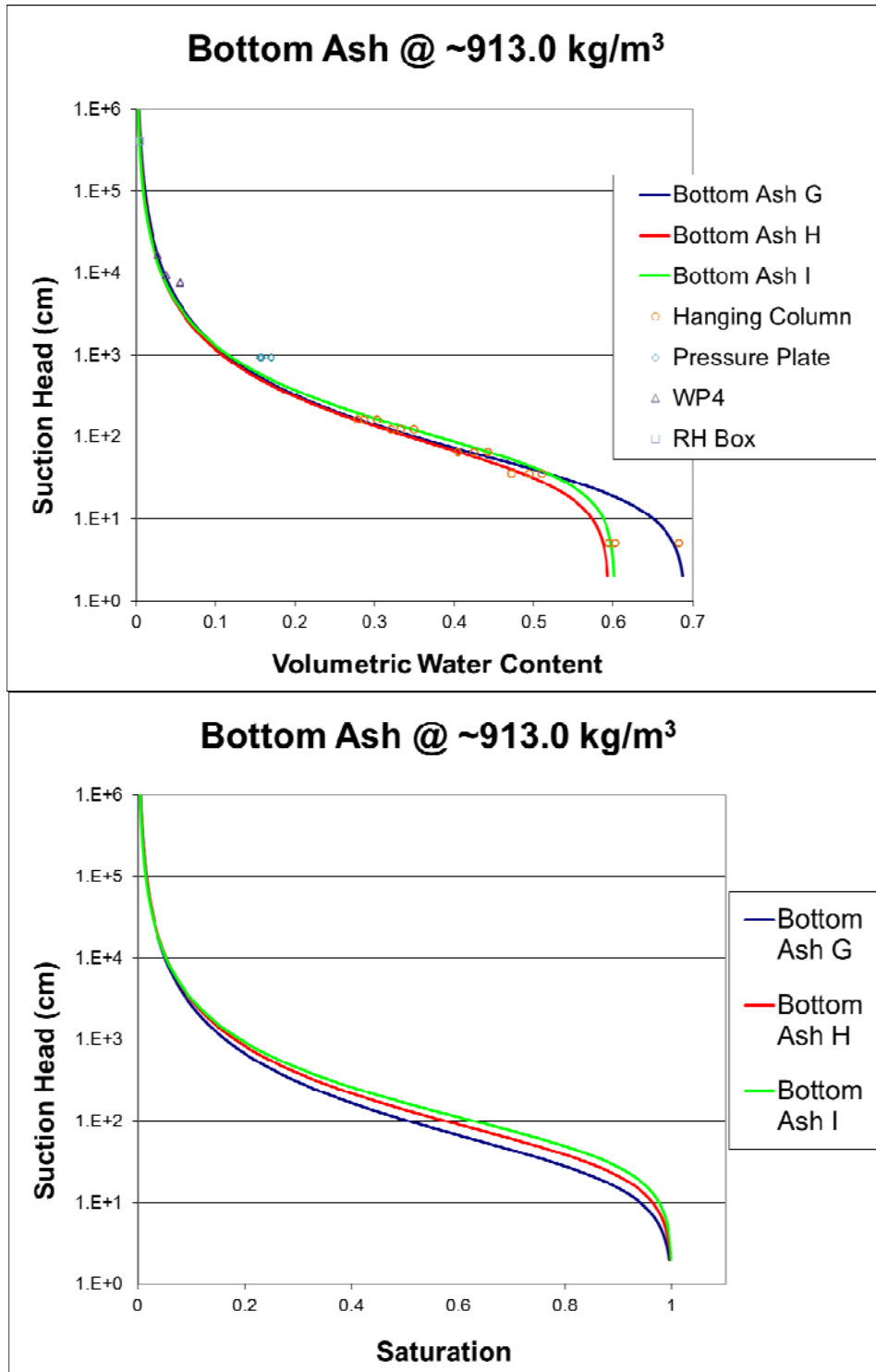


Figure 21. Fitted data (top) and saturation moisture characteristic curves (bottom) for bottom ash at greatest dry density.

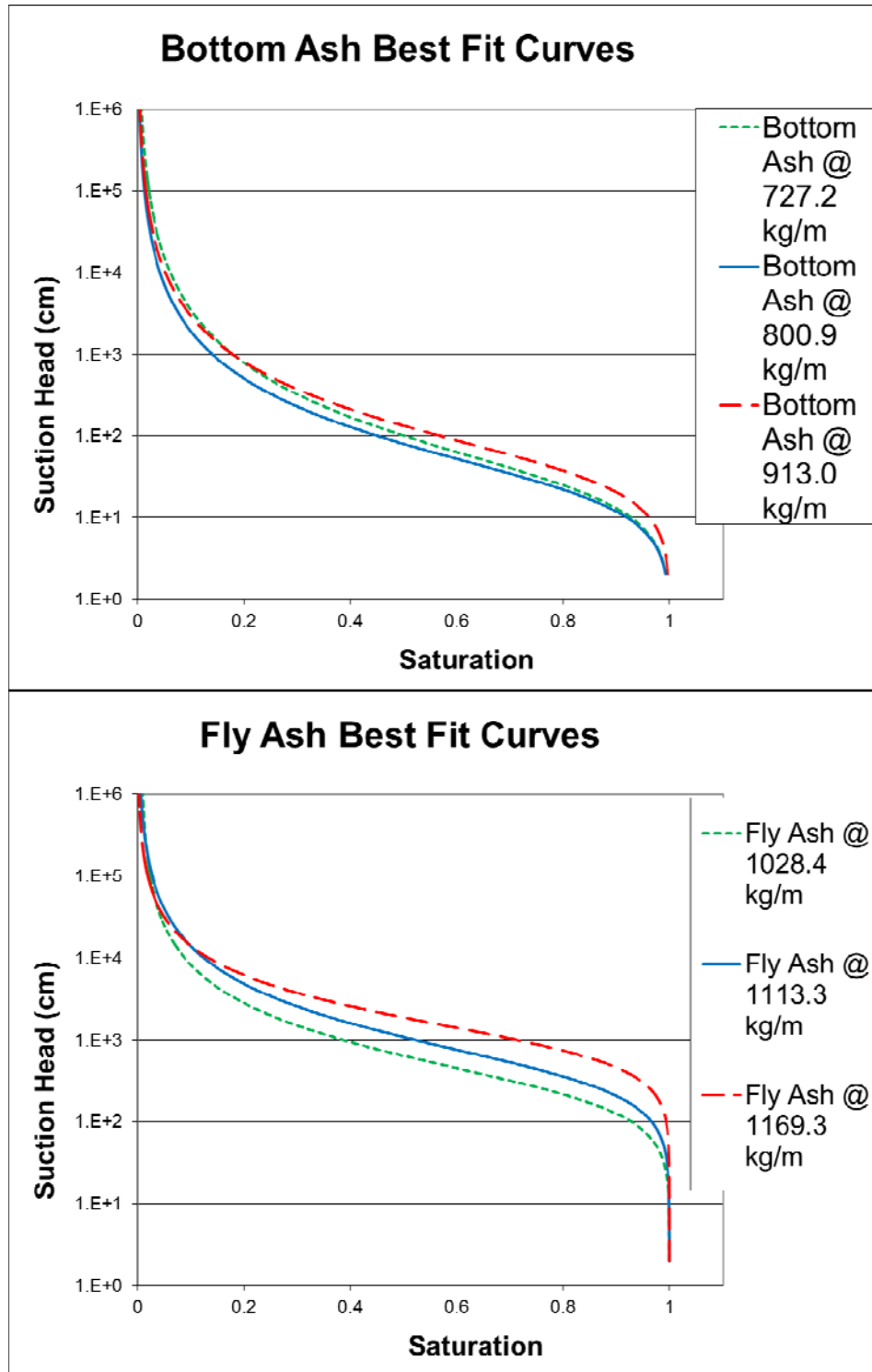


Figure 22. Best fit moisture characteristic curves for fly ash as function of dry density.

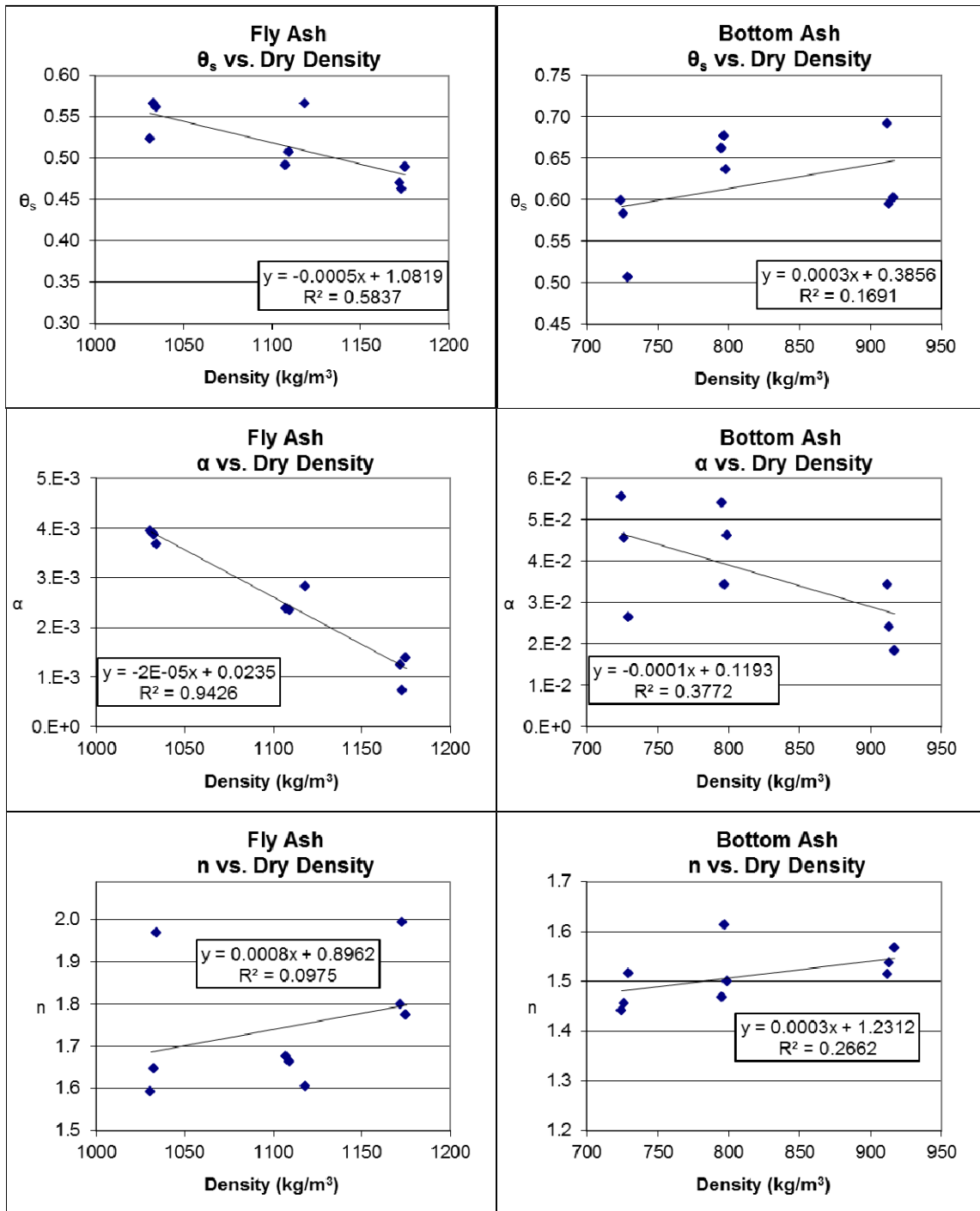


Figure 23. Van Genuchten parameters vs. dry density.

2.5 Discussion of Laboratory Results

2.5.1 Specific Gravity & Calculated Porosity of Fly Ash & Bottom Ash

Specific gravity tests resulted in an average specific gravity of 2.00 for fly ash and 2.06 for bottom ash. These results are within the range of results from other studies (El-Mogazi et al., 1988; Palmer et al., 2000; Prashanth et al., 1998; Seals et al., 1972). Porosity was calculated using the following equation:

$$\eta = 1 - \frac{\rho}{\rho_w G_s} \quad (4)$$

Where:

η = porosity (dimensionless)

ρ = sample density in g/cm^3

ρ_w = density of water in g/cm^3

G_s = specific gravity of material

When porosities are compared to fitted θ_s values, most samples appear to be over saturated. That is, the fitted θ_s is larger than the porosity calculated using the measured specific gravity (Table 8). This result is consistent throughout all samples except for bottom ash samples with a target dry density of 727.0 kg/m^3 .

It is highly unlikely that the samples were over saturated at the fitted θ_s values. It can be seen in the MCCs fitted with data (Figure 16 through Figure 21) that the fitted θ_s values (Table 6) are often less than the volumetric water content measured at -5 cm. Oversaturation is not likely to occur after equilibration at a pressure head of -5 cm.

A possible reason that some of the bottom ash samples appear under saturated may be that some of the particles have large hollow cores that are inaccessible to water. Attention was given during saturation to ensure fully saturated samples. There were no observations during testing to support that any of the samples were over or under saturated. Therefore, calculated porosities using specific gravity results are not used further.

Table 8. Calculated Porosity and Saturated Water Content Comparison.

Sample	Target Dry Density (kg/m ³)	Actual Dry Density (kg/m ³)	G _s	calculated porosity (%)	Θ _s (cm ³ /cm ³)	% saturated
FA A	1028.4	1030.8	2.00	48.5	0.52	108.0
FA B	1028.4	1033.1	2.00	48.3	0.57	117.1
FA C	1028.4	1034.7	2.00	48.3	0.56	116.6
FA D	1113.3	1,113.3	2.00	44.5	0.51	114.1
FA E	1113.3	1,113.3	2.00	44.6	0.49	110.2
FA F	1113.3	1,118.8	2.00	44.1	0.57	128.5
FA G	1169.3	1172.1	2.00	41.4	0.47	113.8
FA H	1169.3	1173.4	2.00	41.3	0.46	112.0
FA I	1169.3	1,175.2	2.00	41.2	0.49	118.8
BA A	727.2	729.2	2.06	64.6	0.51	78.5
BA B	727.2	726.5	2.06	64.7	0.58	90.1
BA C	727.2	724.2	2.06	64.8	0.60	92.5
BA D	800.9	795.2	2.06	61.4	0.66	107.8
BA E	800.9	797.1	2.06	61.3	0.68	110.5
BA F	800.9	798.7	2.06	61.2	0.64	103.9
BA G	913.1	912.3	2.06	55.7	0.69	124.1
BA H	913.1	913.5	2.06	55.7	0.60	106.9
BA I	913.1	916.9	2.06	55.5	0.60	108.6

2.5.2 Fly Ash

Equation (1) can be used to reasonably describe the relationship between load and dry density of fly ash for the range of applied loads expected at the SJCM. Similar results were obtained for all four samples of fly ash that were subjected to one-dimensional loadings used in this study.

Overall, saturated hydraulic conductivity results between fly ash samples of the same dry densities are comparable with one another. The results of the saturated hydraulic conductivity for fly ash show greater variability in the samples with lower dry densities. It can be speculated that this is caused by less uniform pore size distribution at lower densities which becomes more uniform with increasing dry density. These results provide a trend of K_{sat} decreasing as dry density increases, consistent with previous studies on fly ash. The values found in this study are comparable to what other studies have found (Campbell et al., 1983; Joshi et al., 1994; Prashanth et al., 2001).

The van Genuchten model parameters of fly ash also display a trend in variation with density. Values of θ_s , which is related to the amount of pore space within the sample, are shown to decrease with increased density as expected. Values of α , commonly interpreted as the inverse of air entry pressure head (Mudd et al., 2007), also decrease with increases in dry density; this can be attributed to smaller pores in higher density materials being able to retain water at greater

negative pressure heads. Values of air entry for fly ash are similar to what was found in previous studies (Mudd et al., 2007; Chakrabarti et al., 2005).

It is important to note that, for fly ash, values of n show little variation with increasing density; all values are between 1.5 and 2.0. This result is reflected in the similar shapes of MCCs for all fly ash samples. All three samples at each dry density of fly ash provided similar results, indicating that the methods used to estimate unsaturated hydraulic properties are appropriate for fly ash materials.

The saturated and unsaturated hydraulic properties of fly ash are similar to the values expected for silty soils (e.g., Assouline, 1997; Lu and Likos, 2004; Richard et al., 2001). Since both materials have similar particle size distributions this is not surprising.

2.5.3 Bottom Ash

The compressibility measurements for bottom ash materials showed less variation between samples than for fly ash. Equation (1) can be used to describe the relationship between load and dry density of bottom ash for the range of applied loads used. Similar results were obtained for all four samples of bottom ash that were subjected to one-dimensional loading for this study.

K_{sat} values measured for bottom ash samples showed a general linear trend of decreasing as density increases but with considerable variability.

Unsaturated properties of bottom ash show similar variability in the results. θ_s values show little linear trend as dry density increases, with a linear R^2 value of 0.17. θ_s values for bottom ash tend to increase slightly as density increases, which conflicts with expectations. This may be attributed to lack of homogeneity in the material. The structure of the bottom ash has been observed to be heterogenous with pieces of unburned coal appearing at times and even larger pieces of gravel sized rocks. Lack of homogeneity within the bottom ash material brings complications in creating samples that have structures which are consistent with one another. The structure and porosity of a material has a strong impact on the saturated and unsaturated hydraulic properties of a material (Lu and Likos, 2004).

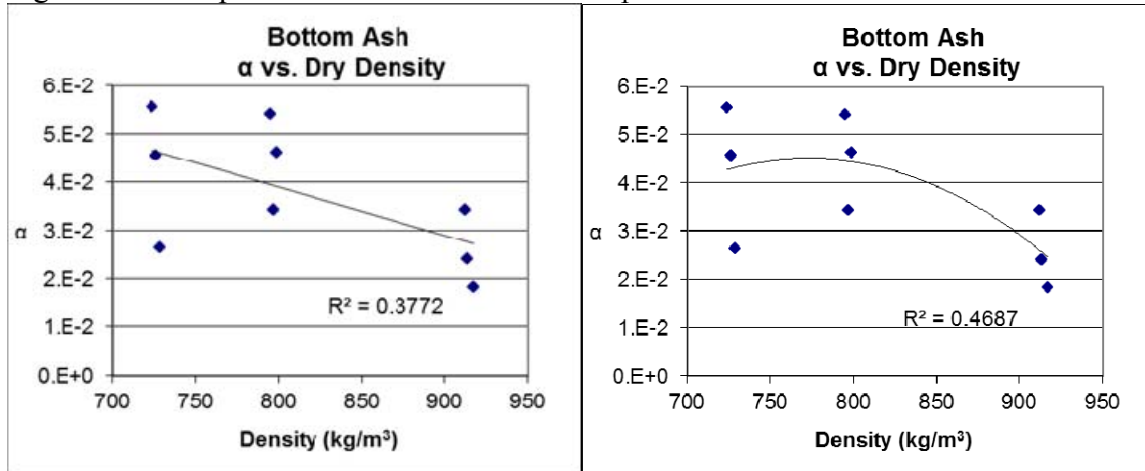
Values of α for bottom ash are similar to those found in other studies (Mudd et al., 2007; Chakrabarti et al., 2005). A linear trend line provides a relatively low R^2 value of 0.38; however, if the data is fit to a second order polynomial trend line, the R^2 value rises to 0.47 (Figure 24). This suggests that, for bottom ash, unsaturated properties such as α may not be affected by increases in dry density until a threshold density is reached. Further testing would be required to support this speculation.

Values of n for bottom ash show less variation than fly ash values; all values are between 1.4 and ~1.6. This shows that the shapes of MCCs, for all bottom ash samples, are more similar relative to fly ash samples. The resulting MCCs for each dry density plot along similar curves providing further evidence that these methods are consistent in estimating unsaturated properties of bottom ash materials.

The variability in bottom ash properties compared to fly ash may be due to more heterogeneity in bottom ash. Larger sample volumes could provide less variability in results for K_{sat} and MCC measurements.

The saturated and unsaturated hydraulic properties of bottom ash are similar to the properties exhibited by a sandy soil (e.g., Assouline, 1997; Lu and Likos, 2004). Since both materials have similar particle size distributions this appears to be a reasonable result.

Figure 24 - Comparison of linear trend line and parabolic trend line



2.6 Conclusions

Fly ash K_{sat} values are shown to decrease as dry density increases. Unsaturated hydraulic properties for fly ash as measured by θ_s and α , decrease with increases in dry density.

Bottom ash compressibility shows little variability whereas hydraulic properties have more variability relative to those of fly ash. K_{sat} values of bottom ash samples tend to decrease as dry density increases. Unsaturated properties of bottom ash show little trend in variations with changes in dry density. Test results may reflect the lack of homogeneity in bottom ash.

This study has shown that methods commonly used in soil testing may be utilized to measure the saturated and unsaturated hydraulic properties of fly ash and bottom ash as a function of their density.

Part II – Geochemical Properties of Coal Combustion By-Products and Cover Materials

3.1 Introduction

Due to the very high temperatures in coal fired power plants organic matter is combusted and inorganic material is captured as fly or bottom ash. This ash is principally composed of aluminosilicates associated with minerals and soil present in the coal. Metals present in the coal remain in the ash or are captured in the flue gas desulfurization process and include many that are toxic or hazardous such as As, B, Ni, Cu, Se, Mo, Cd, Zn and Pb. Constituents in the CCBs may be leached by water added for dust suppression or atmospheric precipitation that percolates through the buried wastes. In addition to the trace metals, other constituents such as alkalinity, chlorides and sulfates may be contained in these leachates. Their presence may affect leaching of the metals (Manskinen, Poykio, and Nurmesniemi 2011).

In the western U.S. CCBs are typically disposed in empty surface mine pits consequently space is generally not a concern. Old surface mining pits provide an economical disposal site when available and the volume of the disposed material reduces the need for other material to provide a final grading plan that is consistent with the surrounding topography. When disposed in an open pit water is often added to the waste to limit dust generation. In addition, wastes from the flue gas desulfurization process usually has a high water content because it originates from wet scrubbers. This moisture may contribute to migration of water through the buried material and its chemistry may influence the long term chemical stability of the buried CCBs.

This phase of the study focused on determining the potential constituents within CCBs and evaluating the resulting leachate. This was accomplished by comparing the differences in mineralogical and geochemical make up of freshly generated ash compared to buried ash from the reclaimed area to determine if the ash was aging. To determine if constituents were being transported to underlying ground water chemical markers in the leachate were identified which would be attributed to the disposed CCBs.

3.2 Background Information

Coal Combustion Byproducts from the San Juan Generating Station consist of a combination of three types of waste generated from burning coal and the associated air pollution control processes: fly ash (FA), bottom ash (BA) and flue gas desulfurization (FGD) sludge. Overall properties of CCBs are dependent mostly on the properties of the parent coal in addition to the condition during incineration and efficiency of the recapture equipment at the specific power plant. However, each sub group has unique characteristics which the following discusses briefly (El-Mogazi, Lisk, and Weinstein 1988). Their characteristics are described below

3.2.1 Fly Ash

Fly ash is a very fine gray powder that is captured from the exhaust gases of furnaces by electrostatic precipitators and scrubbers (ACAA 2011). Physical features of fly ash include spherical particles that constitute a glassy, amorphous (non-crystalline) matrix (El-Mogazi, Lisk, and Weinstein 1988). The spherical shape is a result of molten droplets of fused inorganic constituents being carried upward and cooled in a stream of flue gasses (Dudas and Warren 1987). The size of FA particles is typically similar to silt particles, 2 μm to 50 μm (Chang et al. 1979). The specific surface areas of FA particles vary from 1.27 to 0.45 m^2g^{-1} with large, porous and carbonaceous features on the surface (El-Mogazi, Lisk, and Weinstein 1988), (Fisher, Chang, and Brummer 1976).

Fly ash generated from the coal combustion process is similar to volcanic ash in that both are primarily composed of aluminosilicate glass and may eventually form clay minerals as a result of weathering processes (Zevenbergen et al. 1999). Major elements within fly ash are, in decreasing abundance Si, Al, O, Fe, Ca, C, Mg, K, Na S, Ti, P and Mn (Zevenbergen et al. 1999; Dzombak and Morel 1990; El-Mogazi, Lisk, and Weinstein 1988; Dudas and Warren 1987; Bhangare et al. 2011; Fisher, Chang, and Brummer 1976). Fly has pozzolan properties due to the high alumina and silica composition which means the fly ash will form a weak cement as a result of precipitation silicate and carbonate minerals under high pH conditions (You, UM, and et al. 2009).

The principal component of fly ash is amorphous aluminosilicate glass which is relatively inert in the environment. However, many of the trace elements associated with fly ash (As, Se, Mo, Cd and Zn) are located in the surface layers and are more available for leaching. The explanation for this phenomenon is that these elements are volatilized during combustion and subsequently condense onto the surface of the ash as the flue gas cools in the emissions control processes (El-Mogazi, Lisk, and Weinstein 1988).

Analysis of FA from different types of coal sampled across the United States show western Cretaceous coal typically has higher pH and increased concentrations of B, Ca, and Na than that contained in FA from eastern coal. Higher Ca concentrations can contribute to higher alkalinity within CCBs due to the increased carbonate concentrations (Dudas and Warren 1987);(Shannon and Fine 1974; James et al. 1982). The solubility characteristics of the various chemical species within the FA are directly affected by the leachate solution pH (El-Mogazi, Lisk, and Weinstein 1988), (D. J. Hassett, Hassett, and Brobjorg 1988). To determine a specific ash's potential

environmental effects leach tests must be conducted to identify the trace constituents as well as the effect of FA on solution pH.

A leach test consists of adding a specific ratio of water to soil samples for a specific amount of time. A batch leach tests is a different leach tests that uses a high water ratio to soil ratio 20:1, which are meant to characterize the types of constituents that have the potential to leach in the presence of water. Other tests with much smaller fractions of water to soil ratios are used to characterize concentrations of leachate similar to field conditions like column tests (Bin-Shafique et al. 2006),(Ram et al. 2007).

Experiments demonstrate that different constituents and concentrations leach with different leach tests. One study found that the range of leaching metals concentration changes in descending order for each of the following tests: buffer columns, aqueous columns, aqueous shake, and buffer shake tests (Ram et al. 2007). Recent column leach studies found that decreasing the pH (ph<4) resulted in higher metal ions (As, B, Cd, Cr, Zn, Pb, Hg and Se) concentrations in the leachate. This is most likely due to the instability of the mineral phase of the fly ash as these lower pH ranges (Baba et al. 2008), (Zhao et al. 2006). Previous leaching studies conducted with deionized water are summarized in Table 9. They were conducted by SJCM staff and found high concentration of Ba and F (Luther, Musslewhite, and Brown 2009).

Table 9. Dissolved trace element concentrations in groundwater and deionized water leachate (Luther, Musslewhite, and Brown 2009).

Parameter	Groundwater mg/L	CCB Leachate mg/L
Aluminum	<0.05	2.2
Arsenic	<0.003	<0.003
Barium	0.21	0.28
Boron	<0.009	0.44
Cadmium	<0.002	<0.002
Chromium	<0.001	<0.001
Cobalt	<0.006	<0.006
Copper	<0.001	<0.001
Cyanide	0.53	<0.02
Fluoride	2.1	2.4
Iron	0.37	2
Lead	0.02	0.01
Manganese	0.18	0.16
Mercury	<0.002	<0.002
Nickel	0.004	0.006
Selenium	<0.003	<0.003
Silver	<0.002	0.006
Zinc	0.87	0.01

Leachate composition from fly ash is also dependent on its mineralogy. Fly ash is generally amorphous glass identified as but may include mullite, quartz and magnetic spinel (i.e. magnetite, hematite and ferrite). The magnetic spinel matrix has a high reactivity and a high

potential for carrying and releasing toxic elements such as arsenic, boron and selenium (El-Mogazi, Lisk, and Weinstein 1988), (Ward and French 2006). A unique mineralogical aspect of fly ash that is not found in bottom ash is the presence of hematite (Fe₂O₃) (Sultana, Das, and et al. 2011; Ward and French 2006; Manskinen, Poykio, and Nurmesniemi 2011).

3.2.2 Bottom Ash

Bottom ash (BA) is grey to black and consists of angular particles that are porous. It forms on the wall or floor of coal furnaces and is too large to be carried up the stack by flue gases. It is collected through open grates into ash hoppers at the bottom of the furnaces and later combined with FA and FGDS for disposal (ACAA 2011).

Bottom ash consists of a mix of large particles and the amorphous fused spheres that comprise FA. The particle size of BA is larger than FA is usually in the range associated with fine sands to fine gravel (62.5 µm - 75 µm) (You, UM, and et al. 2009).

Bottom ash is typically composed of the similar elements found in fly ash of Si, Al, Fe, Ca, C, Mg, K, Na, Si, Zn, and Mn (Table 10) (El-Mogazi, Lisk, and Weinstein 1988; You, UM, and et al. 2009). Bottom ash typically has a lower Total Organic Carbon content than FA and when mixed in water, produces a solution with lower electrical conductivity (Manskinen, Poykio, and Nurmesniemi 2011).

Table 10. Mean trace element concentrations in Bottom Ash, Fly Ash and Overburden at the SJCM (Luther, Musslewhite, and Brown 2009)

Parameter	Mean BA mg/Kg	Mean FA mg/Kg	Mean Spoil mg/Kg
Aluminum	7079	6062	7428
Arsenic	2.76	10.8	2.85
Barium	505	758	141
Boron	51.1	200	NA
Cadmium	0.42	0.45	3.01
Chromium	2.68	5.83	5.66
Copper	18.6	12.7	33.4
Iron	4648	3471	NA
Lead	8.46	5.52	10.2
Manganese	59.4	80.5	NA
Molybdenum	3.44	5.82	NA
Nickel	2.15	1.79	9.1
Selenium	0.55	0.58	0.39
Silver	<1.0	<1.0	<1.0
Zinc	37.7	25.8	73.9

The dominant morphology of bottom ash is amorphous glass matrices are identified as glass, mullite-quartz and magnetic spinel (i.e. magnetite, dolomite hematite and ferrite) (Sultana, Das, and et al. 2011) (Ward and French 2006). Again the magnetic matrix is high reactivity and has a high potential for carrying and releasing toxic elements within the bottom ash (El-Mogazi, Lisk,

and Weinstein 1988). Dolomite ($\text{CaMg}(\text{CO}_3)_2$) is found only in bottom ash from a mineralogical stand point (Sultana, Das, and et al. 2011; You, UM, and et al. 2009).

3.2.3 Flue Gas Desulfurization Sludge

Flue gas desulfurization sludge (FGDS) is the material produced by emissions control systems (scrubbers) that remove sulfur dioxide (SO_2), a key component to acid rain, from power plant flue gas streams (ACAA 2011). The scrubbers consist of a tower where the flue gas containing SO_2 is introduced at the bottom and flows upward. A slurry of water and lime (CaCO_3) is sprayed as a mist at the top of the tower and contacts the rising gas stream as it falls through the scrubber. SO_2 is absorbed in the solution which is collected at the bottom of the scrubber as a dilute solution of sulfuric (H_2SO_4) and sulfurous acids (H_2SO_3). The acid is neutralized by addition of limestone (CaCO_3) which subsequently forms a slurry of calcium sulfate (CaSO_4) and calcium sulfite (CaSO_3). The sulfite slurry is further oxidized with air to produce gypsum ($\text{CaSO}_4 \cdot 2\text{H}_2\text{O}$) as a final product. The end composition of the FGD sludge is depends on the power plant design, type of equipment used for incineration, coal composition, composition of the limestone, forced oxidation and end treatment (i.e type of dewatering process used) (Baligar et al. 2011). If there is a market for gypsum, the FGD process is able to produce gypsum with the same chemical composition as mined gypsum. A study conducted on 12 different FGDS showed the following results of the primarily composition of Ca, S, Al, Fe, and Si, an average pH around 9 and an electrical conductivity around 2.3 $\mu\text{S}/\text{cm}$ (Baligar et al. 2011).

3.2.4 Reuse of Coal Combustion Byproducts

Strategies for limiting the volume of CCBs buried in landfills by developing methods for reusing CCBs are being developed. Reuse of CCBs has focused on exploiting the specific physical and chemical properties of the ash.

For instance, fly ash is often used as a concrete additive due to its pozzolanic characteristics; use of FA allows reduced use of more expensive cement and increases the strength of some concrete mixtures (You, UM, and et al. 2009). These characteristics lead to a longer life span of concrete. Other uses for fly ash include a supplement in feed stock and in embankments, soil modification/stabilization and road bases. Bottom ash can be reused as aggregate due to its angular and well-graded size in embankments, road bases and concrete products. Flue gas desulfurization sludge can be used in wallboard, cement and geotechnical applications. The agricultural industry also uses gypsum to treat soils and improve crop performance (ACAA 2011).

3.2.5 Potential Impacts of Coal Combustion Byproduct Disposal

There are two potential impacts associated with the disposal of CCBs: 1) physical characteristics that may lead to catastrophic failure of a CCB disposal facility and 2) chemical characteristics that may threaten human health and the environment as a result of release of leachates from the disposal cell. As previously stated, the main concern of CCBs as they relate to common disposal practices is that they retain the heavy, non volatile contaminants associated with the parent coal. Such components include silver (Ag), arsenic (As), barium (Ba), cadmium (Cd), chromium (Cr), copper (Cu), iron (Fe), mercury (Hg), manganese (Mn), lead (Pb), selenium (Se), strontium (Sr), zinc (Zn), fluorine (F) and chlorine (Cl). These potential contaminants have demonstrated

adverse affects in exposed populations when released into the environment (Ruhl et al. 2010),(White et al. 1994). The heavy metals of concern in western CCBs are generally As, B, Cd, Hg, Pb, and Se. At high concentrations these metals pose acute and chronic health problems, developmental problems in children, and most are considered to be carcinogenic (El-Mogazi, Lisk, and Weinstein 1988). Allowable concentrations of these constituents in drinking water are regulated by the Environmental Protection Agency (EPA) while concentrations in ground water are regulated by the states. Regulations regarding disposal of CCBs are left to individual state regulatory agencies. Typically the chemical analysis of a batch leach and measurement of the total elemental composition are required. New Mexico both tests must be conducted quarterly and the results submitted to the Mining and Minerals Division of the NM Energy Minerals and Natural Resources Department (Mining and Minerals Division, New Mexico 2011; Luther, Musslewhite, and Brown 2009). Table 11 compares the range of values of water quality measurements from SJCM monitoring wells to NM groundwater standards for domestic and irrigated agricultural use.

The major constituents in CCBs are commonly alkali metals and alkaline earth metals, especially N, K, Ca, Mg, the transition metals Al and Fe, Si, and O. Minerals formed from these elements are referred to as aluminosilicates and have very high melting points. They have limited solubility in water. These characteristics allow the analytes to either remain in a solid form during the combustion of the coal or to vaporize during combustion and then condense onto the surfaces layers of the fly ash as the flue gas cools. Either way results in metals being associated with the CCBs and have the potential to leach when water is introduced to the ash. The principal concern is the solubility of these minerals because toxic and hazardous elements, once dissolved in water, can be transported from the disposal cell by ground and surface water flow (Ruhl et al. 2010).

Table 11. Comparison of New Mexico ground water standards for domestic consumption and irrigation use to the range of water quality in SJCM monitoring wells.

Parameter	NM Groundwater Standards		Water Quality Data	
	Domestic	Irrig.	Low	High
pH			4.85	12.61
Spec cond (uS/cm)				
TDS	1000		30	69800
TOC			0.001	415
K			0.001	286
PO ₄			0.001	34.8
Ca				4600
Mg			0.1	2270
Na			0.1	27800
H ₂ S			0.2	386
Phenols	0.005		0.001	7.8
HCO ₃			0.001	2970
CO ₃			75	
Cl	250			16700
F	1.6		0.1	54
SO ₄	600		0.01	52000
NO ₃	10		0.5	180
Al		5	0.5	31
As	0.1		0.05	2.41
B		0.75	0.005	10
Ba	1		0.001	51.6
Cd	0.01		5E-05	0.5
Cr	0.05		0.001	0.5
Cu	1		0.0001	8.7
Co		0.05	0.0003	0.3
Fe	1		0.001	72.3
Pb	0.05		0.0001	2.82
Mn	0.2		0.0005	12.4
Hg	0.002		0.0001	0.06
Mo			0.001	0.07
Ni		0.02	0.001	0.2
Se	0.05		0.001	15.4
Ag	0.05		5E-05	0.5
V			0.0001	2
U	5		1E-05	150
Zn	10		0.001	5.98
Ra-226			0	579

3.3 Research Methods

Samples of CCBs of varying ages were collected from disposed material in the SJCM by a direct push and ultrasonic drilling methods. Samples were collected from reclaimed areas of the mine and compared to fresh samples collected from the adjacent power generation station to determine the physiochemical characteristics of fresh and aged CCBs.

The New Mexico MMD has historical records of the quarterly ash samples available from when the SJCM originally opened through current disposal operations. This data was used to identify sample locations so that samples collected from the power plant and from the disposal pits would be representative of normal operation. Ash data from present until 1995 was compared for all the constituents and no significant difference in between the ash samples was found. This allowed development of general conclusions based on the necessarily limited sample testing conducted during this research.

3.3.1 Sample Collection and Preservation

Fresh samples from the power plant were collected using the same protocol as quarterly samples collected to determine compliance with MMD regulations. Fly ash was collected once per week from each of the four fly ash collector units at the unloader site of each ash bin. Bottom ash was collected twice per month from each of the 3 units where the collection hoppers dump into the transport trucks. FGDS was collected once per week in one liter grabs sampled off the conveyer. Each of the weekly samples were then combined to create a composite sample representative of the 3 months for each FA unit, each BA unit and the FGD sludge (Chee 2009).

Core samples were collected in rigid clear plastic pipe during the direct push sampling program or double bagged in gallon plastic bags from the ultrasonic drilling program. Samples were stored in a cooler at 4 °C and transported to the UNM campus where they were stored in a refrigerator at 4 °C prior to analysis. Samples were prepared according to part 2540 Solids Procedures in Standard Methods (Eaton et al. 2005).

3.3.1.1 Core Sampling

Direct push technology was utilized to collect buried CCB samples from the SJCM. From Sept 13th, 2010 to Sept 17th, 2010 the US Geological Survey (USGS) collected core samples using a Geoprobe® 540UD with an operations crew to collect samples at the Yucca Ramp and Juniper Pit storage locations as seen in Figure 3.

Sites were selected to maximize recovery of CCB sample by drilling in areas where CCB material was known to have been disposed. Jim O'Hara, from the New Mexico Mining and Minerals Division (MMD), assisted in identifying location of the core sampling. Samples were collected from each of 8 sites. When possible, direct push sample collection technology is preferable since it is rapid, inexpensive and samples collected by this method are less disturbed by the sample collection process than if a drilling method is used. Two inch diameter cores were collected in plastic. The direct push method cannot penetrate cobbles or large rocks which resulted in the inability to penetrate to depths ranging from 10ft to 20ft, referred to as refusal. However, coring at the Yucca Ramp did produce some CCB material near 25 ft depth. Figure 25 shows the soil profile of each of the 8 sites sampled (New Mexico Mining and Minerals Division

2009). The horizontal red lines indicate the depth at which core material was selected and subjected to analysis of their physical and chemical properties.

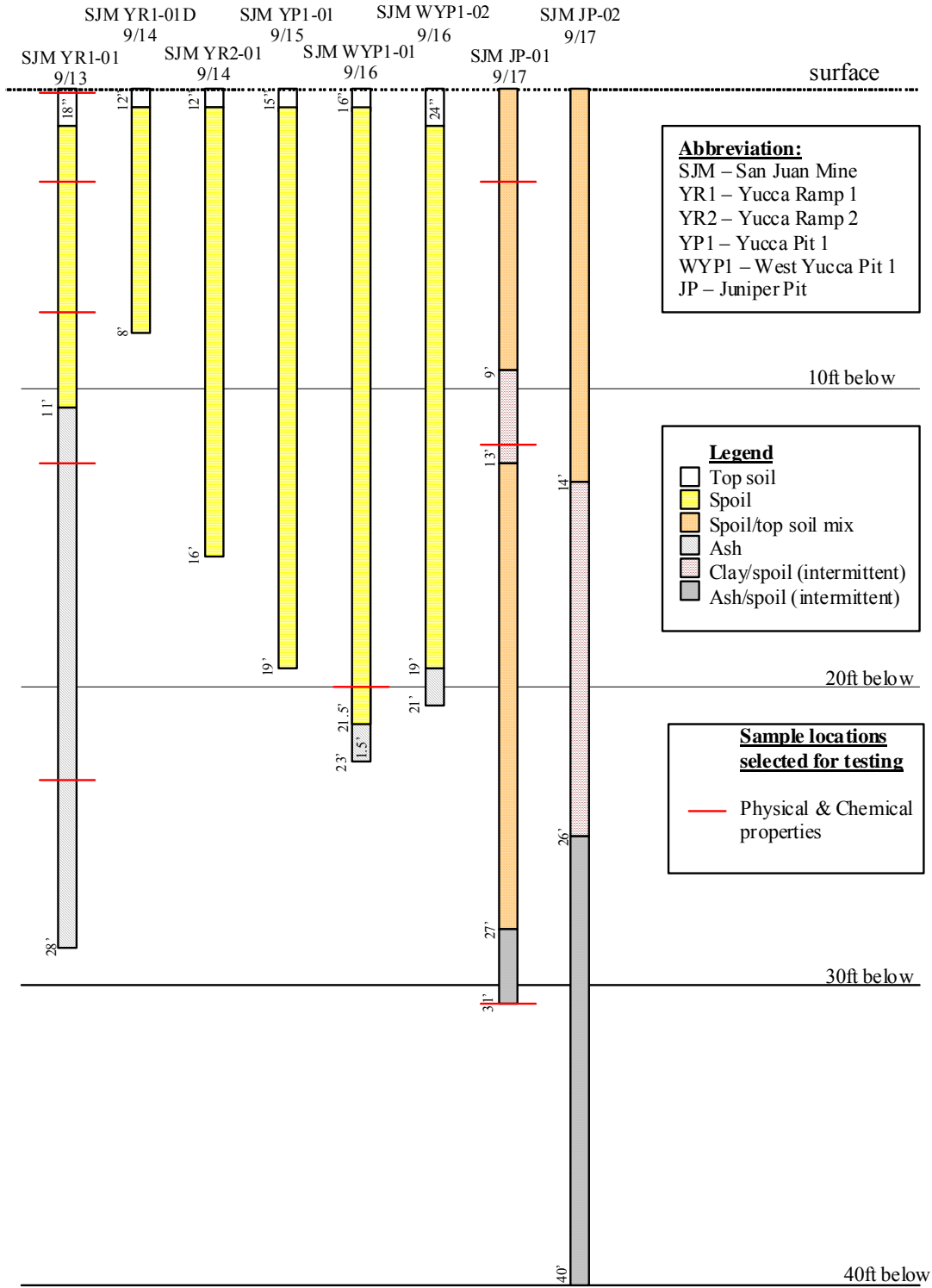


Figure 25. Geoprobe® coring samples diagram

A second set of samples was collected during a coring and monitoring well installation program in the summer of 2011. This drilling program produced samples from the Juniper Pit (JP) area (see Figure 2. Sonic drilling was employed because of its speed, the fact that water or drilling mud is not needed, and it produces a continuous sequence of core material which facilitates detailed and accurate logging of subsurface strata. Drilling occurred from April 28, 2011 to May 1, 2011. Samples collected from the sonic drilling program were used solely for geochemical analysis as the drilling program pulverizes the material making it unsuitable for measurement of physical or hydraulic characteristics. A total of seven locations were drilled. The first was the in the Juniper Pit Surface Material 04 (SJCM- SM-04). A picture of the complete core removed from SJCM-SM-04 is presented in Figure 26 and is discussed below.



Figure 26. Example photo of core samples from sonic drilling.

The depth at which samples were collected is loosely correlated to its age, as information on date and elevation of disposal is not available. Relatively young fly ash (FA) (i.e. material from shallow depths) was collected from the first layer of ash located ten feet below the surface. The core was consistently uniform fly ash for the next 100 feet and no deeper samples were collected. At 109.5 feet below the surface, samples were collected from a layer that was six inches thick of what appeared to be bottom ash (BA) due to the presence of smelter slag chunks and grainier ash material. A sample was collected at 120 feet depth, a 4 inch layer that appeared to be FGDS, based on its higher moisture content and grainier appearance. This layer turned out to be fly ash (FA) as determined by subsequent SEM and XRD analyses. At 124 ft, drilling encountered dry

FA and samples were collected at the bottom layer that rested on PCS at 125 ft below the surface. The well screen and casing was then set to serve as a monitoring well.

The second site for sonic drilling was the SJCM KPC 03 (SJCM-KPC-03) site, on the edge of the reclaimed area. Material at this site mainly consisted of PCS, with a small section between 34 and 41 feet of what appeared to be a mix of ash and sandstone due to a finer powder. However, these samples were deemed unusable for geochemical purposes due to the high fraction of sandstone which would make data interpretation difficult. A total of 10 samples were collected during the sonic drilling program. Figure 27 shows the stratigraphy of each of the drill holes and the depth at which samples were collected for subsequent chemical and geochemical analyses.

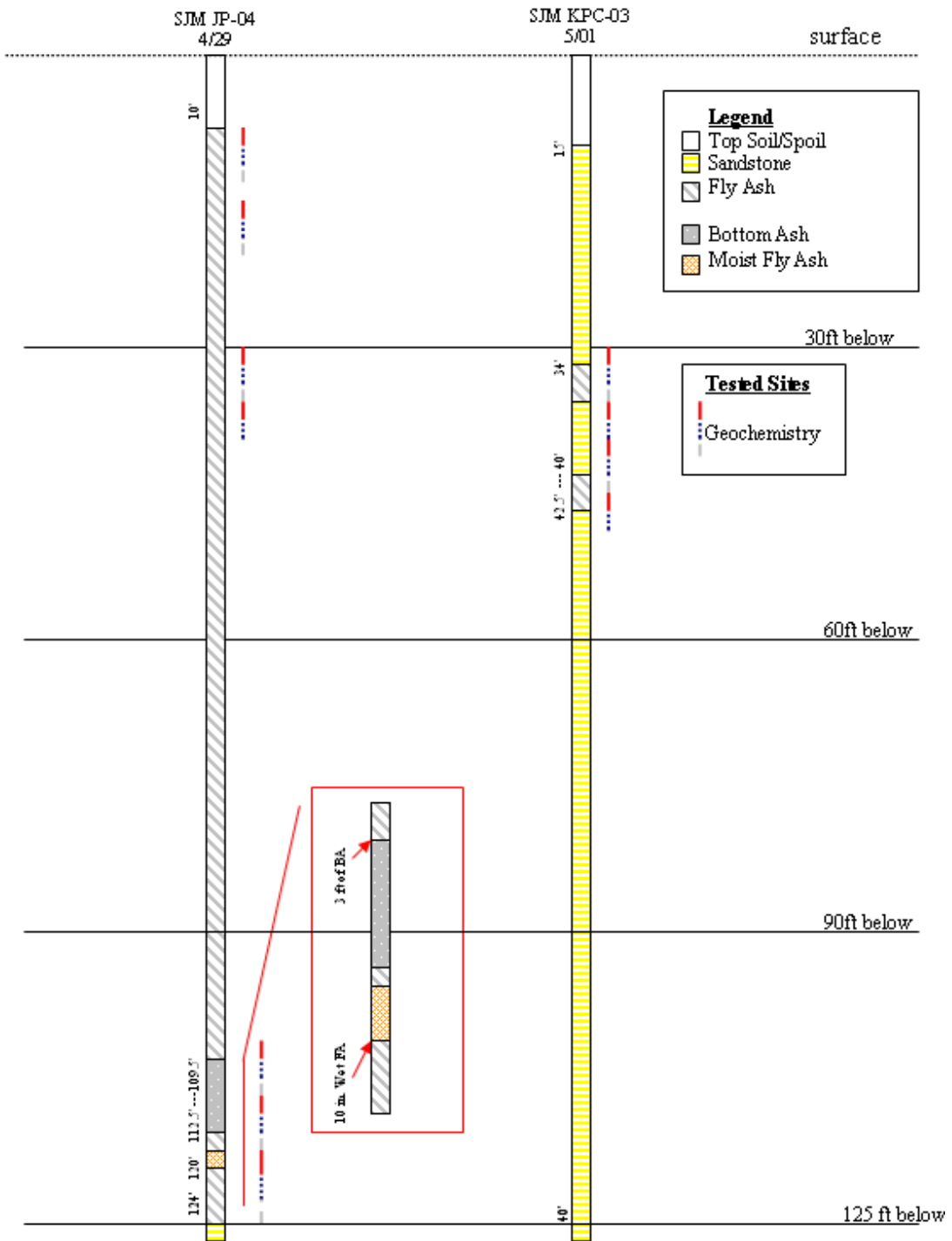


Figure 27. Logs of holes drilled by sonic drilled showing location at which samples were collected.

3.3.1.2 Sample Preparation

A total of 24 samples were collected (9 samples from the Geoprobe drilling samples, 7 samples from the sonic drilling samples and 8 samples of fresh ash collected from the power generating station). Sixteen of these were selected for geochemical analysis. Table 12 shows each classification and site location for the samples.

Thirteen of the 16 samples were determined to consist of buried CCB materials. Three samples of fresh CCB material from the power generating station were analyzed and served as control samples to allow determination of the effects of aging. In addition, samples consisting of spoil/top cover from Yucca Ramp, CCB from Yucca Ramp 01, Juniper Pit 01, Surface Material 04 and KPC 03 were collected for analysis. The samples from the power station consisted of fly ash collected from furnace #1, bottom ash from furnace units 1 & 2 and FGDS.

As previously described, in the actual disposal of the CCBs all three waste products (FA, BA, and FGD sludge) were often combined into a single truck load and disposed of together. However, the fresh samples were collected separately using procedure similar to those established by MMD for compliance monitoring.

The samples were classified as: fresh (unburied CCB), young (CCB from the reclaimed pits near the surface) and old (CCB from the reclaimed pits near bedrock). Initially it was hoped that an accurate age of buried materials could be determine, however, mine disposal records were not sufficiently detailed to permit anything other than an approximate age.

The mass and overall appearance was noted of all samples. The samples were oven dried at 105 °C for 24 hours with their mass and appearance recorded again. Samples that contained larger material were then crushed in a mortar and pestle to shatter box size. Approximately 15 grams were then sent to the University of New Mexico's Earth and Planetary Science Analytical Geochemistry Laboratory (UNM-EPS-AGL) for a suite of geochemical analysis tests.

3.3.2 Chemical Analysis

Chemical analyses were conducted to determine the chemical composition of each of the CCB and spoil/cover samples. Analysis also assists in determining what constituents would be expected to occur in leachates. Testing was done following procedures comparable to the EPA Method 200.2 and ASTM D3987-06 Shake Extraction of Solid Waste with Water respectively. An acid digestion of the samples was also performed to determine their elemental composition.

Table 12. Locations of the sample groups used for each test procedure

CCBs Sample Classification and Location									
Geoprobe 10 Samples		Sonic Collection 11 Samples		Acid Dig./DI Extract 16 Samples		XRD/SEM 10 Samples		Column Test 8 Samples	
Type	Name	Type	Name	Type	Name	Type	Name	Type	Name
Spoil	YR1-01-01T	YFA	SM4-01-01B	Spoil	YR1-01-01T	Fresh	NE-FA-01	Fresh	NE-FA-01
Spoil	YR1-01-01B	YFA	SM4-02-01B	Spoil	YR1-01-01B	Fresh	NE-BA-01	Fresh	NE-BA-01
Spoil	YR1-01-02B	OFA	SM4-03-01B	Spoil	YR1-01-02B	Fresh	NE-FGD-01	Spoil	YR1-01-01T
Spoil	YR1-01-03B	OBA	SM4-04-01B	Spoil	YR1-01-03B	Spoil	YR1-01-01T	OBA	SM4-04-01B
YFA	YR1-01-05B	OFA	SM4-05-01B	YFA	YR1-01-05B	OBA	SM4-04-01B	OFA	SM4-06-01B
YFA	YR1-01-06B	OFA	SM4-06-01B	YFA	YR1-01-06B	OFA	SM4-05-01B	YFA	JP4-01-01B
Spoil	JP1-01-01B	Mix	KPC3-01-01B	Spoil	JP1-01-01B	OFA	SM4-06-01B	Fresh*	NE-FA-01
Spoil	JP1-01-03B	Mix	KPC3-02-01B	Spoil	JP1-01-03B	YFA	JP4-01-01B	OFA	SM4-05-01B
Spoil	JP1-01-08B	Fresh	NE-FA-01	Spoil	JP1-01-08B	Spoil	JP1-01-03B	* = No 8 Coal Seam Water Used	
Spoil	WPR1-01-01B	Fresh	NE-BA-01	Fresh	NE-FA-01				
		Fresh	NE-FGD-01	Fresh	NE-BA-01				
				Fresh	NE-FGD-01				
				OBA	SM4-04-01B				
				OFA	SM4-05-01B				
				OFA	SM4-06-01B				
				Spoil	KPC3-01-01B				

KEY	
Fresh	Fresh unburied
Spoil	Top Spoil
YFA	Young Fly Ash
OFA	Old Fly Ash
OBA	Old Bottom Ash

3.3.2.1 Sample Digestion & Leaching

An analysis using EPA Method 200.2 acid digestion involving acid digestion with nitric (HNO₃) and hydrochloric (HCl) acids was performed to determine elemental composition of 16 of the CCB samples (column 3 of Table 12). This test was employed to compare the composition of fresh and buried CCBs as well as the composition of spoil/cover material. Samples were dried and then ground in a laboratory ball mill. Acids were added then the samples were heated and digested for two hours at 95°C. The samples were analyzed for the elements listed in

on a Perkin-Elmer Optima 5300 DV Inductively Coupled Plasma-Atomic Emission Spectrometer (ICP-AES).

Deionized water extraction was performed on aliquots of the same 16 samples to determine the readily leachable concentrations of following anions: Fluoride (F), Chloride (Cl), Nitrite (NO₂), Bromide (Br), Nitrate (NO₃), Phosphate (PO₄) and Sulfate (SO₄). The purpose of the test was to determine the difference in leachable concentrations of these anions between old, young, and fresh CCBs as differences in anion leachate characteristics are believed to be one indication of secondary mineralization as a result of aging of the buried materials.

The ASTM D3987-06 Shake Extraction of Solid Waste with Water method was used for the deionized water leach procedure. Two grams from each of the sixteen samples were added to 40 mL of deionized water for a 1:20 ratio. A photo of the filled vials is presented in Figure 28. The vials were then fitted onto a mixing wheel (Figure 29) and agitated for 18.5 hours at 30 rotations per minute as required in the procedure.



Figure 28. Photo of samples before leach tests by ASTM D3987-06

After the samples were mixed they were placed in a centrifuge for two minutes each to settle out silt and clay particles. The supernatant was then filtered through 0.47 μ m membrane filters.

Filtered samples were analyzed at the UNM GeoAnalytical Chemistry Laboratory by ion chromatography using a Dionex DX 500 Ion Chromatograph (IC) to determine anions in the aqueous samples, and by ICP-AES (Perkin Elmer 5300 DV) to determine dissolved metals.



Figure 29. Samples placed in mixer for leach tests

3.3.2.2 Mineralogical Characterization

Scanning Electron Microscopy (SEM) and X-Ray Diffraction (XRD) analysis was employed to determine the morphological characteristics and mineralogy of the CCB samples and to look for signs of aging. The intent was to compare the fresh CCB materials to the buried samples collected by the direct push and drilling programs for differences in physical and mineralogical compositions. Of particular interest were changes in the samples from an amorphous glassy structure to more crystalline-clay structures along with the appearance of secondary mineral phases such as carbonates, hydroxides or sulfates.

Ten samples were selected for SEM analysis: spoil from Juniper Pit 01 and Yucca Ramp 01, young fly ash from Yucca Ramp 01, old fly ash from Juniper Pit 04, old bottom ash from Juniper Pit 04, fresh fly ash from furnace unit 1, fresh bottom ash from furnace units 1 & 2 and fresh FGDS, see Table 12 for location of samples.

The samples were analyzed at the UNM-EPS Institute of Meteoritics using a JEOL JSM5800LV variable pressure scanning electron microscope equipped with an Oxford Instruments Energy Dispersive X-ray Spectrometer (EDX) and an Oxford X-ray analyzer (Spilde 2011). Samples were analyzed with both secondary electron (SE) imaging to display sample surface morphology and backscattered electron (BSE) imaging that produces images in which higher and lower atomic number materials appear brighter and darker respectively. All samples were coated in an

EmiTech K950 vacuum evaporator with gold-palladium alloy prior to analysis and examined at an acceleration voltage of 20 kV and a beam current of 0.4 nA (Spilde 2011).

Samples subjected to X-ray Diffraction (XRD) analysis (see Table 12) were analyzed at UNM- EPS XRD Laboratory on a Scintag PAD V Diffractometer/Goniometer with a Scintillation detector. Datascan software (Materials Data, Inc.) for diffractometer automation and data collection, Jade Software (Version 9.1, also from MDI) which can access the complete IDCC Powder diffraction filed database was used to assist in data analysis and interpretation. Some of the samples required a significant amount of grinding to create homogeneous specimens for XRD analysis. For the first runs a standard sample run condition was 5-65 deg 2-theta in a continuous scan mode at 1/2 deg/min and a standard slit configuration (2-4-1-0.3mm) was used which resulted in a total run time of 2 hr per sample (Connolly 2011).

The major mineral phases identified in the FA consisted of aluminosilicate minerals as expected, and included: quartz, mullite, glass, and minor phases of anorthite and hematite (Table 13) (You, et al. 2009; (Ward and French 2006). Minor phases including calcite, feldspar, quartz, and anorthite may also have been present and have been reported by other investigators (Ward and French 2006). Samples subjected to XRD analyses were run using Plexiglas sample holders that give a notable amorphous background "hump" in the 10-20 deg 2-theta range. In many of these samples there was substantial background noise in the 20-35 deg 2-theta range overprinting the sample background which was indicative of significant amorphous constituents(s) in the specimens run. These results are consistent with the presence of glassy constituents that were apparent in SEM images of the fly and bottom ash samples (Connolly 2011).

Table 13. Mineral phases present in the fly ash, bottom ash, and flue gas desulfurization sludge.

Sample Description	Major Phases		Minor Phases		
Fly Ash	Quartz	Mullite	Hematite		
Bottom Ash	Mullite	Quartz	Calcite	Feldspar	Anorthite
Flue Gas Desulf. Sludge	Gypsum		Quartz		

3.3.2.3 Column Studies

The intent of the column study was to simulate the effects of the infiltration of rain water or natural ground water through buried CCBs and to determine the sequence of constituents that would be present in leachates from material disposed in the unlined SJCM.

Columns were constructed from clear acrylic Excelon R - 4000 Transparent Rigid pipe. Two inch ID pipe was used. Each column was 10 inches long and was fitted with clear acrylic 1 inch thick caps that contained an O-ring and ½ inch drilled holes through each cap to allow installation of barbed fittings for attaching flexible tubing. Jaco - Kynar®, nylon, and polypropylene tube and hose connector fittings were used to connect hosing to the columns to Erlenmeyer flasks as seen in Figure 30.



Figure 30. Photo of 2 in ID by 10 in tall columns used in column leach studies.

Eight samples were selected for the column leach tests which were selected to be representative of fresh, young and old buried ash. These samples consisted of fly ash (two fresh, one young, two old), bottom ash (one each fresh and old) and spoil/top cover material. Water collected from the number 8 Coal Seam at SJCM was applied to the second set of samples of fresh and buried fly ash.

No 8 Coal Seam water provided by BHP Billiton was used to simulate the effects of ground water migration through the buried waste. Its composition is compared to historical monitoring information provided by MMD from the G-26 and G-3 well at the SJCM and the results are shown in Table 14.

Table 14. Comparison of the composition of No 8 Coal Seam Water used in column leach studies to the range of water quality measurements from monitoring data.

Parameter	No. 8 Coal Seam*	No 8 Coal Seam Since 2005	
	Column Water	Low	High
pH		7.9	8.7
Spec cond (uS/cm)		5160	7280
TDS		3190	4850
TOC		4.4	50
K	4.4	3.5	4.9
PO ₄		0.06	0.46
Ca	14.27	7.9	20
Mg	5.2	2.5	8
Na	1959	1090	1650
H ₂ S		0.22	171
Phenols			
HCO ₃		760	1720
CO ₃		1	220
Cl		58	520
F		1.9	4
SO ₄		580	3000
NO ₃		0.02	2
Al	-0.047	0.1	0.1
As	-0.043	0.0005	0.005
B	1.6	0.8	1.4
Ba	0.013	0.0179	0.2671
Cd	-0.039	0.00005	0.001
Cr	-0.033	0.001	0.095
Cu	0	0.0001	2.4
Co	-0.038	0.01	0.0161
Fe	-0.063	0.03	0.08
Pb	-0.053	0.0001	0.01
Mn	-0.034	0.005	0.023
Hg		0.002	0.002
Mo	-0.022	0.005	0.005
Ni	-0.044		
Se	-0.107	0.005	0.025
Ag	0.043		
V	-0.009	0.0005	0.1
U		0.00001	0.001
Zn	-0.054	0.007	0.16
Ra-226		0.23	1

*Analysis of No. 8 Coal Seam Water Used in Column Studies

No. 8 Coal Seam water was used to simulate the effect of ground water inflow into the buried waste from the surrounding aquifer that will occur after underground mining was completed. DI water was applied to the other 6 columns to simulate the effect of rainwater infiltrating through the buried CCBs.

The physical characteristics of fresh and aged CCBs collected during the field sampling campaigns were determined by UNM graduate student Ryan Webb in a companion study (Webb et al. 2012). The columns were packed to a density of 64.2 lb/ft^3 which corresponds to the approximate density and porosity of CCBs buried in the mine. This produced an estimated interstitial pore volume of 34.3 mL in each column. During the leach tests one pore volume of fluid was added each day for a period of 30 to 37 days. The intent was to simulate accelerated leaching under unsaturated conditions, and these conditions were confirmed by visual inspection of each column during the study. Leachate samples were collected every 2 days producing a total of 12 to 16 samples, each representing 2 pore volumes of sample. These samples were analyzed by UNM-EPS Geochemical Laboratory for the contaminants listed on the drinking water standards in Table 11.

3.4 Results and Discussion

3.4.1 Chemical Characteristics of CCBs

3.4.1.1 Composition of CCBs and Leachate Characteristics

A number of studies have been conducted on the chemical composition of the CCBs at the SJCM as part of the mine’s quarterly testing requirements of the MMD (Table 15). The results of these tests are similar to the results observed in the column study. Slight differences in MMD quarterly reports compared to the UNM column studies may be due to difference in CCB samples, analytical methods and leaching procedures.

Table 15. Previous leach tests of CCBs from the San Juan Coal Mine and results for key parameters.

Study	Date	Parameters					
		pH s.u.	Arsenic mg/Kg	Boron mg/Kg	Barium mg/Kg	Magnesium mg/Kg mg/L	
Intermountain Laboratories, Inc.	January-98	11.92	0.160	230	360	720	<0.2
Intermountain Laboratories, Inc.	May-02	12	0.110	250	470	900	<1
Current Study	April-11	11.64	0.185	340	1934	656	0.56

Table 16. Elemental composition of CCBs following nitric acid digestion.

Sample (mg/Kg)	Spoil			Fresh			Buried		
	min	max	ave	min	max	ave	min	max	ave
Analyte									
Ag									
Al	19327	29838	24417	43650	43650	43650	32327	39540	36003
As	0.091	0.091	0.091	0.062	0.185	0.124	0.110	0.236	0.185
B	3355	5639	4266	338	342	340	525	3145	1275
Ba	1403	2238	1802	223	1561	892	1422	2534	1934
Be									
Ca	743	5839	3610	7669	8186	7928	4500	6269	5692
Cd									
Co	5	13	9	7	9	8	5	12	8
Cr	15	25	19	14	17	15	13	17	14
Cu	12	43	22	31	37	34	30	39	35
Fe	17383	22562	19440	20804	20941	20873	19798	22908	21529
K	3714	11370	8318	3564	3962	3763	2171	3815	3069
Li	70	606	357	730	774	752	442	601	545
Mg	180	929	450	492	656	574	340	484	392
Mn	125	357	233	115	119	117	122	169	137
Mo									
Na	8381	17216	13710	8535	8945	8740	7016	9437	8400
Ni	7	14	10	6	7	7	6	9	7
Pb	3	24	10	12	13	12	7	19	13
Se									
Si	90463	220434	150222	56692	82234	69463	68352	163049	111161
Sr	32	110	57	82	124	103	89	110	100
V	37	67	50	41	51	46	42	60	48
Zn	43	73	53	39	99	69	22	40	30

The results shown in Table 16 are consistent with previous reports which show that CCBs from western coal contains elevated levels of calcium and iron (Manskinen, Poykio, and Nurmesniemi 2011). Silicon is the most abundant element as expected since silica is a major constituent of most dirt/clay earthen materials. It is usually present in the form of glass (SiO₂) due to the high temperatures in the combustion furnaces where the coal is burned. Sodium and Barium are the most abundant trace elements in the fresh CCBs.

The FA and BA samples have higher levels of Al and Fe than in spoil samples. Also, the alkali and alkaline earth elements such as Na, Ba and Ca all have higher concentrations in the buried fly ash than the fresh fly ash. These higher concentrations are likely the result of leaching from the buried CCBs as mineral phases associated with these elements are often somewhat soluble. The BA has a similar composition to that of FA. Boron concentrations were approximately 2% in the FGD sludge and higher than those in FA and BA which were generally less than 1% on a mass basis.

Deionized (DI) water extractions were used to help identify constituents that have the potential to leach as a result of rain water and snow melt passing through the material. Studies conducted for the mine have found that DI water leachate from CCBs will result in appreciable concentrations of Ca, SO₄ and Na (Luther, Musslewhite, and Brown 2009). The results of the DI water leach studies are presented in Table 17 for selected constituents with a full data set available in the Appendix .

Table 17. Anionic constituents in DI water extracts for surface cover materials (spoil), fresh and buried ash samples

(mg/Kg)	Surface Cover Material			Fresh Ash			Buried Ash		
Analyte Name	min	max	avg	min	max	avg	min	max	avg
F	1.10	10	3	14.0	14	14	6	7	6
Cl	3	106	43	34	41	34	11	15	13
NO ₂	0.04	5	0.8	0.3	3	3	0.73	1.22	1
Br	0.04	0.15		57.3	57	57		0.64	1
NO ₃	18	65	41	90.2	90	90	3	4	4
PO ₄	0.26	0.26							
SO ₄	3008	66300	24465	1034	1034	1034	2044	2386	2207

The elevated concentrations of Fe, Pb, As and Ba in buried ash is believed to be due to the reactivity of the ash materials with water. Barium had the highest concentrations in the buried ash which is believed to be due to the high solubility in water. Water is added to the CCBs during transport to the mine in part for dust suppression and this water may have resulted in leaching of Ba from the upper levels of the disposal cell into the lower levels and accumulating there. Native soil used as cover for the CCB pits contained high concentrations of vanadium (V) and sulfate (SO₄²⁻). These constituents are characteristic of soils in the area.

The constituent concentrations from the leach tests for fresh and buried CCB samples were compared to determine changes in composition with time. Fresh CCB samples showed elevated concentration of nitrite (NO_2^-), nitrate (NO_3^-), Ca, Mg and Sr. These constituents occur naturally in CCBs. Buried CCB samples contained higher concentrations of As, Ba, Fe, and Pb than fresh CCB samples.

While there is a difference between the leachate composition for the spoil, fresh, and old CCBs, it is not possible to which of these is the principal source of constituents in leachate from the buried waste. This is because the mine contains a mixture of all three waste types. Furthermore, the concentrations of the constituents in the leachate of the CCBs is similar to that from the spoil or top cover material. The leachate composition is also not too dissimilar from the composition of native ground water as represented by the chemical characteristics of No. 8 Coal Seam water.

Arsenic concentrations in leachate from the CCBs and the spoil exceed the EPA drinking water standard of 10 $\mu\text{g/L}$. Figure 31 shows the different total concentration of arsenic present in the spoil, fresh fly ash, fresh bottom ash, old fly ash, old bottom ash, and young fly ash. Leachate from FA has roughly twice the As concentration of leachate from BA. The leachate concentration of As from buried samples is higher than in fresh samples. Although As is relatively soluble in water is thus subject to aqueous transport, it is not clear what mechanism is responsible for this difference. It could be due to weathering and partial dissolution of amorphous materials in the CCBs or simply differences in the As content of fresh CCBs in contrast to those produced by coal combustion several decades in the past.

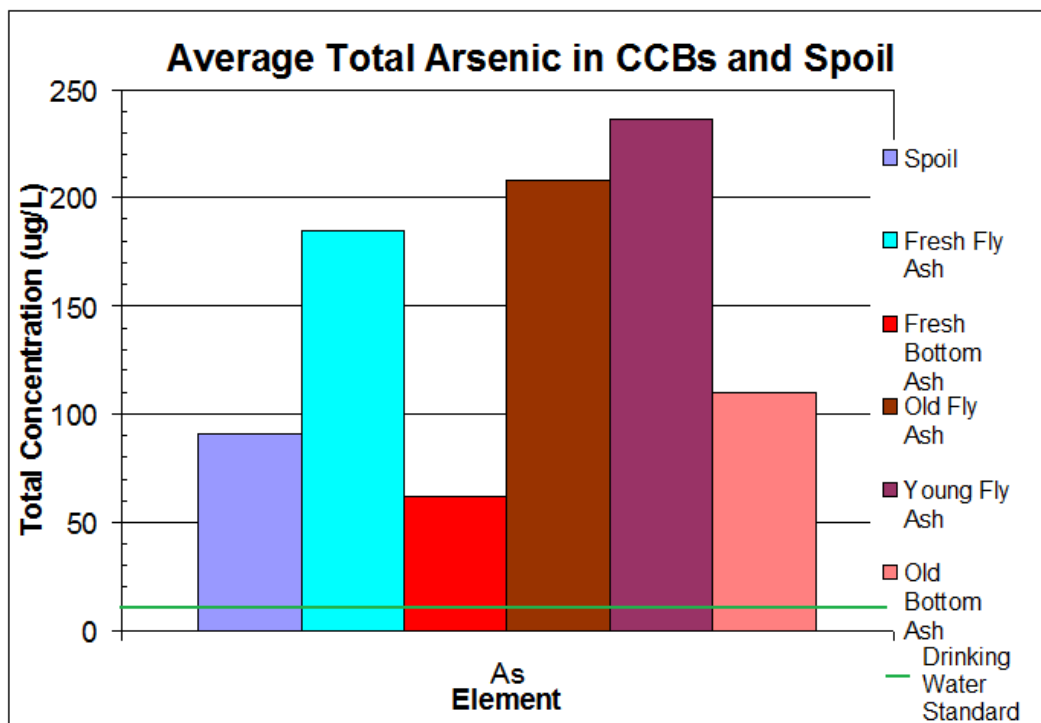


Figure 31. Average total arsenic concentrations in fresh and aged CCBs and spoil material.

3.4.1.2 Variation of CCB Composition with Depth

One of the objectives of this study was to determine if the composition of CCBs vary with time as a result of either geochemical processes within the fill, or perhaps as a result of different chemistry of the source coal. The depth of buried CCBs serves as an approximate indicator of their age; deeper material is older than material near the top of the landfill. The results of acid digestion of buried ash materials are compared in this section. The total concentrations for each constituent for the fresh fly ash and old fly ash samples taken from SM04 were plotted against depth. As previously stated exact ages of the buried CCBs is not known. However, it is clear that age increases with depth with the deepest CCBs being buried approximately 30 years ago.

Nickel concentrations remained fairly constant over depth but showed a slight trend downward as depth increased. This downward trend may be due to Ni leaching from the buried CCBs by water in the disposal cell.

Analyses of acid extracts of buried CCBs found an increasing concentration of Ba and possibly B (Figure 33) with depth while the other constituents did not appear to change with depth of sample. The concentrations of Ba is highest in the oldest samples which may be due to weathering of the shallow material and transport to deeper sediments in the mine. It could also be due to changes in air pollution control equipment at the power plant. This deep ash is presumably older than the EPA's regulations on discharge, allowing for the increased capture or release of each parameter respectively, as seen in Figure 32 through Figure 34.

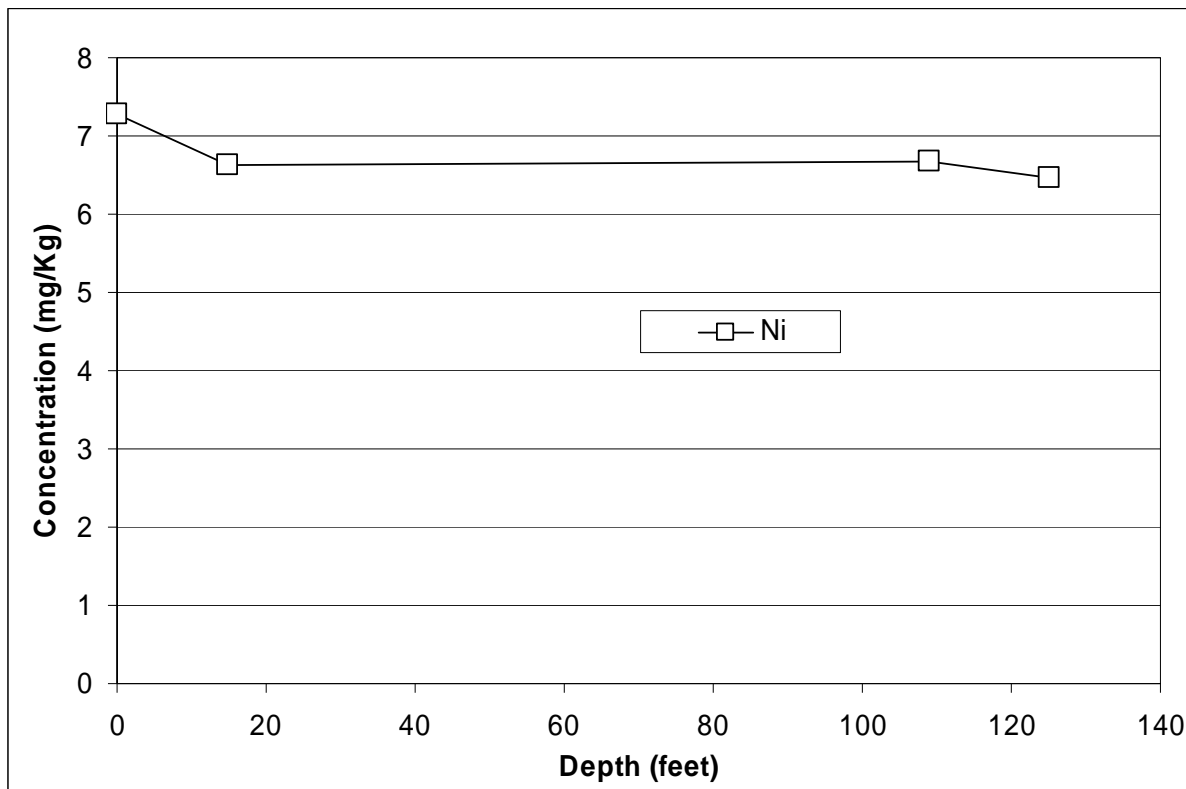


Figure 32. Concentration of Nickel in buried CCBs versus sample depth

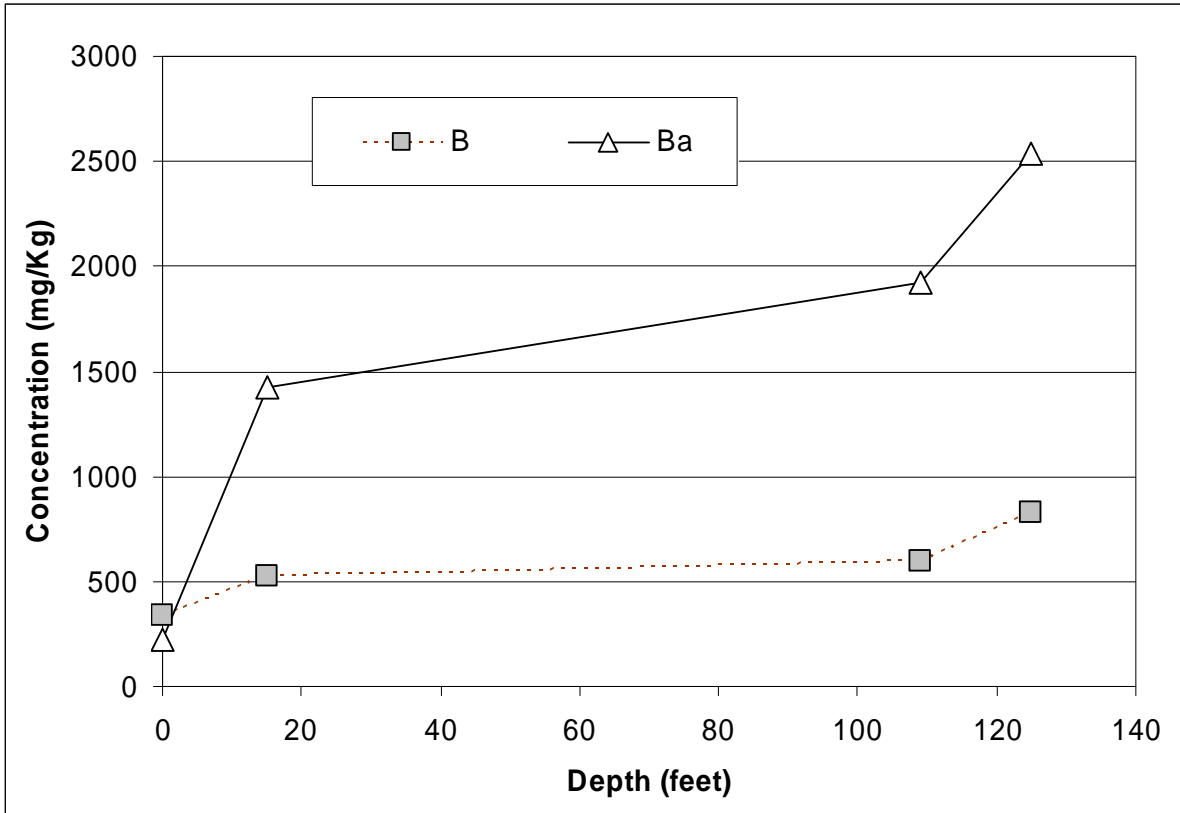


Figure 33. Concentration of Barium and Boron in buried CCBs versus sample depth

Iron (Fe) concentrations increased with depth then leveled off before dropping at the greatest depth (Figure 34). The high concentrations at intermediate depth may be due to geochemical transformations within the CCBs while the drop at the end could be due to changes in coal composition or changes in the material captured by air pollution control equipment at the power plant.

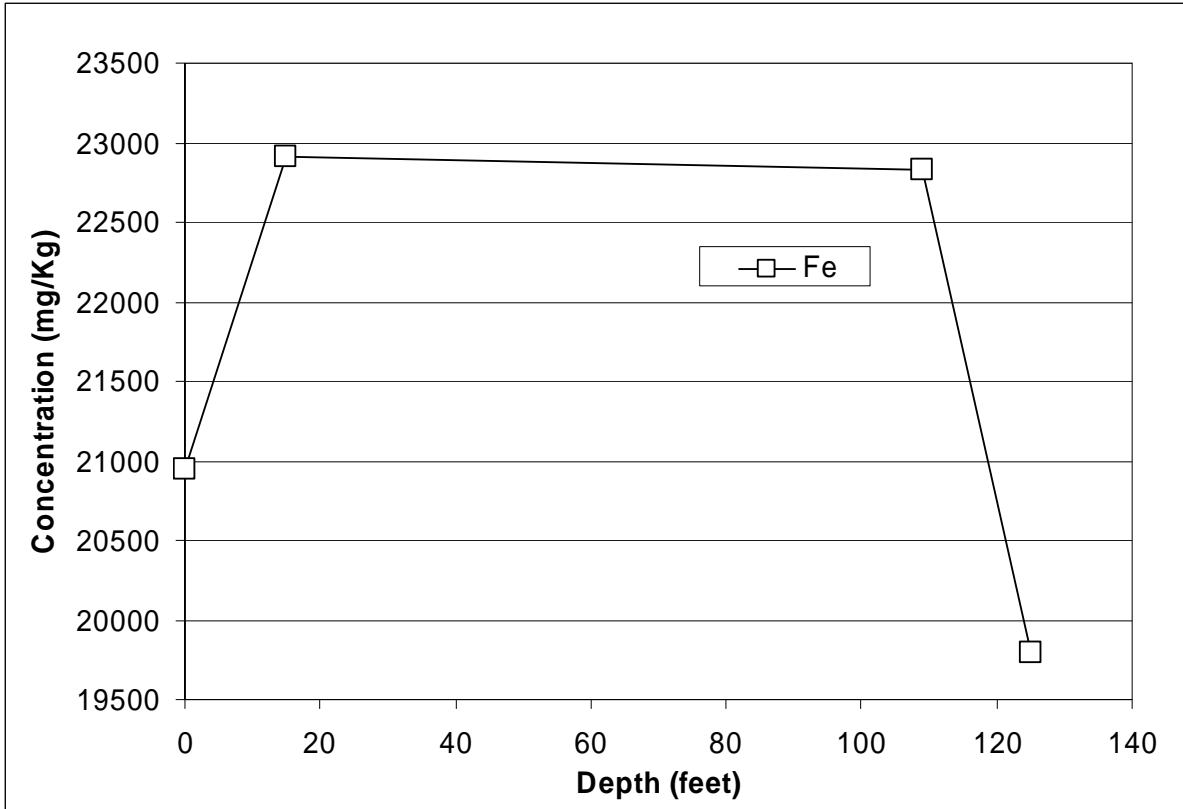


Figure 34. Concentration of Iron in buried CCBs versus sample depth

The concentration of Sr and Mg in acid extracts declined from initial fresh concentrations, but did not decrease below 10 feet in depth which is shown in Figure 35 and Figure 36. Strontium and Mg both have solution chemistry that is similar to Ba and Ca and are relatively soluble in ground water (Patnaik 2002). Thus, leaching of fresh CCBs by water infiltrating through the disposal cell may result in decreased Mg and Sr concentrations of fresh material near the top of the cell. Re-distribution of the dissolved constituents in deeper material may explain the uniform concentrations in deeper material.

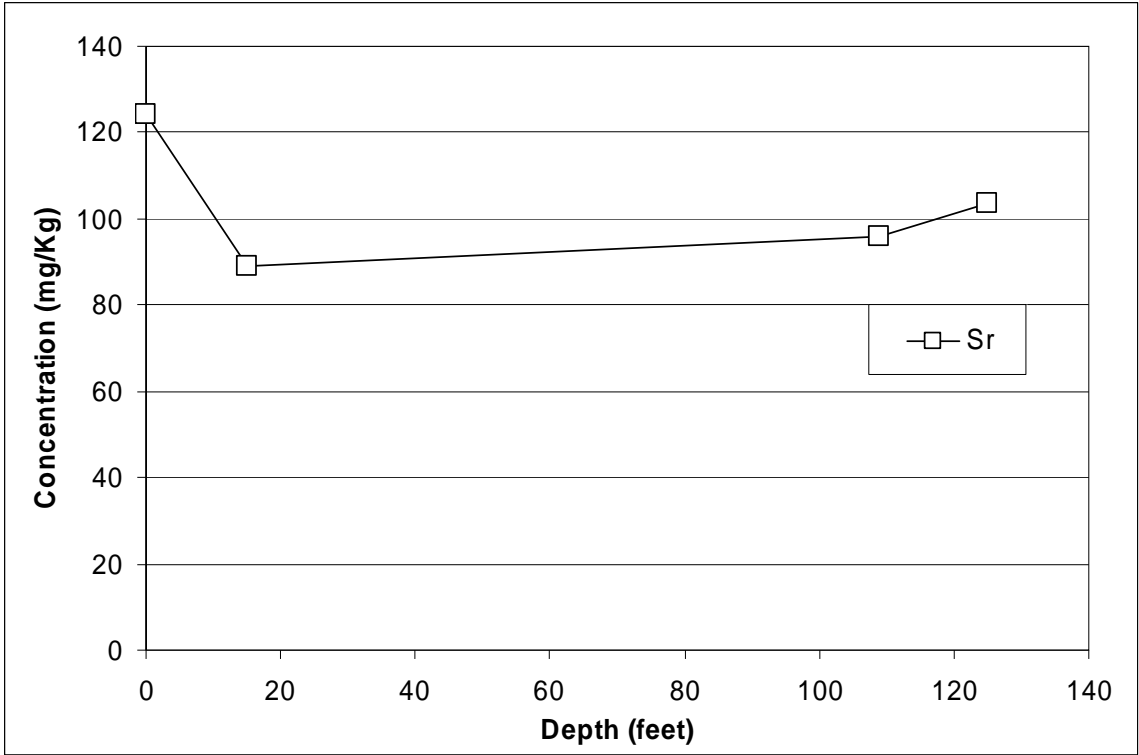


Figure 35. Concentration of Strontium in buried CCBs versus sample depth

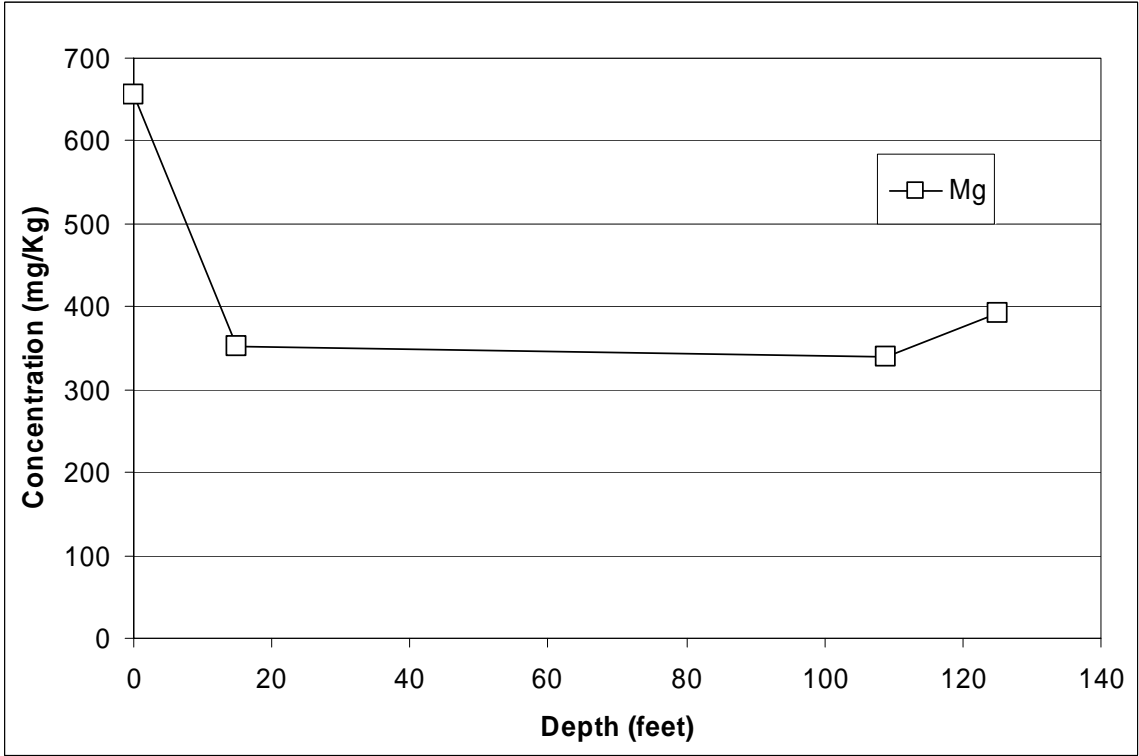


Figure 36. Concentration of Magnesium in buried CCBs versus sample depth

The overall changes in elemental concentration with depth shows that variations in the source coal and type of air pollution control equipment used at the plant may affect the composition of the ash. This is expected and has been reported in other investigations which have found that, aside from the composition of the inorganic constituents in the parent coal, a major factor affecting the chemistry of CCBs is the incineration and type of air pollution control systems (El-Mogazi, Lisk, and Weinstein 1988).

The elemental concentrations of acid extracts from fresh and buried CCBs were normalized by dividing the concentration of each element in the buried samples by their concentration in fresh FA. This facilitates comparison of constituents with very different concentrations. Normalized concentration plots for all constituents measured in this study are presented in the appendix. The normalized concentrations for As and Ba are plotted versus depth in Figure 37.

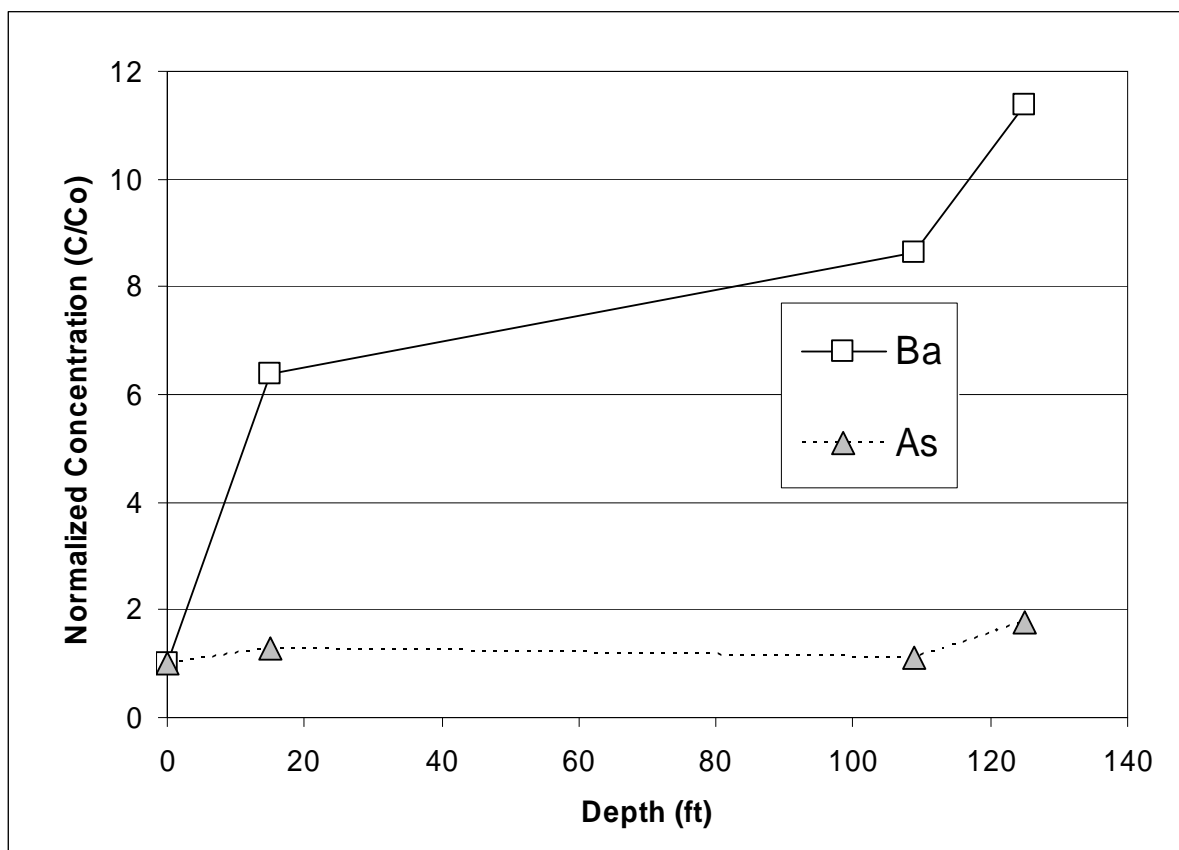


Figure 37. Normalized concentrations of Barium and Arsenic in Fly Ash leachates versus sample depth.

Figure 37 shows that the largest change in concentration with depth was an increase in Ba and As concentrations. Barium and As show elevated concentrations within CCBs compared to the spoil and increase in concentration with depth. This phenomenon may be due to dissolution of As and Ba and vertical transport to depth in the disposed ash. However, because As is naturally present in the ground water at elevated concentrations its presence is a poor indicator of the impact of CCBs on ground water quality (Figure 31).

Normalized concentrations of Boron (B), Cobalt (Co), Chromium (Cr), Nickel (Ni), and Silica (Si) are plotted in Figure 38. A plot of normalized anion concentrations in deionized water leachates of CCB as a function of depth is presented in Figure 41. It should be noted that the decrease/increase on the last data point can be misleading for reasons discussed above which involve the coal burning process.

Other constituents also showed increasing (Figure 38), constant (Figure 40) and decreasing concentration trends (Figure 39) although these differences are not as pronounced as for Ba.

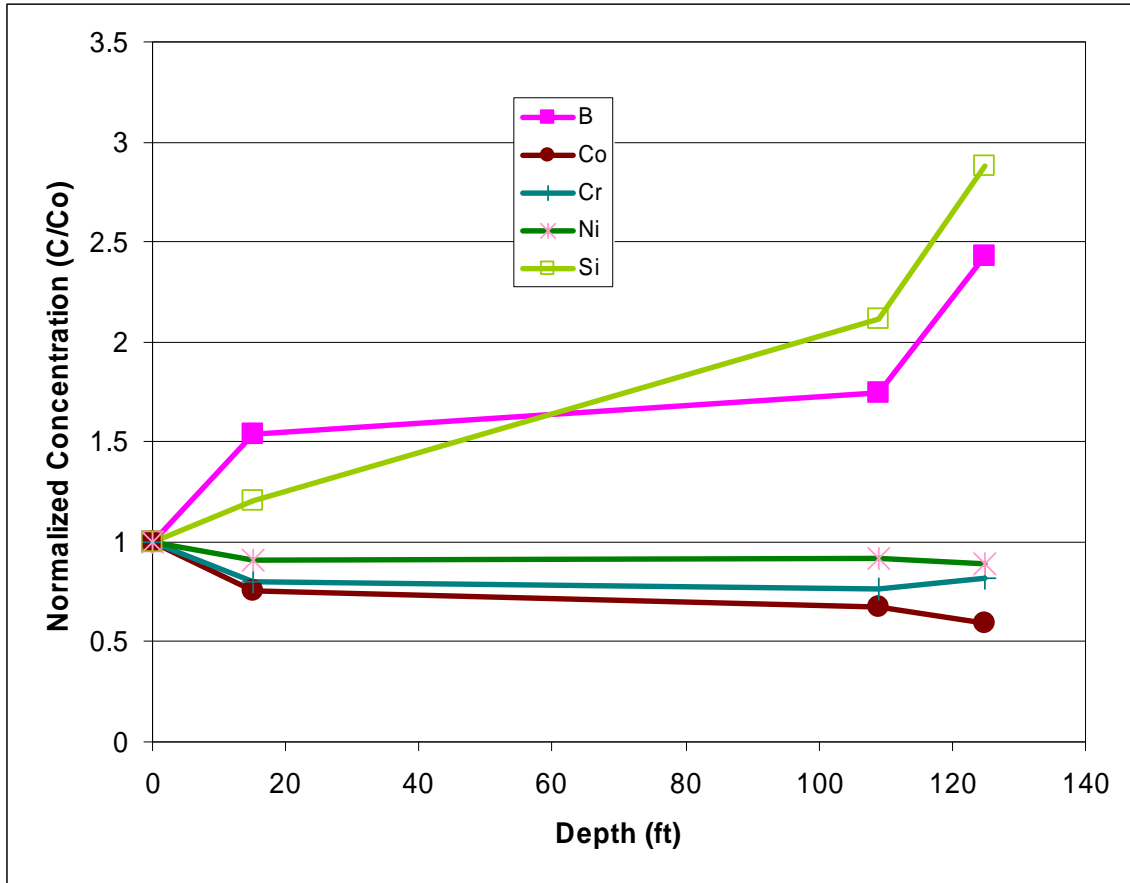


Figure 38. Normalized concentrations of elements with depth (B, Co, Cr, Ni, Si)

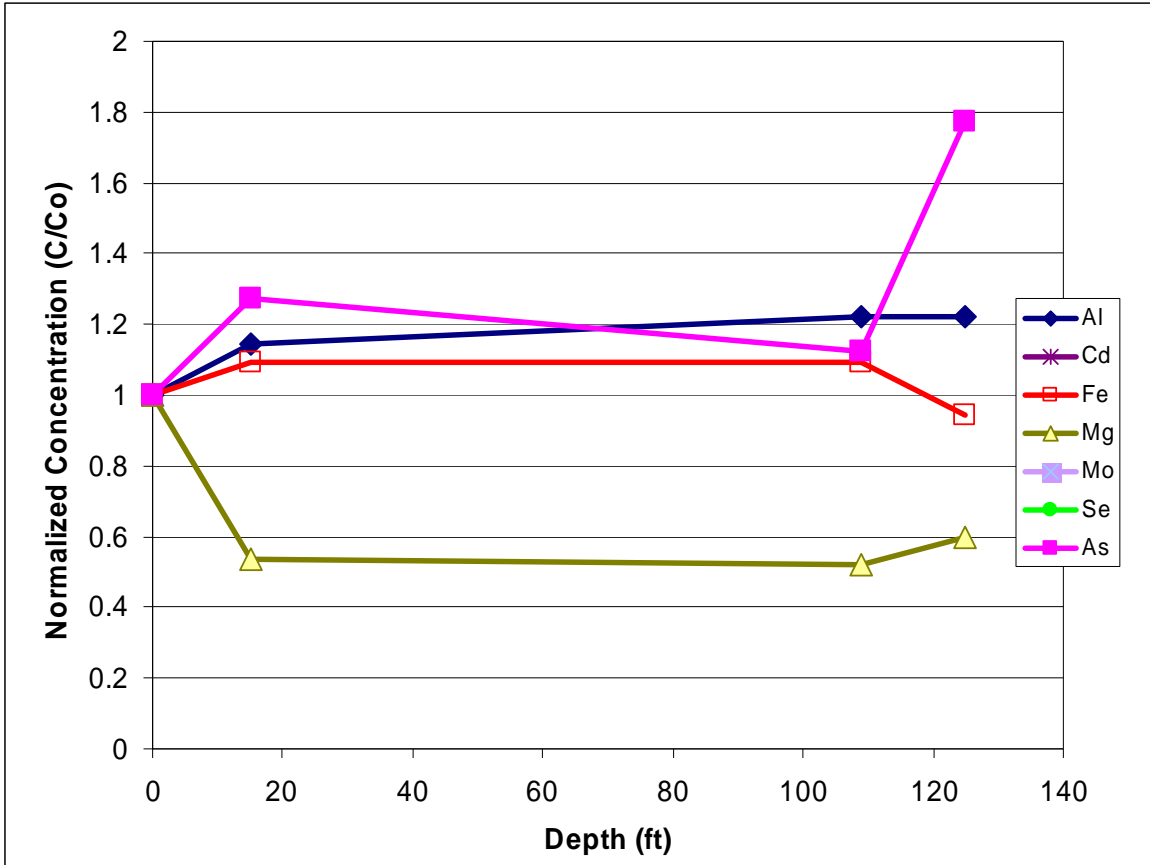


Figure 39. Normalized concentrations of elements with depth (Al, Cd, Fe, Mg, Mo, Se, As).

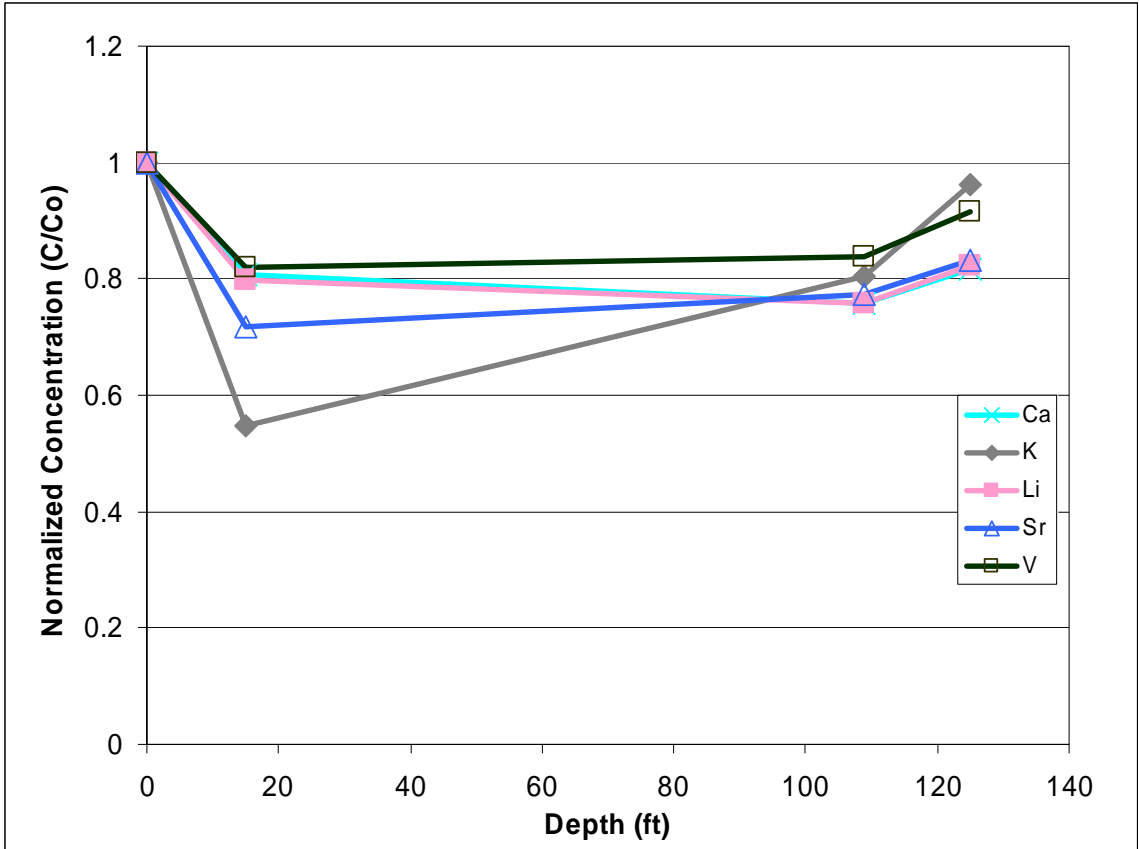


Figure 40. Normalized concentrations of elements which varied little with depth (Ca, K, Li, Sr, V).

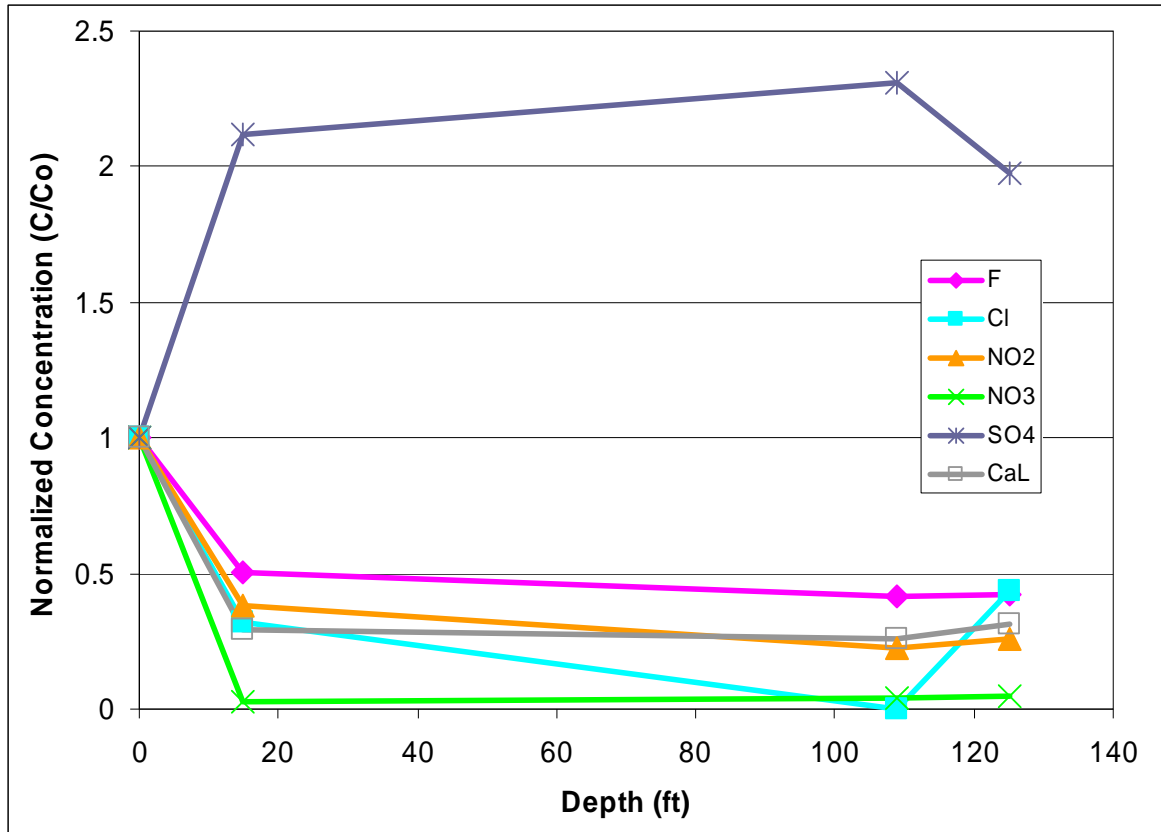


Figure 41. Normalized anion concentrations versus depth (F^- , Cl^- , NO_2^- , NO_3^- , SO_4^{2-} , Alkalinity)

Increasing elemental concentrations in buried samples may be the result of transport of leachates from overlying material migrating to underlying materials. Similarly, decreased constituent concentration in shallow wastes may be the result of leaching by water added to the wastes during disposal and water from atmospheric precipitation. Anions and elements associated with soluble precipitates would be most susceptible to this mechanism. The relatively constant concentration of elements including Al, Cd, Fe, Mg, Mo, Se, Ca, K, Li, Sr, V is likely due to their presence in insoluble phases such as aluminosilicate, feldspar, and quartz minerals.

3.4.1.3 Column Tests

Column leach tests were performed to simulate the percolation of atmospheric precipitation (rain and snow melt) through the ash and FGD sludge to determine the sequence of analytes within the leachate from each material and to gain a better understanding of how composition of the leachate may change with time. The columns were filled with each type of waste material (FA, BA) as well as spoil material that is used for final cover of the buried wastes. Further, both fresh and aged samples from the drilling program were used in the column studies. DI water was used in six of the eight columns to simulate rain water passing through the pit while No 8 Coal Seam water was used in two of the columns to simulate inflow of regional groundwater into the mine. Table 18 shows the historical average and range of water quality data for No 8 Coal Seam water which is the native ground water that is likely to migrate into the SJCM when dewatering operations terminate.

The results of the column leach tests are described in this section. Plots of the concentrations for all constituents measured are presented in Appendix I. Generally the behavior of these constituents fall into two categories. The first group are elements which are not present in soluble minerals. The concentrations of these elements decreases asymptotically with time as they are washed through the columns. These elements include B, Ca, Mo, Na and Sr. The second group of elements are those which are associated with minerals or solid materials that may dissolve with time. These include Al, Li, Si, and V. The column studies found that the concentration of these constituents will increase with time until a new solution equilibrium state is reached after which their concentration will decrease with time similar to the other elements. This section discusses these results.

Table 18. Water Quality Results for No 8 Coal Seam Water used for column leach and historical data compared to typical water quality data

Parameter	No 8 Coal Seam Since 2005			Water Quality Data	
	Low	High	Average	Low	High
pH	7.9	8.7	8.143333	4.85	12.61
Spec cond (uS/cm)	5160	7280	5900		
TDS	3190	4850	4141	30	69800
TOC	4.4	50	13.9	0.001	415
K	3.5	4.9	4.04	0.001	286
PO ₄	0.06	0.46	0.168	0.001	34.8
Ca	7.9	20	13.88		4600
Mg	2.5	8	4.93	0.1	2270
Na	1090	1650	1371	0.1	27800
H ₂ S	0.22	171	83.19125	0.2	386
Phenols				0.001	7.8
HCO ₃	760	1720	1248	0.001	2970
CO ₃	1	220	61	75	
Cl	58	520	217.4		16700
F	1.9	4	2.333333	0.1	54
SO ₄	580	3000	1948	0.01	52000
NO ₃	0.02	2	0.295	0.5	180
Al	0.1	0.1	0.1	0.5	31
As	0.0005	0.005	0.00318	0.05	2.41
B	0.8	1.4	1.09	0.005	10
Ba	0.0179	0.2671	0.104256	0.001	51.6
Cd	0.00005	0.001	0.000441	0.00005	0.5
Cr	0.001	0.095	0.023	0.001	0.5
Cu	0.0001	2.4	0.26542	0.0001	8.7
Co	0.01	0.0161	0.01122	0.00028	0.3
Fe	0.03	0.08	0.048889	0.001	72.3
Pb	0.0001	0.01	0.00432	0.0001	2.82
Mn	0.005	0.023	0.009778	0.0005	12.4
Hg	0.002	0.002	0.002	0.0001	0.06
Mo	0.005	0.005	0.005	0.001	0.07
Ni				0.001	0.2
Se	0.005	0.025	0.0512	0.001	15.4
Ag				0.00005	0.5
V	0.0005	0.1	0.04499	0.0001	2
U	0.00001	0.001	0.000444	0.00001	150
Zn	0.007	0.16	0.05204	0.001	5.98
Ra-226	0.23	1	0.5925	0	579

The ratio of mass of water-to-mass of soil in the column tests was different than that used in the batch DI water extraction tests. The DI water extraction test used mass of water-to-mass of soil ratio of 20 while the ratio used in the columns tests was 0.14. Recall that one pore volume of water was passed through the columns each day, which explains this very low mass ratio. Others

report that low water-to-soil mass ratios can be representative when samples are corrected for water content (Bin-Shafique et al. 2006)(Ram et al. 2007).

The initial concentration of the dissolved metals and anions in the column tests varied widely depended on both the constituent being measured and the type of material in the column. This is illustrated by the concentrations of Na in the columns. Sodium is the most soluble metal in both FA and BA and its concentration from 2270 mg/Kg for Na in old buried bottom ash material to 0.18 mg/Kg for Ni in spoil material (Figure 42). Due to their very low concentrations, leachate results for Ag, Be, Pb, Zn, Mg, Cu, Mn, Ni, Co, Cd and Fe are not reported here. Results for these constituents are contained in the Appendix.

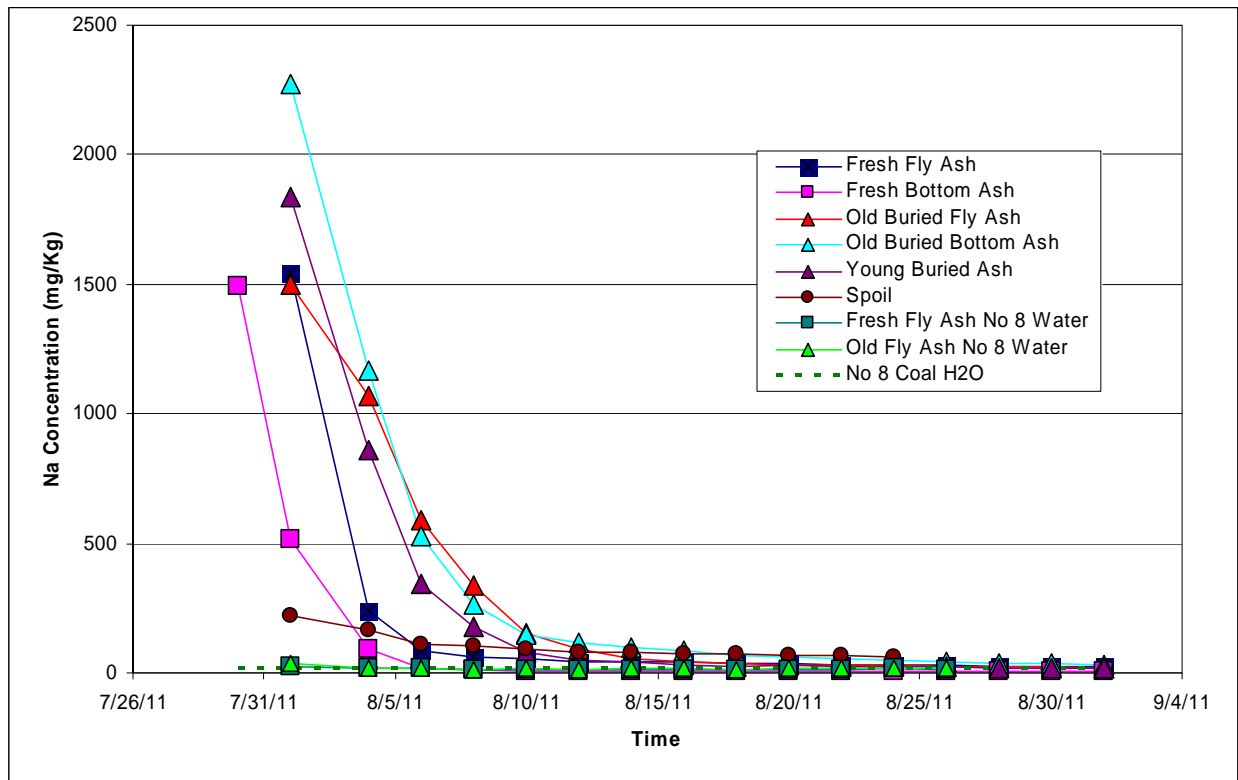


Figure 42. Column test concentration changes over time for Na with largest initial concentration

As with the batch leach results, normalized concentrations of each constituent were plotted to facilitate graphical display and comparison of leach behavior. The constituent concentrations were normalized by plotting the ratio $C/C_{initial}$ where $C_{initial}$ was the concentration in the first pore volume of water passing through the column (Figure 43 through Figure 53).

Though all columns were packed to the same approximate density of 64.2 lb/ft^3 , the differences in particle size resulted in very different hydraulic conductivities as discussed in Chapter 2 of this report. For example, it took DI water six days to pass through the column of fresh FA and samples were collected over the next 37 days. This was the only column in which precipitates appeared in the collected leachate. 18 days after the start of the leach test a white amorphous precipitate was noted and was consistently present in samples collected over the next eight days, then disappeared. The precipitate was believed to be an aluminum hydroxide. Results show that

Ba had the highest normalized concentration in the leachate and it was one of the constituents to leach first followed by Sr which then slowly declined with time. Calcium, Li and Al all appeared after 6 days but did not exhibit the very high normalized concentration increase as did Ba (Figure 43).

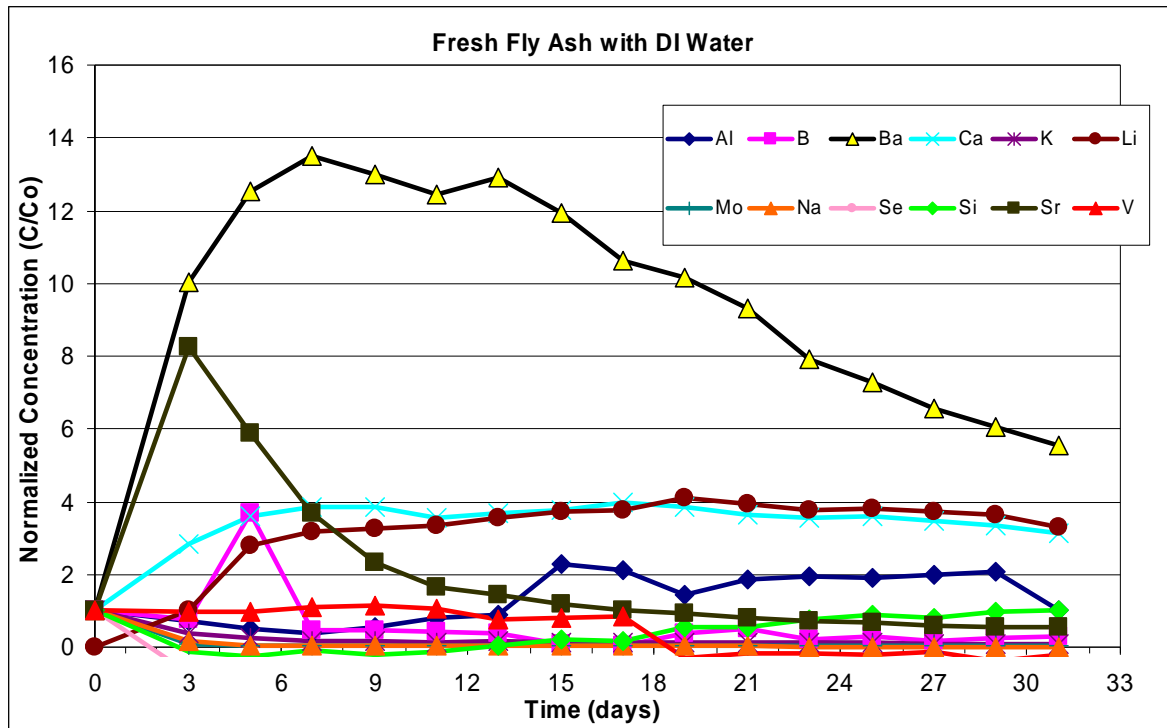


Figure 43. Normalized concentrations of constituents in DI water column leachate of fresh fly ash

The results of Figure 44 show that the concentration of Ca and Li initially spiked then leveled off. Boron, Na, K, Mo, Na and Se all showed the leaching behavior expected of readily soluble constituents that asymptotically approach zero as succeeding pore volumes of water pass through the column. Aluminum and Si displayed results that suggest dissolution of soluble minerals in which their concentrations spiked after 20 day then continued a slow increase. Mineral dissolution of aluminosilicates would result in this type of behavior and has been reported by others (Dudas and Warren 1987).

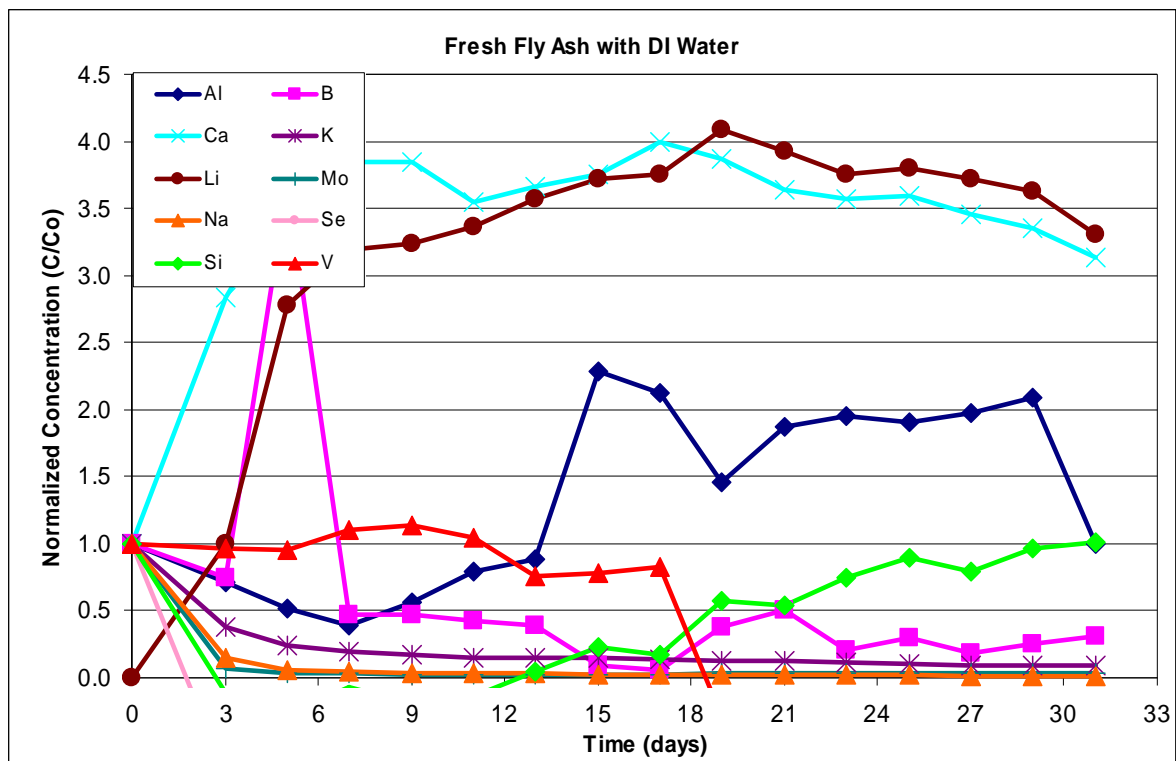


Figure 44. Normalized concentrations of constituents in DI water column leachate of fresh fly ash with Ba, and Sr removed

The column containing fresh BA took 5 days for DI water to pass through after which water was added to the column daily for 37 more days. The results shown in Figure 45 show that the concentration of most of the elements asymptotically decline and approached zero within 12 days. The concentration of Li and Al peaked slightly but then resumed an asymptotic decline (Figure 43). After 14 days the normalized V concentrations then resumed a slow decline which was similar to the leach behavior of the fly ash particles (Figure 43). The cause of this spike is not known.

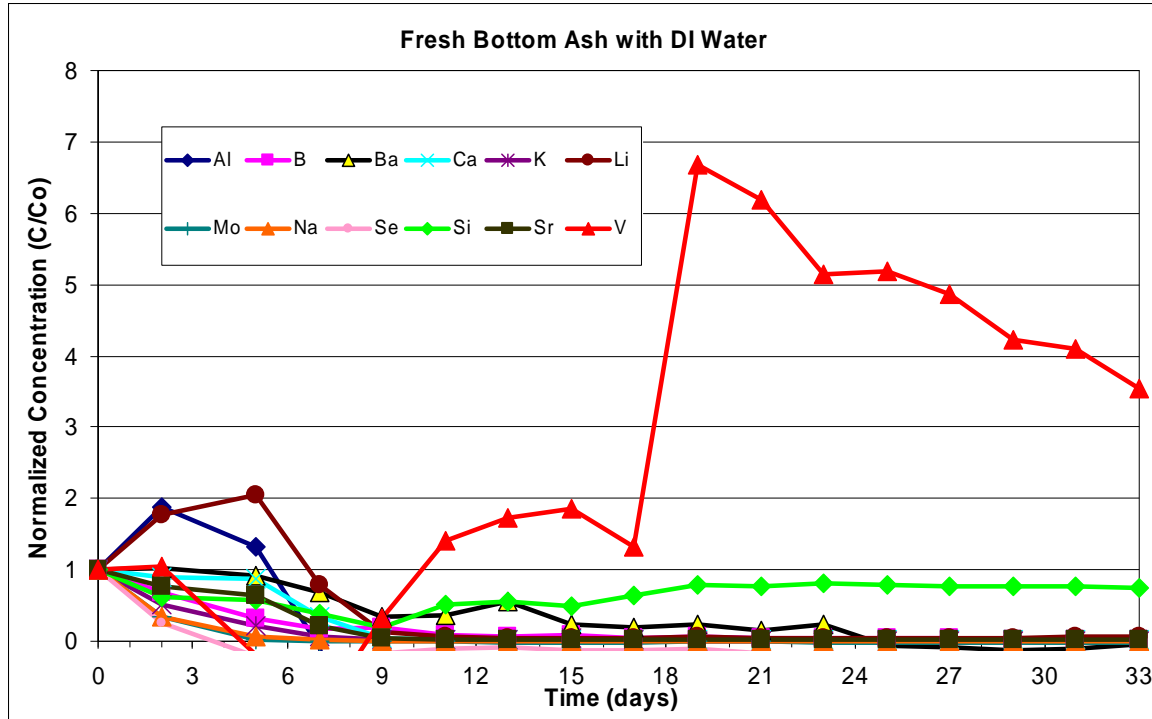


Figure 45: Normalized concentrations of constituents in DI water column leachate of fresh bottom ash

The column containing old buried FA took six days for the DI water to pass through. One pore volume of DI water was added daily and samples collected for another 31 days. Lithium was the only element that showed a dramatic change in normalized concentration relative to the other analytes (Figure 46). Except for except Ca, V and B, most of the constituents exhibited an asymptotic declining leaching trend. The concentrations of B, Ca and V remained constant throughout the 37 day period however, they were present at lower concentrations (1.5 C/C_o) than those found in fresh fly ash (2 C/C_o). This implies less weathering or mineral dissolution within the old fly ash than fresh fly ash over the same time period.

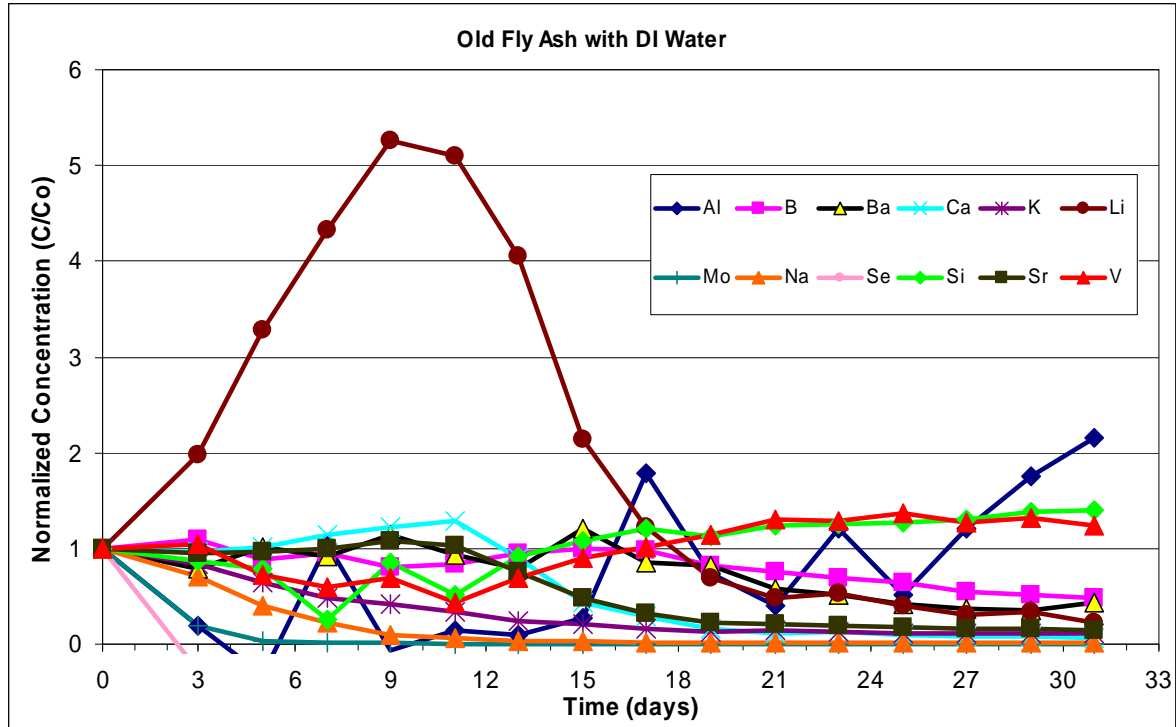


Figure 46: Normalized concentrations of constituents in DI water column leachate of old buried fly ash

The column containing old buried BA and leached with DI water took seven days for water to pass through and then leachate samples were collected for 31 more days. The leaching results (Figure 47) were more similar to those for old FA than the fresh BA leach column, with the majority of the elements following a characteristic asymptotically declining leach profile. The largest normalized leach concentration was for Li. The highest Li concentration was found in the old buried bottom ash, leached with DI water. The concentrations were twice those found in old fly ash and approximately six times larger than those leached from fresh bottom ash material. Vanadium, which leached to a large extent within the fresh bottom ash, showed a slowly increasing trend. Aluminum and Si showed a dissolution trend similar to that observed in other columns but at their highest the Al concentration were approximately three times higher than those seen in fresh BA (Figure 45).

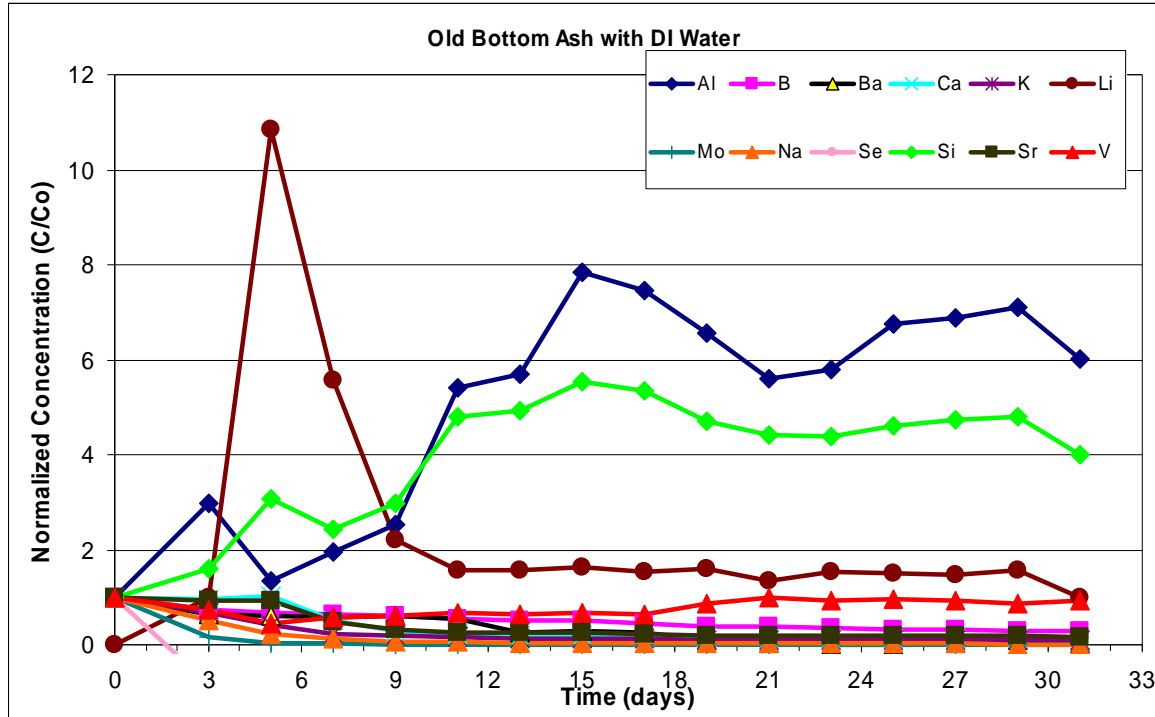


Figure 47: Normalized concentrations of constituents in DI water column leachate of old buried bottom ash

The column containing young FA leached with DI water took 6 days for water to pas through and then leachate samples were collected for another 31 days. The normalized concentration trends displayed in Figure 48 are similar to the leach sequence seen in the other FA columns (Figure 46 and Figure 43) with most the elements showing asymptotically decreasing leach profiles. Aluminum, Si, Li and V showed increasing concentration trends indicative of dissolution of CCB minerals with Al concentrations that were similar to those in old BA. The third Si data point is uncharacteristic of the trend and is believed to be an analytical error.

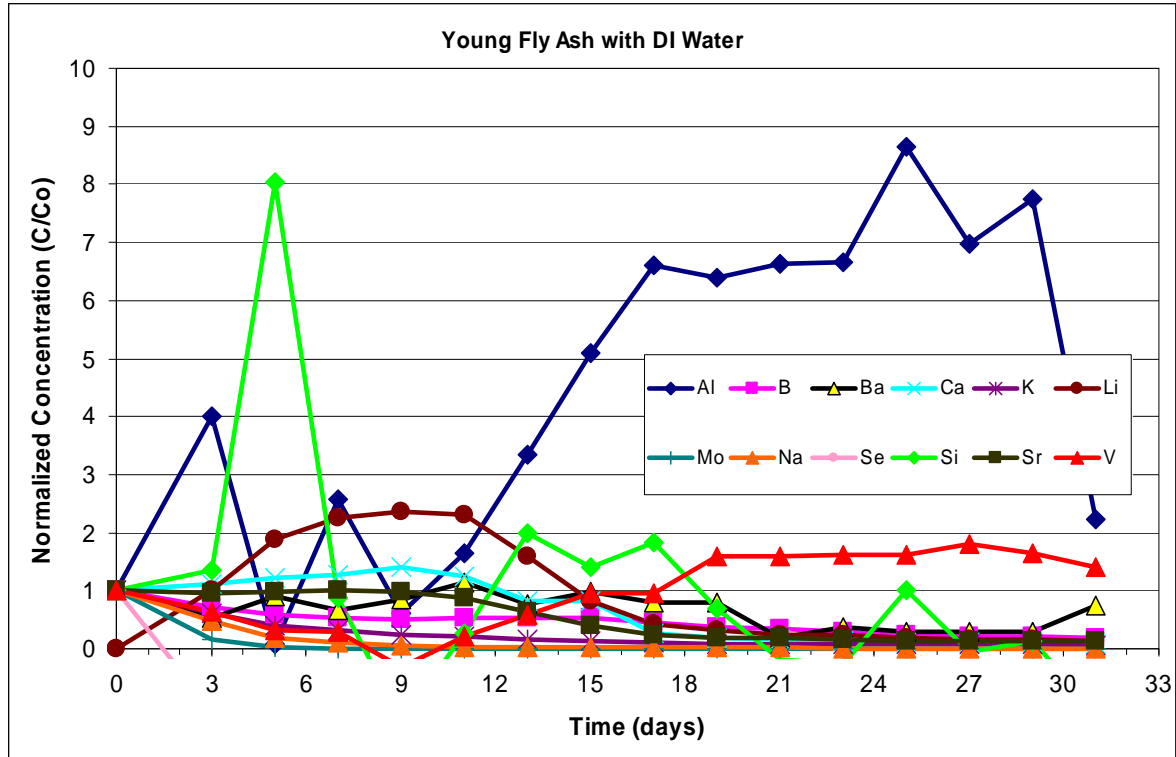


Figure 48: Normalized concentrations of constituents in DI water column leachate of young buried fly ash

The column containing spoil/top cover material was leached with DI water for 37 days. The hydraulic conductivity of this material was much lower than for the CCB materials which limited the amount of water that could be passed through this column. It took 14 days from the start of the test for water to pass through the column and no more than 10 mL was ever collected during the two day sampling interval, although 34.3 mL (one calculated pore volume) was added to the column daily for the first three days. By the fourth day the head space above the spoil material in the column was completely full of water as the water leached through at a much slower rate than the CCBs. Water was added until the head space above the spoil material was filled and then daily addition of water was discontinued except to keep the head space full. A total volume of 1,269 mL was added to the columns containing CCBs over 37 days while the spoil column only passed a total volume of 267.2 mL over 37 days. Clay in the spoil material results in a very low saturated hydraulic conductivity estimated at 10^{-6} cm/sec which prevented flow of water through the column. The normalized concentrations of constituents in the leachate from the spoil column are presented in Figure 49. DI water leachate from the spoil had higher B concentrations than in any of the CCB columns. Boron also leached first but after 2 days its concentration declined. Molybdenum was the next constituent to leach and took 12 days to decline and only showed up in trace amounts in other CCB columns. The rest of the constituents showed characteristic asymptotic leach curves with Li remaining fairly constant. The concentration of Al, Si and Li in the leachate from the column filled with spoil material did not increase in contrast to the other columns containing CCBs.

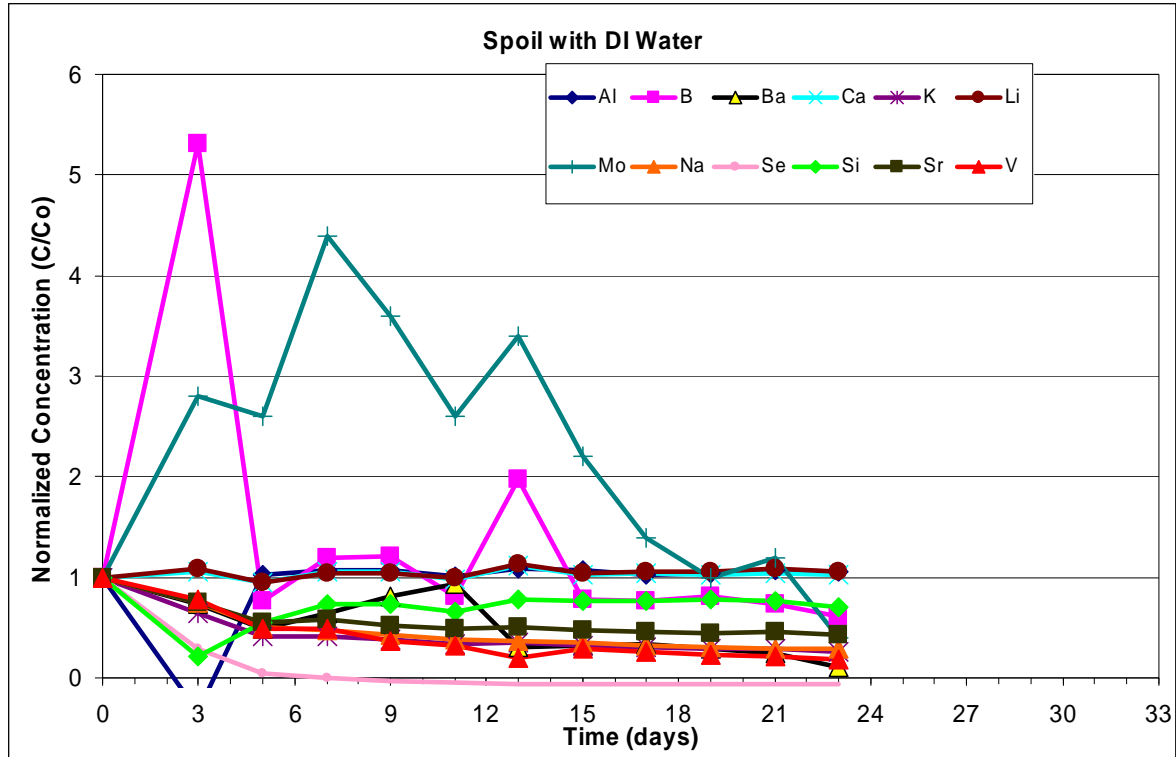


Figure 49: Normalized concentrations of constituents in DI water column leachate of spoil

A column of fresh FA was leached with No 8 Coal Seam water for 30 days. It took seven days for water to initially pass through the column. Normalized concentrations for this test are shown in Figure 50. Many constituents such as Se, Mo and Ba showed an expected decreasing concentration trend. Aluminum concentrations increased similar to young FA leached with DI water (Figure 48). Aluminum, Li and Si all showed distinct increasing concentration trends with time representative of mineral dissolution. Vanadium had higher normalized concentrations in fresh FA this column than the other columns and shows an increasing trend with time. The cause is not known.

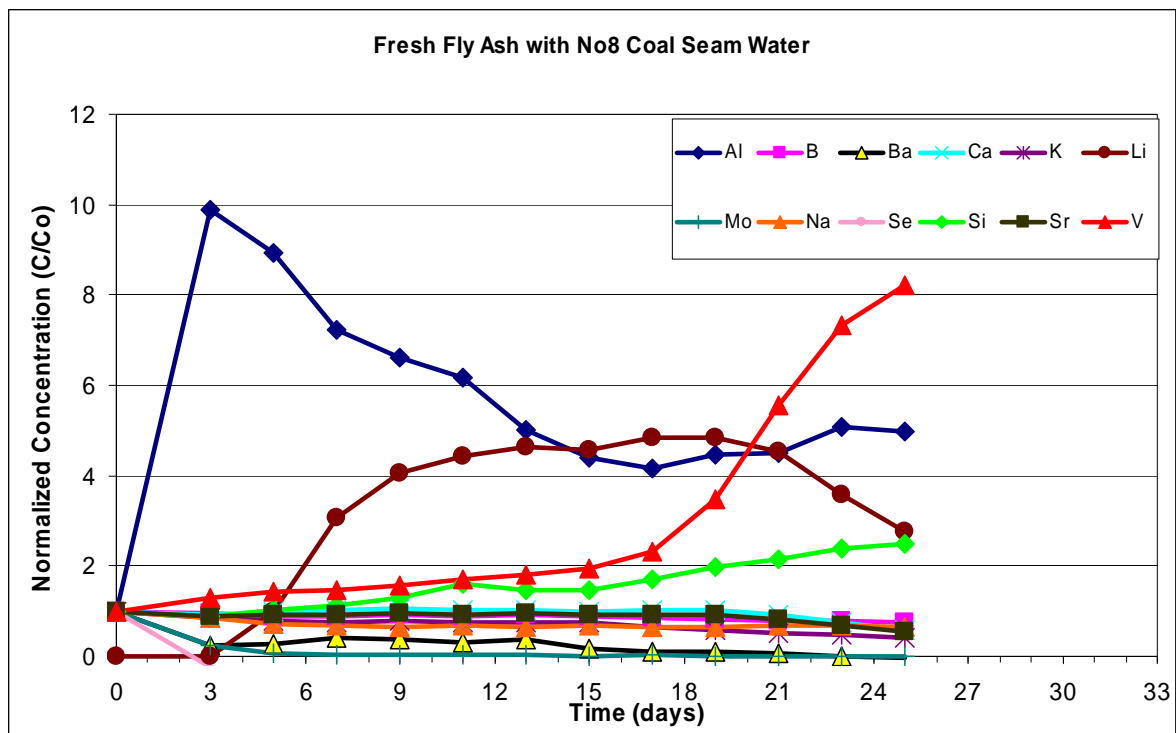


Figure 50: Normalized concentrations of constituents in No 8 Coal Seam Water column leachate of fresh fly ash

Figure 51 shows a plot of the leachate concentrations for the fresh FA leached with No. 8 Coal Seam water in which the concentration profiles of Al, Li, V and Si are eliminated to facilitate visualization of the concentration trends of the other constituents. Strontium and Na show a relatively consistent normalized concentration over time while the Se and Mo concentrations decrease quickly. The initial concentrations of these constituents, however, are small, near the detection limit of the analytical procedure used and results of subsequent samples was below the detection limit. Thus, the appearance of a rapid drop in their concentration would not likely be exhibited if a more sensitive analytical procedure was used.

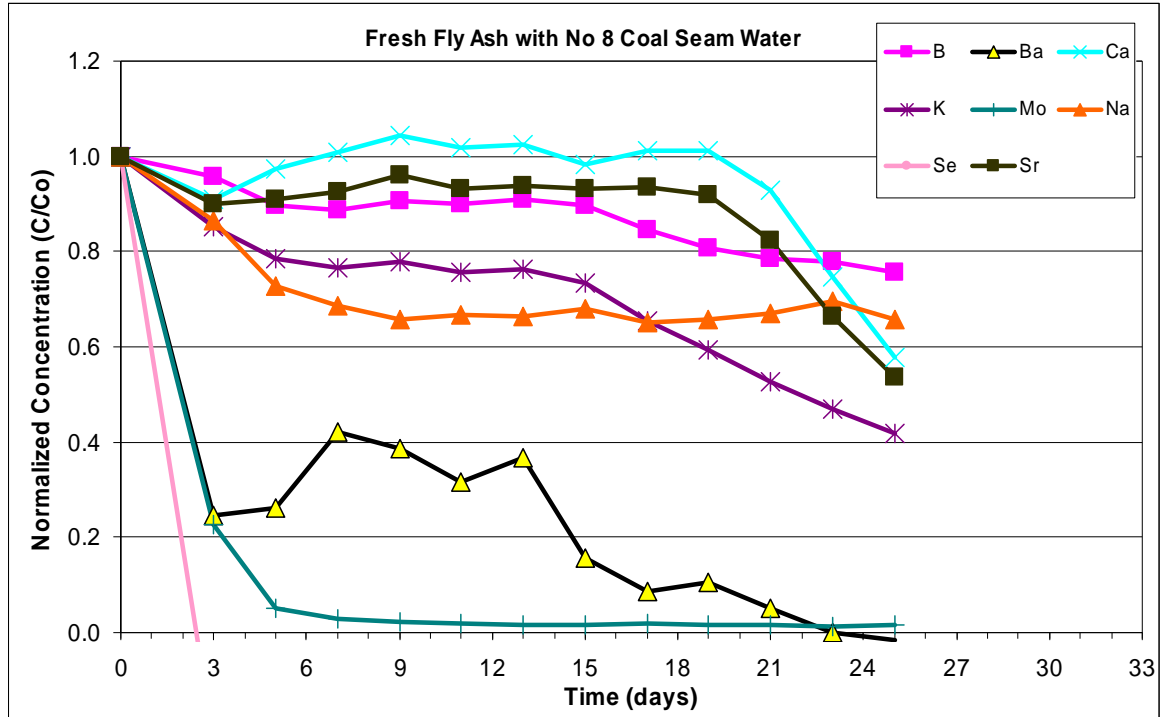


Figure 51: Normalized concentrations of constituents in No 8 Coal Seam Water column leachate of fresh fly ash with Al, Li and V not plotted

No. 8 Coal Seam water was passed through a column of old FA for 30 days (Figure 52). It took 7 days for water to initially pass through the column. Concentration of elements in the leachate show similar trends to fly ash leached with DI water. Barium had the highest normalized concentration in the leachate of all the columns and took 18 days to completely drop back to its original concentration. Aluminum and Si concentrations increased with time when leached with No. 8 Coal Seam water implying dissolution of aluminosilicate minerals.

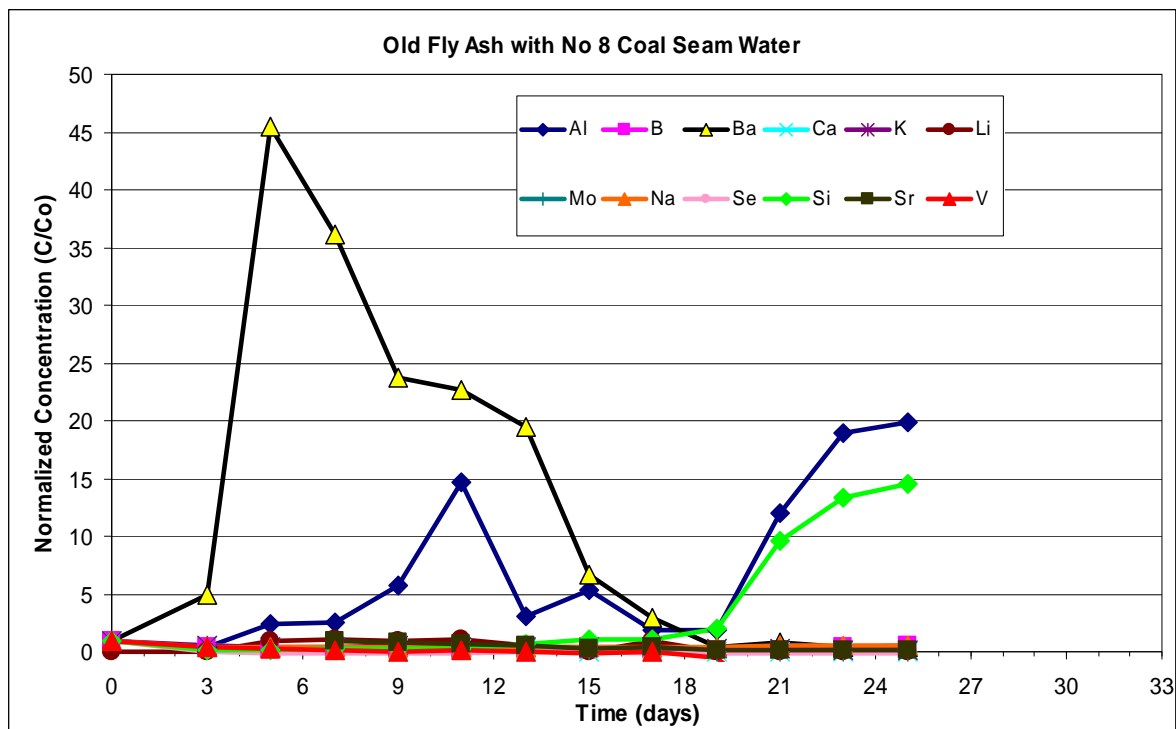


Figure 52: Normalized concentrations of constituents in No 8 Coal Seam Water column leachate of old buried fly ash

Removing Ba, Al and Si, from the data of Figure 52 facilitates examination of the leaching behavior of the other constituents (Figure 53). Lithium increased with time which is consistent with its appearance due to mineral dissolution trend while the remaining constituents show asymptotically decreasing concentrations. Strontium concentrations were not available for the first three data points thus the plot that appears to show delayed leaching is simply the result of using the results from the third sample as the normalizing concentration.

The trends of asymptotic concentration declines shown in Figure 53 demonstrate the consistency of the results. Such trends were seen throughout all the data with minimal jumps in concentrations such as that seen in Figure 53 on the 9th data point of Li. This, or the point immediately before it, is an anomaly that is believed to be due to analytical error.

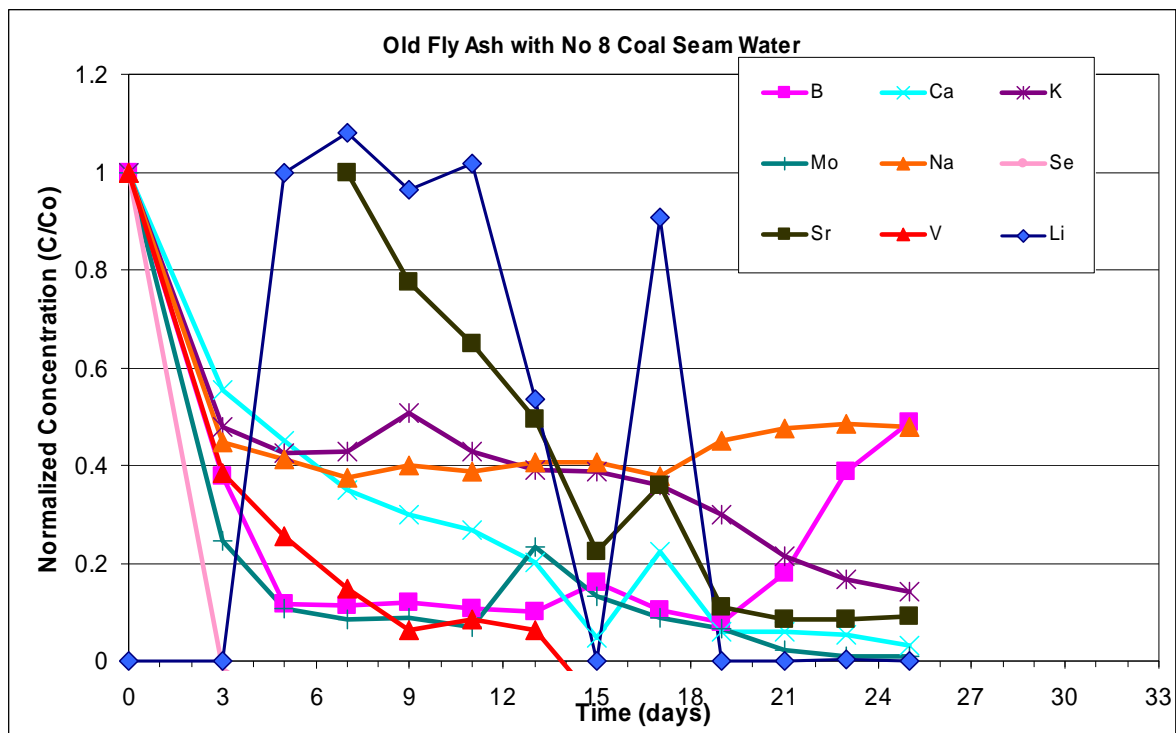


Figure 53: Normalized concentrations of constituents in No 8 Coal Seam Water column leachate of old buried fly ash with Ba, Al and Si removed

The results of the column leach studies show that the range of constituent concentrations depends in large part on the characteristics of the water that is in contact with the buried CCBs. The pit stratigraphy and the material contained in them varies with location as CCBs were used to fill low spots and were not necessarily placed uniformly throughout the pit (Ginn, Perkins, and O’Hayre 2009). The pits range from being completely surrounded by spoil material or surrounded on the top and sides by spoil material with PCS closing along the bottom (Ginn, Perkins, and O’Hayre 2009). It is expected that leachate from the CCBs should be similar to that from the columns leached with No 8 Coal Seam water resulting in initial dissolution of CCB minerals and consequent high Ba concentrations.

In considering the results of the leach tests it is important to remember that the water flow rate through the pit would be many orders of magnitude slower than that used in the laboratory column studies. Whereas the laboratory columns were fed one pore volume of fluid per day, unsaturated flow through the buried CCBs may be on the order of one pore volume per century or less. Unsaturated flow through the pit depends on a number of parameters and is discussed quantitatively in Section III of this report.

3.4.2 Mineralogical Results

The mineralogy of fresh CCB samples was compared to that of buried samples collected by the drilling and direct push methods to determine differences in their characteristics which might be evidence of chemical transformations associated with aging of the buried material. SEM images showed evidence of aging and lath-like crystal growth. XRD results showed evolution of the

samples from a highly amorphous structure to one in which more crystalline clay structure along with formation of secondary elements was apparent.

3.4.2.1 SEM Investigations

Scanning electron microscopy (SEM) of the CCB samples found that the Fly Ash particles principally consisted of small spheres with only a few other irregular or elongated features. The spheres ranged in size from 100 μm to 50 nm. The elemental composition of the spheres consisted mostly of Si (10-28 weight%), Al (5-23 weight %) and O along with variable trace amounts of Na, Mg, S, P, K, Ca, Ti and Fe. Images were collected using two detectors, secondary electron imaging and backscattered electron imaging. A secondary electron imaging (SE) produces an image which provides topographical information about the surface. Backscattered electron imaging (BSE) generates an image which provides information about the location of heterogeneities in the elemental composition in which elements with the highest atomic number appear as brighter material and elements with low atomic number are associated with darker regions (Spilde 2011). Figure 54 and Figure 55 show the range of size and clumping of the silica spheres.

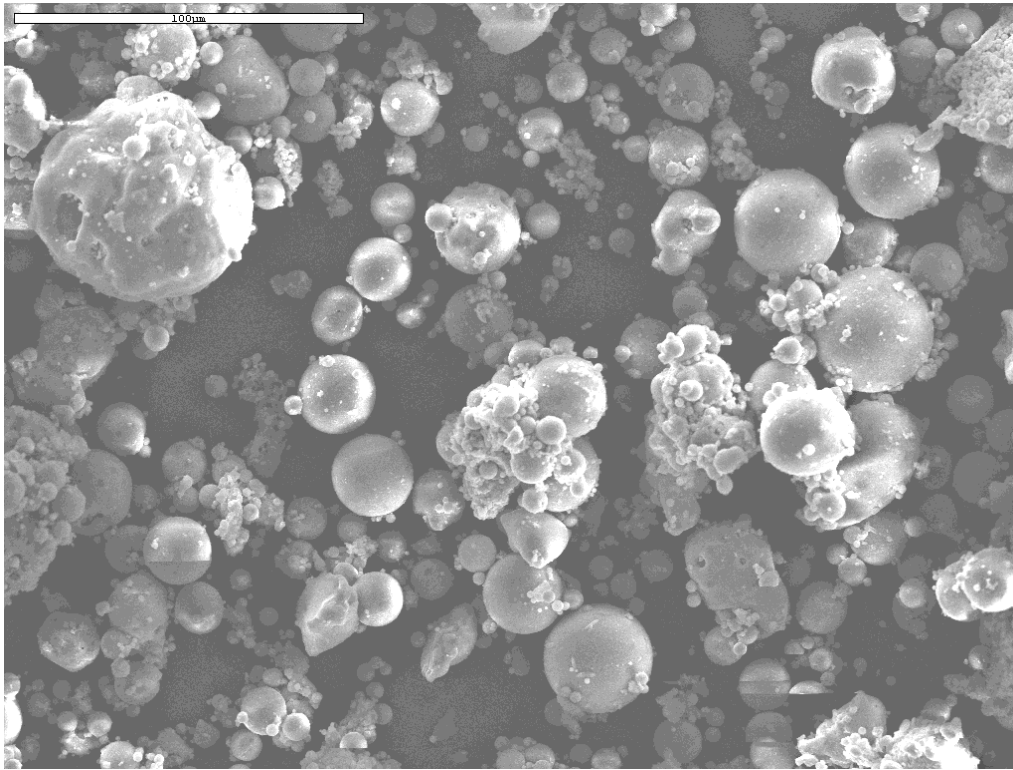


Figure 54. SEM micrograph of fly ash using secondary electron imaging showing spherical morphology of particles. Original magnification = 400x. Scale bar = 100µm.

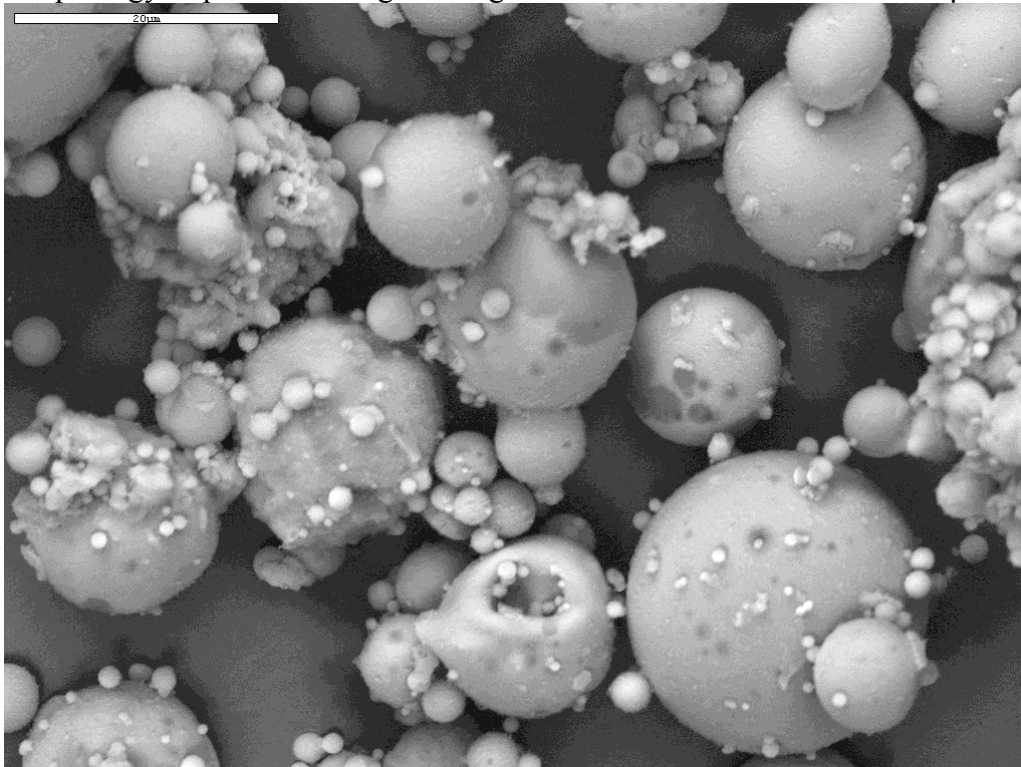


Figure 55. SEM micrograph of fly ash using back scattered electron imaging. Original magnification = 1500x. Scale bar = 20µm.

SEM images of BA samples showed them to include both rough and irregular grainy material along with spherical particles. The samples had a similar chemical composition to FA and consisted primarily of Si and Al with trace amounts of Na, Mg, K, Ca, Ti and Fe similar to the fly ash. One difference was that the BA samples had higher levels of carbon which comprised up to 45 weight %. An SEM micrograph of BA material is presented in Figure 56. Bottom ash samples also showed that some of the spherical particles were fused together by amorphous Si_xO_y material as seen in Figure 57 (Spilde 2011).

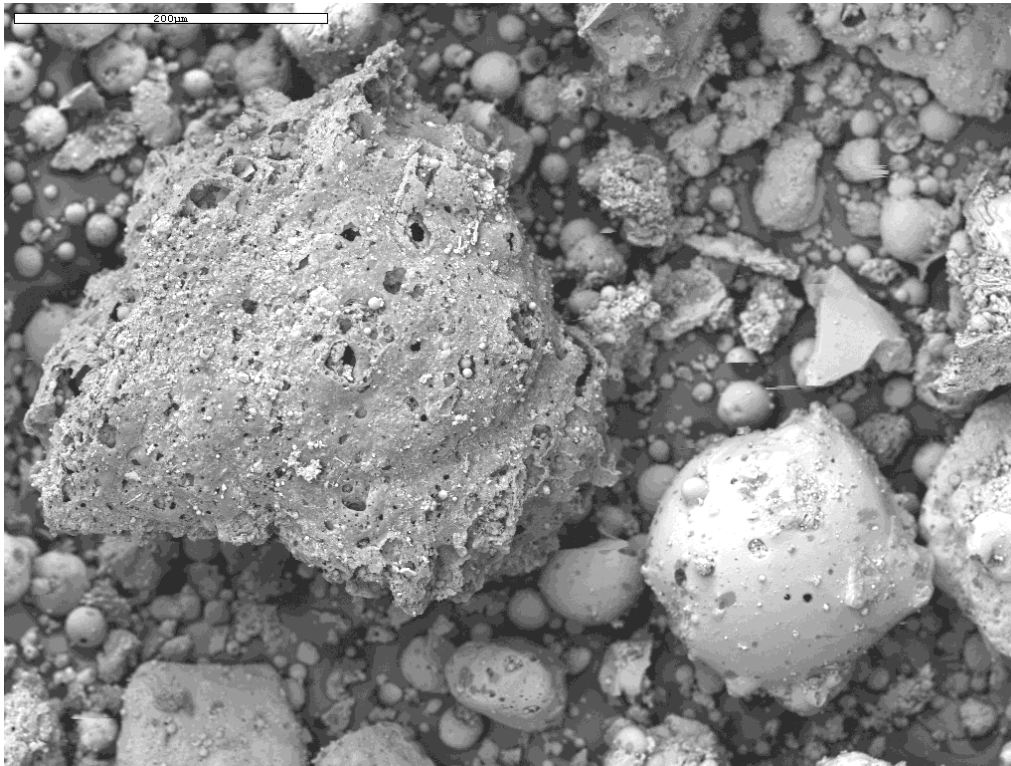


Figure 56. SEM image of bottom ash samples using back scattered electron imaging. Original magnification = 180x. Scale bar =200µm.

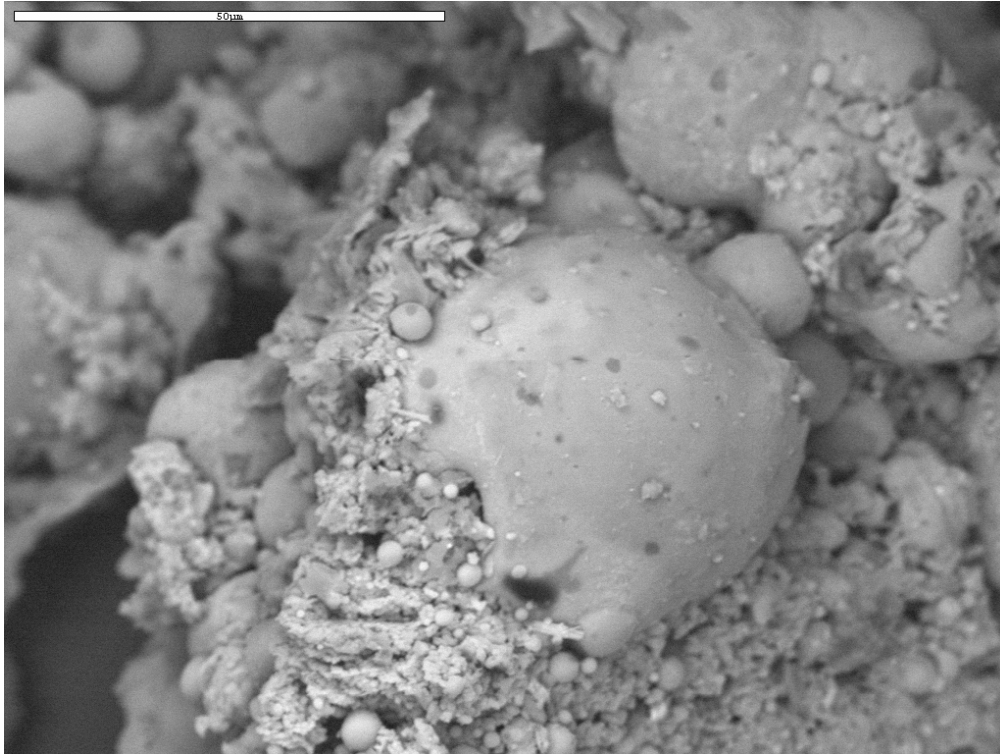


Figure 57. SEM micrograph of bottom ash using back scattered electron imaging. Original magnification = 1000x. Scale bar = 50µm.

Flue gas desulfurization (FGD) sludge samples, as expected, consisted primarily of calcium sulfate crystals. The crystals were subhedral to euhedral and showed a monoclinic crystal habit that is common in gypsum. Figure 58 is a BSE image of an FGD sludge sample showing the characteristic gypsum crystals (Spilde 2011).

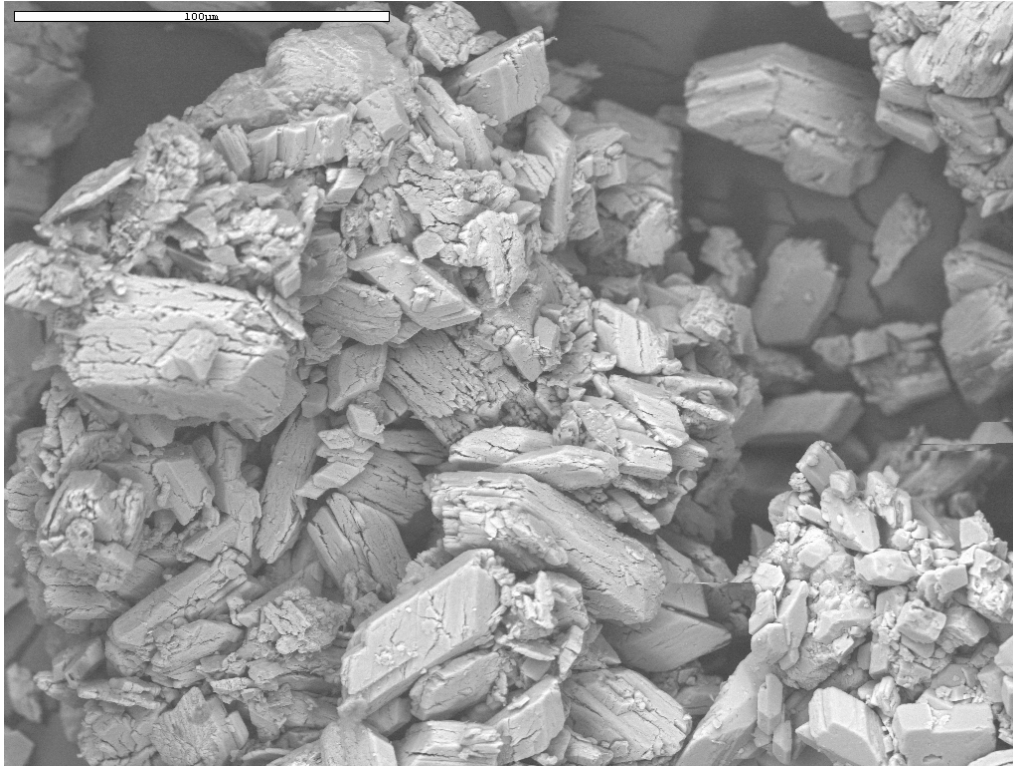


Figure 58. SEM micrograph of flue gas desulfurization (FGD) sludge using back scattered electron imaging. Original magnification = 430x. Scale bar = 100µm.

Old ash samples from the drilling and core sampling program show similar composition to that of fresh samples and the presence of characteristic micro-spheres as found in fresh samples. However, the older samples also showed significant alteration and degradation with more fracturing of spheres, irregular blobs and fine material that appears to cement the spheres together. The mesh of lath-like crystals between spheres is shown in Figure 60. Their major elemental composition includes Si, Al and Ca while the composition of the mesh could not be determined (Spilde 2011).

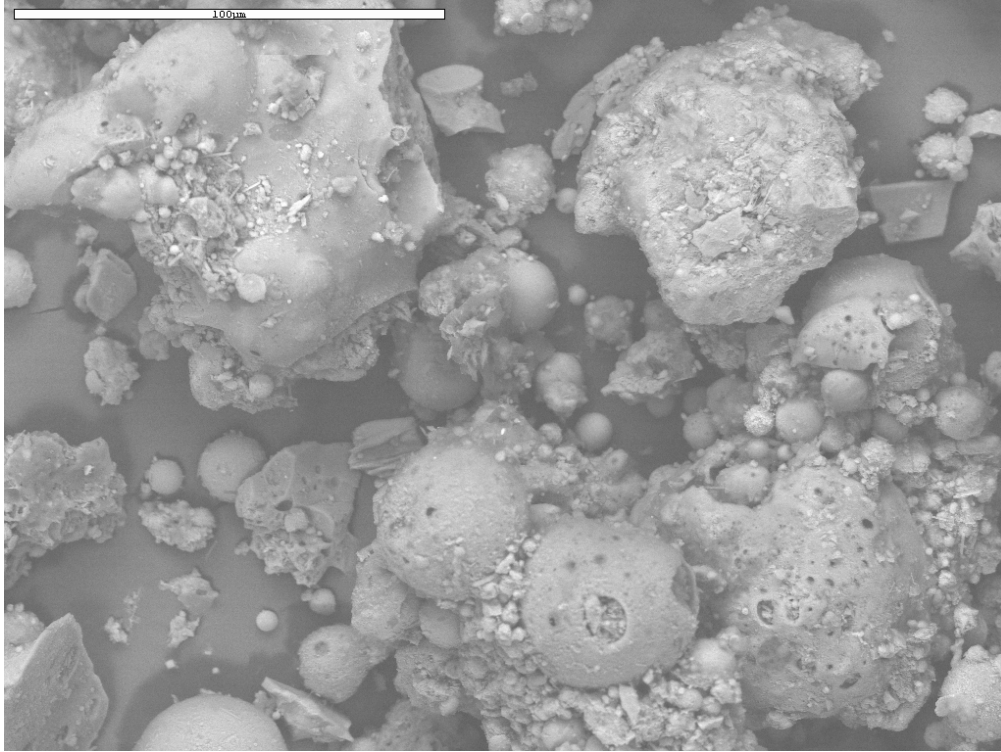


Figure 59. SEM micrograph of old buried bottom ash using back scattered electron imaging. Original magnification = 500x. Scale bar = 100µm.

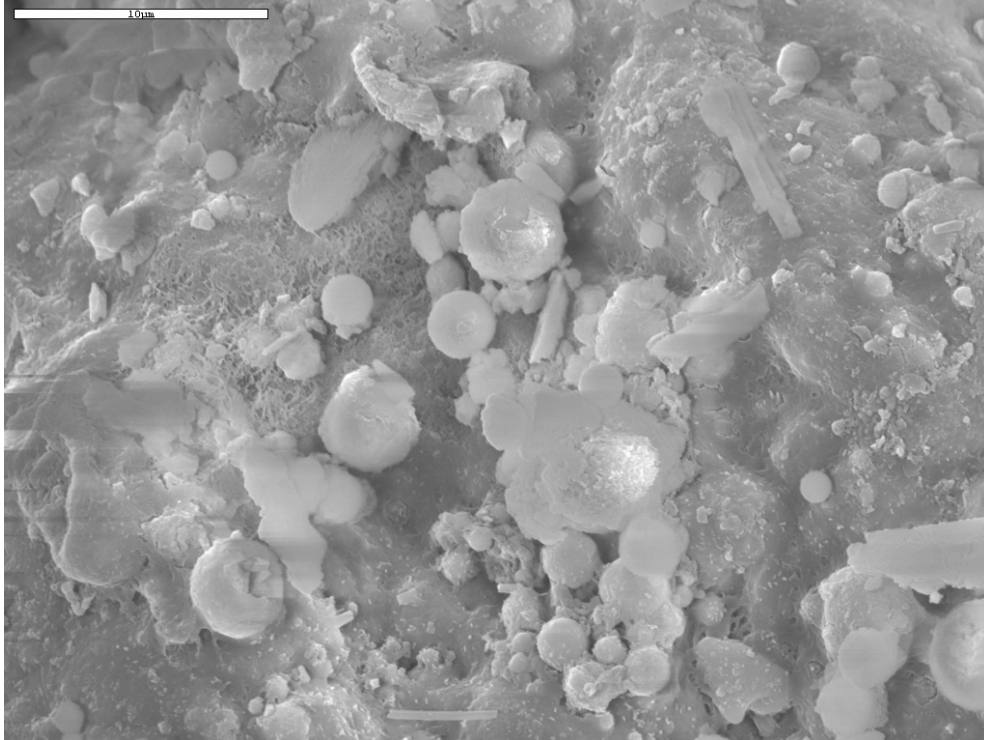


Figure 60. SEM micrograph of old buried fly ash using secondary electron imaging. Original magnification = 3000x. Scale bar = 10 μ m.

3.4.2.2 X-Ray Diffraction Investigation

Previous studies of CCBs done using XRD to determine their mineralogy reported that the primary composition consists of quartz, mullite and glass with minor phases of cristobalite, magnetite, maghemite and hematite. The minor phases are variable and depend on the chemical composition and mineralogy of the parent coal and are usually consist of amorphous materials (You, UM, and et al. 2009; You, UM, and et al. 2009; Sultana, Das, and et al. 2011; Ward and French 2006; Connolly 2011).

X-ray diffraction studies of fresh fly ash samples produced diffraction patterns that matched quartz (SiO_2) and mullite ($\text{Al}_6\text{Si}_2\text{O}_{13}$) (Table 13). The X-ray diffraction pattern also displayed a substantial background peak indicating significant amorphous constituents, which with manual comparison matched data patterns of hematite (Fe_2O_3) (Connolly 2011). Figure 61 shows the diffraction pattern for fresh fly ash and the library patterns for mullite (top), quartz (middle) and hematite (bottom).

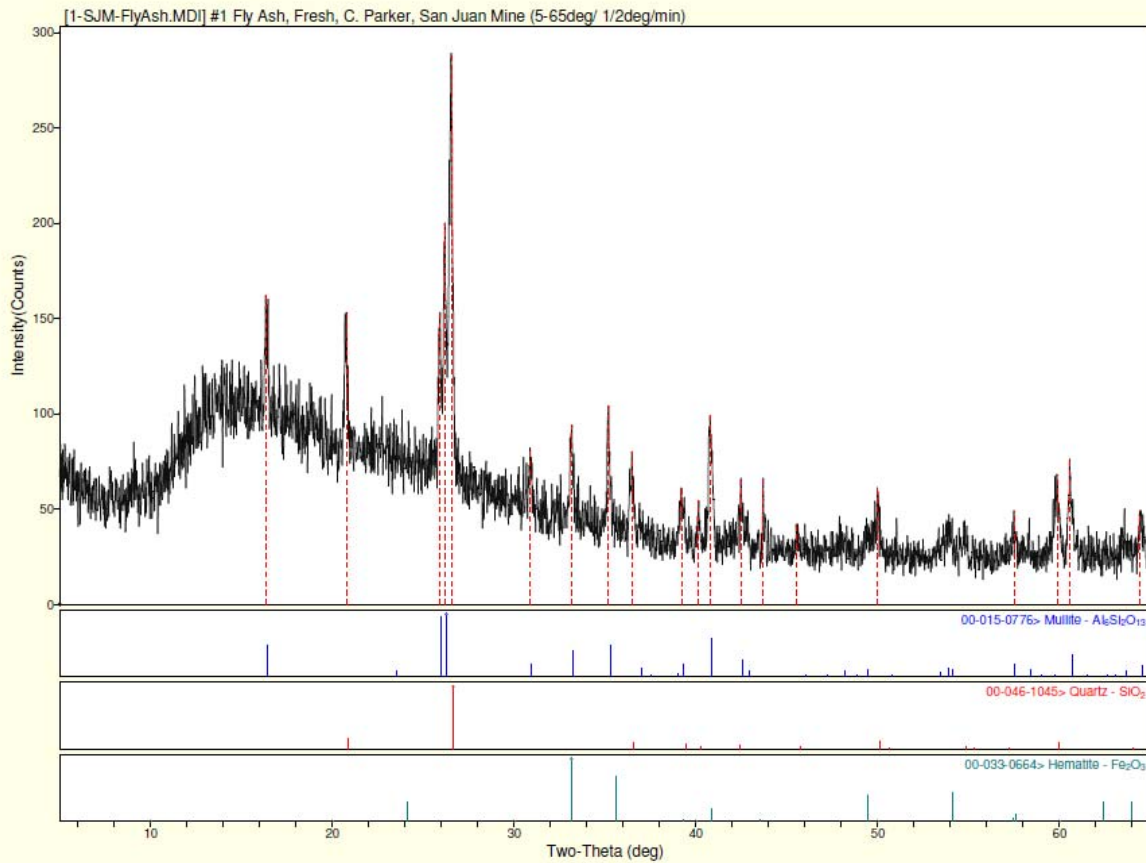


Figure 61. XRD pattern for fresh fly ash. The library patterns are for mullite (top), quartz (middle) and hematite (bottom).

The diffraction pattern of fresh bottom ash displayed matches for mullite and quartz as the dominant phases. There is an apparent amorphous peak, however it is not as distinctive as in the FA samples implying that the amount of amorphous components may be smaller. There were two peaks that were consistent with the presence of Calcite (CaCO₃) and Feldspar (Albite NaAlSi₃O₈) which is shown in Figure 62.



Figure 62. XRD pattern for fresh bottom ash. The library patterns are for mullite (top), quartz (second from top), calcite (third from top) and albite (bottom).

The FGDS diffraction pattern indicate the presence of gypsum with a well defined crystalline structure. Trace amounts of calcite and quartz were also found and are shown in (Figure 63) (Connolly 2011).

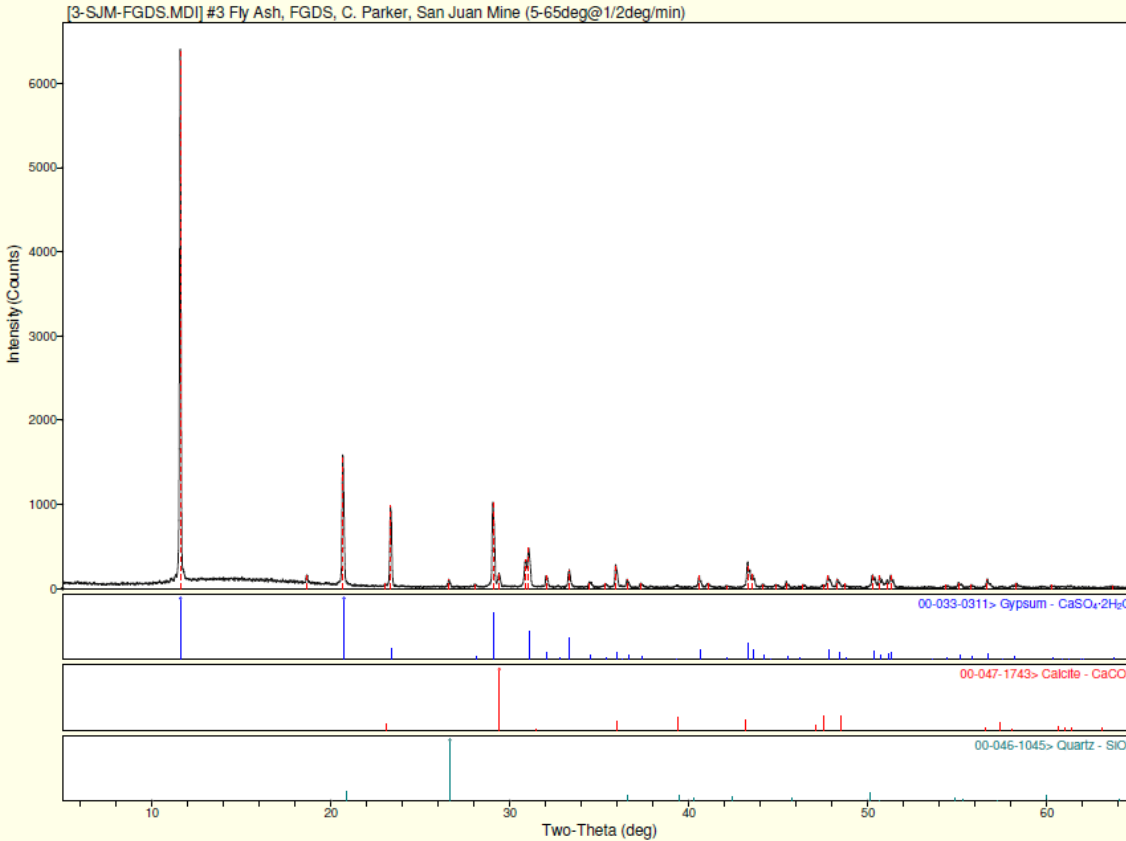


Figure 63. XRD pattern for fresh flue gas desulfurization ash. The library patterns are for gypsum (top), calcite (middle) and quartz (bottom).

Old fly ash samples showed a diffraction pattern similar to the fresh FA samples with a clear match for the diffraction patterns for quartz and mullite. It appears that the old fly ash contains more crystalline structure which is supported by a smaller region associated with amorphous material (compare the Two Theta region below 20° in Figure 64 and Figure 64). A clear calcite peak is present that was not in the fresh FA diffraction pattern. A peak at 9.07 degrees has possible matches for aluminum phosphate, ferrierite, clintonite and paragonite but were not positively identified due to their small concentration in the samples. The diffraction pattern for old FA is presented in Figure 64 (Connolly 2011).

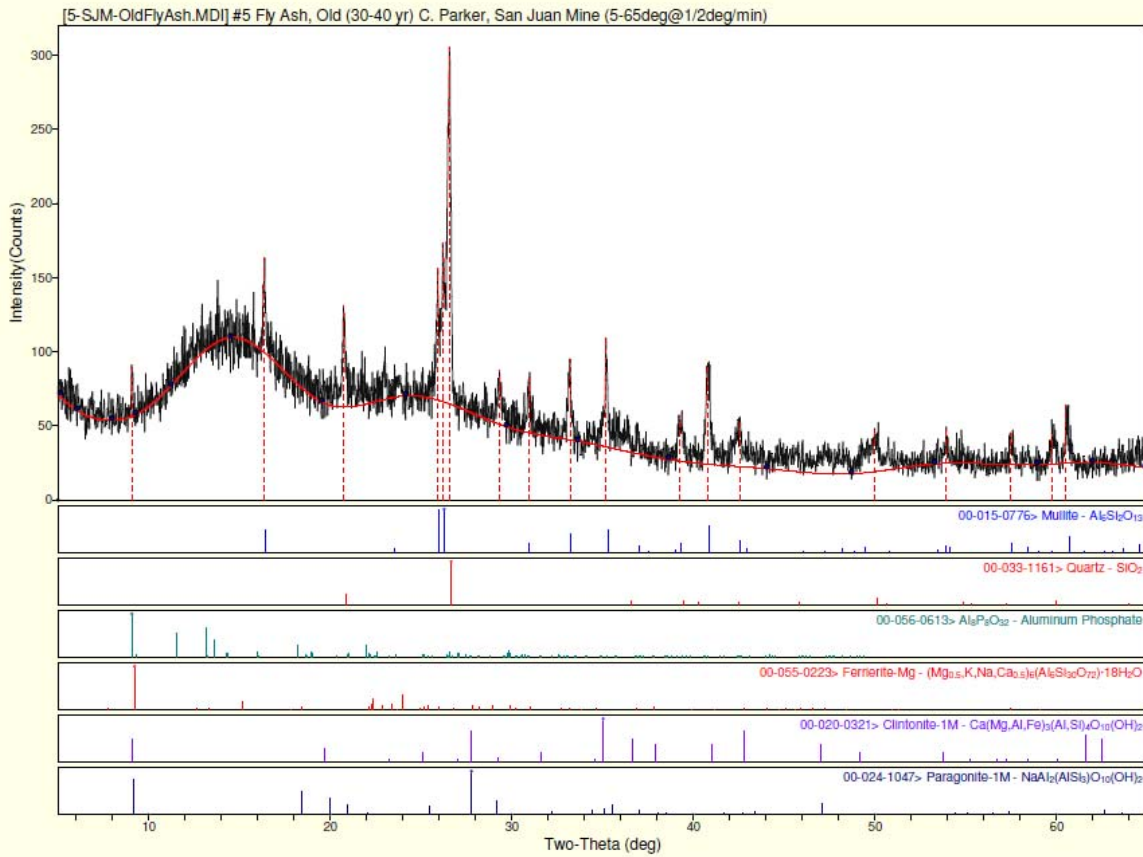


Figure 64. XRD pattern for old fly ash. The library patterns are for mullite (top), quartz (second from top), aluminum phosphate (third from top), ferrierite (fourth from top), clintonite (fifth from top), and paragonite (bottom).

The diffraction pattern for old BA was similar to that for the fresh BA pattern in indicating the presence of mullite and quartz with calcite and feldspar peaks. The intensity peaks of quartz were lower than in the fresh BA samples. Figure 65 shows the match for the XRD pattern for old BA with these constituents (Connolly 2011).

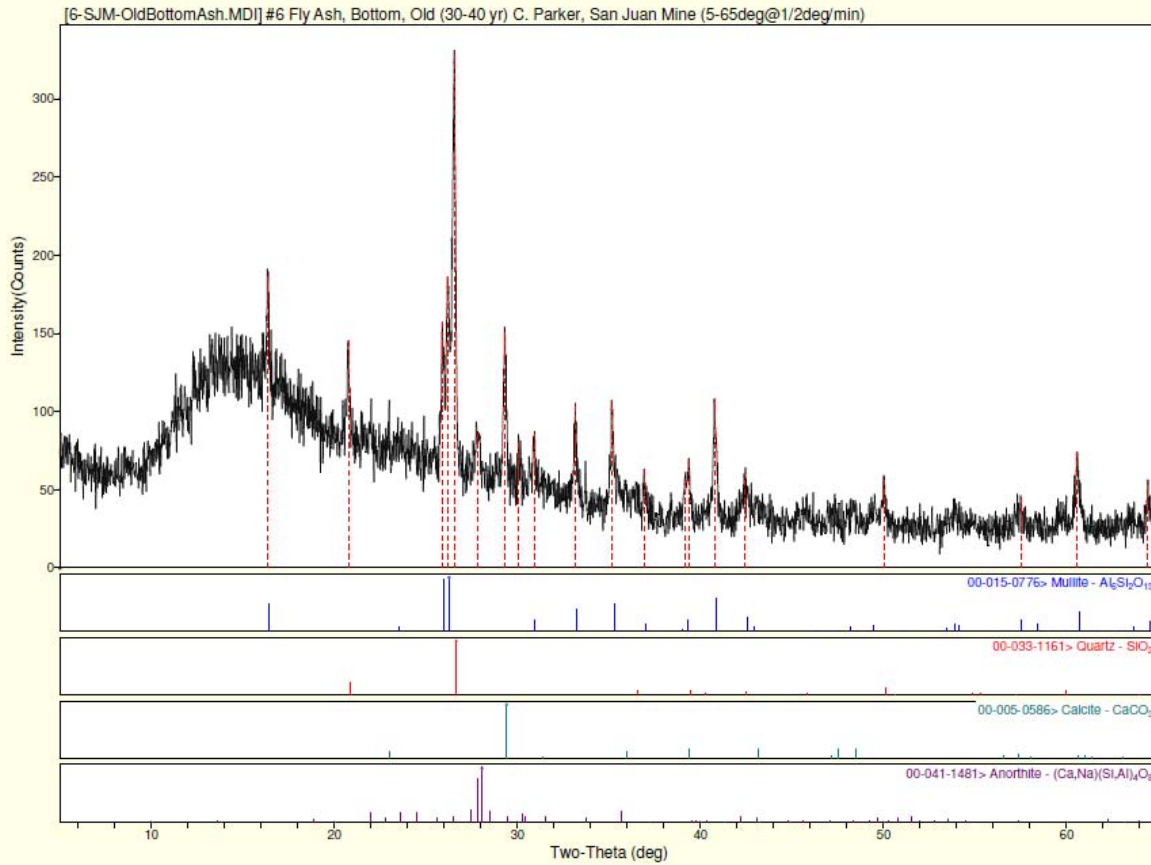


Figure 65. XRD pattern for fresh bottom ash. The library patterns are for mullite (top), quartz (second from top), calcite (third from top), ferrierite (fourth from top), and anorthite (bottom).

The XRD diffraction pattern of a spoil/top cover sample showed the presence of quartz and nontronite, an iron rich clay, along with the likely presence of other various clay phases. The presence of a high fraction of clay minerals is responsible for very low hydraulic conductivity of the soil that has been used to cover the filled mine pits. These phases can be seen in the diffraction pattern in Figure 66 (Connolly 2011).

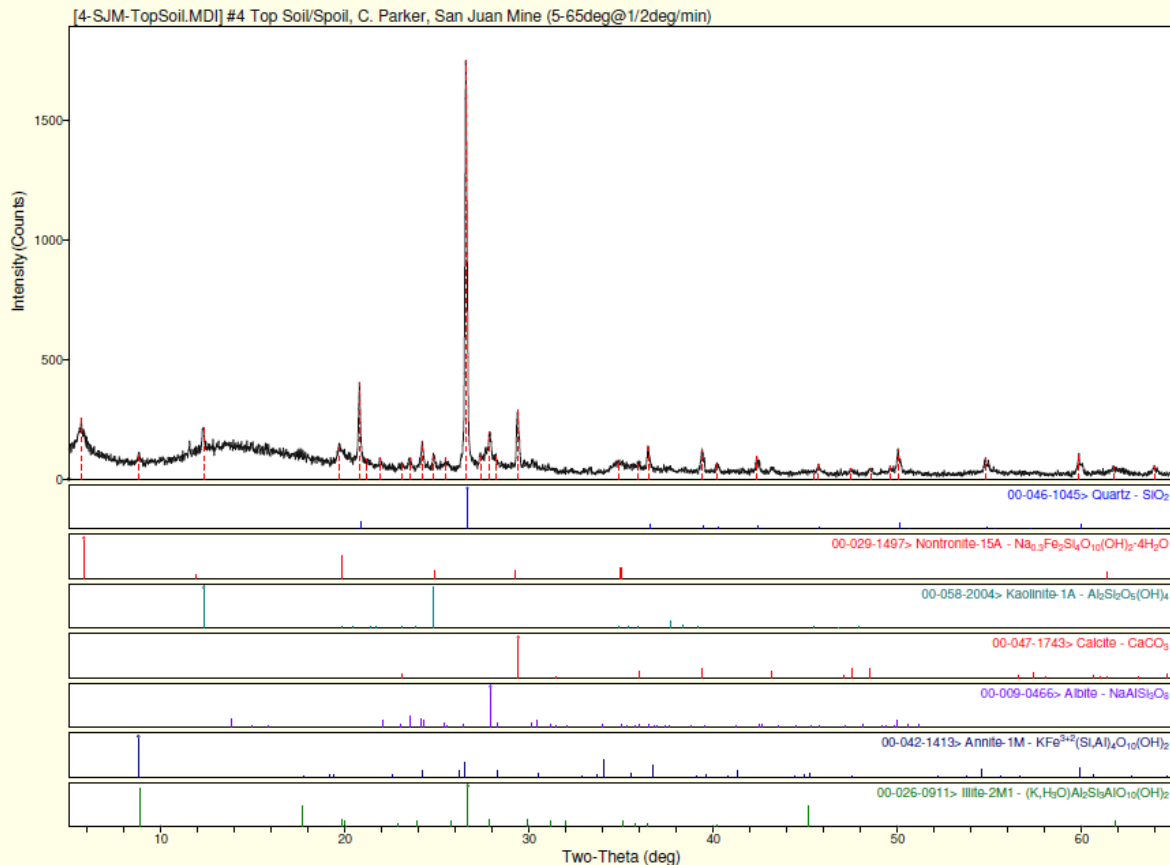


Figure 66. XRD pattern for spoil material. The library patterns are for quartz (top), nontronite (second from top), kaolinite (third from top), calcite (fourth from top), albite (fifth from top), annite (sixth from top) and illite (bottom).

The XRD diffraction patterns for fresh and aged FA are compared in Figure 67. The top pattern is fresh FA that has never been buried and shows a diffraction pattern that is similar to those described previously. The middle pattern is buried fly ash from a sample from a sample collected at a depth of 10 ft from hole SM04 and is similar to that of the fresh FA but includes the presence of a small calcite peak. The bottom diffraction pattern is from a sample collected at a depth of 125 ft from hole SM04 and shows a much larger calcite peak. A clear resemblance can be seen in the overall pattern to the library patterns for mullite and quartz. The buried samples (the middle and bottom patterns) show a peak indicating the presence of calcite. The oldest samples (bottom pattern) display a series of small low angle peaks which suggests the presence of clay minerals that are not present in the fresh FA and younger sample material. Interpretation of the XRD patterns suggests occurrence of diagenetic processes resulting in the formation of secondary calcite and possible generation clay material as a result of alteration of the ash (Connolly 2011).

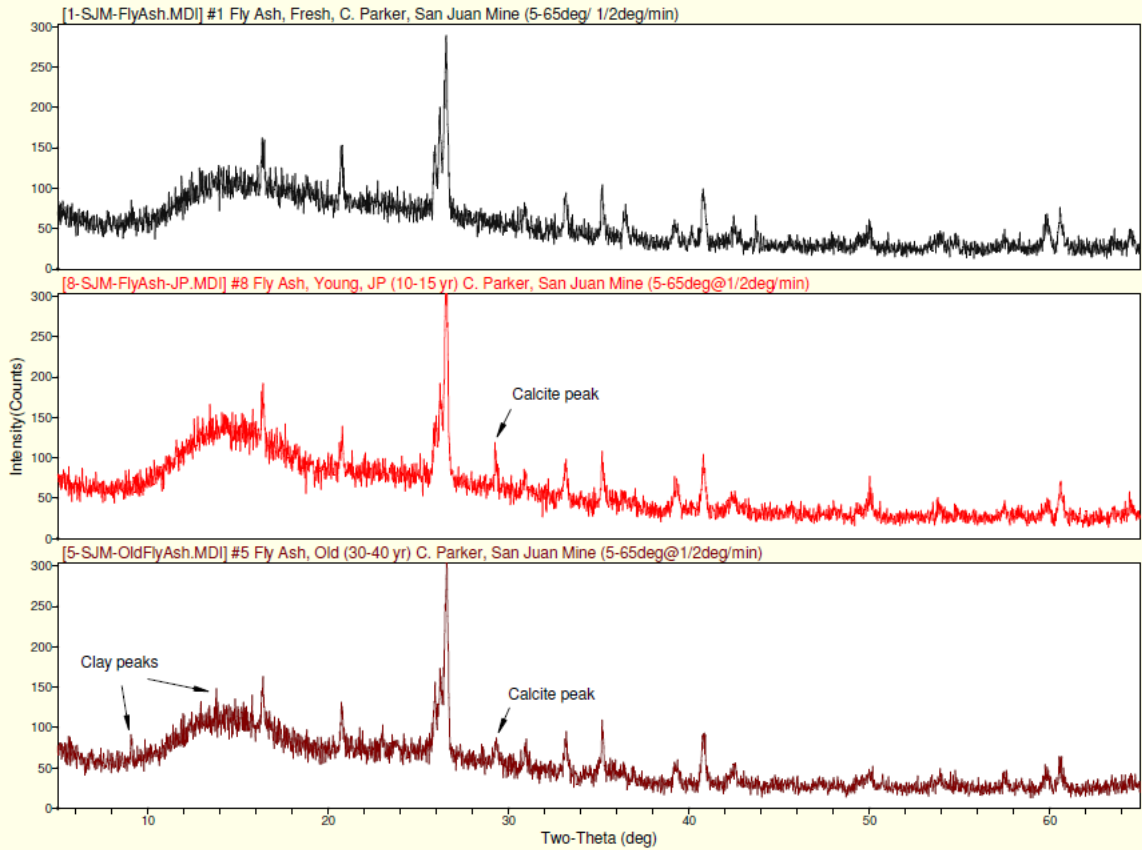


Figure 67. XRD diffraction patterns for fresh fly ash (top), fly ash buried at 10 ft (middle) and fly ash buried at 125 ft (bottom).

Diffraction patterns for buried BA samples of different ages (i.e. buried at different depths) are compared in Figure 68. The top pattern is that for fresh ash and shows the bottom ash characteristic feldspar and calcite peak. The red line is from a sample collected at a depth of 120 ft from hole SM04 that when collected was coarse and showed physical characteristics (color and granulation) expected of BA. The bottom pattern is the diffraction pattern of BA collected from the SM04 hole at 109 feet below the surface and appeared to be BA. The diffraction patterns reveal that what was believed to be BA was actually FA as it lacks the feldspar and calcite peak characteristic of BA. The older BA sample shows a less prominent peak of quartz than the fresh sample and there is evidence of non clay peaks in the pattern (Connolly 2011). This set of samples shows the value of XRD in determining whether buried samples are FA or BA as the two often cannot be distinguished by their visual characteristics.

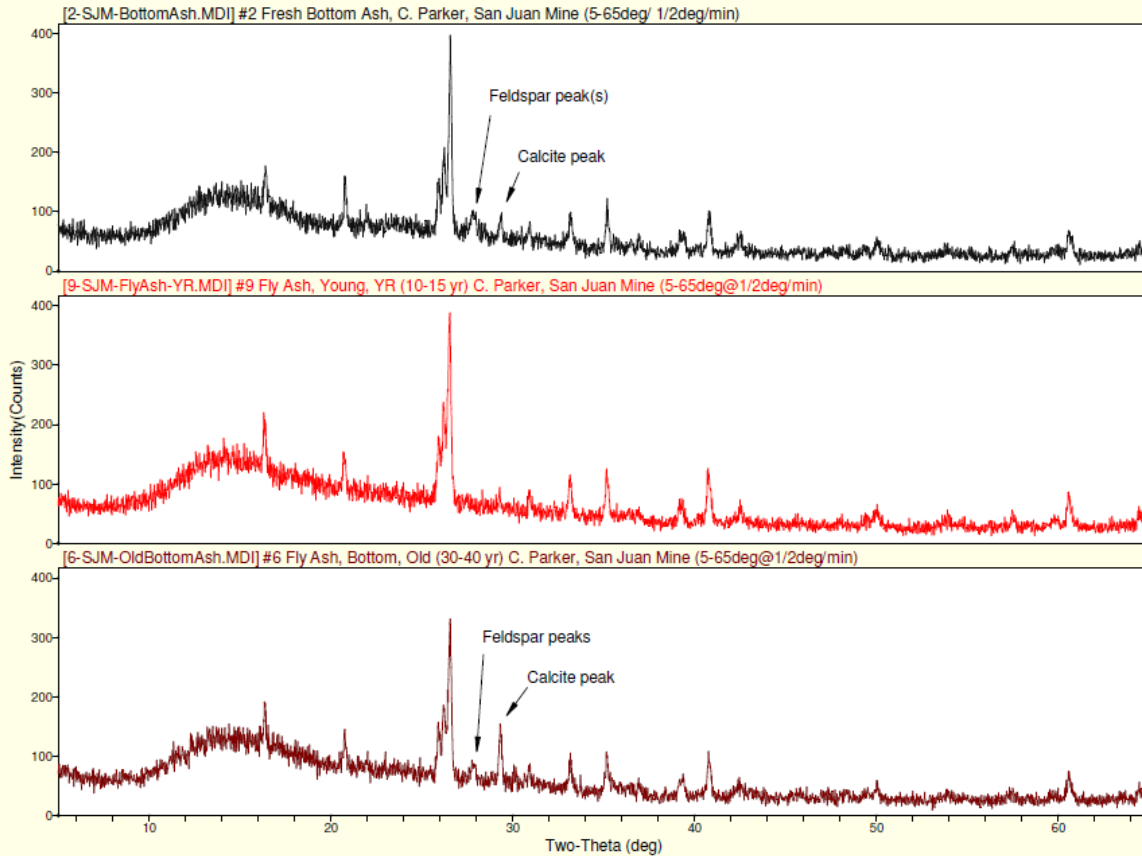


Figure 68. XRD diffraction patterns for fresh bottom ash (top), fly ash buried at 120 ft (middle) and bottom ash buried at 109 ft (bottom).

The results show that evidence of aging and the ash mineralogy changing from a glassy amorphous phase to a more clay/crystalline structure. The presence of calcite in the FA as a secondary phase is also cited as further evidence of aging as it would not survive the furnace temperatures. Evidence from the XRD patterns is consistent with the observation of lath-like crystals in the SEM micrographs.

3.4.3 Potential Ground Water Impacts of Leachate from Buried CCBs

To determine the potential effect of the CCB leachate on underlying groundwater quality at the SJCM the maximum concentration of key constituents from the column leach tests was compared to underlying ground water chemistry from monitoring well GL (see Figure 9). This well is that which is nearest to the disposal pit containing CCB samples analyzed in this study. Constituents that have higher concentrations in the CCB column leachates than in the GL water samples include: Al, B, Ba, Ca, Li, Mo, Si, Sr and V. Table 19 summarizes the leachate quality for fresh and old FA and BA, spoil/top cover material, and the quality of ground water from the GL monitoring well.

Caution must be exercised in comparing the results of the column leach tests to the quality of native ground water because the leach tests constitute a highly simplistic system in which DI water is quickly passed through the CCB or soil material. The exposure time in this study was a

couple of days whereas shallow ground water at the SJCM is likely to have been in contact with the aquifer material for many decades or centuries, depending on location. Furthermore, DI water is a much more aggressive leaching solution than ground water because the latter solution is strongly buffered (i.e. has high alkalinity) and high concentrations of dissolved salts that will limit the solubility of many of the minerals associated with buried CCBs and soil materials.

Table 19. Comparison of maximum concentration of elements in CCB column leachate to concentrations in SJCM ground water. All concentrations in mg/L.

Parameter (mg/kg)	Recharge GW	Column Tests						Recharge GW	
		FFA	FBA	DI WATER		YFA	Spoil	FFA	OFA
				OFA	OBA				
Al	0.005	1.503	0.273	0.315	1.55	5.667	0.031	2.064	3.273
B	1.13	2.146	67.64	29.6	33.51	33.26	7.406	40.26	11.34
Ba	0.1	6.42	0.067	0.058	0.053	0.052	0.154	0.057	4.32
Ca	508	436.6	665.2	605.7	454.2	591.2	317.5	403.4	472.7
Se	0.0105	0.125	0.244	0.182	0.088	0.078	1.934	0.191	0.935
Si	10.25	0.768	6.334	8.093	4.316	2.256	8.766	1.97	27.12
V	0.1	0.026	0.147	0.24	0.141	0.136	-0.024	0.757	0.49

High CCB Leach

Abbreviations

GW = ground water

FFA = fresh fly ash

FBA = fresh bottom ash

OFA = old fly ash

OBA = old bottom ash

YFA = young fly ash

The results of the column leaching studies show that the concentrations of B, Ca, Mo and Sr will likely follow an asymptotically decreasing trend and quickly decline to background concentrations in the water in the soil matrix. This water may be either unsaturated water in the vadose zone or regional ground water, depending on the buried depth of the CCBs and the future ground water elevations in the pit. Al, Li, Si, and V are elements that are associated with dissolution of minerals in the buried CCBs. Their concentrations in both the DI water and No. 8 Coal Seam ground water leach is close to or exceeds their solubility for minerals detected in the geochemical studies. It is suggested that their elevated concentrations are the result of dissolution of amorphous phases. Subsequent precipitation and formation of quartz and clay minerals will quickly decrease their concentration to levels similar to that in the native ground water.

Material buried in the SJCM will remain unsaturated until the mine dewatering stops and ground water levels are re-established in the mine. It is expected that ground water will enter the mine by two mechanisms: 1) horizontal flow of water from the No. 8 Coal Seam into the mine, and 2) vertical flow of ground water as regional ground water levels rise. Infiltration of water from the land surface into the buried material will be small due to the very low hydraulic conductivity of the spoil material used for cover at the mine ($< 10^{-6}$ cm/s).

3.5 Conclusions

3.5.1 Analytes of Concern

Barium and As were established as the primary analytes of concern at the SJCM because of their relatively high concentration in leachates from CCBs in most ash analyses collected since 1972. Results from CCB leach studies presented here also indentify Ba and As as constituents with elevated concentrations (Luther, Musslewhite, and Brown 2009) (Mining and Minerals Division, New Mexico 2011). Of particular interest is that this study found that the Ba and As concentrations increase with depth.

Selenium and B, which have been frequently reported in other studies of CCBs as having elevated concentrations, were not found at high concentrations in SJCM ash (Zhao et al. 2006; Yuan 2009; Baba et al. 2008; Bhangare et al. 2011). In addition their concentrations did not approach drinking water MCLs in any of the CCB or spoil samples.

This study found little difference in constituent leachate concentrations between CCBs and spoil/top cover material. For example, as shown in Figure 34 CCBs have an average concentration of Fe of 20,900 mg/Kg which is statistically significantly different from the average concentration of Fe in the spoil material of 19,400 mg/kg. However, the Fe concentration difference between the spoil and the ash is less than 10% which is not a large value. Further, the mass of spoil in the pit is several orders of magnitude larger than the mass of ash, except in the immediate vicinity of ash disposal areas. Therefore, it is not possible to determine the relative contributions of Fe to underlying ground water.

The concentrations of all constituents associated with the CCB leachates is not high enough to result in exceedence of ground water standards for any parameters except for potential Ba and As. It is likely that oxidation-reduction and precipitation reactions as well as dilution will result in little or no measurable increase in the concentrations of these constituents in ground water underneath the SJCM.

3.5.2 Leaching Sequence

Most of the constituents in CCB leachates decreased exponentially with time when leached with either DI water or No. 8 Coal Seam ground water as expected. Constituents typically disappeared within 14 days of the start of the leach tests. Barium was a notable exception as its highest concentration was observed 16 days after initial leaching with DI water and No 8 Coal Seam water suggesting its appearance was the result of dissolution of solids in the waste material.

Aluminum and Si concentrations peaked after about 28 days of leaching which was interpreted as evidence of dissolution of aluminosilicate minerals occurring in all of the CCB materials obtained in the sampling program. Samples leached with DI water showed a slower dissolution rate than those with No 8 Coal Seam water. Overall, the highest Al and Si concentrations were observed when buried old CCB samples were leached with No 8 Coal Seam water. Higher ionic strength and alkalinity present in the coal seam water is believed to have resulted in increased solubility of amorphous mineral phases in the CCBs.

3.5.3 Evidence of Aging of Buried CCBs

SEM analysis of buried CCBs showed evidence of partial dissolution when compared to fresh CCB samples in the form of rounded edges and fractures of glassy FA particles. There was also evidence of the presence of calcite, a secondary mineral, in the buried ash. XRD analysis verified the presence of calcite within the buried CCB samples as well as the oldest samples showing higher crystalline structure than that of young buried CCBs.

The spoil material which is used as final cover of SJCM pits has a high fraction of sodium-saturated smectitic clay with secondary accumulation of sulfate and carbonate salts. As with most smectite clays, these swelled when water was introduced resulting in very low hydraulic conductivity. Consequently very little water infiltrated through the unsaturated columns filled with spoil. These results suggest that very little water will infiltrate through the spoil cover and reach the buried ash.

3.5.4 Comparison of Results with Historical Data

A difference was observed between results of leaching fresh and aged materials, as well as differences in leach results from past studies. This difference is believed to be due to different composition of the coal as mining progressed, differences in air pollution control equipment over the 40 years the power plant has been in operation and differences in sampling and analysis procedures. The majority of CCB samples tested were collected from the Juniper Pit area and were selected to understand leachate chemistry as ground water fills the pit after dewatering is concluded. The No 8 Coal Seam water is believed to be representative of the ground water that will eventually fill the mine when mine dewatering stops. Potentiometric maps suggest that the No 8 Coal Seam water will enter the waste through the side of the Juniper Pits due to horizontal flow.

The interaction of ground water at the SJCM is different from that resulting from the spill at the Tennessee Valley Authority (TVA) Kingston, TN coal power plant in several ways. The TVA plant used water to transport their CCB waste as a slurry in flumes to the ash detention ponds. CCBs from the San Juan Generating Station are transported in haul trunks with a low water content that is added for dust suppression and a bit of residual water associated with the FGD sludge. TVA stored their CCBs in above grade ponds while CCBs at the SJCM are placed below grade in mined-out sections of the open pit mine. Because the wastes are unsaturated at the SJCM, there is no hydraulic gradient forcing water flow through the buried waste and out of the mine. In addition, there is no hydrostatic pressure that decreases the stability of a tailings dam. The scenario of a berm failure as happened at the Kingston facility cannot occur at the SJCM since the CCBs are stored within the ground; there is no tailings dam or berm. TVA is likely to contaminate surface water due to the detention pond structure while SJCM is likely to contaminate groundwater due to their CCB disposal pits. SJCM does not line its disposal pits so there is a possibility of off site transport of contaminants from the waste. However, unsaturated ground water flow through the waste is virtually non-existent as explained in the following section. Thus, the only credible scenario by which CCBs disposed at the SJCM can impact the environment is when inundation of the buried material occurs following termination of mine dewatering. The chemical, geochemical, and leaching studies described in this section suggest that future impacts on ground water quality at the SJCM will be very small and possibly not measurable.

Part III One Dimensional Modeling of Unsaturated Flow

4.1 Introduction

An important question related to the impact of CCB disposal in the SJCM pits on underlying ground water quality is whether water is moving downward from the ground surface and into the disposal pits. This could result in a scenario in which contaminants could be leached from the CCBs and subsequently transported through the bottom of the mine resulting in contamination of the regional aquifer. Understanding unsaturated water movement through the mine cover and buried waste is an important component in evaluating the potential for contamination from this disposal facility.

Water movement from the surface, through the CCBs, then into underlying strata and eventually reaching the regional water table is complicated by a number of factors, including:

- The land-atmosphere interface is a time-dependent boundary condition depending principally on the climatic conditions at a particular time; precipitation will result in infiltration through the ground surface, whereas dry conditions will often result in water loss by evaporation and transpiration.
- The buried materials are expected to remain unsaturated (or partially saturated). Thus, the hydraulic properties of the buried materials are not constant, but rather are a function of saturation.
- The profile from the surface to the ground water consists of layers of materials with different properties. Further, the properties are a function of the depth of burial.

Because of the complexity a numerical solution of the flow equations for water in unsaturated porous material is required to estimate the rate and amount of water that can be expected to move through the waste to the underlying ground water.

4.2 Previous research

Numerical solutions of the equations of unsaturated ground water flow have been widely used to estimate water movement through unsaturated soil profiles. There are a number of programs that have been developed to simulate flow under these conditions (e.g., HYDRUS1D, VS2D, UNSAT-H). All have different advantages, limitations, features, and intended applications. Numerical solutions have been developed for particular applications, including buried waste (e.g., solid waste was considered by El-Fadel et al., 1997). Water movement through soils that are similar to granular CCBs, particularly in applications in which granular materials are used as subgrade material beneath pavements, was considered by Cetin et al. (2012), Apul et al. (2003). However, no previous studies have been identified in which the unsaturated flow of water through buried CCBs in the configuration and climatic conditions of the San Juan Mine has been modeled.

4.2.1 Methods

Modeling of one-dimensional water movement through soil cover and buried CCBs was conducted to simulate water movement through the buried waste in the SJCM. The modeling program HYDRUS1D (Simunek et al., 2008) was used in this study. HYDRUS 1D is a software package designed to simulate the movement of water, heat, and dissolved constituents in variably saturated media. Only water movement was simulated in this study. The program numerically solves the Richards equation for variably saturated water flow and includes a sink term to account for root water uptake. The program is capable of analyzing water and solute transport in unsaturated, partially saturated, as well as fully saturated porous media. The water flow portion of the model is capable of incorporating boundaries controlled by prescribed head and flux, atmospheric conditions, and free drainage. The governing flow and transport equations are solved numerically using a Galerkin-type linear finite element scheme.

The one-dimensional model developed for this study represents a vertical profile from the ground surface, through two meter of soil cover, then 33 m of buried CCBs into the underlying sandstone formation. For most simulations, the upper boundary was modeled using daily-varying climate data. The lower boundary was modeled as a no-flow boundary at a large distance below the CCB-sandstone contact. This was done to assure that the lower boundary condition had no impact on migration through the buried CCB waste. Additional simulations were conducted with focused recharge conditions at the surface and with a water table at the CCB-sandstone contact. The initial condition in the soil profile consisted of an assumed water content, which was selected based on values measured in field samples. The initial water content was also varied in the modeling program to determine its impact on unsaturated water movement.

The model profile was created using 1001 nodes with a varying nodal density that resulted in a spacing of 0.33 cm at the top of the soil column and 16.67 cm at the bottom. The time units used were days with an initial time step of 0.01, a minimum time step of 1e-6 d and a maximum step of 1 d. A water content tolerance of 0.0001 was set with a maximum number of iterations per time step of 200.

Profiles were 85 m in total depth with the top 2 m representing soil cover, the next 33 m represented buried CCB in the pit, and the bottom 50 m consisted of basement rock associated with the Pictured Cliffs Sandstone. Initial volumetric moisture contents used were that of 20% throughout CCB materials and pictured cliffs, with 5% for the top soil. These initial moisture contents were based on average measured values from CCB samples recovered from the SJM in 2010 (Chan, 2010). Observation points were placed in the model at depths of 2, 7, 12, 17, 22, 27, 32, and 35 m to collect data on fluxes, water content, and potential within the profile during simulations.

4.2.1.1 Profile Development

Ash disposal at the SJM involved the placement of different types of CCBs in the pits as they were produced at the San Juan Generating Station. Quarterly reports of ash disposal at the SJM (SJM, 2011) indicate a fairly constant ratio of fly ash to bottom ash production of 78% to 22%, but there are no records as to the specific profile of ash in the landfill sites. Therefore, 15 different profiles of landfill composition were developed in order to capture different possible

landfill compositions. To create the different profiles, the total CCB pit depth (33 m) was divided into 18 layers, each 1.83 m thick. For a particular profile, each layer was randomly assigned the properties of FA or BA while maintaining the overall ratio of FA to BA in the column profile. Each of these profiles was therefore different in the arrangement of the layers of FA and BA.

Two additional profiles were also developed, one of which the CCB material is solely FA and another of solely BA. Flue gas desulfurization byproducts were also disposed of in these pits, but were not included in the modeling as material properties were not available. This is further justified by the fact the FGD sludge represents a very small component of the material disposed at the SJCM.

4.2.1.2 Material Properties

Top soil in situ density and hydraulic properties obtained from the investigation conducted by Chan (2010) were used for the model. Pictured Cliffs Sandstone properties were those determined by other studies. The saturated hydraulic conductivity of the Pictured Cliffs Sandstone was determined by Kernodle (1996). Unsaturated properties from a study conducted by Van Genuchten (1989) for hygiene sandstone formation located near Boulder, CO were used for the MCC fitting parameters. Both hygiene sandstone and pictured cliffs sandstone were formed in the late cretaceous period and have low permeability (Kernodle, 1996, Kiteley, 1977). A summary of the material properties for the top soil and the Pictured Cliffs Sandstone are given in Table 20.

Table 20. Hydraulic Properties of Top Soil and Pictured Cliffs Sandstone.

Material	θ_r (cm ³ /cm ³)	θ_s (cm ³ /cm ³)	α (cm ⁻¹)	n	K _s (cm/d)
Top Soil	.02018	0.44	0.0323	1.39	0.730
Pictured Cliffs	0.0	0.256	.00562	3.27	0.213

The densities of the CCB materials were calculated using a weighted average density curve from the compressibility results in Part I (see for example Figure 69). Parameters of equation (1) were weighted to the R² value of each fitted curve using the following equation:

$$FP = \frac{T_1 \cdot R_1^2 + T_2 \cdot R_2^2 + T_3 \cdot R_3^2 + T_4 \cdot R_4^2}{\sum R_n^2} \quad (5)$$

Where:

- FP = fitting parameter being calculated
- T_n = fitting parameter for trial number n
- R²_n = R² value for trial number n

Figure 70 shows one of the spreadsheets used to develop random profiles for the model. The top soil is highlighted in brown, the bottom ash in green, and the fly ash is not highlighted. Sandstone is not represented in this profile due to the fact that the properties of sandstone were assumed to be constant and did not depend upon material densities or the weight of material in

the disposal cell above it. Each segment of material had a calculated dry density from the weighted average density curves and a total density could then be calculated by adding the appropriate mass associated with the gravimetric moisture content. The overburden weight was calculated as the total density of the material multiplied by the depth of the segment (1.83 m for CCBs) and a total overburden pressure for each cell is the sum of pressures for all segments above the cell in question. Saturated and unsaturated properties of each material were then calculated using the trend lines calculated from the laboratory results as a function of dry density given in Part I.

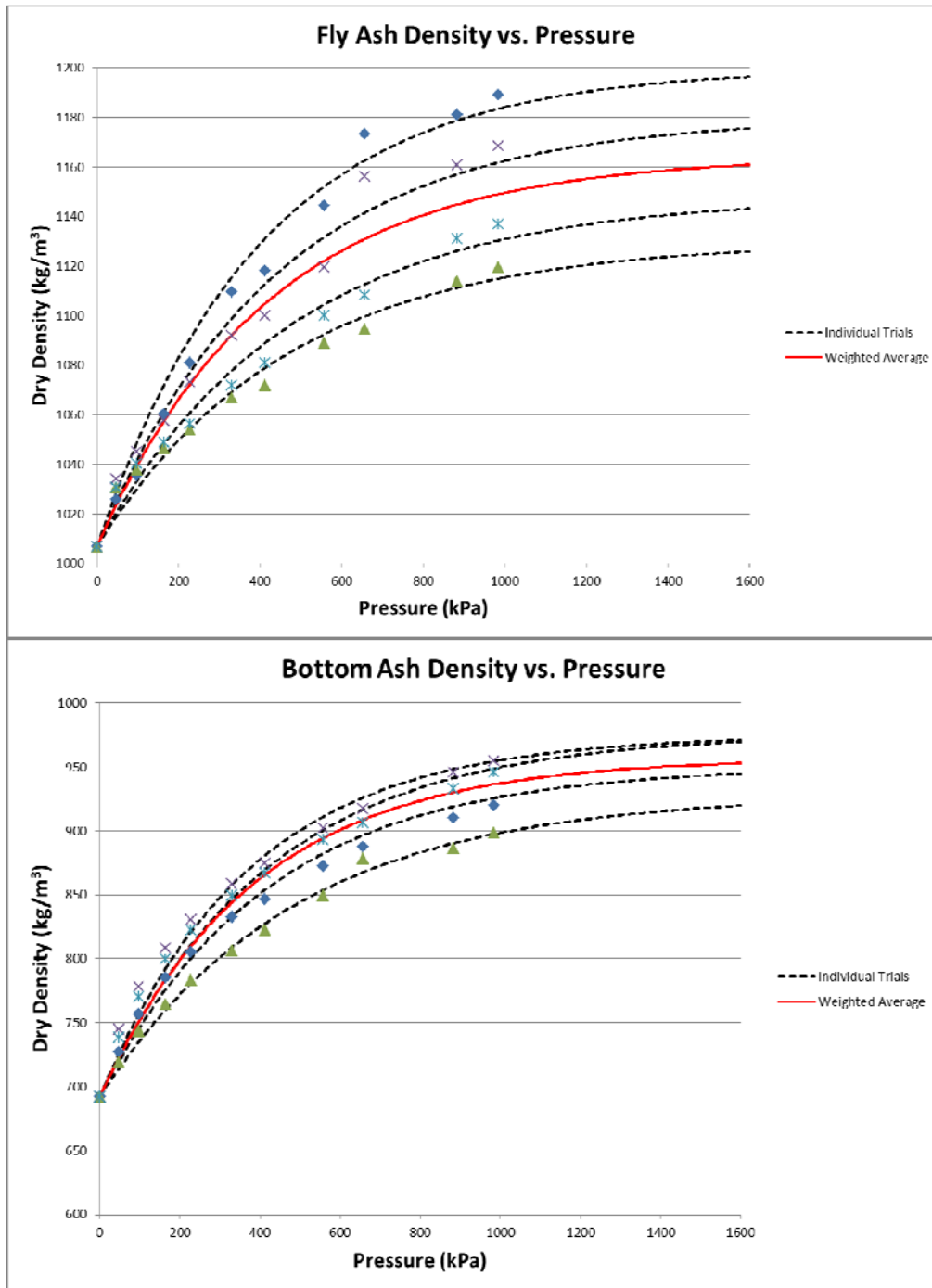


Figure 69. Fly Ash (top) and Bottom Ash (bottom) Dry Density vs. Pressure Curves

random	depth (m)	material	moisture (%)	tot. overburden (kg/m ³)	tot. overburden (kpa)	dry density (kg/m ³)	tot. density (kg/m ³)	Ksat (cm/s)	Ksat (cm/day)	ThetaR	ThetaS	alpha	n	air entry (cm)
	2.00	Top Soil	0.05	3529	35	1680	1764	8.45E-06	7.30E-01	0.02018	0.44	3.23E-02	1.39	31
17.0	3.83	FA	0.20	6763	66	1030	1236	1.02E-04	8.77E+00	0	0.55	3.94E-03	1.69	254
33.0	5.67	FA	0.20	9029	89	1037	1244	9.92E-05	8.57E+00	0	0.55	3.81E-03	1.69	262
65.5	7.50	FA	0.20	11309	111	1043	1252	9.69E-05	8.38E+00	0	0.55	3.69E-03	1.70	271
28.3	9.33	FA	0.20	13604	133	1049	1259	9.48E-05	8.19E+00	0	0.54	3.57E-03	1.70	280
99.2	11.17	BA	0.20	15913	156	780	936	4.37E-03	3.77E+02	0	0.61	4.10E-02	1.50	24
73.8	13.00	FA	0.20	17629	173	1060	1272	9.14E-05	7.89E+00	0	0.54	3.38E-03	1.71	296
39.5	14.83	FA	0.20	19960	196	1065	1278	8.95E-05	7.73E+00	0	0.54	3.27E-03	1.71	306
77.1	16.67	FA	0.20	22303	219	1070	1284	8.77E-05	7.58E+00	0	0.53	3.17E-03	1.72	315
76.6	18.50	FA	0.20	24658	242	1075	1290	8.60E-05	7.43E+00	0	0.53	3.08E-03	1.72	325
17.5	20.33	FA	0.20	27024	265	1080	1296	8.44E-05	7.29E+00	0	0.53	2.99E-03	1.72	335
66.5	22.17	FA	0.20	29400	288	1085	1302	8.29E-05	7.16E+00	0	0.53	2.90E-03	1.73	345
25.8	24.00	FA	0.20	31787	312	1089	1307	8.14E-05	7.04E+00	0	0.52	2.82E-03	1.73	355
23.5	25.83	FA	0.20	34182	335	1093	1312	8.00E-05	6.92E+00	0	0.52	2.74E-03	1.73	365
32.7	27.67	FA	0.20	36587	359	1097	1316	7.87E-05	6.80E+00	0	0.52	2.67E-03	1.74	375
29.7	29.50	FA	0.20	39000	382	1101	1321	7.75E-05	6.70E+00	0	0.52	2.60E-03	1.74	385
74.3	31.33	FA	0.20	41421	406	1104	1325	7.63E-05	6.59E+00	0	0.52	2.53E-03	1.74	395
85.4	33.17	BA	0.20	43850	430	870	1044	3.24E-03	2.80E+02	0	0.63	3.20E-02	1.53	31
59.0	35.00	FA	0.20	45763	449	1110	1332	7.43E-05	6.42E+00	0	0.51	2.42E-03	1.75	413

Figure 70. Example of Profile Spreadsheet

4.2.1.3 Upper Boundary Condition for Baseline Model

The upper boundary condition for the baseline model incorporated climate data from the NMCC station located at the Farmington Agricultural Science Center, approximately 14 km from the SJM. Meteorological data obtained from this site included daily temperature maximum and minimums, precipitation, and wind data. The climate data was plugged into the Penman Monteith equation by the HYDRUS 1D model to estimate evapotranspiration. Data between January, 1995 and December, 2004 was selected for this study in part because it was complete (no missing data) and was used for these simulations. For simulations longer than 10 years, this 10 year period of data is repeated. The atmospheric boundary condition allowed a maximum depth of 5 cm of standing water to accumulate on the soil surface prior to runoff occurring.

4.2.1.4 Baseline Root Water Uptake

The root water uptake for this model was adopted from Garcia et al. (2011), who investigated the root water uptake for the creosote bush present in the Mojave Desert. The creosote bush study conducted by Garcia et al. (2011) displays similar transpiration as great basin shrubs present near the SJM (Steinwand et al., 2001).

The Feddes model was used to calculate root water uptake by the HYDRUS 1D model. The leaf area index used for the simulation was set to a constant 0.38 according to Steinwand's study (2001), and a radiation extinction value of 0.6 was assumed. The pressure head below which plants will begin to uptake water was set to 0; maximum water uptake was set to occur between -2,000 and -7,000 cm; water uptake rate decreases between -7,000 and -40,000 cm with a wilting point of -80,000 cm of root zone pressure head. The maximum transpiration rate was set to 0.5 cm/day and a lower rate of 0.1 cm/day. The root zone was set to a depth of 1 m from the top of the soil profile. The root distribution values used as input for the model are presented in Table 21.

Table 21 - Root Distribution Input Values

Depth (cm)	Root Distribution
0-10	0
10-20	0.1
20-30	0.2
30-40	0.2
40-50	0.3
50-60	0.3
60-70	0.1
70-80	0.1
80-90	0.1
90-100	0.1

4.2.1.5 Lower Boundary Condition for Baseline Model

The boundary condition at the bottom of the 85 m vertical profile was a zero constant flux. It was observed that this lower boundary was sufficiently far from the bottom of the disposal pit that it did not affect water movement at the interface between the disposal cell and the Pictured Cliffs Sandstone. Figure 71 displays a diagram of the profile of material in the baseline model.

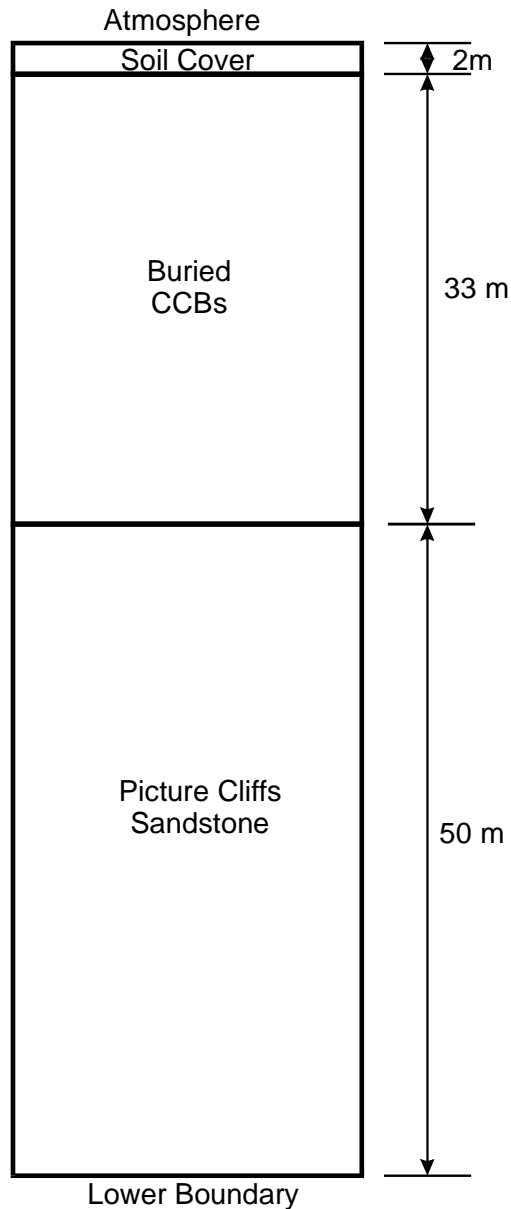


Figure 71. Diagram of baseline model materials and boundary conditions

4.2.1.6 Initial Moisture Content

Four of the randomly generated profiles were selected to investigate the sensitivity to the initial moisture content different from that of the baseline model based on the number of and spacing between BA materials in the profile. Also, FA only and BA only profiles were used to investigate the sensitivity of the model to the initial moisture content of the buried materials. The initial moisture content of the top soil was 5% for all simulations. The CCBs and Pictured Cliffs Sandstone initial moisture contents were changed from the baseline value of 20% to values of 10, 15, 25, 30, and 40% to investigate the effect that this had on soil water content and movement at the interface between the buried CCBs and the sandstone.

4.2.1.7 Root Water Uptake

Simulations were conducted with and without root water uptake to assess its impact on the model results for FA and BA only profiles. All other aspects of the model were those used in the baseline model.

4.2.1.8 Upper Boundary Condition

The upper boundary condition was changed from using actual meteorological data to zero constant flux in order to determine if any moisture was infiltrating through the top boundary under baseline conditions, or if the observed fluxes at the interface between the topsoil and the CCB were due to initial conditions. Root water uptake was also not included during this analysis.

4.2.1.9 Extended Simulation Duration

The duration for the FA only and BA only profiles of the baseline model were extended for a period of 100 years to determine the time needed for the system to come to equilibrium. The upper boundary condition was set to zero constant flux and root water uptake was not simulated.

4.2.1.10 Focused Recharge on Surface

Once the pit has been filled, covered, and closed it is possible that its surface may experience differential settlement that may provide natural sinks through which focused recharge may occur. In order to account for this, an analysis was conducted in which standing water was allowed to occur to simulate focused recharge that may occur. This analysis was performed for the FA and BA only profiles.

The maximum allowed pressure head at the soil surface (i.e. depth of standing water) was changed from 5 cm to 0 cm to investigate how much runoff might occur under the given meteorological conditions. The graphs showing precipitation and surface runoff for this scenario are presented in Figure 72. The amount of surface runoff for each precipitation event producing runoff was then multiplied by 10 to account for a watershed area 10 times larger than the ponding area of the sink. The dates and magnitudes of runoff events can be seen in Table 22. The calculated runoff of the watershed was then added to the precipitation occurring on the runoff dates in the meteorological input data for the baseline model. The maximum allowed pressure head at the soil surface was then changed from 0 to 100 cm to simulate ponding and focused recharge. This simulation was executed for a time period of 20 years on FA only and BA only profiles.

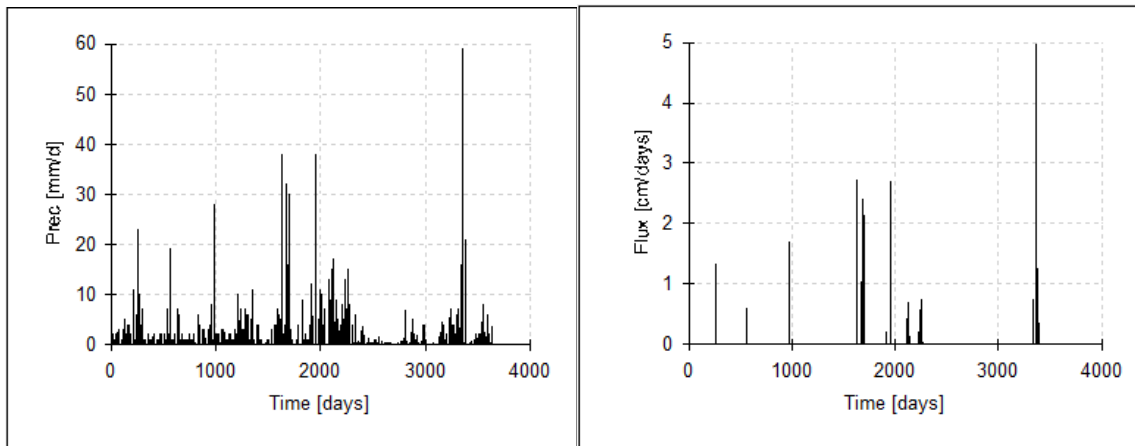


Figure 72. Precipitation (left) and Surface Runoff (right)

Table 22. Day and Magnitude of Runoff Events

Day in Model	Runoff (cm)	Excess for 10 m ² (cm)
251	1.38	13.75
558	0.81	8.13
976	1.88	18.75
1622	2.81	28.13
1666	1.13	11.25
1671	2.50	25.00
1676	2.25	22.50
1914	0.31	3.13
1957	2.75	27.50
2108	0.50	5.00
2121	0.81	8.13
2231	0.56	5.63
2258	0.69	6.88
3342	0.75	7.50
3362	5.00	50.00
3381	1.25	12.50
3386	0.38	3.75

4.2.1.11 Presence of Water Table

Simulations that included the presence of a water table at the base of the disposal pit were conducted for the FA only and BA only profiles. Alterations were made to the baseline model to create a scenario in which a water table occurred at a depth of 35 m from the soil surface. The depth of the profile was changed from 85 to 35 m to remove the Pictured Cliffs Sandstone and the bottom boundary condition was set to a constant (saturated) water content; these water contents were 51% for FA only and 65% for BA only profiles.

4.2.1.12 Lowering of Water Table

The scenario in which the landfill pit equilibrates with the water table at 35 m depth and then the water table is significantly lowered was simulated. This was done to simulate the impacts that might be experienced if at some point in the future extensive development of the underlying aquifer occurred causing a large regional drawdown. The profile depth was kept at 85 m with the Pictured Cliffs Sandstone composing the lower 50 m as in the baseline profile. The upper boundary condition was set to a zero constant flux and the root water uptake simulation was removed from the baseline model. This was done to eliminate outside influences so that the results only reflected the consequences of lowering of the water table. Initial conditions for the soil profile were also changed to represent an equilibrium condition with the water table at 35 m.

4.3 Results and Discussion

The model profiles containing FA only, BA only, and two representative random profiles have been selected to display the results for the baseline model and the sensitivity of the model results to initial soil moisture content. The random profiles are identified as profile numbers 3 and 8; these profiles were chosen because they represent the highest and lowest fluxes of the 15 random profiles at the observation points. Material discretization for profiles 3 and 8 can be seen in Table 23. All other profiles show flux rates bounded by the two selected profiles. The figures display water flux for each observation point as a function of time and moisture content with depth at selected time steps.

4.3.1 Results of Baseline Model Simulation

A summary of the range of values for fluxes and water contents for the baseline are presented in Table 24. A positive flux value represents upward water movement and a negative flux represents downward movement. All baseline model simulations indicate the Pictured Cliffs Sandstone becoming saturated at the bottom of the material and drying near the interface with the CCB pit. The top soil shows little change in moisture content over the duration of the simulations.

The FA only profile simulation shows that the moisture content of the CCB material at the bottom of the pit as the interface with top soil dries, though it does not become fully saturated. The BA only profile simulation also shows an increase in moisture content of CCB material at the bottom of the pit, though it too does not become fully saturated. This profile shows intermittent wetting and drying sections between the top soil and bottom of the pit. The profile 3 and 8 simulations display the CCB pit wetting at the bottom of fly ash sections, though not fully saturated, and drying within the bottom ash materials. No downward water movement is observed at the interface between the soil cover and CCB pit interface for any of these simulations. These results can be seen in Figure 73 through Figure 76.

Table 23. Material distribution for random vertical profiles 3 and 8

Depth (m)	Profile 3 Material	Profile 8 Material
0-2	Topsoil	Topsoil
2-3.8	BA	FA
3.8-5.7	FA	FA
5.7-7.5	FA	FA
7.5-9.3	FA	BA
9.3-11.2	FA	FA
11.2-13.0	FA	BA
13.0-14.8	BA	FA
14.8-16.7	FA	BA
16.7-18.5	FA	FA
18.5 - 20.3	FA	FA
20.3 - 22.2	FA	BA
22.2 - 24.0	FA	FA
24.0 - 25.8	FA	FA
25.8 - 27.7	FA	FA
27.7 - 29.5	FA	FA
29.5 - 31.3	BA	BA
31.3 - 33.2	BA	FA
33.2 - 35.0	BA	FA
35.0 - 85.0	Sandstone	Sandstone

Table 24. Range of fluxes and water contents for the baseline model simulation.

Profile	Total Range of Observation Point Fluxes (cm/day)	Total Range of Water Contents (cm/cm)	CCB pit range of Water Contents (cm/cm)
FA only	-0.02 - 0.09	0.01 - 0.33	0.16 - 0.33
BA only	0.0 - 0.12	0.01 - 0.27	0.19 - 0.27
Profile 3	-0.03 - 0.02	0.08 - 0.32	0.08 - 0.32
Profile 8	-0.1 - 0.05	0.01 - 0.31	0.08 - 0.31

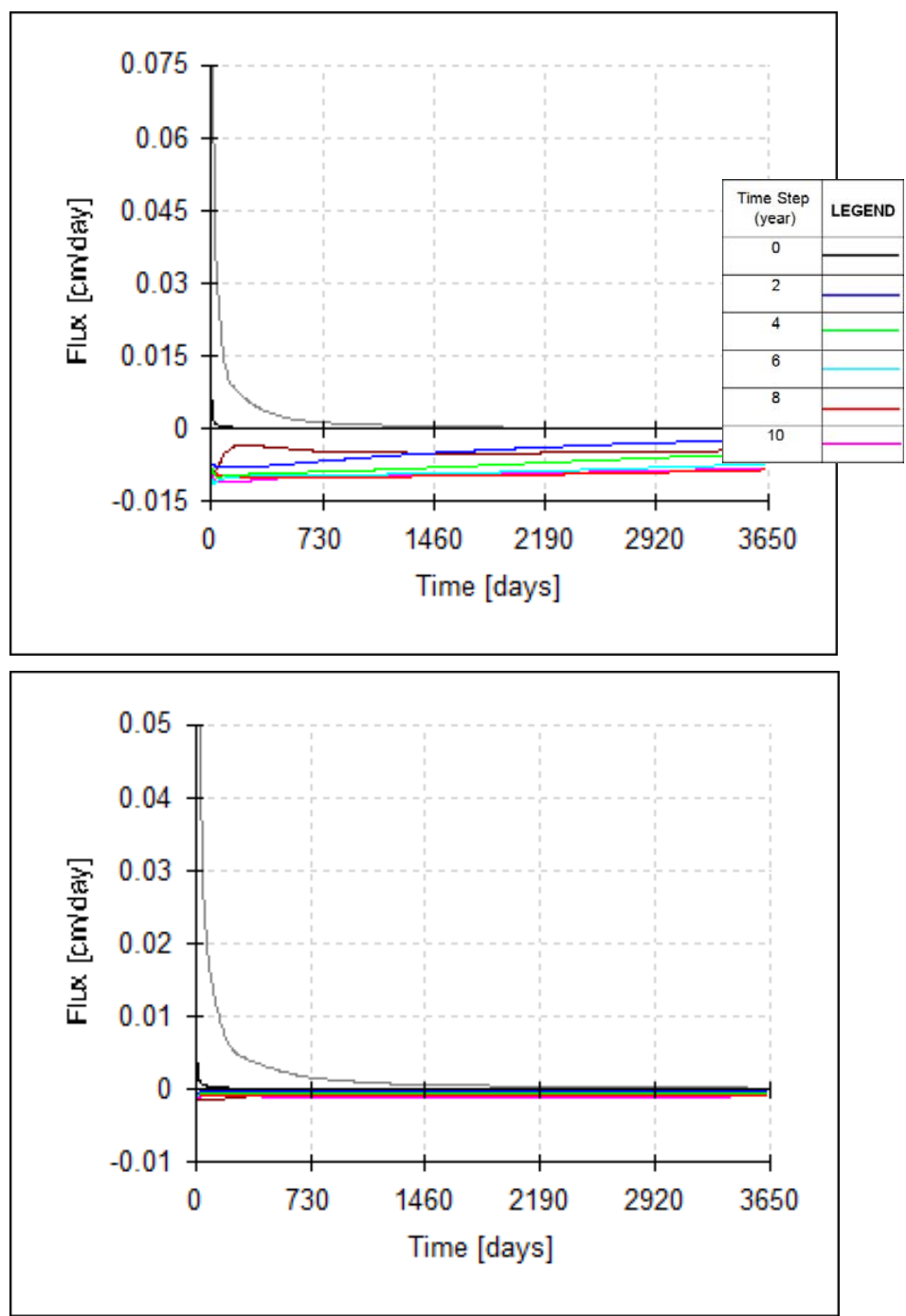


Figure 73. Soil water flux predictions for fly ash only profile (top) and bottom ash only profile (bottom).

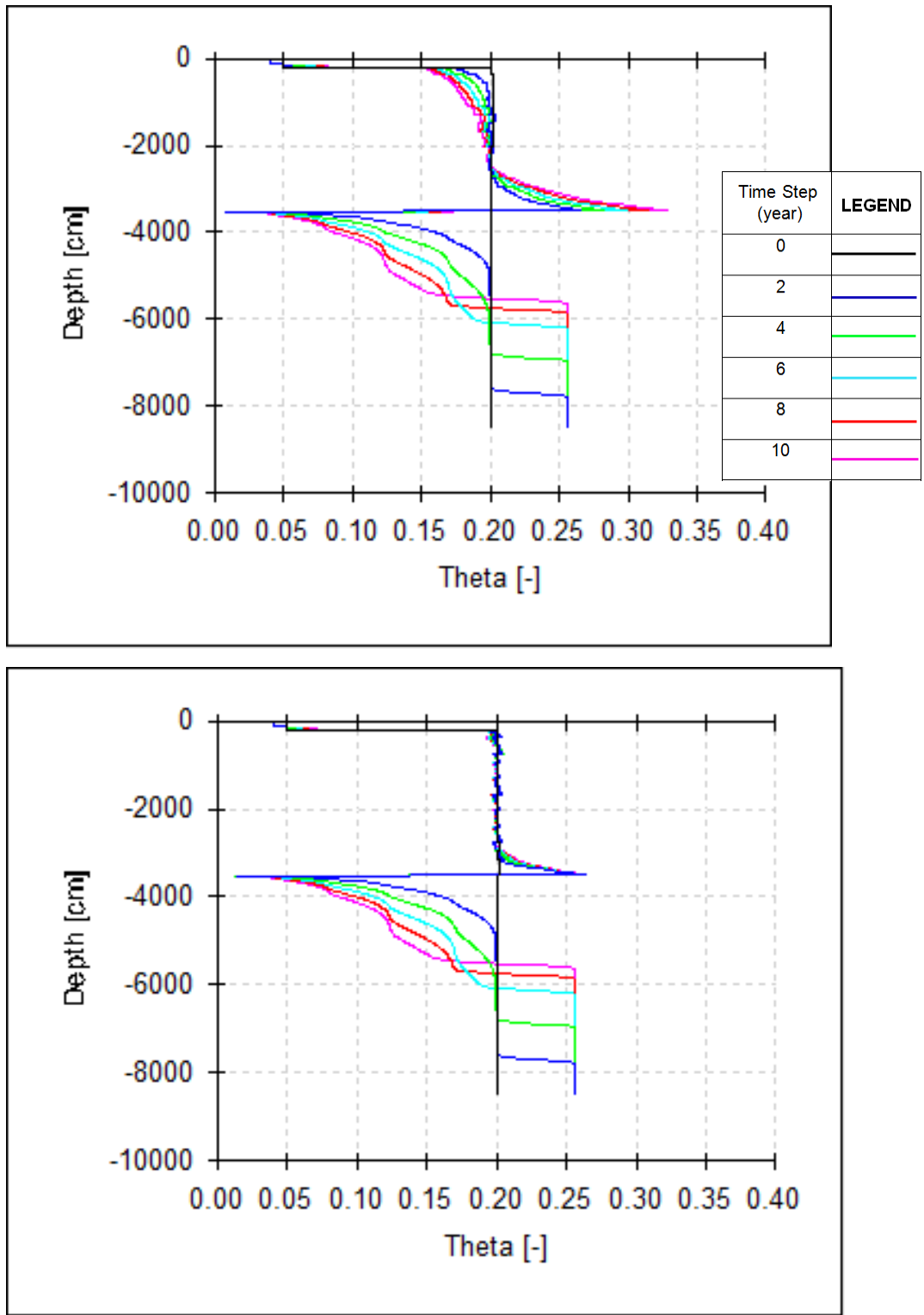


Figure 74. Soil moisture content vs. depth for fly ash only profile (top) and bottom ash only profile (bottom).

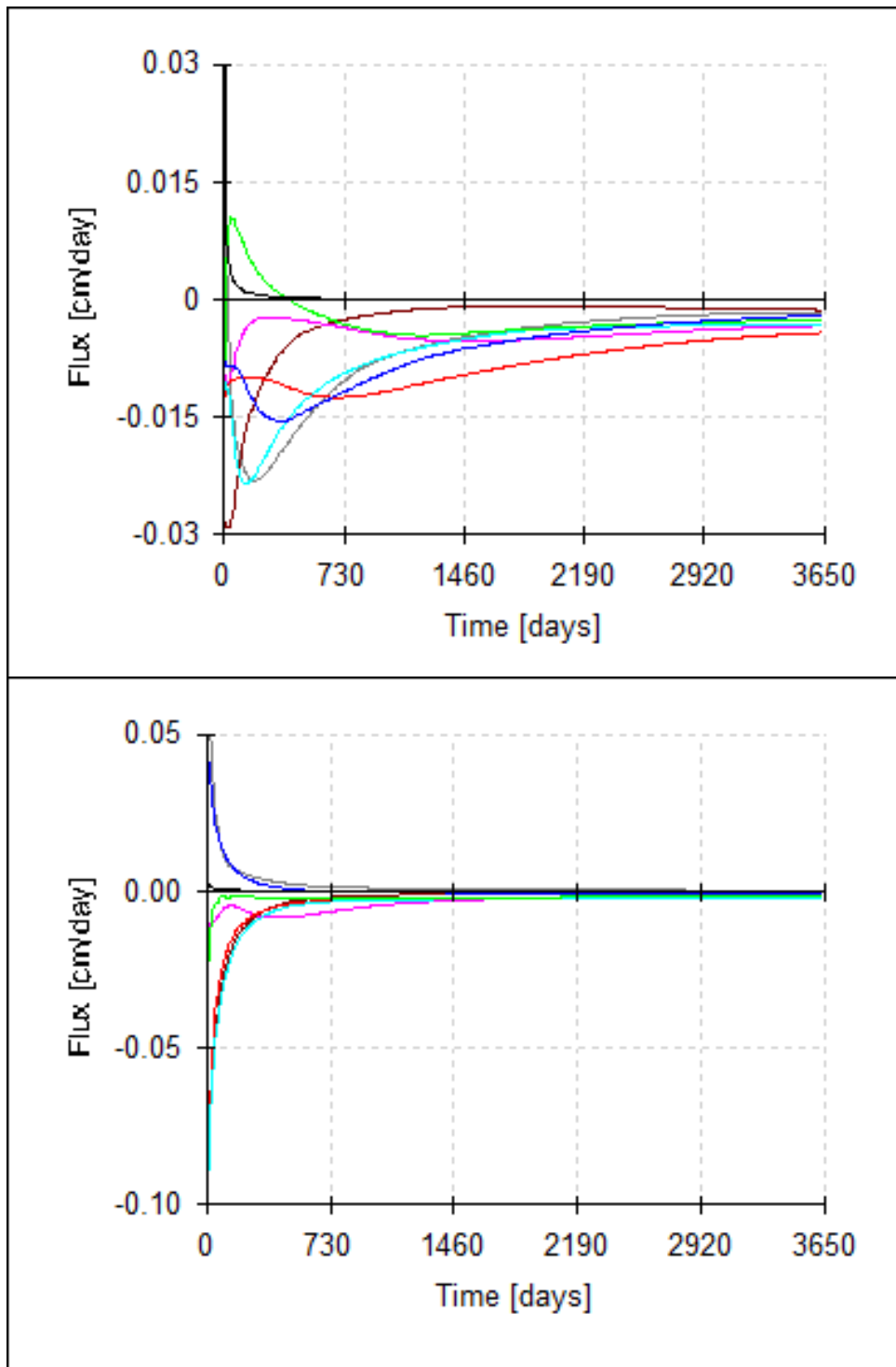


Figure 75. Soil water flux predictions for random profiles 3 (top) and 8 (bottom).

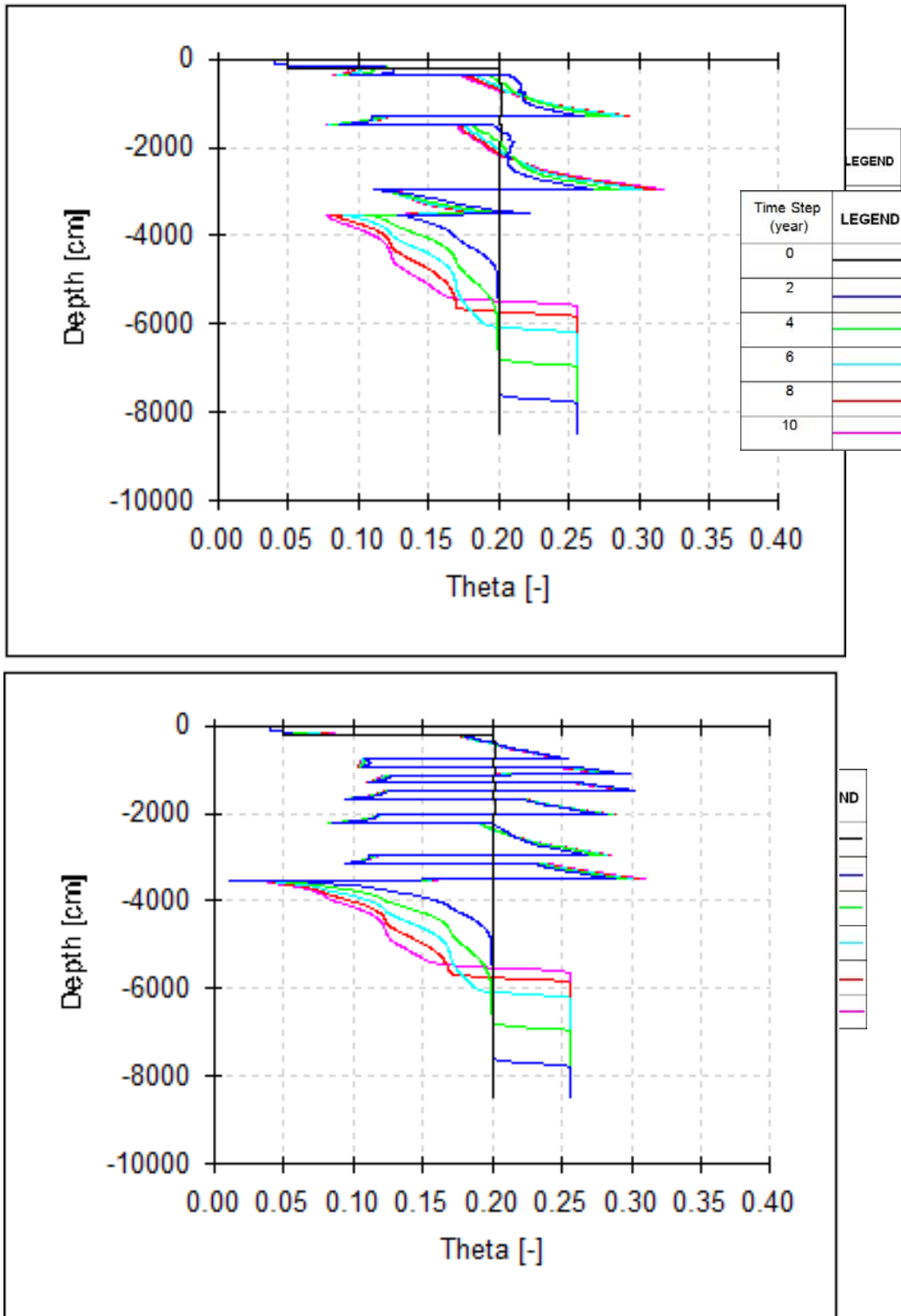


Figure 76. Soil moisture content vs. depth for random profiles 3 (top) and 8 (bottom).

4.3.1.1 Initial Moisture Content

Model calculations for the FA only profile predict downward fluxes at the bottom of the CCB pit at an initial water content of 30 and 40%. The BA only profile displays a downward flux only at an initial water content of 40%. Random Profile 3 shows downward fluxes at the bottom of the CCB pit at initial water contents of 20, 25, 30, and 40%. Random Profile 8 displays a downward flux at the bottom of the CCB pit only at an initial water content of 40%. The maximum flux vs. initial water content predicted for each profile is shown in Figure 77. Maximum flux is defined here as either the maximum upward value if no downward flux is predicted or the maximum downward value predicted during the 10 year time period of the simulation. For all simulations, the maximum flux occurred briefly, during the first 1 to 2 years of the simulation and likely reflects equilibration of water present initially in the soil column.

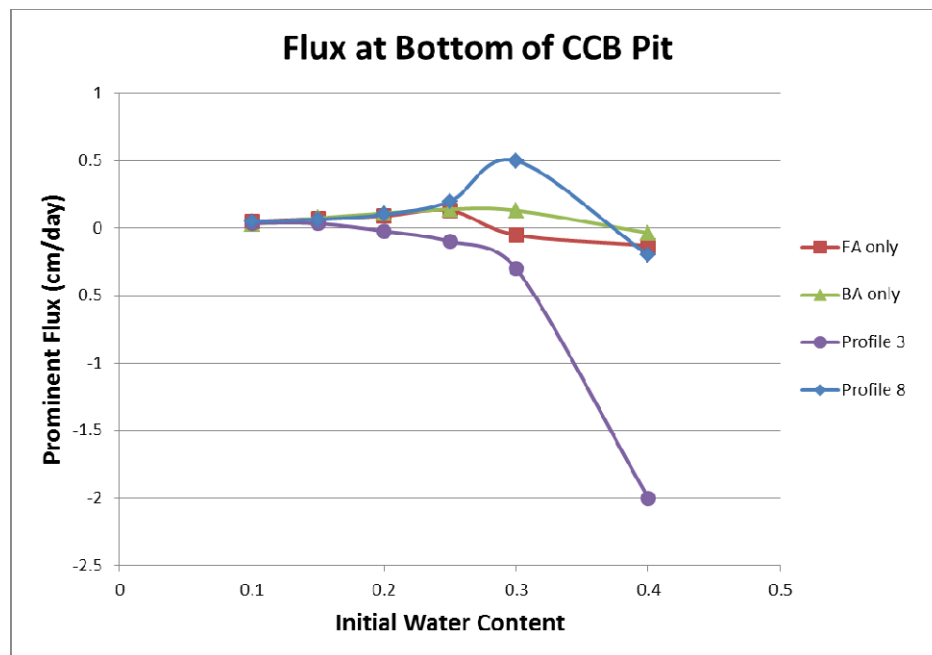


Figure 77. Flux at bottom of CCB pit as a function of initial water content.

4.3.1.2 Effect of Root Water Uptake

Results of the model simulation without root water uptake show no significant impact on the flux at the interface between the soil cover buried CCBs for both the FA only and BA only profiles during the 10 year simulation. The baseline model included about 40 cm of evapotranspiration; this water was principally stored in the top soil when the simulation was conducted without root water uptake (i.e., no evapotranspiration). In addition, because the soil cover was wetter than in the baseline case, somewhat more evaporation occurred when root water uptake was excluded from the simulation. Results of surface infiltration, root water uptake, and evaporation both with and without root water uptake simulation can be seen in Figure 78 through Figure 80.

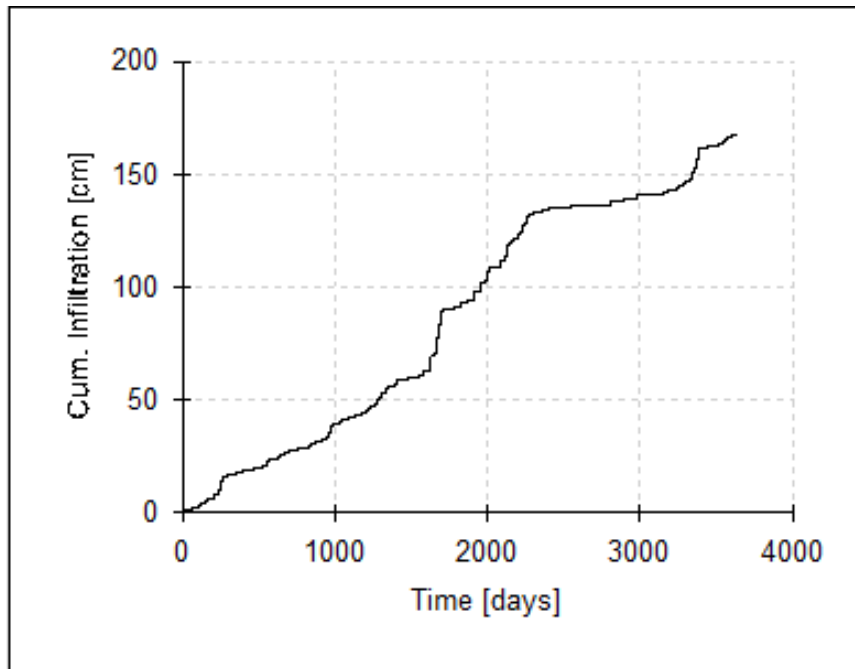


Figure 78. Baseline results: cumulative infiltration.

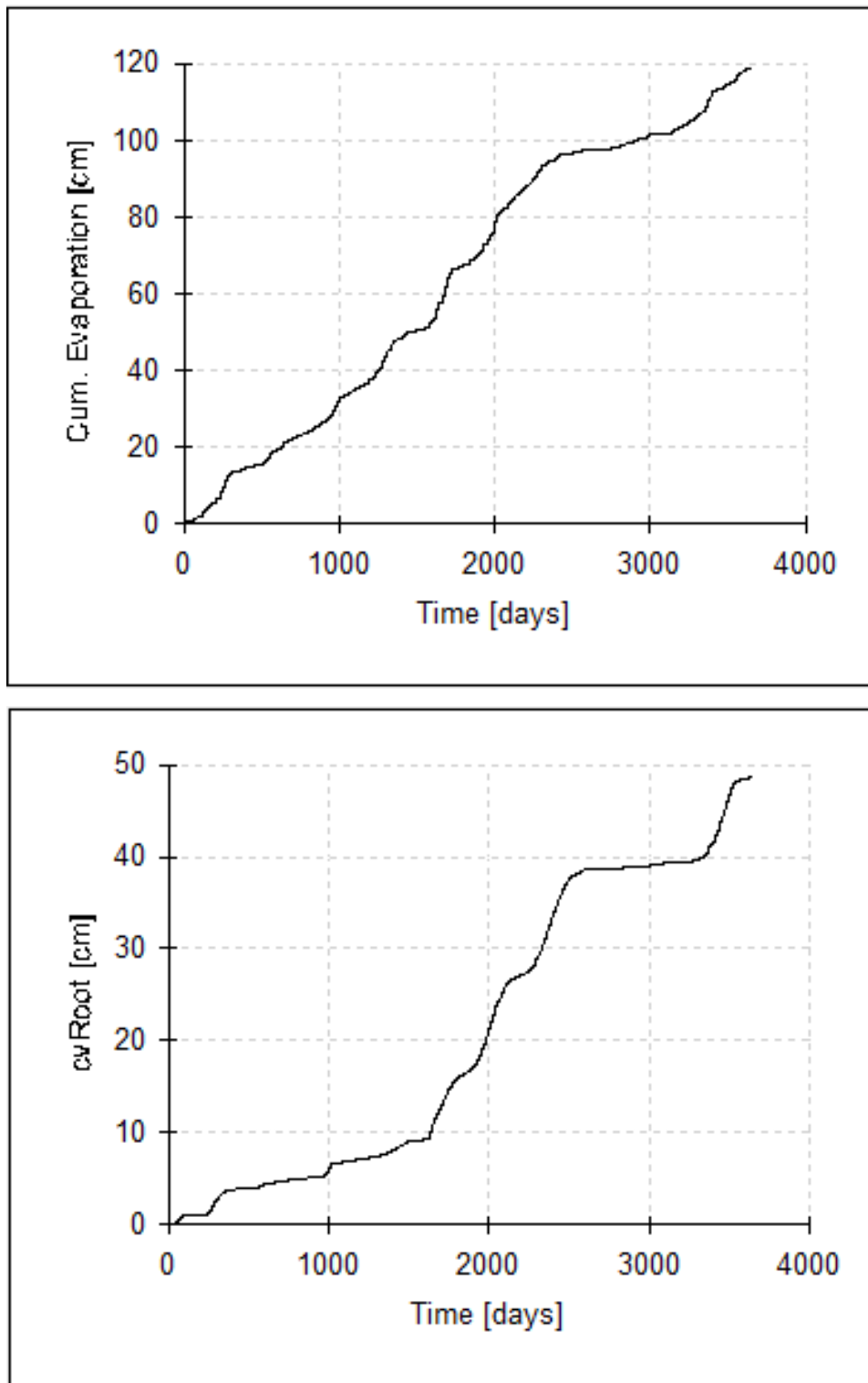


Figure 79. Cumulative root water uptake (top) and cumulative evaporation (bottom) for baseline model.

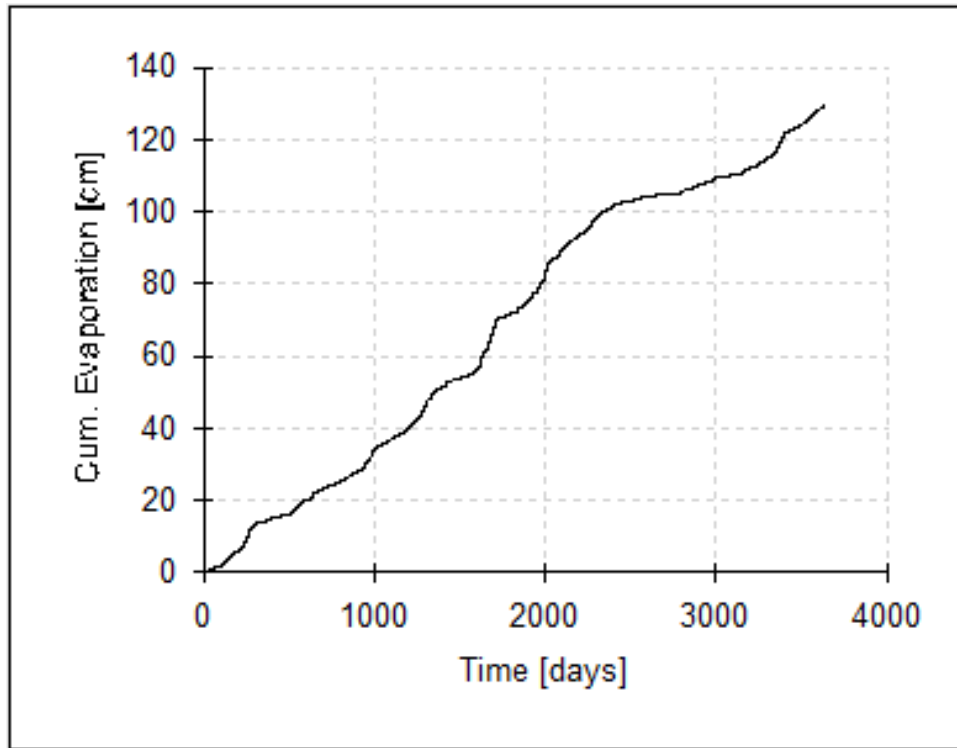


Figure 80. Cumulative evaporation without root water uptake.

4.3.1.3 Impact of the Upper Boundary Condition

Results from the model simulation with the upper boundary condition set to a zero constant flux and no root water uptake simulation showed no significant impact on the movement of water within or below the CCB pit for the baseline FA only and BA only profiles. These were the only profiles simulated for this boundary condition, but both show the relative insensitivity of water movement through the unsaturated soil to the upper boundary condition.

4.3.1.4 Extended Simulation Duration

The results for the 100 year simulation indicate equilibrium had not been reached within this period for both the FA only and BA only profiles. Very small fluxes (less than 5×10^{-4} cm/day) were still occurring throughout the profiles at the end of the 100 year duration, but these should be contrasted with fluxes up to 2 cm/d in the first year or two of the simulations (Figure 77).

4.3.1.5 Impact of Focused Surface Recharge

The cumulative surface infiltration results from the focused recharge (i.e. ponding) scenario is shown in Figure 81 and shows greater infiltration than in the baseline model. A plot of flux vs. time and water content with depth for the focused surface recharge scenario is presented in Figure 82 and Figure 83. The soil cover shows highly variable moisture content during the focused recharge simulation which is consistent with up to 100 cm of ponded water as the upper boundary condition

The FA only profile simulation results from focused recharge show the CCB pit wetting throughout the entire depth of the pit over the 10 year duration of the simulation. The Pictured Cliffs Sandstone material begins to show wetting at the interface with the CCB pit near the end of the simulation. The simulation for the soil profile consisting of BA only shows increased moisture in the unsaturated material at the interface of the soil cover and buried CCBs after 8 years and continued wetting downward through the pit throughout the simulation period. The model shows that the buried CCB never experiences wetting at the bottom of the pit for the BA only profile, even at the end of the 20 year simulation period.

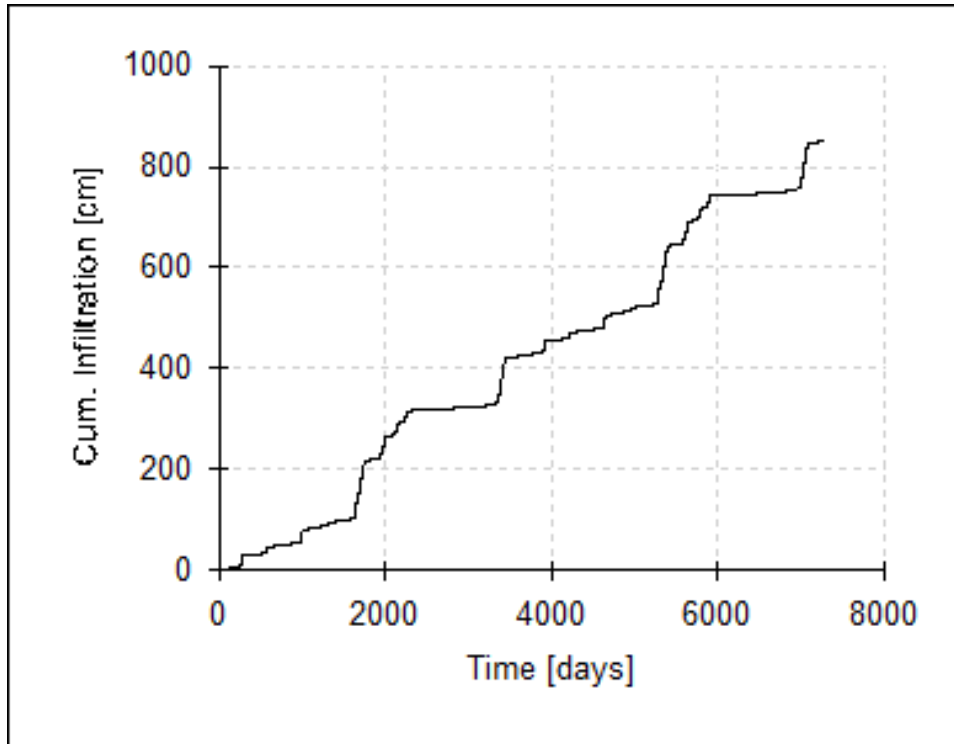


Figure 81. Cumulative infiltration for focused recharge scenario.

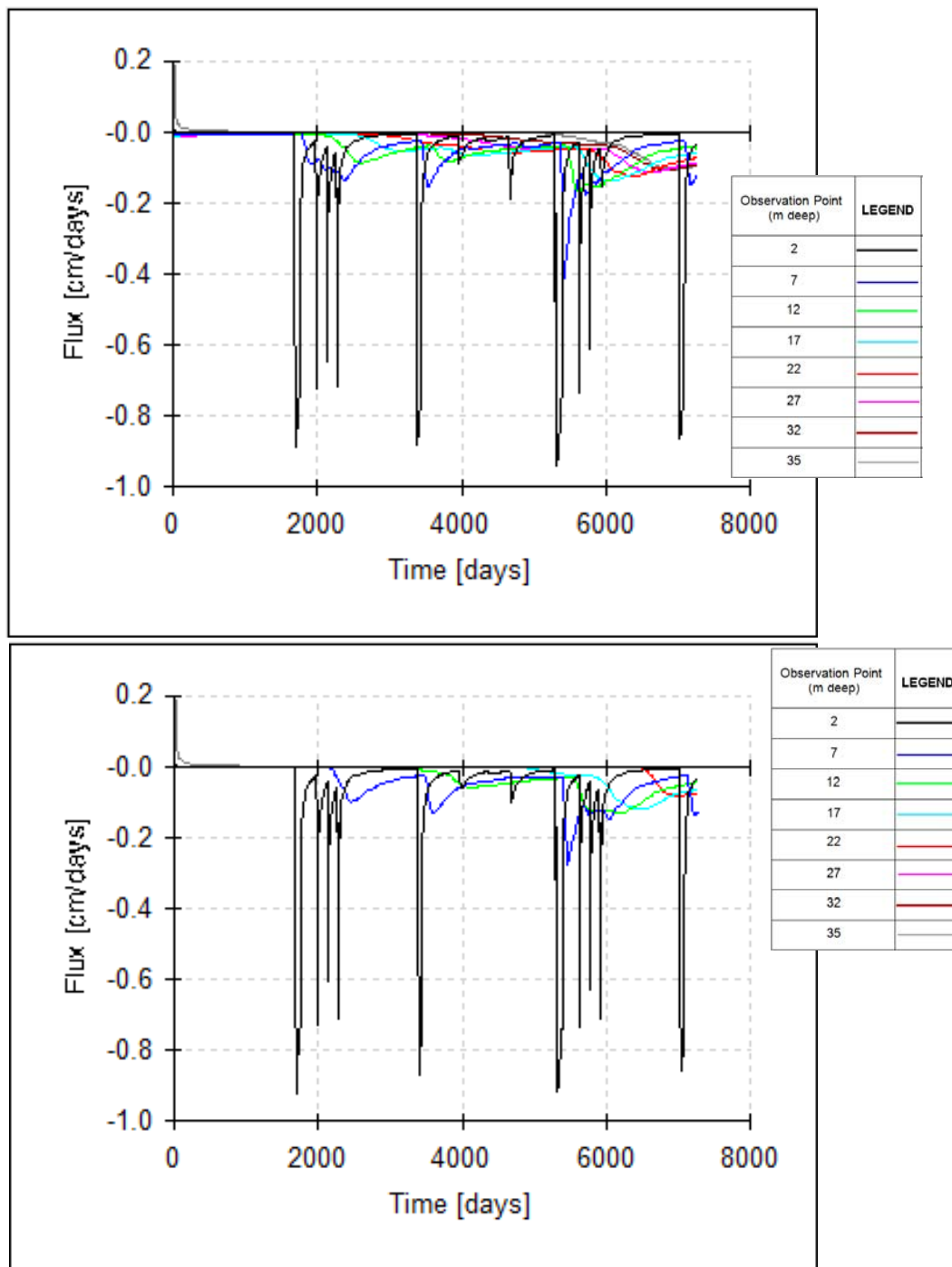


Figure 82 - Focused recharge scenario: Flux for fly ash only profile (top) and bottom ash only profile (bottom)

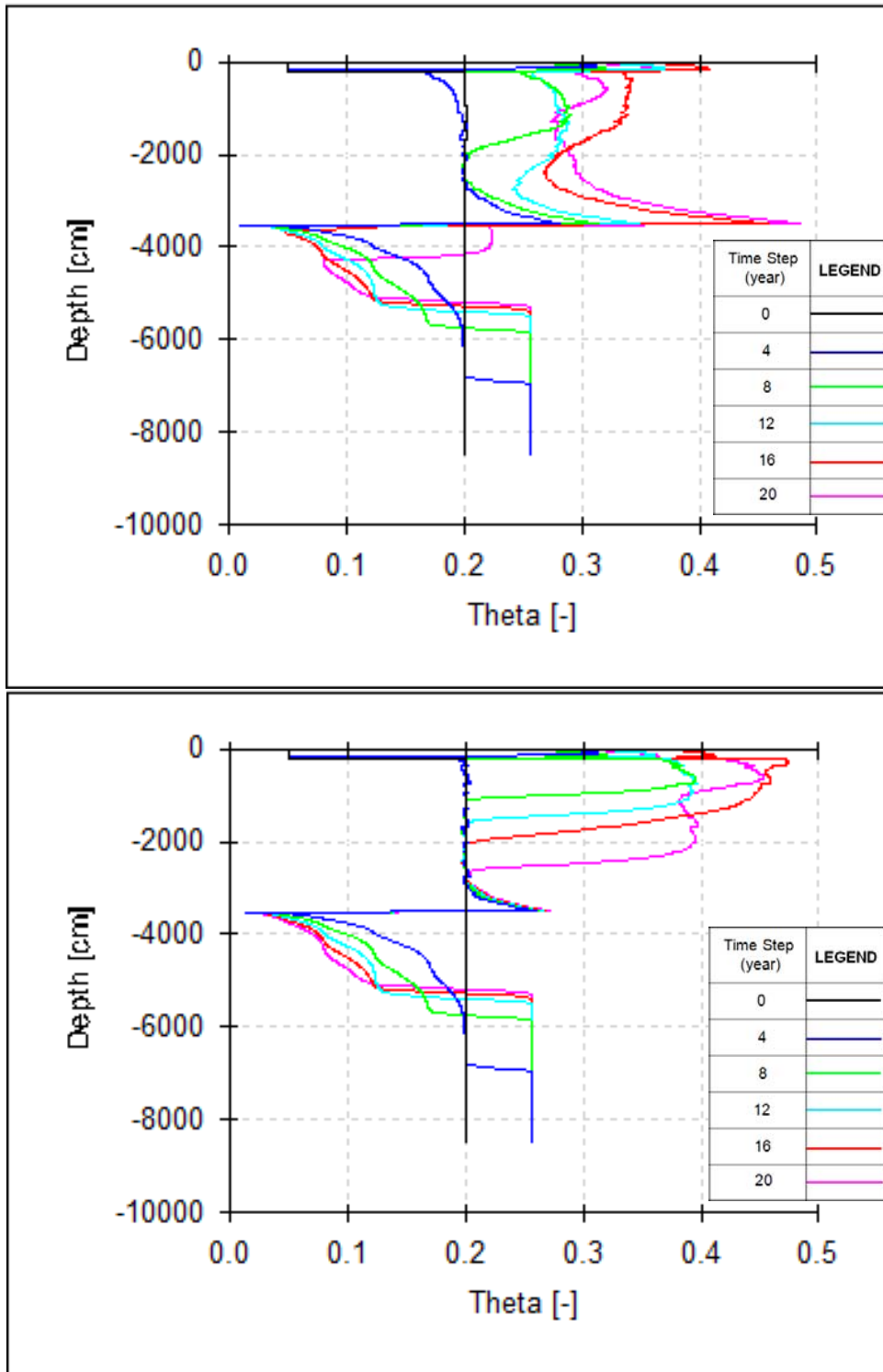


Figure 83. Plot of simulated water content vs depth for the focused recharge scenario for the fly ash (top) and bottom ash (bottom) only profiles

4.3.1.6 Impact of the Presence of a Water Table

Simulation results in which a water table is present at the bottom of the CCB pit are shown in Figure 84 and Figure 85. It is important to note the difference in the scale of the vertical axis in these figures compared to previous figures; the depth shown below the surface only extends to 35 m which is the base of the pit. For both the FA only and BA only profiles, there is a large, initial upward soil water flux at the bottom of the pit during the first year of the simulation as the dry ash equilibrates with underlying ground water. Throughout the simulation period material in the top of the FA only pit is drying from the top soil interface downward as initial water present in the buried ash equilibrates with the very dry soil cover. In contrast, the soil moisture profile in the BA only profile reaches rapid equilibrium and doesn't change after the first two years.

4.3.1.7 Impact of Lowering of the Water Table

The results for a scenario in which a water table is lowered from a depth of 35 to 85 m can be viewed in Figure 86 and Figure 87. Both the soil water flux and the moisture content for the FA only and BA only profiles exhibit similar results, an initial downward flux of approximately 0.2 cm /day at the bottom of the CCB pit and little or no effects in the top 20 m of buried ash. The profiles show a drying of the Pictured Cliffs Sandstone as well as the CCB pit, both originating from the interface between the two.

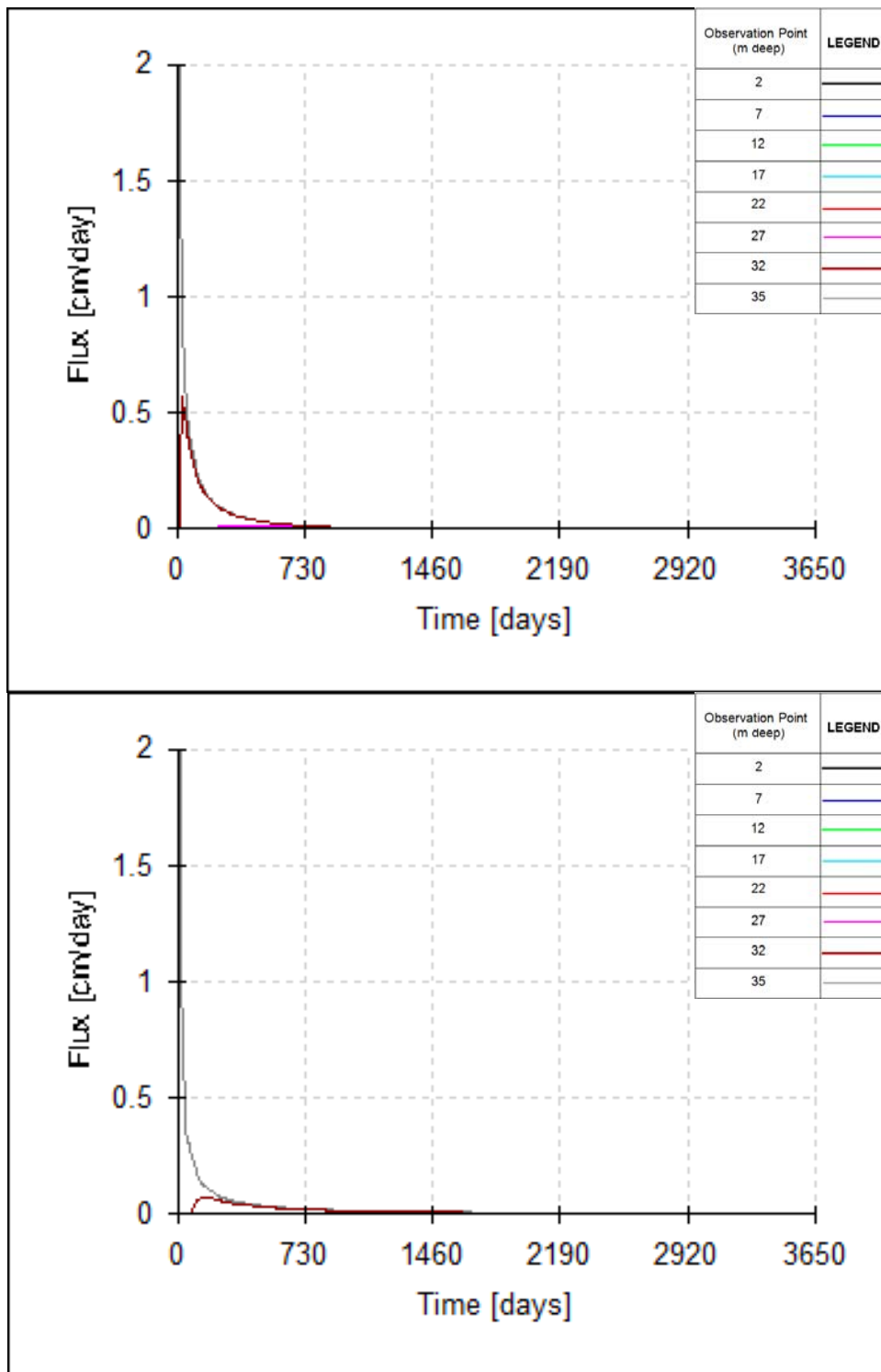


Figure 84. Predicted soil water flux for a water table at bottom of the buried CCB for fly ash (top) and bottom ash (bottom) only profiles

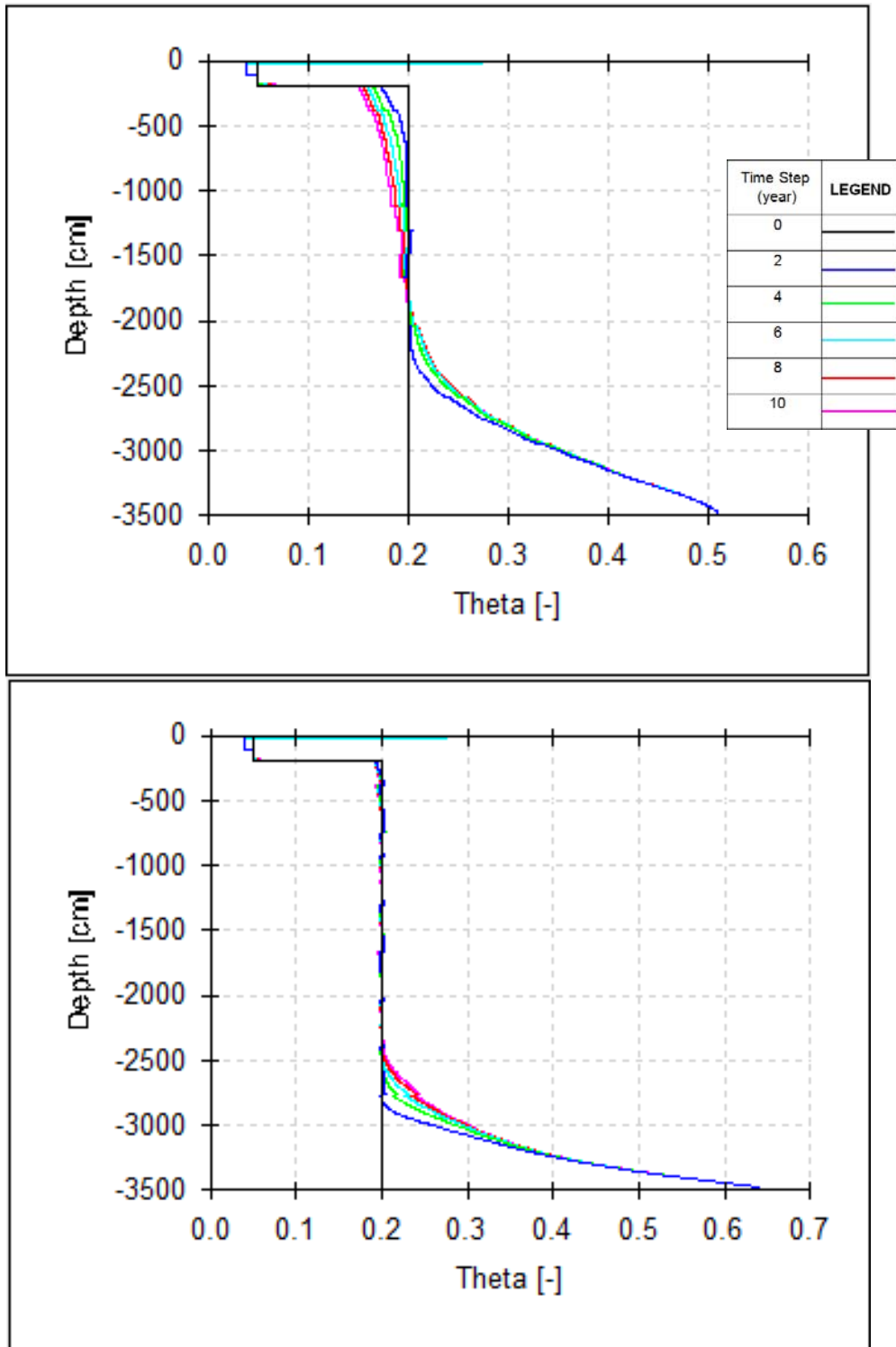


Figure 85. Predicted moisture content for water table located at the bottom of the buried ash for fly ash(top) and bottom ash (bottom) only profiles

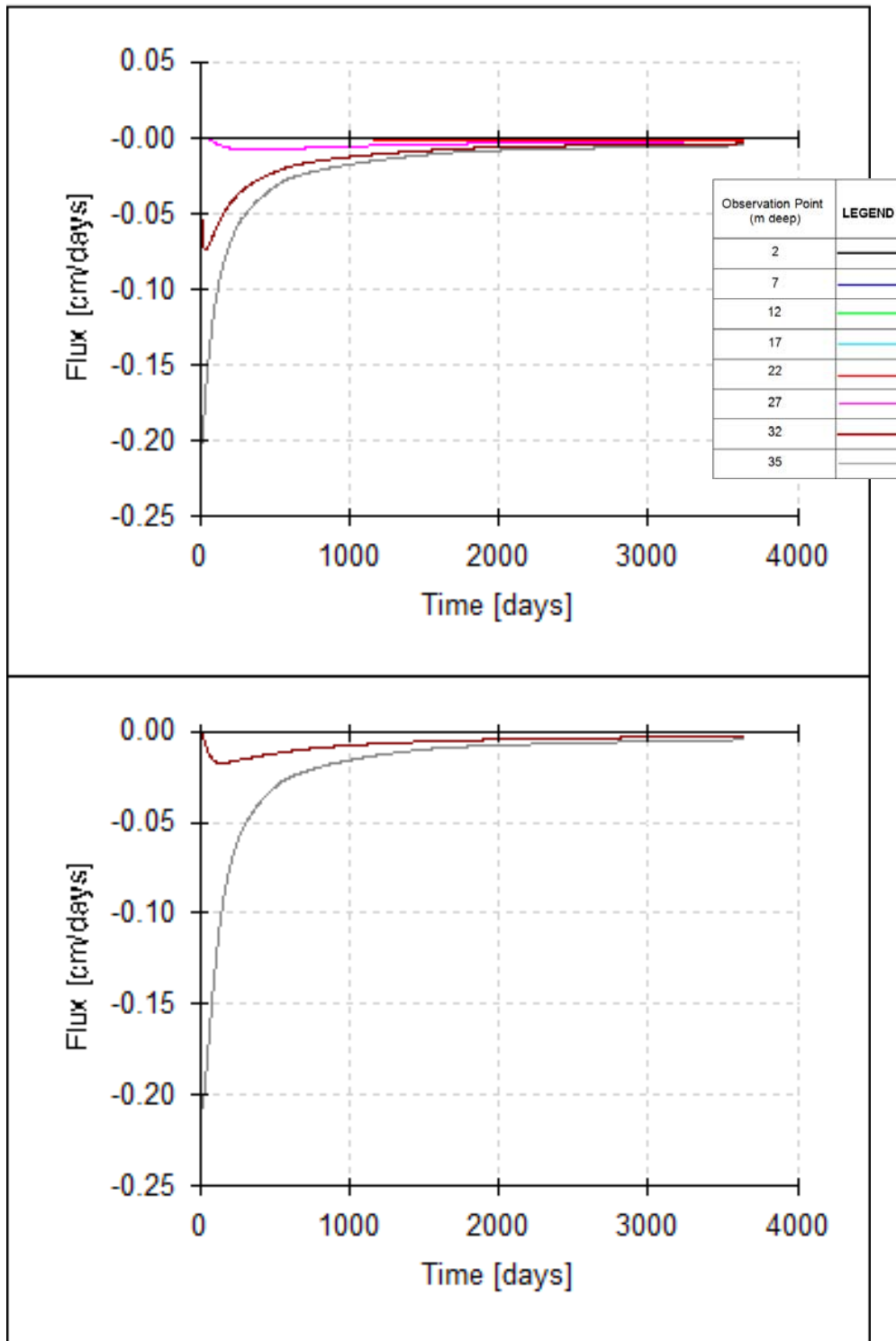


Figure 86. Predicted soil water flux for a drop in water table from the bottom of the pit for fly ash (top) and bottom ash (bottom) only profiles

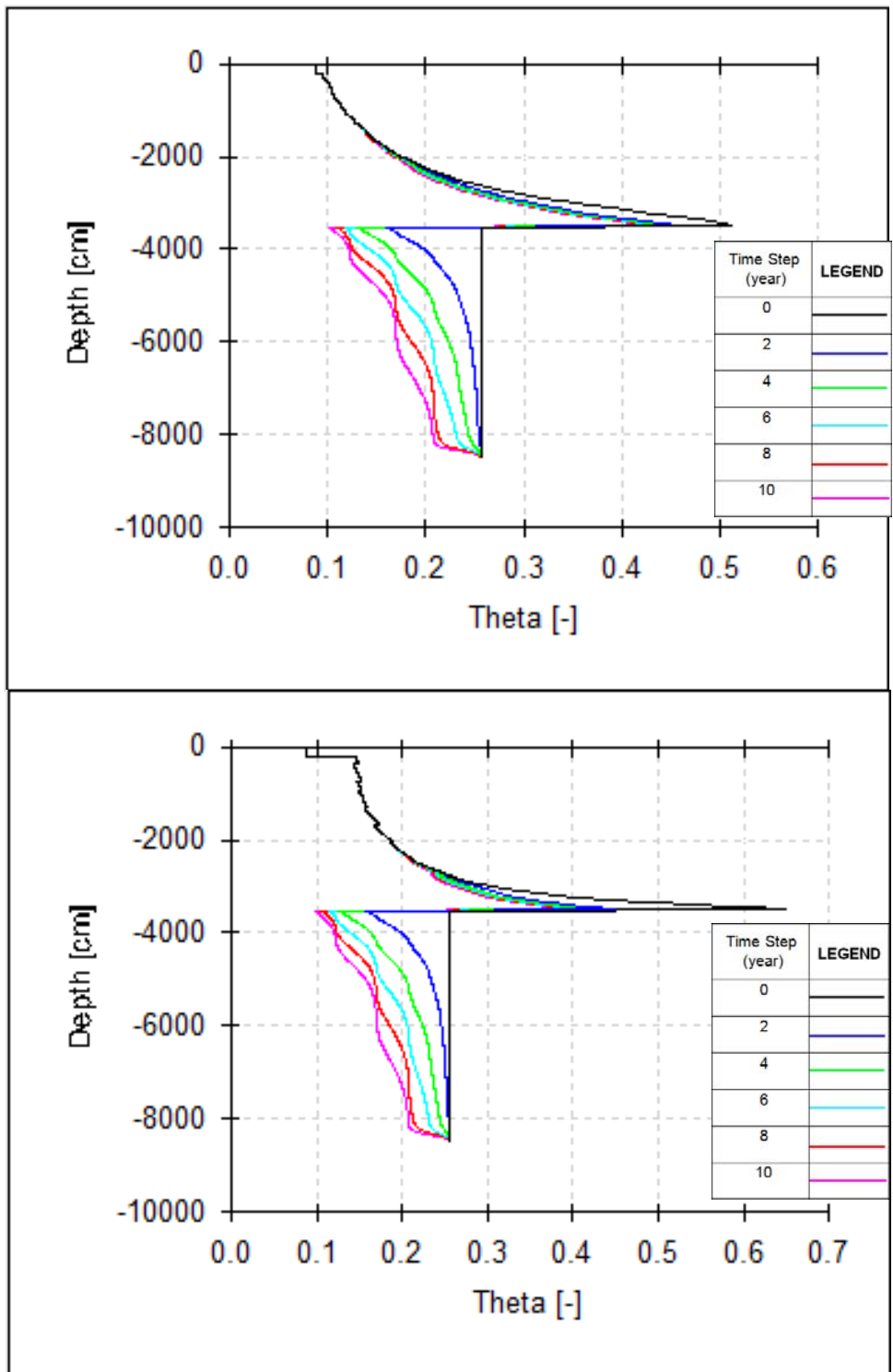


Figure 87. Predicted moisture content for a drop in water table from the bottom of the pit for fly ash (top) and bottom ash (bottom) only profiles

4.4 Discussion

The unsaturated soil water fluxes predicted by the model simulations primarily result from the initial conditions in the buried CCBs. The initial conditions for most simulations were prescribed water contents similar to those observed in the fresh ash and young ash samples. Even when these initial water contents were constant, they result in differences in total head vertically in the profile. Differences in total head produce potential gradients that cause the soil water to move up or down in the buried ash.

Results from the simulations with a zero constant flux upper boundary condition (i.e. no infiltration) and no root water uptake simulation show that water does not infiltrate past the root zone during the 10 year duration of the baseline model. Thus, soil water fluxes in the CCB pit are primarily due to initial water contents and are not being driven by infiltration from the surface. The movement of water through the bottom of the CCB pit into the underlying Pictured Cliffs Sandstone is an upward flux in most simulations. This is a result of initial conditions once again. Variations between material properties resulting in an upward gradient driving the movement of water. A summary of the soil water flux at 2 m and 35 m deep observation points, the top and bottom layers of the CCBs, respectively, are plotted at 1, 5, and 10 years in Figure 88 and Figure 89, respectively. The fluxes represent the average flux for all baseline simulations and the whiskers represent the minimum and maximum fluxes. Recall that negative fluxes as observed in Figure 89 represent upward movement of water towards dryer conditions at the surface.

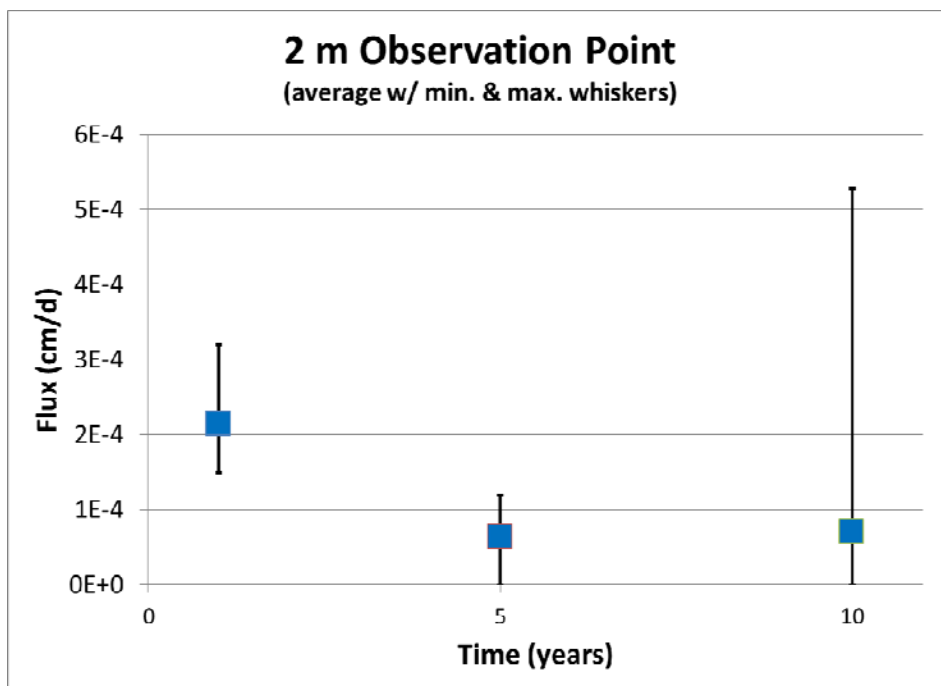


Figure 88. Predicted water flux at the interface between the soil cover and buried CCBs.

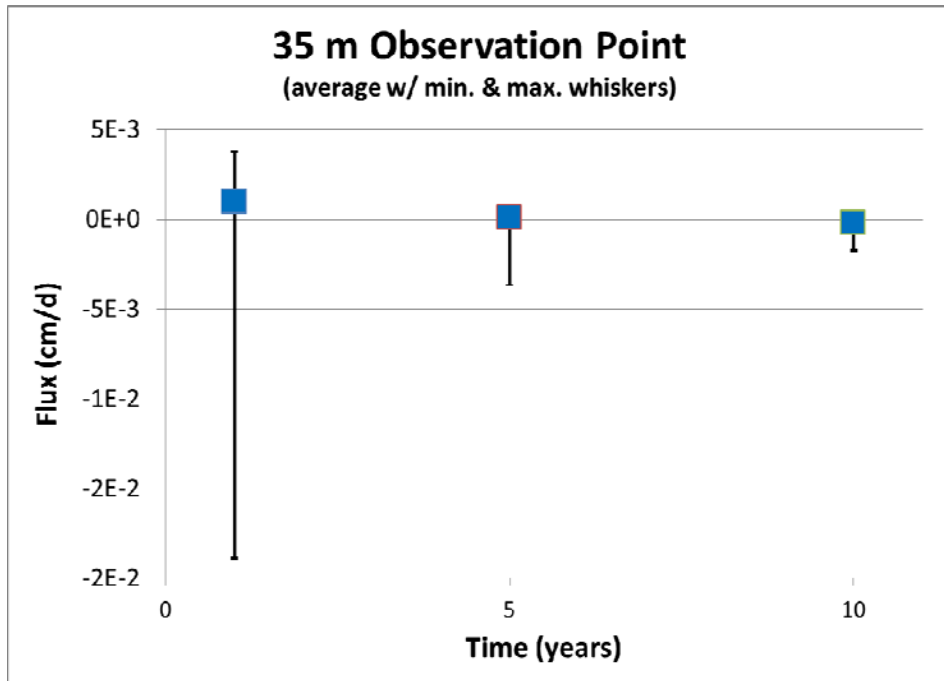


Figure 89. Predicted water flux at the interface between the buried CCBs and the Pictured Cliffs Sandstone.

Layering of the CCBs creates conditions that induce flow in the profile. Figure 90 presents the soil moisture characteristic curve for the different materials used in this modeling study. Figure 91 shows hydraulic conductivity (K) as a function of soil water pressure head (h), and Figure 92 shows the relationship between the hydraulic conductivity (K) and soil moisture content (θ) of materials for profile 3, respectively. It can be seen with these MCCs that the initial conditions existing at the interfaces between different materials (that is, constant water content) results in significant potential head differences which can induce water movement between layers. For example, at the initial moisture content of 0.2, pressure heads of fly ash and bottom ash are approximately 1000 cm and 316 cm, respectively. Thus, water will initially tend to move from bottom ash to fly ash. Water accumulates at the interface between the pictured cliffs sandstone and CCBs because of the initial upward gradient. Also, as water drains towards equilibrium, the K of the pictured cliffs sandstone becomes very low.

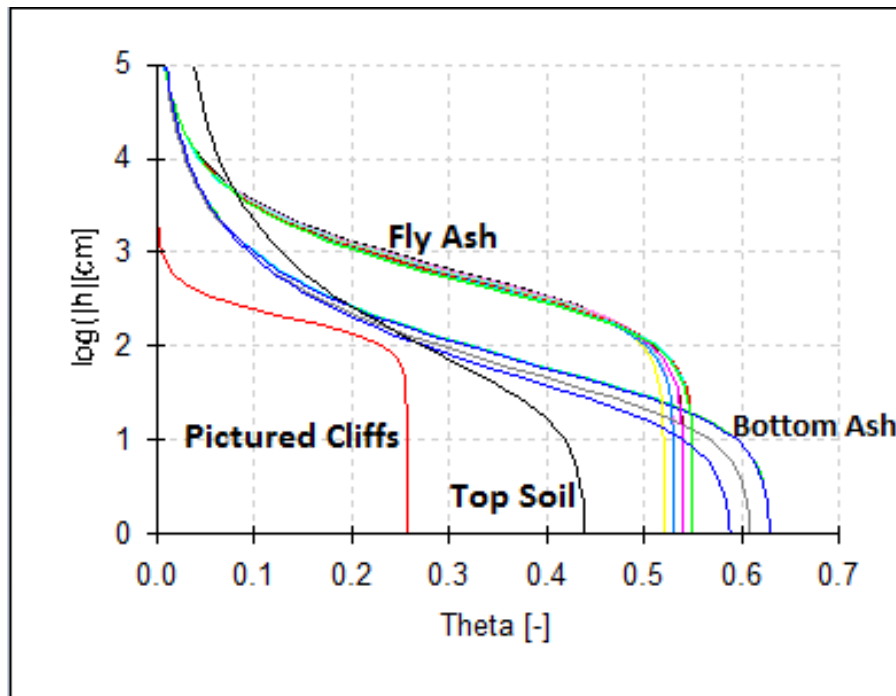


Figure 90. Moisture characteristic curves for materials used in the modeling study.

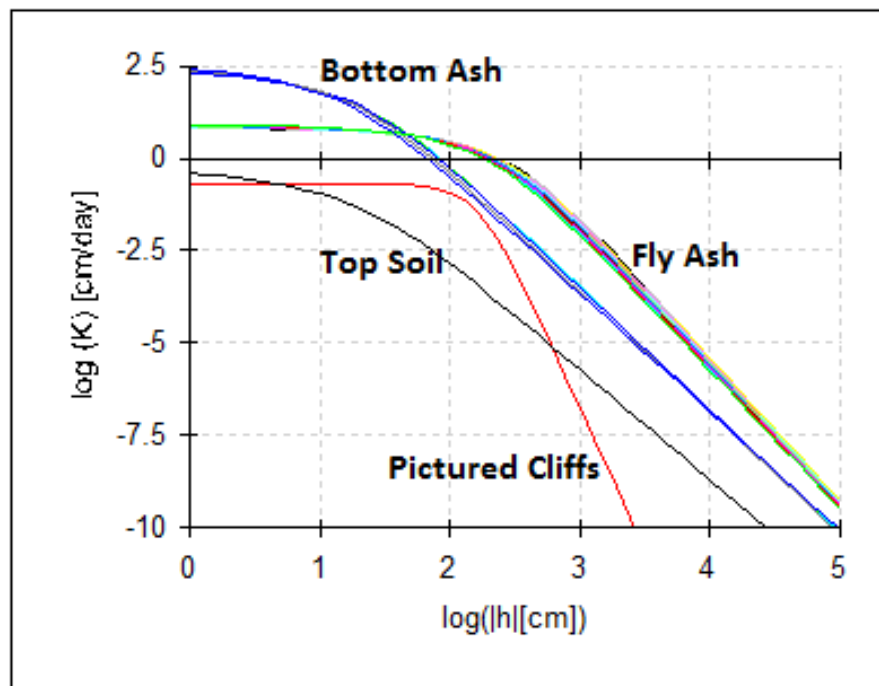


Figure 91. $\log K$ vs. $\log h$ for materials in profile 3

When ponding is allowed on the surface of the soil cover, water is able to infiltrate through the soil cover and into the CCB pit. It can be seen in Figure 83 that water moves more rapidly through the FA only profile than the BA only profile. Water is able to infiltrate through the entire depth of the CCB pit between 8 and 12 years in the FA only profile; whereas in the BA only profile, water still has not infiltrated through the entire CCB pit after 20 years. This difference in infiltration depth is due to the BA requiring a greater moisture content compared to FA in order to transmit water from the soil cover into the buried CCB material. Thus, because it accumulates more moisture to transmit this flux water does not move as deep into the BA profile. This is largely due to the fact that BA material is coarser and its hydraulic conductivity is roughly an order of magnitude less than that for FA at high water contents (Figure 92) The MCCs and K vs. suction head of the top soil and CCBs present beneath the top soil for these simulations are displayed in Figure 93 and Figure 94 respectively.

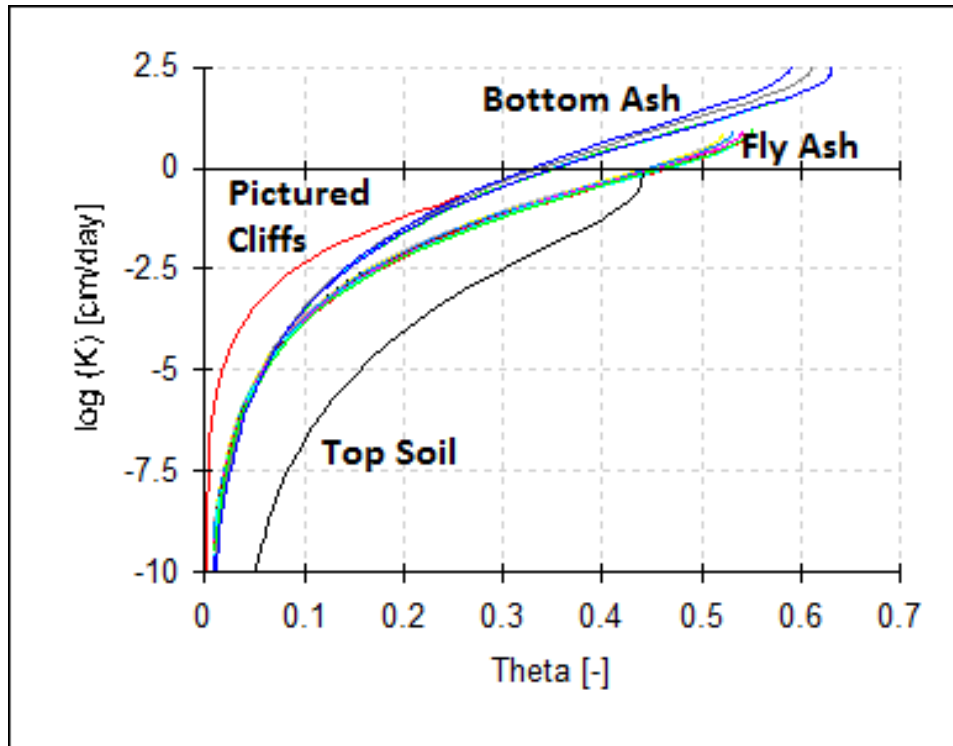


Figure 92. log K vs Water Content for materials in profile 3

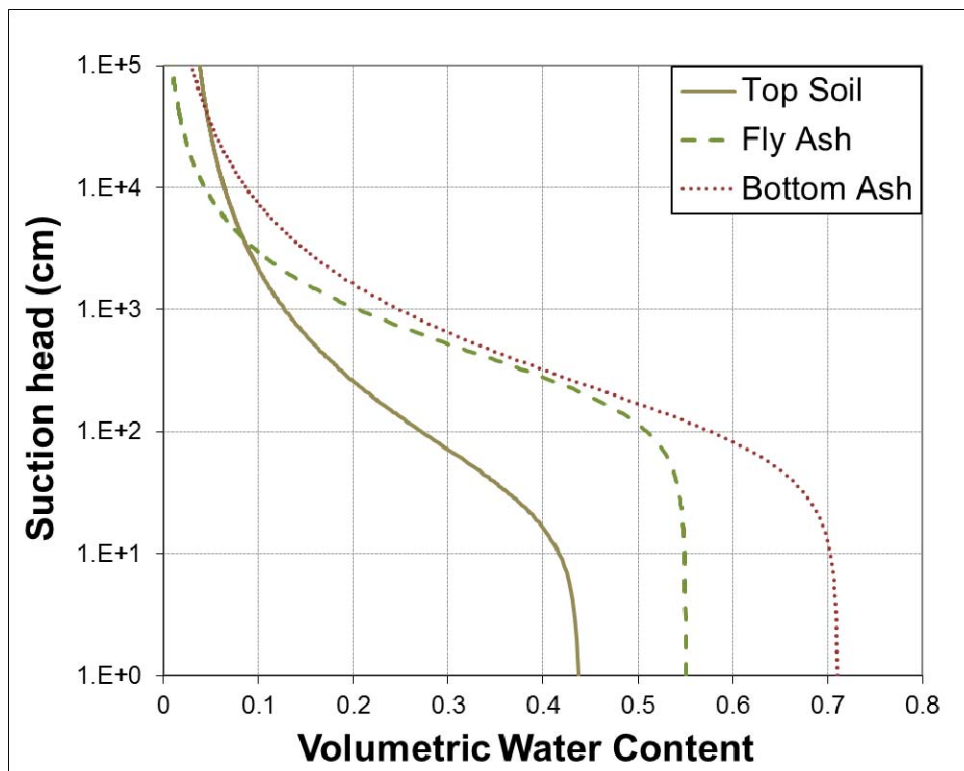


Figure 93. Moisture characteristic curve for top soil, fly ash, and bottom ash at the interface between top soil and CCBs for focused recharge simulations.

The focused recharge scenario only accounts for one dimensional flow, and therefore does not include the effect that horizontal water movement would have on the buried ash. It does, however, display the potential for water movement through a CCB pit if ponding occurs at the surface and subsequently causes focused recharge.

Simulation results for the scenario in which a water table is present at the bottom of the CCB pit show capillary rise occurring above the water table interface. Within the FA only profile, there is also some drying of the CCBs near the top of the interface between soil cover and buried CCBs whereas the BA only profile does not display this behavior. These results are a consequence of the larger size of the BA materials so that the water contents that these materials will have at equilibrium with a water table decreases above the top of the water table.

The simulated lowering of the water table shows little drainage into the Pictured Cliffs Sandstone. The FA only profile shows a downward flux occurring further up from the bottom of the CCB pit than the BA only profile.

4.4.1 Sensitivity Analyses

The numerical modeling shows that the initial water content in the buried ash has a significant impact on the soil water movement at the bottom of the CCB pit. Downward fluxes in excess of 0.05 cm/day occur for simulations with initial water contents of about 25% and above. This result suggests that disposal practices (i.e., wetting of the ash material for dust control) may influence the flux through the bottom of the CCB pits. Significant fluxes at the bottom of the pits occur briefly after disposal then taper off to near zero which demonstrates that fluxes are related to equilibration of initial conditions between materials and not due to infiltration of rainwater through the soil cover.

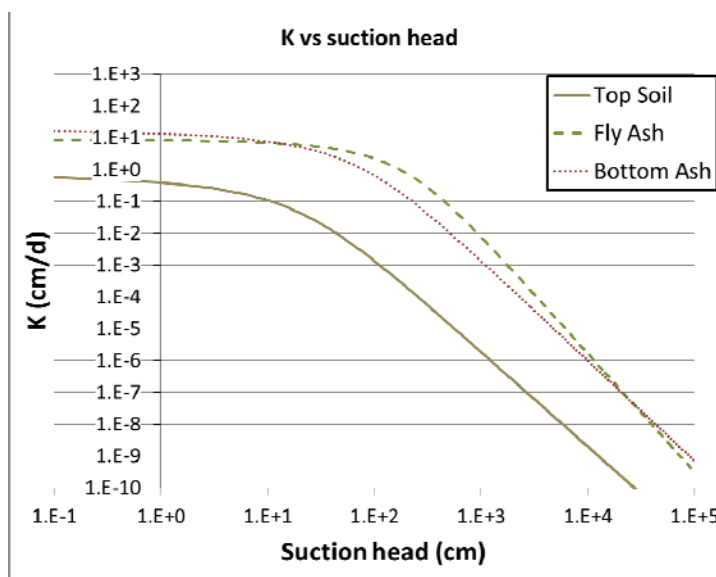


Figure 94. K vs. Suction Head for top soil, fly ash, and bottom ash at interface between top soil and CCBs for focused recharge simulations.

The sensitivity of the simulation to the root water uptake is small over the 10 year modeling duration. With no root water uptake being simulated, there was still not enough infiltration through the soil cover to enter the CCB pit after 10 years. The results also indicate that evaporation is the dominant factor in evapotranspiration. With no root water uptake, water may eventually infiltrate into the CCB pits, but the root water uptake by vegetation likely to be present in the arid climate would most likely eliminate infiltration moving beyond the root zone under the conditions simulated. This is consistent with literature concerning aquifer recharge in arid environments (Scanlon, 2006).

4.4.2 Importance of the Lower Boundary Condition

The modeling showed that the low permeability of the Pictured Cliffs Sandstone is an important factor that affects soil water movement in the lower regions of the buried ash. The low permeability relative to CCB materials forms an impediment to flow at the interface. At a pressure head of about -300 cm, the FA (**Error! Reference source not found.**) has a hydraulic conductivity of 0.316 cm/d while the Pictured Cliffs Sandstone has a hydraulic conductivity of 0.001 cm/d. It should be noted that this sandstone is the only material in the model for which

there were no properties measured in the laboratory. The demonstrated dependence on the lower boundary condition suggests that future studies should obtain samples of the sandstone and determine their unsaturated hydraulic properties to improve confidence in the predictions.

4.4.3 Properties as a Function of Density

Varying the density of the ash materials in the model did not appreciably affect the soil water flux into or out of the pit. This is largely due to the lack of infiltration past the soil cover. Water movement within the CCB pits was influenced by the variable hydraulic properties, but not to a significant degree. For the simulation of the focused recharge scenario, if an average material property would have been used for the CCBs, then exchange of water across the interface between the top soil and CCBs may have been different. For most of the simulations in this study, the modeling of material properties as a function of density did not significantly alter the results.

4.5 Conclusions

The simulations of water movement and soil moisture content using the HYDRUS 1D model demonstrated that water movement in busied CCB materials is primarily due to the redistribution of water between layers due to equilibrating initial conditions. The baseline model did not predict water movement from the soil cover into the CCBs due to the very low hydraulic conductivity of this material resulting from its high clay content. Infiltration through the soil cover into the buried CCBs has the greatest potential of occurring in situations in which focused recharge (i.e. ponding of water at the surface) occurs. In all other scenarios, evapotranspiration from the soil cover and vegetation is effective at keeping the relatively small amount of water that infiltrates at the surface from migrating below root depth of 1 m under the conditions provided for this model.

If a water table is present at the bottom of the CCB pit, the simulation results suggest that water movement will be upward into the CCBs. Should the water table be lowered at a later date, results suggest that little water will drain from the CCBs into the underlying material. Initial water contents of 25% and above result in appreciably more flux at the bottom of the CCB pit. These high water contents are not likely to be caused by infiltration through the soil cover, but rather through addition of water for dust suppression during disposal of the ash materials. Further studies should include testing of the Pictured Cliffs Sandstone to include measured properties of this material in order to better predict fluxes from the CCB pits into the underlying material.

5.0 Overall Project Conclusions

This study consisted of a combination of laboratory measurements and numerical simulations to determine the potential impacts that might be expected following disposal of coal combustion byproducts (CCBs) in a mined out open pit coal mine. This study focused on the San Juan Coal Mine near Farmington, NM. Three types of CCBs have been disposed of in this mine: fly ash, bottom ash, and flue gas desulfurization sludge. Disposal of these materials has been occurring at the mine for over 35 years, with some material being buried at depths in excess of 30 m. The mine is located above aquifers in the Fruitland and Pictured Cliffs Sandstone formations. Aquifers near the mine have very poor water quality with high concentrations of TDS and other constituents that make them unsuitable for human or livestock water supplies. No clear evidence of ground water contamination from past disposal of CCBs has been found, however, questions remain whether such contamination may occur in the future. The purpose of this investigation was to develop a better understanding of the geochemistry of fresh and buried CCBs as well as to determine their physical characteristics that would govern unsaturated flow of water through them.

This investigation had three major components: 1) measurement of physical properties of CCBs and spoil material used to cover them, 2) measurement of chemical properties and geochemical characteristics of fresh and aged CCBs, and 3) numerical modeling of one-dimensional unsaturated flow through buried CCBs to gain improved understanding of the potential water movement through the disposal cell. The conclusions of each of these investigations are briefly summarized below.

5.1.1 Physical Properties

Samples were collected of fresh CCBs as well as buried CCBs. Small samples of undisturbed buried CCB samples were collected by coring with a Geo-probe direct push rig, however, this method was limited to collection of shallow samples (< 12 m). A sonic drill rig was used to obtain samples throughout the entire depth of the pit at two locations. Fresh samples were collected from the coal-fired power plant adjacent to the mine.

The physical properties measured included: grain size distribution, density, compressibility, moisture content, saturated hydraulic conductivity and moisture characteristic curves. Both fly and bottom ash were found to be light materials with minimum dry densities of approximately 1100 kg/m^3 and 800 kg/m^3 respectively. The grain size diameter at which 10% of the material is retained is $4 \text{ }\mu\text{m}$ for fresh fly ash and $20 \text{ }\mu\text{m}$ for fresh bottom ash; there are few clay sized particles in both materials which is important to their hydraulic properties.

The fly ash and bottom ash were found to be quite compressible; consequently, hydraulic properties were measured at densities corresponding to the range of burial depths. The saturated hydraulic conductivity (K_{sat}) of the fly ash and bottom ash were found to decrease as dry density increased, consistent with previous studies and with other soils. Values of K_{sat} are approximately $1 \times 10^{-4} \text{ cm/s}$ and $5 \times 10^{-3} \text{ cm/s}$ for fly and bottom ash respectively. In contrast the spoil material which is used for covering reclaimed pits had very low values of K_{sat} , less than $8.5 \times 10^{-6} \text{ cm/s}$ due to the high clay fraction.

The soil moisture characteristics of the fly and bottom ash were determined and fitted to a van Genuchten mathematical model for different compacted densities. This information is needed to predict unsaturated flow of water through the CCB materials.

5.1.2 Geochemical Properties

Samples of fresh and buried CCBs were subjected to a variety of chemical and mineralogical analyses. The total elemental composition was determined by conducting an acid digestion of each fraction. The ash materials were principally composed of Al, B, Ba, Ca, Fe, K, Na and Si consistent with other studies of CCBs. The flue gas desulfurization sludge principally consisted of Ca and S in the form of sulfate (SO₄). Total concentrations of metals regulated in NM ground water standards were low. In particular, the As concentration averaged .124 ppm and .185 ppm in fresh and buried ash samples. This was of the same order of magnitude of the As concentration of 0.091 ppm measured in a spoil sample used for surface cover.

Samples of CCBs from different depths were subjected to acid leaching to determine if their composition varied with depth. There was some evidence that B and Ba concentrations in the CCBs increase with depth. Possible explanations for the differences in ash composition include:

- Changes in the composition of coal as mining of the pit has progressed over the past 40 years.
- Changes in the ash material captured by emissions control equipment as older equipment has been replaced by newer technologies.
- Results of leaching and/or formation of secondary minerals through geochemical processes

This study was not able to determine which of these possible scenarios was the proper explanation for the observed changes. Furthermore, due to the limited number of locations from which samples were collected and the limited number of samples it is not certain that there is in fact a trend; the numerical data may simply reflect inherent natural variability. This is an area that may be worthy of further investigation.

A series of columns were prepared containing fly and bottom ash as well as spoil material. They were subjected to leaching with deionized water and No. 8 Coal Seam water to determine the possible leach sequence that might occur over time. The results showed that the concentration of most elements (including B, K, Cr, Mg, Cu, Mo, Na and Ni) asymptotically decreased with time suggesting that they were either weakly adsorbed to the solid phase or associated with the pore fluids. No arsenic was detected in column leachates. Several elements showed an initial increase in concentration followed by a decrease. These included Al, Ba, Ca, and Li, as well as Si and Sr in some columns. This is believed to be due to dissolution of soluble amorphous materials, likely glass formed under the high temperatures in the coal furnace. Arsenic concentrations were low in all of the leachates.

Flow through the columns was intended to be unsaturated and they were fed one pore volume per day for a period of at least 30 days. All of the columns remained unsaturated except for the column filled with spoil material. Due to the very low hydraulic conductivity of this material almost no flow passed through this column, which provided confirmation of conductivity

measurements reported previously. This observation is important because it provides evidence of the effectiveness of this material as a landfill cover at preventing surface infiltration substantially reaching the disposed CCBs.

The mineralogy of the CCBs was investigated by X-ray diffraction (XRD) and scanning electron microscopy (SEM) which found gypsum ($\text{CaSO}_4 \cdot 2\text{H}_2\text{O}$) to be the dominant mineral in the flue gas desulfurization sludge. Fly ash was dominated by amorphous glass spheres. Bottom ash contained similar materials. The principal mineral phases identified were mullite ($\text{Al}_6\text{Si}_2\text{O}_{13}$) and quartz (SiO_2), with calcite (CaCO_3) and clay minerals also detected in some samples. Evidence of aging in some of the deepest and therefore oldest buried CCBs was noted which is consistent with elevated concentrations of some elements in the leaching studies.

This phase of the investigation found that the concentration of Al, B, Ba, Ca, Se, Si, and V were higher than in native ground water. However, most concentrations were comparable. Though the concentrations were elevated the impact of the leachate on underlying ground water also depends on the mass flux of leachate reaching the water table. This is calculated as the product of the concentration of the dissolved constituents and the flow of water through buried waste. The flow of water is very low and in fact is likely close to zero. It was investigated in the third phase of this study.

5.1.3 Modeling Studies

The third phase of this investigation consisted of development of a numerical model of unsaturated flow through buried waste. A one-dimensional model was developed using the HYDRUS 1D code. The model simulated flow through 2 m of cover consisting of spoil material, 33 m of buried CCBs, and 50 m of Pictured Cliffs Sandstone. Physical properties measured in the first phase of the study were used and 10 years of precipitation records was used to simulate rainfall onto the cover. Different mixtures of fly and bottom ash were simulated in the model calculations.

The modeling showed that there was a small initial flux through the CCBs due to the equilibration of the water associated with its placement in the pit during the first 1 to 2 years of simulation. After equilibration, there was little or no flux through the disposal cell due to the high evaporation rates and root water uptake, the very low hydraulic conductivity of the spoil material that is used as cover, and the low conductivity of the unsaturated CCBs. Five years following disposal the flux through the cover into the buried CCBs was predicted by the model to be less than .4 mm/yr. Vertical ground water flow through the bottom of the pit into the underlying Pictured Cliffs Sandstone was predicted to be near zero or possibly upward depending on the boundary conditions and material properties simulated.

A small amount of recharge from the disposal pit could be induced by allowing substantial ponding on the surface. Ponding might occur in low areas due to differential settlement of the wastes or improper grading. Recharge through the ponds is referred to a focused recharge.

The very low (or possibly zero) downward flow of ground water through the unsaturated waste predicted by the modeling study, together with the low concentrations of contaminants in

leachates from buried CCBs provides compelling evidence that the potential for contamination of the underlying regional aquifer at the SJCM is small.

References

- ACAA. 2009. 2009 CCP Production Use Survey. ACAA.
http://acaa.affiniscape.com/associations/8003/files/2009_CCP_Production_Use_Survey_Corrected_020811.pdf.
- ACAA. 2011. What are CCPs? ACAA, August 30.
<http://acaa.affiniscape.com/displaycommon.cfm?an=8>.
- Anon. Climate Ratios.pdf.
http://www.esrl.noaa.gov/gmd/infodata/lesson_plans/Climate%20Ratios.pdf.
- Anon. ESRL NOAA Pan Evaporation by State.
<http://www.wrcc.dri.edu/htmlfiles/westevap.final.html>.
- Assouline, Tavares-Filho, and Tessier, 1997. "Effect of Compaction on Soil Physical and Hydraulic Properties: Experimental Results and Modeling." *Soil Sci. Soc. Of American Jour.* 61:390-398.
- Baba, Alper, Gulbin Gurdal, Fatma Sengunalp, and Ozgur Ozay. 2008. "Effects of leachant temperature and pH on leachability of metals from fly ash. A case study: Can thermal power plant, province of Canakkale, Turkey." *Environmental Monitoring and Assessment*, 139 (1) (April 1): 287-298. doi:10.1007/s10661-007-9834-8.
<http://dx.doi.org/10.1007/s10661-007-9834-8>.
- Baligar, V.C., R.B. Clark, R.F. Korcak, and R.J. Wright. 2011. "Flue Gas Desulfurization Product Use on Agricultural Land." *Advances in Agronomy*, 111: 51-86.
doi:10.1016/B978-0-12-387689-8.00005-9.
- Bhangare, R.C., P.Y. Ajmal, S.K. Sahu, G.G. Pandit, and V.D. Puranik. 2011. "Distribution of trace elements in coal and combustion residues from five thermal power plants in India." *International Journal of Coal Geology*, 86 (4) (June 1): 349-356. doi:16/j.coal.2011.03.008.
<http://www.sciencedirect.com/science/article/pii/S0166516211000620>.
- Bin-Shafique, Sazzad, Craig H. Benson, Tuncer B. Edil, and Kooouho Hwang. 2006. "Leachate Concentrations from Water Leach and Column Leach Tests on Fly Ash-Stabilized Soils." *Environmental Engineering Science*, 23 (1) (January): 53-67. doi:10.1089/ees.2006.23.53.
<http://www.liebertonline.com/doi/abs/10.1089/ees.2006.23.53>.
- Campbell, Fox, Aitken, and Bell, 1983. "Physical Characteristics of Sands Amended with Fly Ash." *Aut. J. Soil Res.* 21:147-154.
- Chakrabarti, Mudd, Kodikara, 2005. "Coupled Atmospheric-Unsaturated Flow Modelling of Leached Ash Disposal in the Latrobe Valley, Australia." *International Conference of Engineering for Waste Treatment*.
- Chan, M. (2011). Unpublished laboratory analyses of samples from the San Juan Mine, Dept. of Civil Engineering, University of New Mexico, Albuquerque, NM.
- Chang, A.C., L.J. Lund, A.L. Page, and J.E. Warneke. 1979. "Physical properties of fly ash-amended soils." *Journal of Environmental Quality*, 6: 267-270.
- Chee, Marianita. 2009. San Juan Mine Permit 09-01: Section 900 Operation Plan: General Requirements. San Juan Coal Co.
- Connolly, Jim. 2011. Report on X-Ray Diffraction analysis of Coal Ash Samples from San Juan Mine power plant, Letter report, Dept. of Earth and Planetary Sciences, University of New Mexico, Albuquerque, NM, June 28, 2011.

- Dudas, M.J., and C.J. Warren. 1987. "Submicroscopic model of fly ash particles." *Geoderma*, 40 (1-2) (September): 101-114. doi:doi: 10.1016/0016-7061(87)90016-4. <http://www.sciencedirect.com/science/article/pii/0016706187900164>.
- Dzombak, D. A., and F. M. M. Morel. 1990. *Surface Complexation Modeling—Hydrous Ferric Oxide*. Ed. null. Vol. null. null.
- Eaton, Andrew D., Lenore S. Clesceri, Eugene W. Rice, and Arnold E. Greenber. 2005. *Standard Methods for the Examination of Water and Wastewater*. 21st ed. American Public Health Association, American Water Works Association, Water Environmental Federation.
- El-Mogazi, Dina, Donald J. Lisk, and Leonard H. Weinstein. 1988. "A Review of Physical, Chemical, and Biological Properties of Fly-Ash and Effects on Agricultural Ecosystems." *The Science of the Total Environment*, 74: 1-37.
- Fisher, G. L., D. P. Y. Chang, and Margaret Brummer. 1976. "Fly Ash Collected from Electrostatic Precipitators: Microcrystalline Structures and the Mystery of the Spheres." *Science* 192 (4239). New Series (May 7): 553-555. <http://www.jstor.org/stable/1741564>.
- Garcia, C.A., Andraski, B.J., Stonestrom, D.A., Copper, C.A., Simunek, J., Wheatcraft, S.W., (2011). Interacting Vegetative and Thermal Contributions to Water Movement in Desert Soil, *Vadose Zone Journal*, 10(2), 552-564.
- Ginn, Mickey, Steven Perkins, and Art O'Hayre. 2009. San Juan Mine Permit 09-01: Section 907 RECLAMATION PLAN: PROTECTION OF HYDROLOGIC BALANCE. BHP-Billiton, San Juan Coal Company.
- Hamilton, Steven J. 2004. "Review of Selenium Toxicity in the Aquatic Food Chain." *The Science of the Total Environment*, 326 (1-3): 1-31.
- Hassett, David J., Debra F. Hassett, and Joseph N. Brobjerg. 1988. Control of Trace Element Solubility in Coal Flysh Leachates. In University of Wisconsin-Madison: Department of Engineering Professional Development, September 14.
- Hill and Sumner, 1967. "Effect of Bulk Density on Moisture Characteristics of Soils." *Soil Sci.* 103:234-238.
- James, W.D., C.C. Graham, M.D. Glascock, and A.G. Hanna. 1982. "Water Leachable Boron From Coal Ashes." *Environmental Science & Technology*, 16: 175-179.
- Lu and Likos, 2004. *Unsaturated Soil Mechanics*. Hoboken, NJ: John Wiley & Sons Inc.
- Luther, J., Musslewhite, B., Brown, C. (2007). The Relationship Between Water Quality (sic) and Coal Combustion By-Product Placement in an Arid Western Coal Mine, 9 p. (www.mcrc.org/PDF/Forums/CCB6/1-1.pdf accessed 2/10/10).
- Luther, James, B. Musslewhite, and C Brown. 2009. The Relationship Between Water Quality and Coal Combustion By-Product Placement in an Arid Western Coal Mine. San Juan Coal Co.
- Manskinen, Kati, Risto Poykio, and Hannu Nurmesniemi. 2011. "Comparison of the total and fractionated heavy metal and sulphur concentrations in bottom ash and fly ash from a large-sized (120 MW) power plant of a fluting board mill." *Lietuvos Mokslu Akademija*, 22 (1): 46-55.
- Martin, Collins, Browning, and Biehl, 1990. "Properties and Use of Fly Ashes for Embankments." *J. of Energy Eng.* 116:71-86.
- Mining and Minerals Division, New Mexico, NM. 2011. Mining and Minerals Division of New Mexico Coal Mine Data. Coal Mine Data Links. <http://www.emnrd.state.nm.us/MMD/coalminewebmap/coalminewebmap.htm>.

- New Mexico Mining and Minerals Division. 2009. Annual Evaluation Summary Report for the Regulatory Program Administered by the State of New Mexico for Evaluation Year 2009. Office of Surface Mining Reclamation and Enforcement, June.
- Norwest. 2009. Groundwater Monitoring Plan for San Juan Mine. Norwest Corporation, June 16.
- NRCS, and University of Oregon PRISM. 2000. NRCS PRISM. <http://www.wcc.nrcs.usda.gov/climate/prism.html>.
- O'Hara, J., Anderson, M.B., Delay, L.S. (2009). Using a Geographic Information System to Identify Coal Ash Disposal Sites at the San Juan Mine, New Mexico, poster prepared by staff of the Mining and Minerals Division, State of New Mexico Energy, Minerals, and Natural Resources Department, Santa Fe, NM.
- Office of Surface Mining Reclamation and Enforcement (2009). Annual Evaluation Summary Report for the Regulatory Program Administered by the State of New Mexico for Evaluation Year 2009 (July 1, 2008 to June 30, 2009), Mining and Minerals Division, Energy Minerals and Natural Resources Department, Santa Fe, NM.
- Palmer, Edil, and Benson, 2000. "Liners for Waste Containment Constructed with Class F and C Fly Ashes." *J. of Hazardous Materials* 76:193-216.
- Parker, C.H. (2011). Analysis of Coal Combustion By-Product Disposal Practices in Arid Climates: Leachate Water Quality, M.S. Thesis, Department of Civil Engineering, University of New Mexico, Albuquerque, NM, 167 p.
- Patnaik, Pradyot. 2002. Handbook of Inorganic Chemicals. 1st ed. McGraw-Hill Professional, November 20.
- Pathan, Aylmore, and Colmer, 2003. "Properties of Several Fly Ash Materials in Relation to Use as Soil Amendments." *J. Environ. Qual.* 32:687-693.
- Prashanth, Sivapullaiah, and Sridharan, 1998. "Compaction Curves on Volume Basis." *Geotechnical Testing Journal* 21:58-65.
- Prashanth, Sivapullaiah, Sridharan, 2001. "Pozzolanic Fly Ash as a Hydraulic Barrier in Land Fills." *Eng. Geology* 60:245-252.
- Ram, Lal, Nishant Srivastava, Ramesh Tripathi, Sanjay Thakur, Awadhesh Sinha, Sangeet Jha, Reginald Masto, and Swapan Mitra. 2007. "Leaching behavior of lignite fly ash with shake and column tests." *Environmental Geology*, 51 (7) (February 1): 1119-1132. doi:10.1007/s00254-006-0403-1. <http://dx.doi.org/10.1007/s00254-006-0403-1>.
- Richard, Cousin, Sillon, Bruand, and Guerif, 2001. "Effect of Compaction on the Porosity of Silty Soil: Influence on Unsaturated Hydraulic Properties." *European Jour. of Soil Sci.* 52:49-58.
- Ruhl, Laura, Avner Vengosh, Gary S. Dwyer, Heileen Hsu-Kim, and Amrika Deonarine. 2010. "Environmental Impacts of the Coal Ash Spill in Kingston, Tennessee: An 18-Month Survey." *Environmental Science & Technology*, 44 (24) (December 15): 9272-9278. doi:doi: 10.1021/es1026739. <http://dx.doi.org/10.1021/es1026739>.
- Ryan Webb, John Stormont, Bruce Thomson, and Mark Stone. 2012. Physicochemical Characteristics of.
- Shannon, D.G., and L.O. Fine. 1974. "Cation Solubilities of Lignite Fly Ashes." *Environmental Science & Technology*, 8: 1026-1028.
- Simunek, J, M. Sejna, H. Saito, M. Sakai, and M. Th. Van Genuchten, 2008. The HYDRUS-1D software package for simulating the movement of water, heat, and multiple solutes in variably saturated media, Version 4.0. HYDRUS Softw. Ser. 3. Dep. Of Environ. Sci., Univ. of California, Riverside.

- Spilde, Mike. 2011. Examination of San Juan Mine coal ash samples by SEM. Letter report, Dept. of Earth and Planetary Sciences, University of New Mexico, Albuquerque, NM, August 16, 2011.
- Steinwand, Harrington, and Groeneveld, 2001. "Transpiration coefficients for three Great Basin shrubs." *Journal of Arid Environments* 49:555-567.
- Sultana, Parveen, Kukhen Das, and et al. 2011. "Mullite formation in coal fly ash is facilitated by the incorporation of magnesium oxide." *Reviews Advanced Material Science* 27: 69-74.
- Truman, C.C., R.C. Nuti, L.R. Truman, J.D. Dean, 2010. "Feasibility of Using FGD Gypsum to Conserve Water and Reduce Erosion from an Agricultural Soil in Georgia." *Catena* 81:234-239
- U.S. Congress 1977. The Surface Mining Control and Reclamation Act (SMCRA) of 1977. U.S. Public Law 95-87. U.S. Public Law 95-87.
- United States Environmental Protection Agency. 2011. Drinking Water Contaminants | Drinking Water Contaminants | US EPA. Drinking Water Contaminants. September 30. <http://water.epa.gov/drink/contaminants/index.cfm>.
- Ward, C. R., and D. French. 2006. Relation between coal and fly ash mineralogy based on quantitative X-ray diffraction methods. In Lexington, KY, April 11.
- White, A. F., N. M. Dubrovsky, W. T. Frankenberger, and S. Benson. 1994. *Selenium in the Environment*. Ed. null. Vol. null. null.
- Yeboah, N., and S. Burns. 2011. "Geological disposal of energy-related waste." *KSCE Journal of Civil Engineering* 15 (4) (April 1): 697-705. doi:10.1007/s12205-011-0010-x. <http://dx.doi.org/10.1007/s12205-011-0010-x>.
- You, Kwang-suk, Nam-il UM, and et al. 2009. Manufacture of cementitious materials with coal combustion bottom ash and FGD gypsum. In Lexington, KY, May 4.
- Young, Andy. Ashes to Ashes: Returning CCBs to the Ground at Navajo Mine, 10 p. (www.mcrc.osmre.gov/PDF/Forums/CCB3/3-1.pdf - accessed 2/10/10).
- Yuan, Chun-Gang. 2009. "Leaching characteristics of metals in fly ash from coal-fired power plant by sequential extraction procedure." *Microchimica Acta*, 165 (1) (April 1): 91-96. doi:10.1007/s00604-008-0103-5. <http://dx.doi.org/10.1007/s00604-008-0103-5>.
- Zevenbergen, Chris, John P. Bradley, L. Piet van Reeuwijk, A. K. Shyam, Ole Hjelmar, and Rob N. J. Comans. 1999. "Clay Formation and Metal Fixation during Weathering of Coal Fly Ash." *Environmental Science & Technology*, 33 (19) (October 1): 3405-3409. doi:doi:10.1021/es9900151. <http://dx.doi.org/10.1021/es9900151>.
- Zhao, Fenghua, Suping Peng, Baoshan Zheng, Yuegang Tang, Zhiyuan Cong, and Deyi Ren. 2006. "The Leaching Behavior of Cadmium, Arsenic, Zinc, and Chlorine in Coal and Its Ash from Coal-Fired Power Plant." *Environmental Engineering Science*, 23 (1) (January): 68-76. doi:10.1089/ees.2006.23.68, <http://www.liebertonline.com/doi/abs/10.1089/ees.2006.23.68>.

Appendix I – Results of Column Leach Tests

Table 25. Chemical analyses of column leach tests.

Column	1 - Fresh Fly Ash - NE-FA-01 (Conc. in mg/Kg)															
Sample ID	1.01	1.02	1.03	1.04	1.05	1.06	1.07	1.08	1.09	1.10	1.11	1.12	1.13	1.14	1.15	1.16
Day No.	0	3	5	7	9	11	13	15	17	19	21	23	25	27	29	31
Analyte	8/1/11	8/4/11	8/6/11	8/8/11	8/10/11	8/12/11	8/14/11	8/16/11	8/18/11	8/20/11	8/22/11	8/24/11	8/26/11	8/28/11	8/30/11	9/1/11
Ag	-0.022	-0.026	-0.024	-0.023	-0.022	-0.02	-0.021	-0.02	-0.02	0.028	0.028	0.028	0.027	0.026	0.028	0.027
Al	0.657	0.464	0.342	0.259	0.369	0.518	0.582	1.503	1.398	0.957	1.229	1.285	1.251	1.299	1.375	0.909
As																
B	0.584	0.439	2.146	0.273	0.273	0.247	0.231	0.052	0.031	0.219	0.294	0.121	0.173	0.109	0.147	0.18
Ba	0.475	4.759	5.948	6.42	6.178	5.919	6.137	5.662	5.044	4.817	4.418	3.75	3.454	3.107	2.883	2.632
Be	-0.075	-0.075	-0.075	-0.075	-0.075	-0.075	-0.075	-0.075	-0.075	-0.073	-0.073	-0.073	-0.073	-0.073	-0.073	-0.073
Ca	109.3	310.3	395.1	419.9	420.2	388	400.6	410	436.6	422.7	397.8	390.1	392.3	377.3	366.4	342.3
Cd	-0.039	-0.039	-0.039	-0.039	-0.039	-0.04	-0.039	-0.039	-0.039	-0.04	-0.04	-0.04	-0.04	-0.04	-0.04	-0.04
Co	-0.041	-0.04	-0.04	-0.04	-0.04	-0.04	-0.04	-0.04	-0.04	-0.04	-0.04	-0.04	-0.04	-0.04	-0.04	-0.04
Cr	0.114	-0.027	-0.031	-0.031	-0.032	-0.033	-0.033	-0.034	-0.034	-0.035	-0.035	-0.035	-0.036	-0.035	-0.036	-0.035
Cu	0.006	0.001	0.001	0.001	0	0.001	0.001	0.002	0.001	0	-0.001	0	0	-0.001	0	0
Fe	-0.06	-0.062	-0.061	-0.062	-0.061	-0.062	-0.062	-0.062	-0.062	-0.063	-0.063	-0.063	-0.063	-0.062	-0.062	-0.063
K	75	28.47	17.83	14.21	12.6	11.04	11.3	11.01	9.984	9.344	9.087	8.914	7.937	7.275	7.034	7.023
Li	-91.47	11.2	31.09	35.75	36.28	37.63	40.05	41.63	42.08	45.8	44	42.06	42.51	41.63	40.63	37.06
Mg	-0.286	-0.281	-0.276	-0.278	-0.278	-0.279	-0.279	-0.28	-0.28	-0.305	-0.305	-0.302	-0.299	-0.303	-0.301	-0.294
Mn	-0.041	-0.041	-0.041	-0.041	-0.041	-0.041	-0.041	-0.041	-0.041	-0.04	-0.04	-0.04	-0.04	-0.04	-0.04	-0.04
Mo	2.956	0.22	0.117	0.099	0.08	0.073	0.08	0.084	0.076	0.101	0.107	0.108	0.108	0.108	0.114	0.111
Na	1539	237.2	84.62	61.91	52.86	45.85	44.52	41	36.58	36.68	33.21	31.11	27.76	24.21	22.18	21.56
Ni	-0.059	-0.046	-0.046	-0.046	-0.046	-0.046	-0.046	-0.047	-0.047	-0.05	-0.049	-0.05	-0.05	-0.05	-0.05	-0.05
Pb	-0.048	-0.046	-0.047	-0.047	-0.047	-0.047	-0.045	-0.045	-0.045	-0.057	-0.058	-0.057	-0.056	-0.057	-0.058	-0.058
Se	0.125	-0.09	-0.103	-0.106	-0.102	-0.103	-0.099	-0.097	-0.102	-0.097	-0.103	-0.099	-0.104	-0.106	-0.095	-0.097
Si	0.762	-0.086	-0.207	-0.054	-0.146	-0.102	0.038	0.174	0.132	0.433	0.411	0.571	0.686	0.604	0.733	0.768
Sr	4.9	40.4	28.9	18	11.39	8.087	7.017	5.846	4.944	4.544	3.99	3.599	3.336	3.004	2.769	2.627
V	-0.065	-0.063	-0.062	-0.072	-0.074	-0.068	-0.049	-0.051	-0.054	0.019	0.012	0.011	0.014	0.008	0.026	0.015
Zn	-0.041	-0.045	-0.034	-0.034	-0.033	-0.039	-0.042	-0.041	-0.041	-0.039	-0.027	-0.031	-0.041	-0.029	-0.041	0.035

Column	2 - Fresh Bottom Ash - NE-BA-01 (Conc. in mg/Kg)																
Sample ID	2.01	2.02	2.03	2.04	2.05	2.06	2.07	2.08	2.09	2.10	2.11	2.12	2.13	2.14	2.15	2.16	2.17
Day No.	0	2	5	7	9	11	13	15	17	19	21	23	25	27	29	31	33
Analyte	7/30/2011	8/1/11	8/4/11	8/6/11	8/8/11	8/10/11	8/12/11	8/14/11	8/16/11	8/18/11	8/20/11	8/22/11	8/24/11	8/26/11	8/28/11	8/30/11	9/1/11
Ag	-0.015	-0.017	-0.018	-0.018	-0.02	-0.021	-0.021	-0.023	-0.022	0.024	0.026	0.025	0.024	0.025	0.026	0.025	0.023
Al	-0.054	-0.101	-0.072	0.005	0.226	0.181	0.101	0.185	0.192	0.208	0.152	0.193	0.215	0.223	0.243	0.273	0.253
As																	
B	67.64	46.55	22.16	11.66	13.09	6.285	4.745	6.057	3.562	3.826	3.187	2.874	2.641	2.35	2.056	1.97	1.889
Ba	0.066	0.067	0.061	0.045	0.023	0.024	0.037	0.015	0.013	0.016	0.01	0.015	-0.004	-0.005	-0.008	-0.007	-0.003
Be	-0.074	-0.074	-0.075	-0.075	-0.075	-0.075	-0.075	-0.075	-0.075	-0.072	-0.072	-0.072	-0.072	-0.072	-0.072	-0.072	-0.073
Ca	665.2	589.9	584.8	228	34.22	20.55	17.59	16.58	15.04	17.55	16.64	16.65	16.99	16.58	16.03	15.77	16.27
Cd	-0.039	-0.04	-0.04	-0.039	-0.04	-0.039	-0.039	-0.039	-0.039	-0.04	-0.039	-0.039	-0.04	-0.04	-0.039	-0.04	-0.039
Co	-0.04	-0.04	-0.039	-0.039	-0.04	-0.04	-0.04	-0.04	-0.039	-0.041	-0.041	-0.041	-0.041	-0.04	-0.041	-0.041	-0.041
Cr	0.091	0.025	-0.016	-0.024	-0.025	-0.026	-0.026	-0.027	-0.027	-0.028	-0.029	-0.03	-0.029	-0.029	-0.03	-0.03	-0.03
Cu	0.007	0.007	0.003	0.002	0.002	0	0	0.006	0	-0.001	-0.001	0	-0.001	0	-0.001	-0.001	0
Fe	-0.059	-0.061	-0.062	-0.062	-0.062	-0.062	-0.062	-0.062	-0.062	-0.063	-0.063	-0.063	-0.063	-0.063	-0.063	-0.063	-0.062
K	29.85	15.54	6.213	1.862	0.881	0.585	0.532	1.197	0.41	0.211	0.108	0.181	0.134	0.012	-0.034	-0.039	-0.049
Li	27.08	48.21	55.21	21.37	3.231	1.665	1.394	1.323	1.222	1.478	1.395	1.434	1.391	1.444	1.444	1.445	1.495
Mg	12.97	11.18	6.334	0.914	0.042	-0.064	-0.071	-0.074	-0.092	-0.071	-0.049	-0.075	-0.047	-0.05	-0.042	-0.032	-0.031
Mn	-0.027	-0.04	-0.039	-0.041	-0.038	-0.041	-0.041	-0.04	-0.041	-0.04	-0.04	-0.04	-0.039	-0.039	-0.039	-0.039	-0.039
Mo	2.064	0.69	0.065	-0.009	-0.017	-0.022	-0.026	-0.028	-0.029	-0.02	-0.022	-0.024	-0.024	-0.026	-0.026	-0.027	-0.028
Na	1494	516.8	92.04	19.55	12.19	8.059	6.81	7.583	5.768	6.805	6.446	5.615	6.367	4.809	4.48	4.334	4.386
Ni	-0.051	-0.047	-0.046	-0.046	-0.046	-0.047	-0.046	-0.044	-0.046	-0.049	-0.049	-0.049	-0.049	-0.049	-0.049	-0.049	-0.049
Pb	-0.057	-0.052	-0.048	-0.044	-0.042	-0.041	-0.041	-0.042	-0.04	-0.053	-0.054	-0.054	-0.052	-0.053	-0.054	-0.052	-0.053
Se	0.244	0.06	-0.05	-0.067	-0.043	-0.025	-0.02	-0.029	-0.029	-0.028	-0.042	-0.055	-0.06	-0.062	-0.068	-0.075	-0.076
Si	6.334	3.853	3.633	2.453	1.258	3.221	3.573	3.046	4.117	4.966	4.9	5.146	5.037	4.903	4.923	4.912	4.732
Sr	3.33	2.591	2.149	0.729	0.169	0.096	0.08	0.074	0.068	0.068	0.063	0.064	0.065	0.061	0.059	0.058	0.059
V	0.022	0.023	-0.004	-0.022	0.007	0.031	0.038	0.041	0.029	0.147	0.136	0.113	0.114	0.107	0.093	0.09	0.078
Zn	-0.02	-0.044	-0.046	-0.049	-0.054	-0.056	-0.054	-0.046	-0.037	-0.041	-0.05	-0.029	-0.017	-0.012	-0.052	-0.05	-0.007

Column	3 - Old Buried Fly Ash - SM4-04-06B (Conc. in mg/Kg)															
Sample ID	3.01	3.02	3.03	3.04	3.05	3.06	3.07	3.08	3.09	3.10	3.11	3.12	3.13	3.14	3.15	3.16
Day No.	0	3	5	7	9	11	13	15	17	19	21	23	25	27	29	31
Analyte	8/1/11	8/4/11	8/6/11	8/8/11	8/10/11	8/12/11	8/14/11	8/16/11	8/18/11	8/20/11	8/22/11	8/24/11	8/26/11	8/28/11	8/30/11	9/1/11
Ag	-0.006	-0.016	-0.019	-0.019	-0.016	-0.018	-0.019	-0.021	-0.021	0.026	0.026	0.025	0.024	0.024	0.025	0.024
Al	0.146	0.028	-0.046	0.153	-0.01	0.022	0.014	0.04	0.261	0.109	0.058	0.175	0.076	0.176	0.257	0.315
As																
B	26.87	29.6	23.57	25.35	21.81	22.67	25.62	26.96	26.27	21.99	20.21	18.62	17.24	14.79	14	12.98
Ba	0.048	0.038	0.049	0.044	0.055	0.045	0.038	0.058	0.041	0.039	0.028	0.025	0.02	0.018	0.017	0.021
Be	-0.073	-0.073	-0.073	-0.074	-0.073	-0.074	-0.073	-0.073	-0.073	-0.072	-0.071	-0.071	-0.071	-0.072	-0.071	-0.071
Ca	471	451.3	479.5	540.3	577.7	605.7	425.9	203.8	135.3	72.3	55.47	57.38	45.14	35.92	38.05	29.15
Cd	-0.039	-0.039	-0.039	-0.039	-0.039	-0.039	-0.04	-0.04	-0.039	-0.041	-0.04	-0.04	-0.041	-0.04	-0.041	-0.04
Co	-0.045	-0.04	-0.039	-0.039	-0.039	-0.039	-0.039	-0.04	-0.04	-0.041	-0.041	-0.041	-0.041	-0.041	-0.041	-0.04
Cr	1.1	0.263	0.038	0.003	-0.004	-0.01	-0.013	-0.017	-0.019	-0.022	-0.022	-0.022	-0.023	-0.024	-0.024	-0.021
Cu	0.011	0.005	0.004	0.001	0.002	0.003	0.003	0.001	0.001	-0.001	-0.001	-0.001	-0.002	-0.001	-0.001	-0.001
Fe	-0.054	-0.06	-0.061	-0.062	-0.062	-0.062	-0.062	-0.062	-0.062	-0.063	-0.063	-0.063	-0.063	-0.063	-0.063	-0.061
K	71.34	59.32	45.39	35	29.32	23.7	17.52	14.39	11.35	9.617	9.945	9.086	8.579	8.178	8.151	7.731
Li	11.01	21.7	36.06	47.6	57.88	56.16	44.68	23.55	13.49	7.558	5.282	5.864	4.431	3.365	3.783	2.503
Mg	0.284	0.163	0.201	0.231	0.274	0.257	0.155	-0.06	-0.151	-0.196	-0.078	-0.226	-0.231	-0.242	-0.242	-0.189
Mn	-0.042	-0.041	-0.04	-0.038	-0.041	-0.041	-0.041	-0.041	-0.041	-0.04	-0.04	-0.04	-0.04	-0.04	-0.04	-0.039
Mo	11.31	2.269	0.394	0.137	0.095	0.07	0.062	0.056	0.05	0.04	0.031	0.033	0.025	0.015	0.015	0.011
Na	1496	1067	590.7	335.5	155.4	91.22	55.89	41.82	34.01	31.97	31.26	28.24	25.85	23.16	22.39	21.19
Ni	-0.095	-0.056	-0.048	-0.047	-0.046	-0.047	-0.047	-0.047	-0.047	-0.051	-0.051	-0.051	-0.051	-0.051	-0.051	-0.04
Pb	-0.082	-0.053	-0.048	-0.05	-0.049	-0.049	-0.048	-0.043	-0.042	-0.053	-0.052	-0.053	-0.053	-0.053	-0.052	-0.053
Se	0.182	-0.051	-0.098	-0.108	-0.102	-0.115	-0.105	-0.108	-0.109	-0.121	-0.111	-0.114	-0.113	-0.114	-0.111	-0.113
Si	5.798	5.032	4.564	1.538	4.906	3.01	5.282	6.267	6.986	6.501	7.16	7.272	7.376	7.582	8	8.093
Sr	3.698	3.496	3.566	3.671	3.979	3.81	2.8	1.771	1.162	0.831	0.791	0.743	0.663	0.6	0.615	0.561
V	0.175	0.184	0.126	0.105	0.122	0.077	0.12	0.159	0.178	0.2	0.228	0.226	0.24	0.222	0.23	0.217
Zn	-0.035	-0.037	-0.038	-0.026	-0.045	-0.045	-0.043	0	-0.05	-0.05	-0.048	-0.049	-0.051	-0.037	-0.051	0.116

Column	4 - Old Buried Bottom Ash -SM4-05-01B (Conc. in mg/Kg)															
Sample ID	4.01	4.02	4.03	4.04	4.05	4.06	4.07	4.08	4.09	4.10	4.11	4.12	4.13	4.14	4.15	4.16
Day No.	0	3	5	7	9	11	13	15	17	19	21	23	25	27	29	31
Analyte	8/1/11	8/4/11	8/6/11	8/8/11	8/10/11	8/12/11	8/14/11	8/16/11	8/18/11	8/20/11	8/22/11	8/24/11	8/26/11	8/28/11	8/30/11	9/1/11
Ag	-0.013	-0.019	-0.019	-0.018	-0.02	-0.021	-0.019	-0.021	-0.021	0.025	0.025	0.026	0.026	0.027	0.026	0.025
Al	0.198	0.587	0.264	0.389	0.502	1.07	1.128	1.55	1.478	1.302	1.11	1.149	1.339	1.36	1.406	1.19
As																
B	33.51	24.24	23	21.19	20.04	18.76	17.39	16.95	15.14	13.21	12.86	12.22	11.14	10.33	10.13	9.776
Ba	0.053	0.034	0.033	0.031	0.032	0.028	0.014	0.016	0.014	0.005	0.002	0	0	0.002	0.005	0.002
Be	-0.073	-0.073	-0.074	-0.074	-0.074	-0.073	-0.073	-0.073	-0.074	-0.072	-0.072	-0.072	-0.072	-0.072	-0.072	-0.072
Ca	437.8	422.8	454.2	218	119.4	91.53	82.06	80.42	72.45	64.03	57.37	60.54	56.94	54.08	57.19	40.58
Cd	-0.039	-0.039	-0.04	-0.04	-0.04	-0.039	-0.039	-0.039	-0.039	-0.04	-0.04	-0.04	-0.04	-0.04	-0.04	-0.041
Co	-0.042	-0.04	-0.039	-0.039	-0.04	-0.04	-0.04	-0.04	-0.04	-0.041	-0.041	-0.041	-0.041	-0.041	-0.041	-0.041
Cr	0.472	0.068	0	-0.017	-0.026	-0.03	-0.032	-0.032	-0.033	-0.033	-0.033	-0.033	-0.034	-0.034	-0.033	-0.033
Cu	0.01	0.005	0.003	0.003	0.01	0.002	0.004	0.001	0.001	-0.001	0	-0.001	-0.001	-0.001	-0.001	-0.001
Fe	-0.058	-0.061	-0.061	-0.06	-0.061	-0.061	-0.061	-0.062	-0.062	-0.063	-0.063	-0.063	-0.063	-0.063	-0.063	-0.063
K	92.82	62.05	37.45	21.93	16.56	13.83	12.8	12.25	10.7	9.492	9.615	8.848	8.254	7.755	7.916	7.469
Li	-28.64	2.666	28.96	14.83	5.887	4.189	4.157	4.32	4.094	4.272	3.589	4.081	3.995	3.943	4.155	2.606
Mg	-0.044	-0.153	-0.162	-0.174	-0.196	-0.233	-0.237	-0.255	-0.252	-0.277	-0.18	-0.277	-0.279	-0.278	-0.282	-0.27
Mn	-0.032	-0.04	-0.041	-0.039	-0.04	-0.041	-0.041	-0.041	-0.041	-0.04	-0.04	-0.04	-0.04	-0.04	-0.04	-0.04
Mo	5.586	0.853	0.218	0.112	0.081	0.055	0.047	0.04	0.03	0.026	0.023	0.023	0.017	0.012	0.014	0.015
Na	2273	1170	526.7	263.5	149.5	116.4	95.85	83.34	68.33	59.74	54.43	48.49	43.88	39.11	36.16	33.39
Ni	-0.069	-0.049	-0.047	-0.032	-0.041	-0.046	-0.045	-0.046	-0.046	-0.051	-0.051	-0.051	-0.05	-0.051	-0.05	-0.05
Pb	-0.064	-0.052	-0.048	-0.045	-0.043	-0.042	-0.041	-0.041	-0.042	-0.054	-0.054	-0.054	-0.054	-0.054	-0.054	-0.053
Se	0.088	-0.072	-0.102	-0.107	-0.107	-0.107	-0.105	-0.103	-0.101	-0.119	-0.117	-0.116	-0.117	-0.118	-0.115	-0.115
Si	0.78	1.244	2.388	1.9	2.31	3.735	3.844	4.316	4.179	3.675	3.456	3.422	3.595	3.696	3.738	3.11
Sr	2.444	2.302	2.28	1.187	0.749	0.632	0.587	0.598	0.552	0.497	0.498	0.5	0.471	0.459	0.486	0.421
V	0.141	0.105	0.063	0.08	0.085	0.096	0.091	0.093	0.088	0.121	0.138	0.129	0.136	0.132	0.122	0.131
Zn	-0.036	-0.046	-0.044	-0.044	-0.043	-0.048	-0.047	-0.05	-0.048	-0.046	-0.049	-0.048	-0.05	-0.048	-0.049	-0.039

Column	5 - Young Buried Ash - SM4-01-01B (Conc. in mg/kg)															
Sample ID	5.01	5.02	5.03	5.04	5.05	5.06	5.07	5.08	5.09	5.10	5.11	5.12	5.13	5.14	5.15	5.16
Day No.	0	3	5	7	9	11	13	15	17	19	21	23	25	27	29	31
Analyte	8/1/11	8/4/11	8/6/11	8/8/11	8/10/11	8/12/11	8/14/11	8/16/11	8/18/11	8/20/11	8/22/11	8/24/11	8/26/11	8/28/11	8/30/11	9/1/11
Ag	-0.017	-0.018	-0.017	-0.016	-0.017	-0.017	-0.02	-0.02	-0.02	0.025	0.027	0.026	0.025	0.024	0.026	0.031
Al	0.655	2.622	0.057	1.683	0.408	1.079	2.197	3.329	4.324	4.182	4.337	4.357	5.667	4.566	5.079	1.452
As																
B	33.26	24.26	19.11	17.51	16.6	17.84	17.53	17.51	15.14	12.29	11.1	9.746	8.241	7.432	6.955	6.458
Ba	0.046	0.025	0.041	0.031	0.039	0.052	0.035	0.045	0.037	0.036	0.009	0.017	0.013	0.014	0.014	0.034
Be	-0.074	-0.074	-0.074	-0.074	-0.075	-0.074	-0.074	-0.074	-0.074	-0.072	-0.072	-0.072	-0.072	-0.072	-0.072	-0.072
Ca	422.1	468.1	513.8	538.2	591.2	521.6	345.3	345.3	108	75.03	63.2	56.03	48.08	40.58	40.49	38.42
Cd	-0.039	-0.04	-0.04	-0.039	-0.039	-0.04	-0.04	-0.04	-0.039	-0.04	-0.04	-0.04	-0.04	-0.04	-0.04	-0.04
Co	-0.043	-0.04	-0.039	-0.039	-0.039	-0.039	-0.039	-0.04	-0.04	-0.041	-0.041	-0.04	-0.041	-0.041	-0.041	-0.04
Cr	0.187	0.02	-0.016	-0.023	-0.025	-0.026	-0.028	-0.029	-0.03	-0.031	-0.03	-0.032	-0.031	-0.032	-0.031	-0.032
Cu	0.012	0.004	0.005	0.003	0.001	0.021	0.004	0.002	0.002	-0.001	0.001	-0.001	-0.001	-0.001	-0.001	-0.001
Fe	-0.055	-0.06	-0.061	-0.061	-0.061	-0.062	-0.062	-0.061	-0.062	-0.063	-0.063	-0.063	-0.063	-0.063	-0.063	-0.063
K	54.17	33.62	21.63	16.94	12.59	11.42	8.269	6.614	5.289	4.957	4.675	4.328	3.829	3.713	3.76	3.359
Li	-1.453	23.25	44	52.5	55.13	53.39	37.02	19.15	9.891	7.144	5.819	5.277	4.429	3.738	3.613	3.313
Mg	0.21	0.167	0.305	0.185	0.308	0.14	-0.02	-0.132	-0.187	-0.21	-0.115	-0.243	-0.245	-0.241	-0.267	-0.255
Mn	-0.039	-0.041	-0.04	-0.041	-0.04	-0.038	-0.041	-0.041	-0.041	-0.04	-0.039	-0.04	-0.04	-0.04	-0.04	-0.04
Mo	9.306	1.57	0.288	0.122	0.098	0.087	0.08	0.083	0.07	0.052	0.047	0.047	0.031	0.022	0.023	0.02
Na	1837	857.1	346.9	180.2	82.55	51.8	41.62	29.79	24.82	28.78	27.33	22.7	21.8	19.92	17.57	15.9
Ni	-0.086	-0.053	-0.047	-0.046	-0.046	-0.045	-0.046	-0.046	-0.046	-0.051	-0.05	-0.05	-0.05	-0.051	-0.05	-0.05
Pb	-0.076	-0.052	-0.048	-0.049	-0.051	-0.049	-0.046	-0.046	-0.042	-0.055	-0.054	-0.054	-0.054	-0.053	-0.054	-0.053
Se	0.078	-0.082	-0.106	-0.109	-0.112	-0.113	-0.114	-0.107	-0.113	-0.122	-0.12	-0.124	-0.118	-0.12	-0.119	-0.119
Si	0.281	0.382	2.256	0.245	-0.351	0.071	0.562	0.394	0.515	0.195	-0.055	-0.073	0.284	-0.013	0.035	-0.308
Sr	1.829	1.732	1.808	1.844	1.79	1.606	1.172	0.704	0.452	0.333	0.318	0.282	0.248	0.23	0.236	0.23
V	0.075	0.047	0.024	0.021	-0.024	0.015	0.044	0.072	0.071	0.119	0.119	0.121	0.122	0.136	0.124	0.105
Zn	-0.031	-0.042	-0.043	-0.031	-0.019	0.007	-0.045	-0.045	-0.049	-0.046	-0.049	-0.047	-0.05	-0.052	-0.052	-0.05

Column	6 - Spoil - YR1-01-01B (Conc. in mg/Kg)											
Sample ID	6.01	6.02	6.03	6.04	6.05	6.06	6.07	6.08	6.09	6.10	6.11	6.12
Day No.	0	3	5	7	9	11	13	15	17	19	21	23
Analyte	8/1/11	8/4/11	8/6/11	8/8/11	8/10/11	8/12/11	8/14/11	8/16/11	8/18/11	8/20/11	8/22/11	8/24/11
Ag	0.024	0.024	0.026	0.027	0.025	0.025	0.026	0.024	0.025	0.026	0.026	0.025
Al	-0.091	0.031	-0.094	-0.098	-0.098	-0.092	-0.099	-0.098	-0.094	-0.095	-0.097	-0.096
As												
B	1.393	7.406	1.068	1.663	1.691	1.128	2.74	1.096	1.07	1.13	1.023	0.852
Ba	0.154	0.113	0.076	0.098	0.125	0.143	0.046	0.049	0.051	0.044	0.037	0.017
Be	-0.075	-0.075	-0.074	-0.074	-0.074	-0.074	-0.074	-0.074	-0.074	-0.074	-0.074	-0.074
Ca	284.1	300.1	267.7	300.6	299.5	280.4	317.5	290.6	296	293.5	297.4	289.6
Cd	-0.039	-0.04	-0.039	-0.039	-0.039	-0.039	-0.04	-0.04	-0.04	-0.04	-0.04	-0.04
Co	-0.001	-0.012	-0.021	-0.023	-0.027	-0.029	-0.031	-0.031	-0.031	-0.033	-0.033	-0.034
Cr	-0.034	-0.037	-0.036	-0.037	-0.037	-0.037	-0.037	-0.037	-0.037	-0.038	-0.038	-0.037
Cu	0.341	0.318	0.161	0.133	0.113	0.094	0.089	0.072	0.063	0.055	0.048	0.039
Fe	0.022	0.006	-0.005	-0.017	-0.027	-0.03	-0.036	-0.032	-0.034	-0.039	-0.042	-0.044
K	179	115.7	73.23	73.5	67.72	59.82	62.2	56.94	54.91	52.62	52.02	47.73
Li	25.67	27.91	24.55	26.59	26.81	25.4	29.2	26.54	27.18	27.02	27.91	27.07
Mg	541.5	425.1	299.1	274.5	239.9	209.9	198.8	193.9	179.4	170.6	164.5	155.6
Mn	0.567	0.243	0.153	0.013	0.002	0.038	0.035	0.119	0.111	0.085	0.064	0.051
Mo	0.005	0.014	0.013	0.022	0.018	0.013	0.017	0.011	0.007	0.005	0.006	0.002
Na	219	163.3	111.5	105.3	94.31	82.16	79.43	76.16	71.64	67.9	64.7	63.5
Ni	0.188	0.128	0.075	0.07	0.054	0.04	0.035	0.032	0.026	0.022	0.021	0.015
Pb	-0.063	-0.064	-0.062	-0.063	-0.063	-0.062	-0.062	-0.061	-0.06	-0.061	-0.062	-0.062
Se	1.934	0.573	0.101	0.002	-0.061	-0.103	-0.121	-0.127	-0.129	-0.125	-0.124	-0.128
Si	8.766	1.937	4.882	6.456	6.413	5.785	6.799	6.775	6.71	6.879	6.748	6.122
Sr	10.39	7.781	5.653	6.019	5.46	5.046	5.287	5.002	4.785	4.691	4.694	4.524
V	-0.13	-0.102	-0.063	-0.064	-0.048	-0.042	-0.025	-0.037	-0.033	-0.029	-0.028	-0.024
Zn	0.054	-0.018	-0.032	-0.041	-0.041	-0.041	-0.043	-0.041	-0.044	-0.029	-0.046	-0.016

Column	7 - Fresh Fly Ash w/ No 8 Coal Seam Water - NE-FA-01 (Conc. in mg/Kg)												
Sample ID	7.01	7.02	7.03	7.04	7.05	7.06	7.07	7.08	7.09	7.10	7.11	7.12	7.13
Day No.	0	3	5	7	9	11	13	15	17	19	21	23	25
Analyte	8/1/11	8/4/11	8/6/11	8/8/11	8/10/11	8/12/11	8/14/11	8/16/11	8/18/11	8/20/11	8/22/11	8/24/11	8/26/11
Ag	0.039	0.034	0.032	0.036	0.035	0.031	0.028	0.029	0.03	0.031	0.047	0.274	0.028
Al	0.209	2.064	1.87	1.512	1.384	1.29	1.046	0.922	0.87	0.935	0.941	1.063	1.043
As													
B	40.26	38.58	36.14	35.73	36.43	36.23	36.57	36.09	34.09	32.5	31.63	31.37	30.51
Ba	0.057	0.014	0.015	0.024	0.022	0.018	0.021	0.009	0.005	0.006	0.003	0	-0.001
Be	-0.072	-0.072	-0.072	-0.072	-0.072	-0.072	-0.072	-0.072	-0.072	-0.071	-0.069	-0.068	-0.067
Ca	386.5	351.7	376.3	389.6	403.4	393.2	395.5	379.8	390.6	390.5	359.3	289.2	222.9
Cd	-0.04	-0.041	-0.041	-0.041	-0.041	-0.041	-0.041	-0.041	-0.041	-0.041	-0.041	-0.041	-0.041
Co	-0.044	-0.041	-0.04	-0.04	-0.04	-0.04	-0.04	-0.04	-0.04	-0.04	-0.04	-0.04	-0.04
Cr	0.773	0.208	0.047	0.012	-0.01	-0.021	-0.029	-0.033	-0.034	-0.035	-0.034	-0.035	-0.034
Cu	0.011	0.002	0	0	-0.001	-0.001	-0.001	0.001	-0.002	0	-0.001	-0.001	-0.001
Fe	-0.056	-0.061	-0.062	-0.063	-0.062	-0.062	-0.063	-0.06	-0.063	-0.062	-0.063	-0.063	-0.063
K	88.77	75.68	69.72	68.06	69.23	67.18	67.72	65.12	58.07	52.73	46.73	41.75	37.16
Li	-42.32	-24.23	7.925	24.37	32.2	35.18	36.62	36.15	38.4	38.29	36.03	28.26	21.84
Mg	0.215	0.132	-0.072	-0.071	-0.068	-0.061	-0.046	0.369	-0.046	-0.043	-0.073	-0.121	-0.155
Mn	-0.041	-0.04	-0.04	-0.04	-0.04	-0.04	-0.04	-0.039	-0.04	-0.04	-0.04	-0.04	-0.04
Mo	10.74	2.445	0.555	0.299	0.236	0.214	0.185	0.18	0.192	0.18	0.165	0.15	0.156
Na	22.16	19.19	16.12	15.18	14.59	14.79	14.72	15.04	14.4	14.59	14.84	15.4	14.58
Ni	-0.097	-0.062	-0.053	-0.051	-0.051	-0.052	-0.051	-0.051	-0.052	-0.052	-0.051	-0.051	-0.051
Pb	-0.095	-0.069	-0.061	-0.06	-0.061	-0.061	-0.06	-0.061	-0.06	-0.06	-0.06	-0.058	-0.058
Se	0.191	-0.043	-0.101	-0.112	-0.117	-0.124	-0.115	-0.118	-0.116	-0.111	-0.111	-0.104	-0.1
Si	0.794	0.702	0.82	0.903	1.039	1.267	1.171	1.165	1.356	1.576	1.709	1.904	1.97
Sr	2.403	2.164	2.184	2.224	2.306	2.24	2.258	2.238	2.244	2.206	1.978	1.598	1.285
V	0.092	0.118	0.132	0.135	0.145	0.156	0.166	0.18	0.214	0.321	0.511	0.674	0.757
Zn	-0.043	-0.043	-0.044	-0.043	-0.044	-0.044	-0.044	-0.044	-0.045	-0.004	-0.045	-0.043	-0.046

Column	8 - Old Fly Ash w/ No 8 Coal Seam Water - SM4-04-06B (Conc. in mg/Kg)												
Sample ID	8.01	8.02	8.03	8.04	8.05	8.06	8.07	8.08	8.09	8.10	8.11	8.12	8.13
Day No.	0	3	5	7	9	11	13	15	17	19	21	23	25
Analyte	8/1/11	8/4/11	8/6/11	8/8/11	8/10/11	8/12/11	8/14/11	8/16/11	8/18/11	8/20/11	8/22/11	8/24/11	8/26/11
Ag	0.038	0.025	0.022	0.022	0.024	0.023	0.026	0.029	0.027	0.026	0.026	0.025	0.025
Al	0.165	0.063	0.386	0.412	0.955	2.415	0.511	0.884	0.316	0.307	1.981	3.117	3.273
As													
B	11.34	4.294	1.315	1.289	1.356	1.221	1.147	1.823	1.185	0.881	2.038	4.41	5.541
Ba	0.095	0.474	4.32	3.435	2.257	2.158	1.847	0.63	0.284	0.038	0.074	0.044	0.035
Be	-0.073	-0.073	-0.073	-0.073	-0.073	-0.073	-0.073	-0.073	-0.073	-0.073	-0.071	-0.07	-0.069
Ca	472.7	262.7	212.6	165.7	141.9	126.5	95.23	22.56	106.4	27.71	28.34	24.8	14.33
Cd	-0.04	-0.04	-0.04	-0.04	-0.04	-0.04	-0.04	-0.04	-0.04	-0.04	-0.04	-0.04	-0.04
Co	-0.044	-0.041	-0.041	-0.04	-0.04	-0.04	-0.042	-0.041	-0.041	-0.041	-0.041	-0.04	-0.04
Cr	0.367	0.004	-0.032	-0.034	-0.033	-0.034	-0.033	-0.033	-0.034	-0.033	-0.033	-0.034	-0.034
Cu	0.03	0.003	0.004	0.002	0.034	0.001	0.002	0.003	0.001	0	0	0.001	0
Fe	-0.057	-0.061	-0.062	-0.062	-0.059	-0.063	-0.062	-0.061	-0.062	-0.062	-0.062	-0.06	-0.059
K	144.4	69.13	61.49	61.92	73.19	62.07	56.6	56.06	51.66	43.39	31.05	24.29	20.62
Li	-97.11	-13.87	5.558	6.001	5.363	5.65	2.98	-3.871	5.045	-1.769	-0.327	0.025	-0.709
Mg	-0.311	-0.311	-0.31	-0.311	-0.299	-0.311	-0.31	-0.311	-0.309	-0.308	-0.298	-0.288	-0.273
Mn	-0.041	-0.04	-0.04	-0.04	-0.039	-0.04	-0.04	-0.04	-0.04	-0.04	-0.04	-0.04	-0.039
Mo	10.65	2.612	1.152	0.902	0.931	0.745	2.466	1.399	0.924	0.71	0.243	0.114	0.097
Na	38.77	17.4	15.98	14.51	15.47	15.03	15.79	15.77	14.66	17.5	18.39	18.79	18.57
Ni	-0.096	-0.06	-0.054	-0.053	-0.05	-0.052	-0.06	-0.055	-0.053	-0.052	-0.05	-0.05	-0.05
Pb	-0.087	-0.064	-0.056	-0.056	-0.035	-0.054	-0.061	-0.058	-0.056	-0.057	-0.054	-0.054	-0.054
Se	0.935	-0.015	-0.096	-0.1	-0.089	-0.089	-0.058	-0.038	-0.095	-0.11	-0.115	-0.112	-0.091
Si	1.863	0.365	0.325	0.423	0.572	0.616	1.168	1.989	1.949	3.641	17.96	24.83	27.12
Sr				12.92	10.02	8.372	6.407	2.893	4.622	1.443	1.082	1.113	1.177
V	-0.047	-0.018	-0.012	-0.007	-0.003	-0.004	-0.003	0.004	0.003	0.025	0.252	0.438	0.49
Zn	0.086	0.018	-0.028	-0.04	0.027	-0.031	-0.023	-0.047	-0.043	-0.044	-0.019	-0.048	-0.053

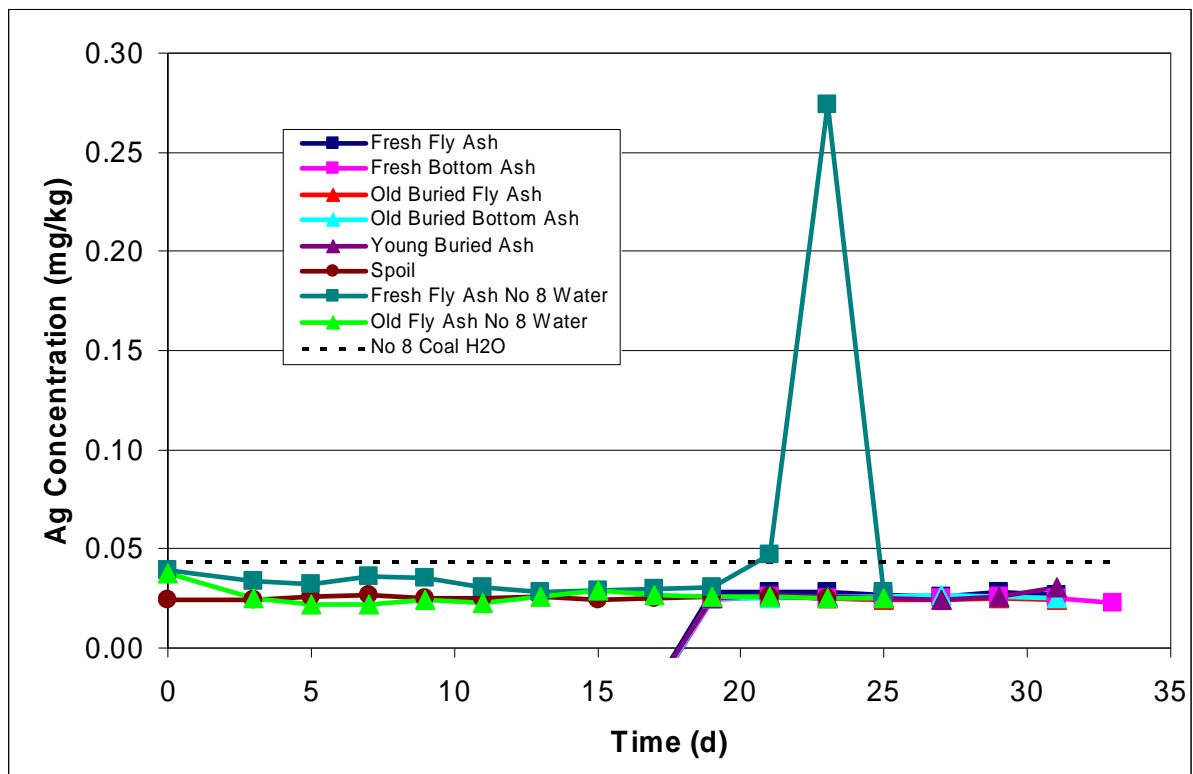


Figure 95 : Results of column leach tests for silver (Ag).

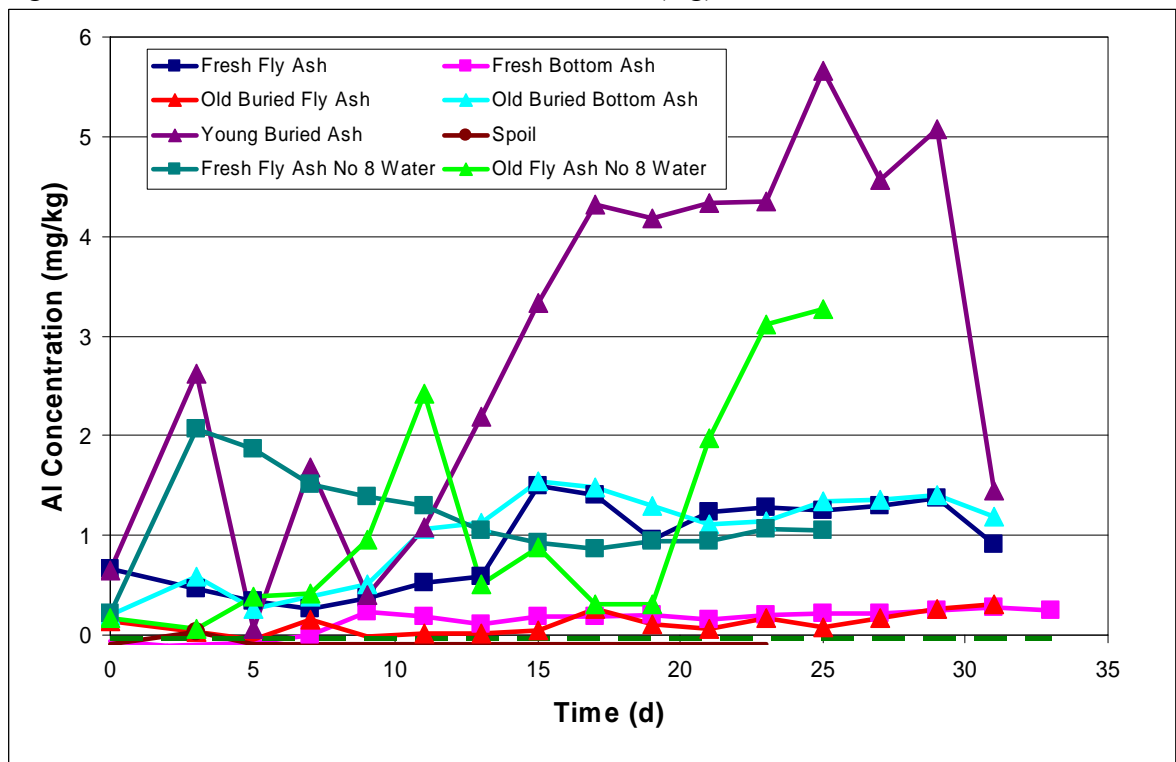


Figure 96: Results of column leach tests for aluminum (Al)

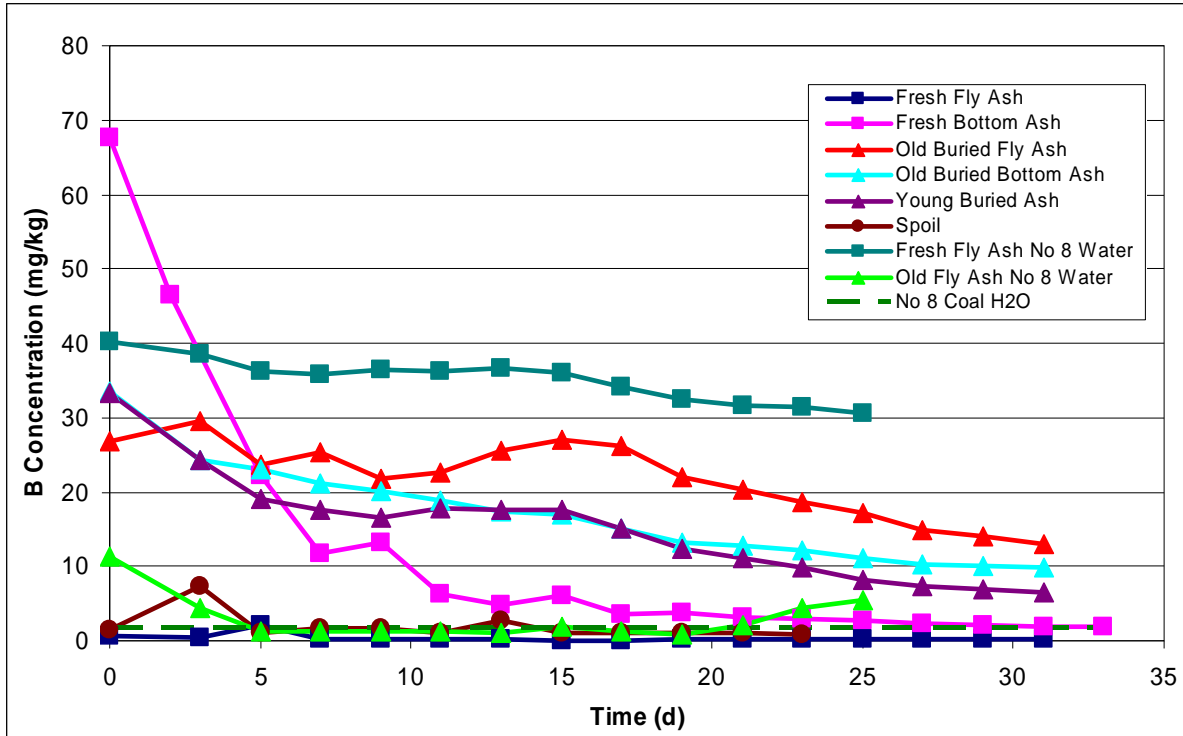


Figure 97: Results of column leach tests for boron (B)

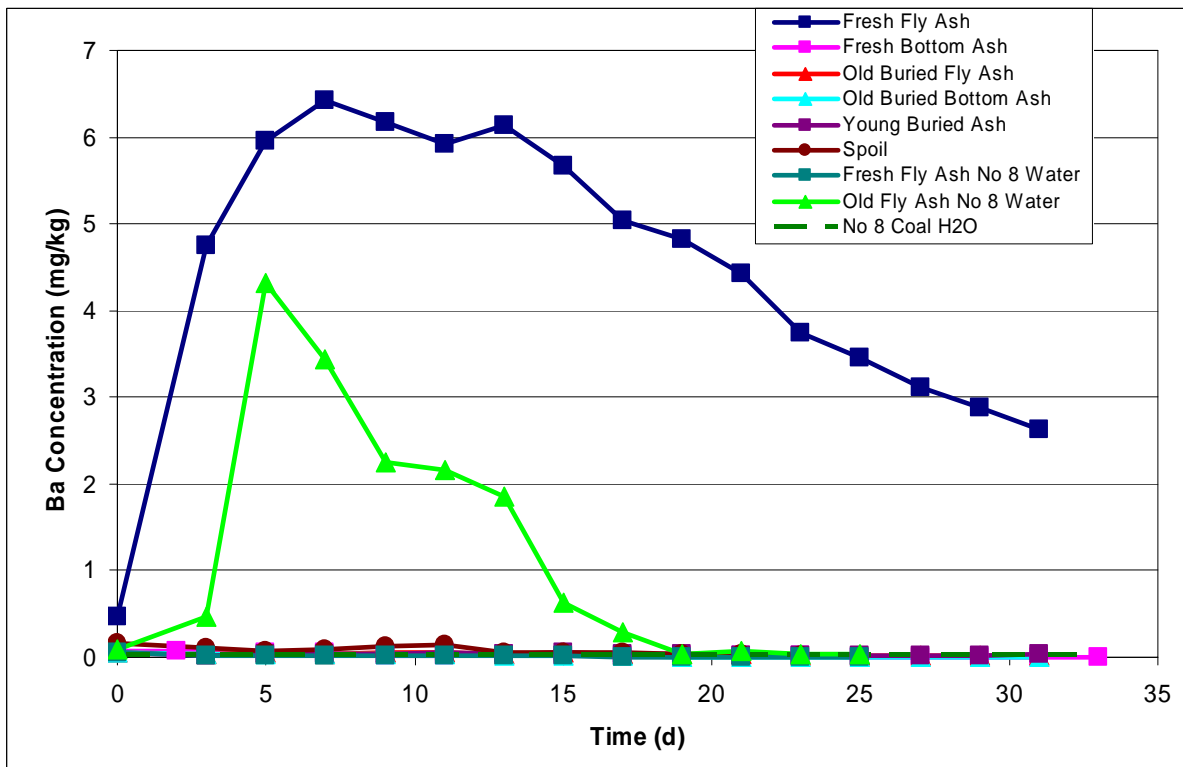


Figure 98: Results of column leach tests for barium (Ba)

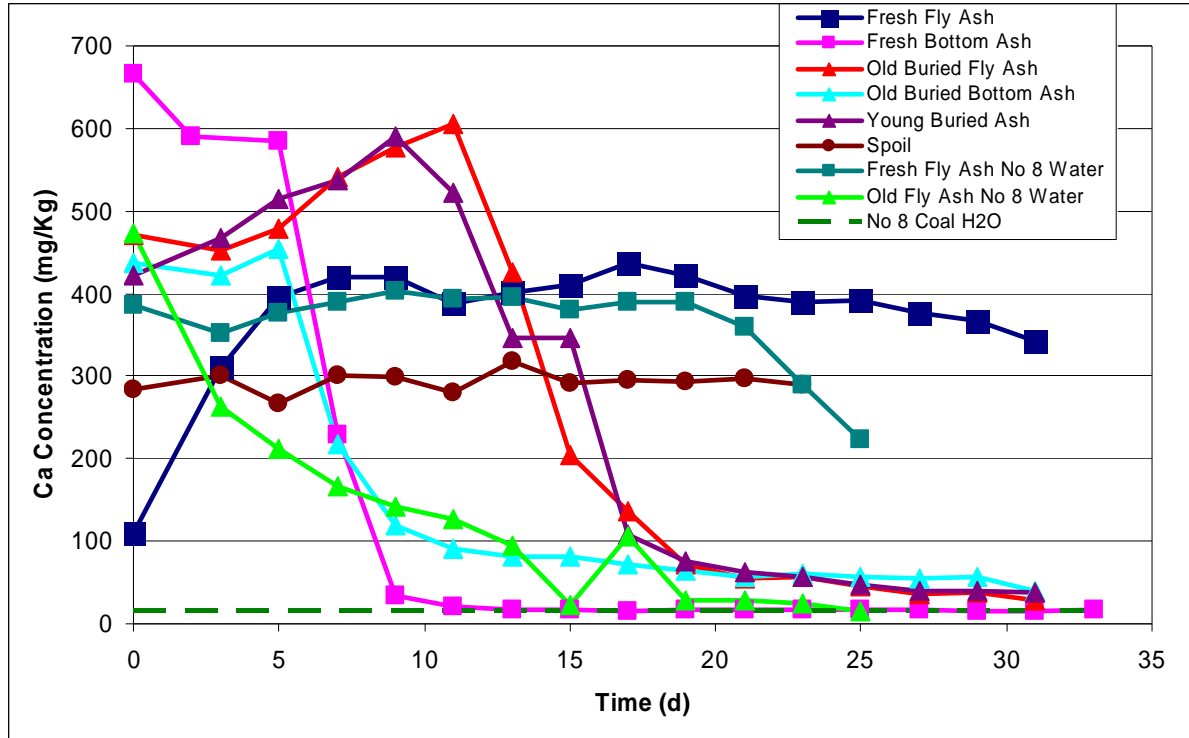


Figure 99: Results of column leach tests for calcium (Ca)

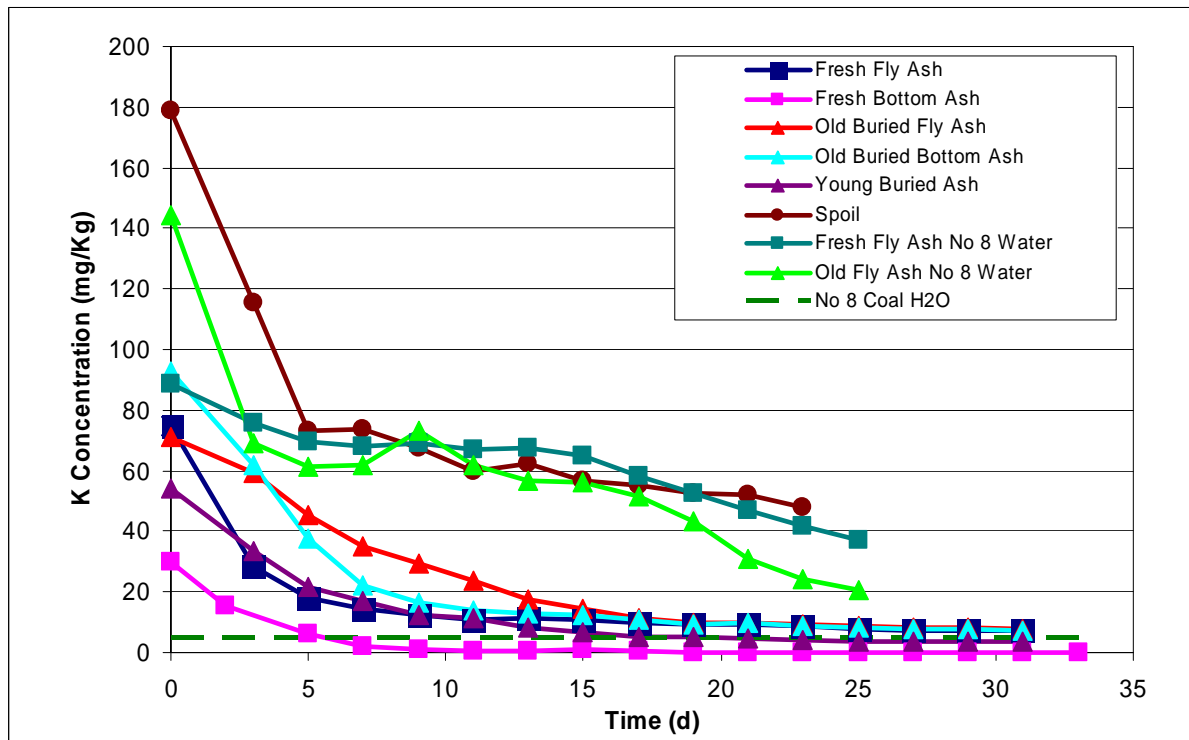


Figure 100: Results of column leach tests for potassium (K)

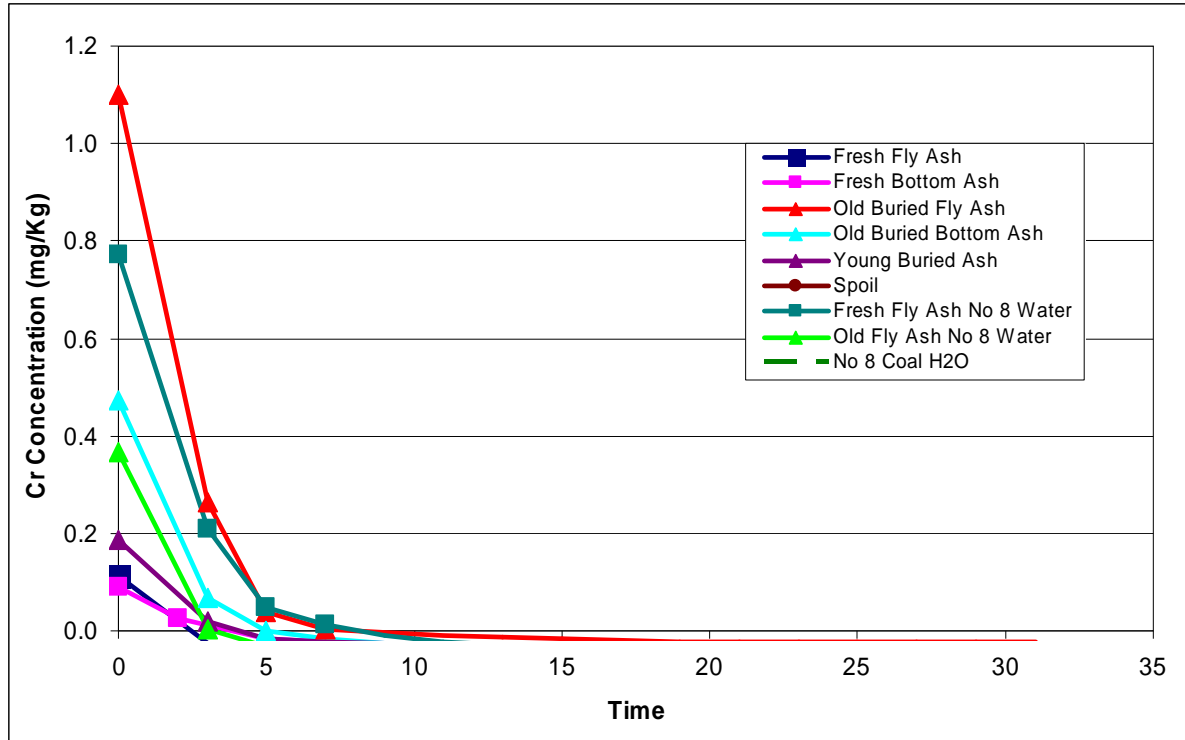


Figure 101: Results of column leach tests for chromium (Cr)

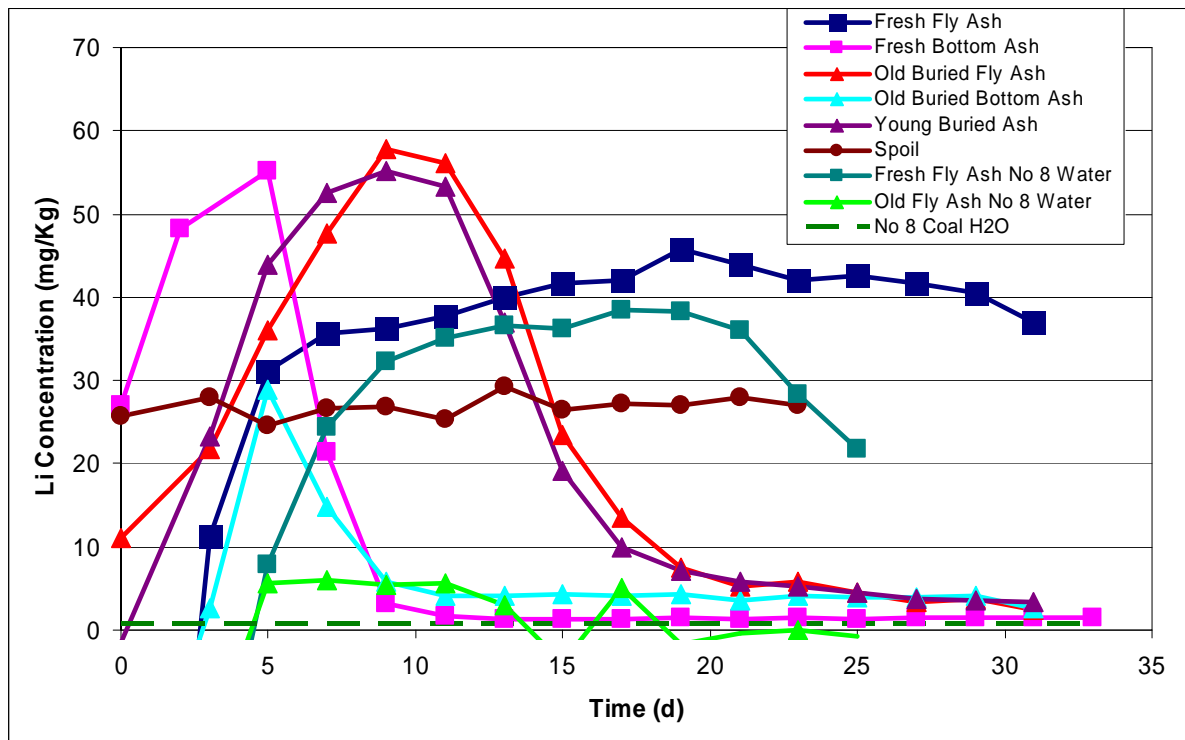


Figure 102: Results of column leach tests for lithium (Li)

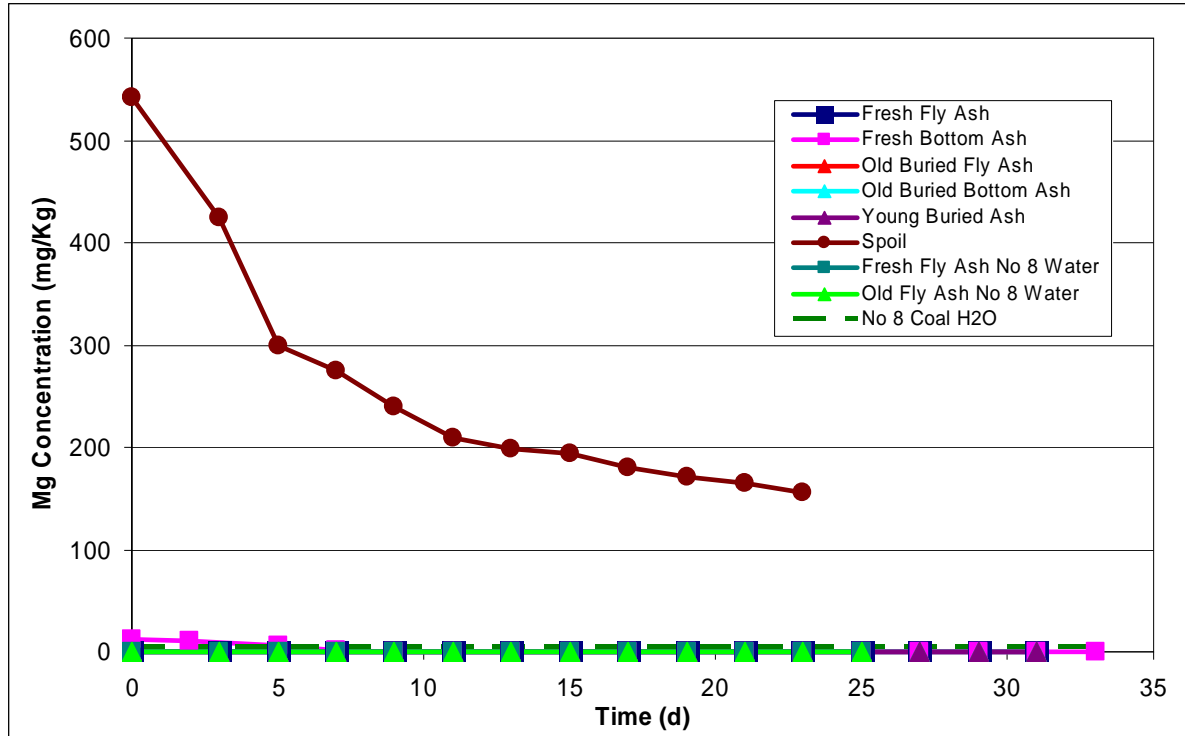


Figure 103: Results of column leach tests for magnesium (Mg)

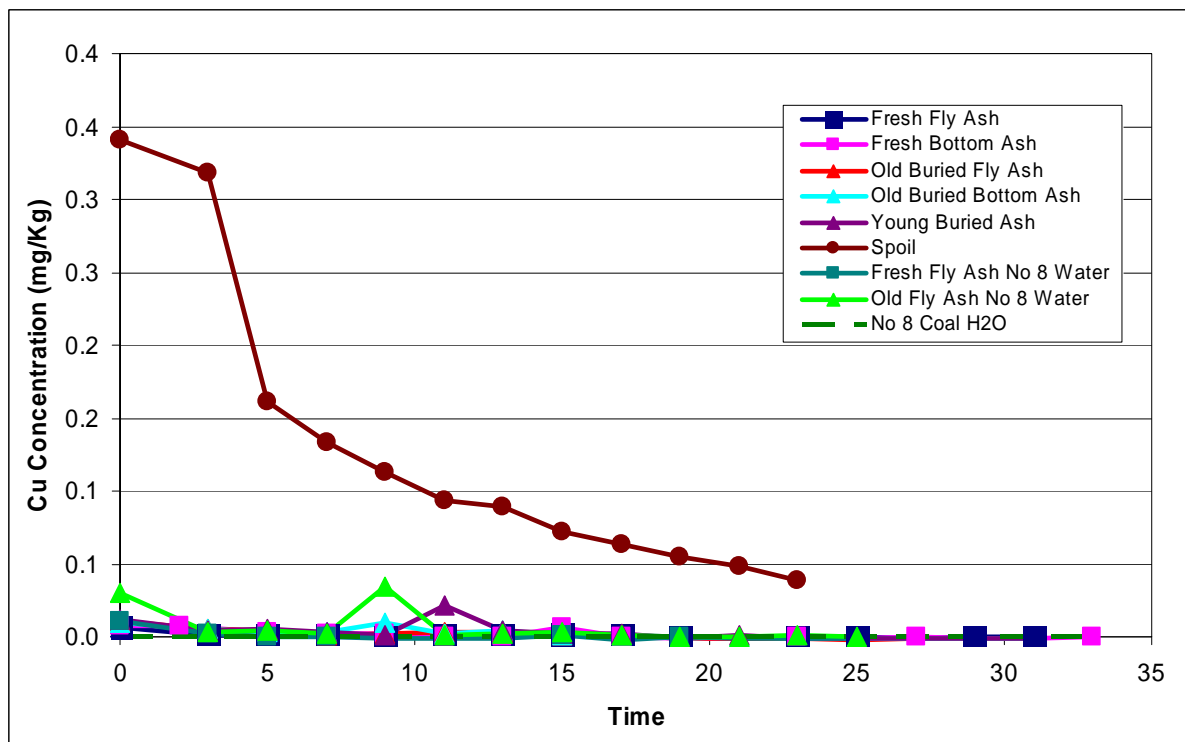


Figure 104: Results of column leach tests for copper (Cu)

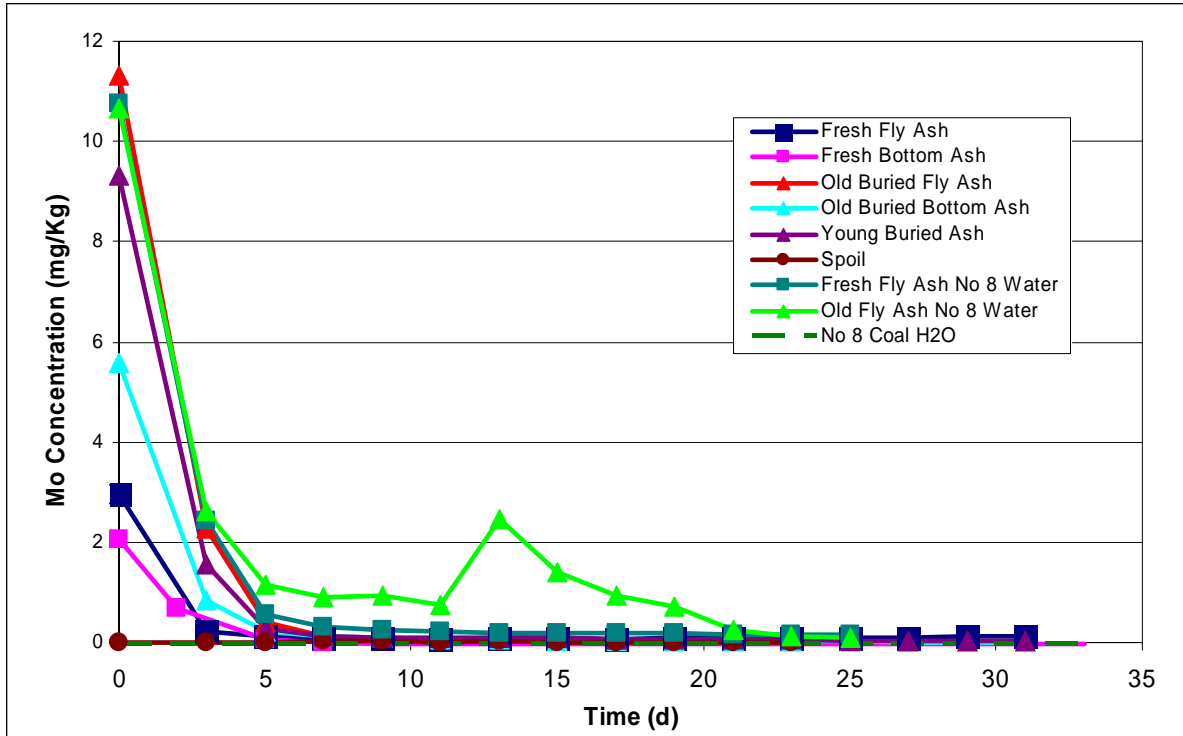


Figure 105: Results of column leach tests for molybdenum (Mo)

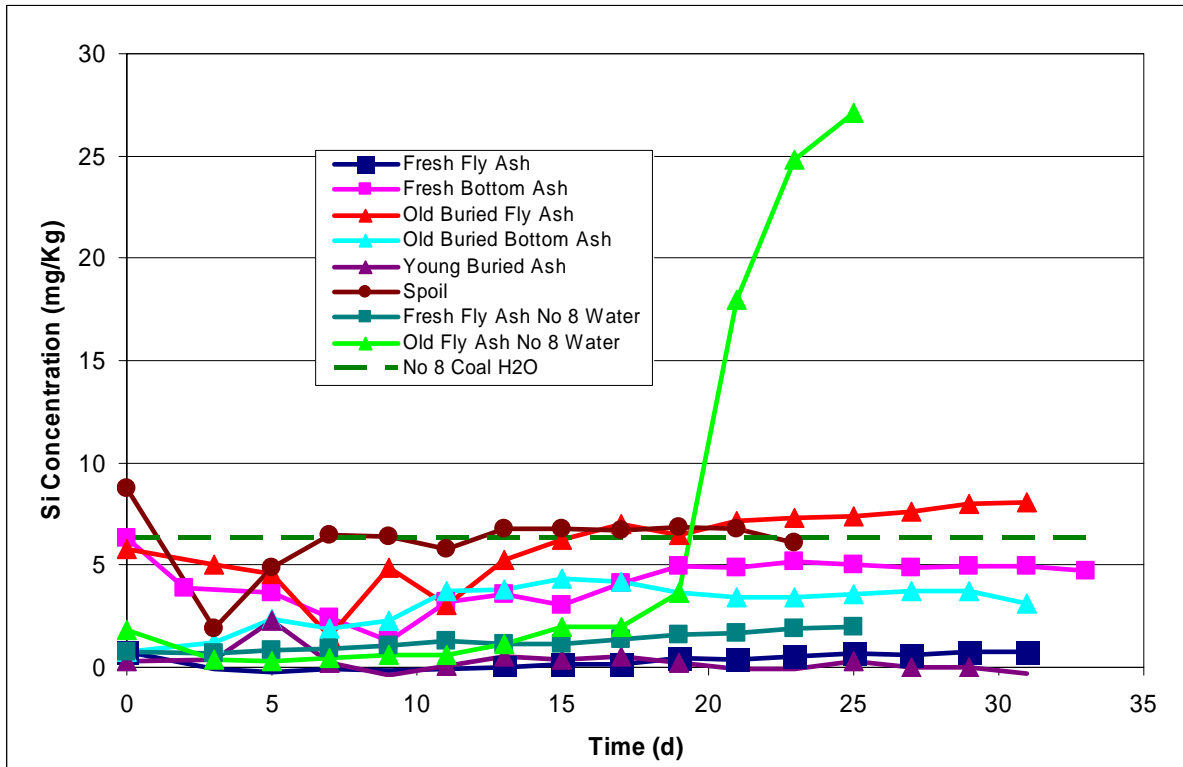


Figure 106: Results of column leach tests for silicon (Si)

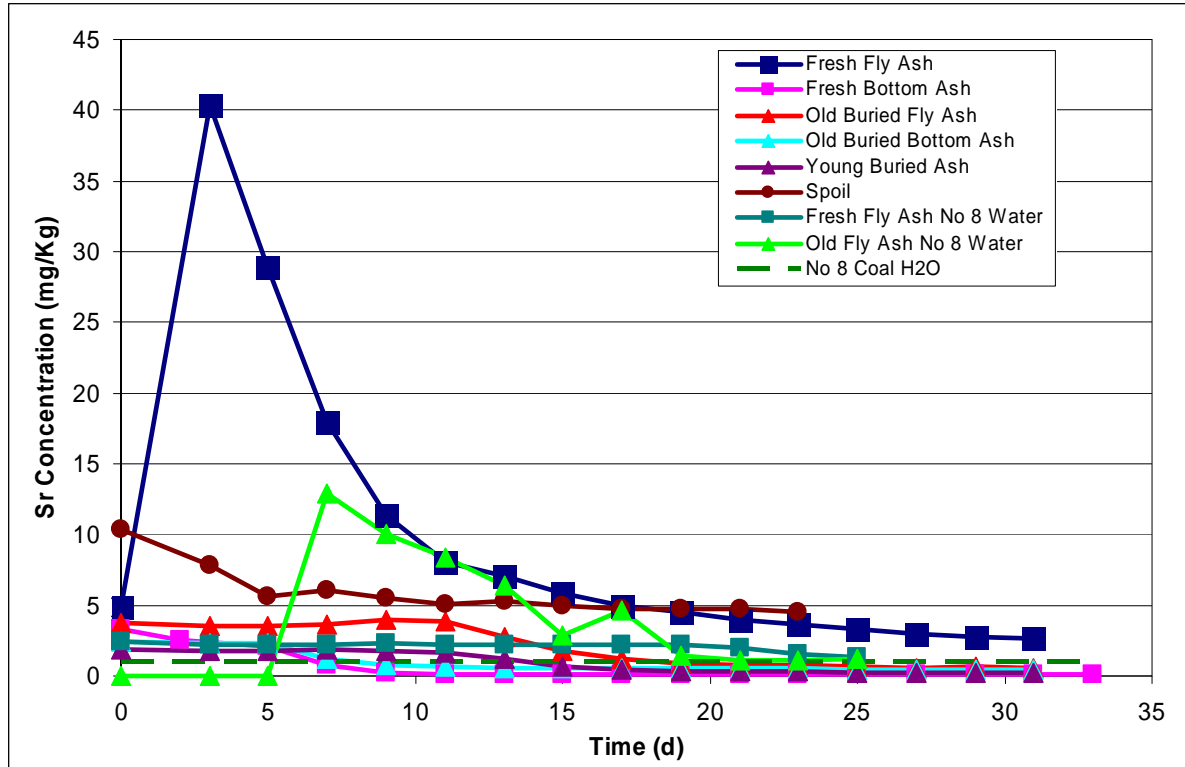


Figure 107: Results of column leach tests for strontium (Sr)

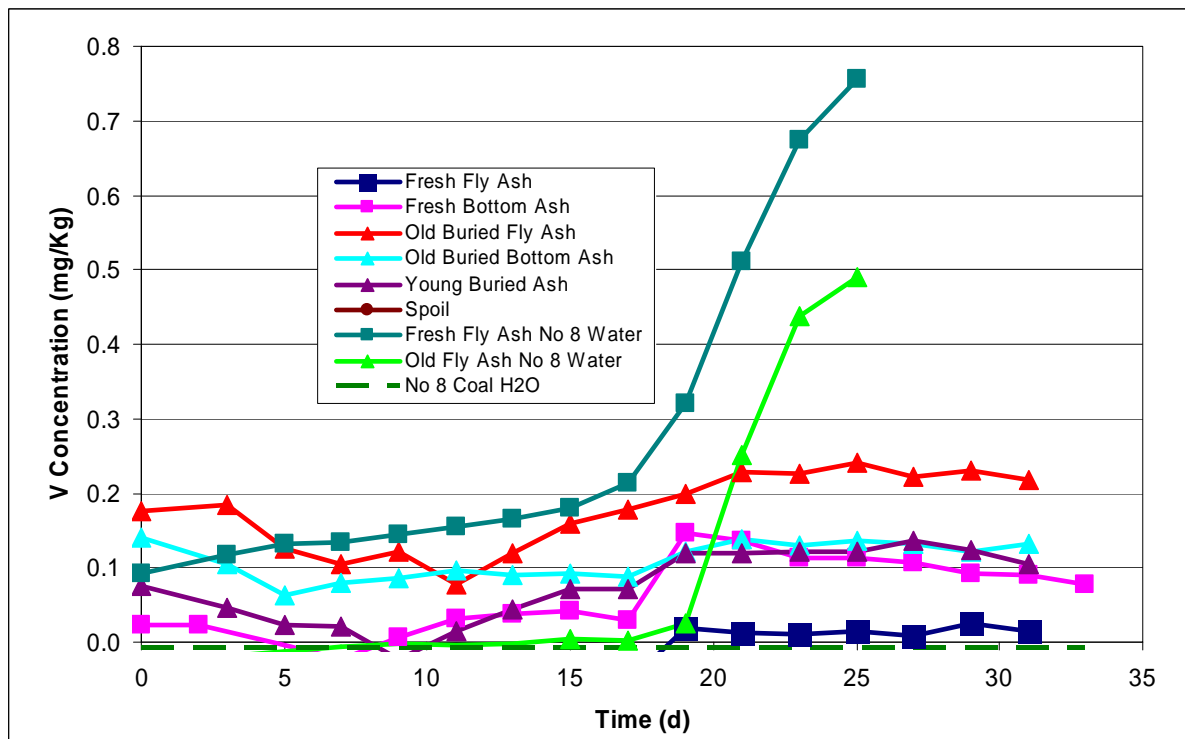


Figure 108: Results of column leach tests for vanadium (V)

Appendix II - Abbreviations

BA	Bottom ash
CCBs	Coal Combustion By-Products
DI water	Deionized water
EPA	Environmental Protection Agency
FA	Fly ash
FBA	Fresh bottom ash
FFA	Fresh fly ash
FGD	Flue gas desulfurization
MCC	Moisture characteristic curves
MCL	Maximum contaminant level
MMD	Mining and Minerals Division of the New Mexico Energy, Minerals and Natural Resources Department
NMCC	New Mexico Climate Center
NMED	New Mexico Environment Department
OBA	Old bottom ash
OFA	Old fly ash
SJCM	San Juan Coal Mine
SMCRA	Surface Mining Control and Reclamation Act